PHD

Electrochemical studies on ultramicroelectrodes

Menolasina, Sabino Jose

Award date:
1996

Awarding institution:
University of Bath

Electrochemical studies on ultramicroelectrodes

Submitted by Sabino José Menolasina
for the degree of PhD
of the University of Bath
1996

COPYRIGHT

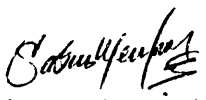

Sabino José Menolasina

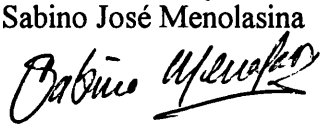

ProQuest LLC
789 East Eisenhower Parkway
P.O. Box 1346
Ann Arbor, MI 48106-1346

University of Bath

Electrochemical studies on ultramicroelectrodes

School of Chemistry

Sabino José Menolasina Monrreal

November 1996

University of Bath

Abstract

School of Chemistry

Doctor of Philosophy

Electrochemical studies on ultramicroelectrodes

by

Sabino José Menolasina Monrreal

The applications of ultramicroelectrodes have had an impact on applied electrochemistry in the last fifteen years due to their high immunity to ohmic drop phenomena and the high mass transfer obtained due to their small size.

In the present work, carbon and gold ultramicroelectrodes, 4 and 5 μm in radius respectively, were prepared and characterised using electrochemical techniques and scanning electronmicroscopy (SEM). It was found that a good quality seal, can be obtained by chemical treatment of the carbon fibres.

Ultramicroelectrode studies of underpotential deposition (*upd*) of lead were carried out. A monolayer of lead and Au-Pb alloys are formed simultaneously in the *upd* region.

Ultramicroelectrode studies of the oxidation and reduction of hexacyano-ferrate couple have shown that the electrochemical process is affected by the concentration of the KF supporting electrolyte. Determination of the rate constants for the hexacyanoferrate couple for the free (unpaired) anionic species seems to be impossible. Even at the lower concentrations and after correction for double layer effects, the reaction is still dominated by ion pair effects.

The oxygen reduction reaction was investigated using Pt polycrystalline ultramicroelectrodes and Pt modified carbon ultramicroelectrodes. The mechanism of oxygen reduction to water, seems to be dependent on the mass transfer conditions and the roughness of the electrode surface.

Acknowledgements

I would like to express my gratitude to my supervisor Prof. L.M. Peter for his guidance and advice over the last three years.

Many thanks to Dr. Jason Riley, Dr. Mike Bailes for their support and help in some stages of my studies.

Many thanks to all my laboratory colleagues who shared bad and good moments with me during the last three years.

Many thanks to the glassblower Mr. M. Lock for his help during the preparation of the first ultramicroelectrodes and for making innumerable ultramicroelectrodes after that.

I wish to thank Zoraida, my wife, and my children for their encouragement and understanding during this work and for keeping me in good spirits. I would like also to thank David Fermín, Enrique Millán, Dr. José Miguel Ortega and Dr. Carlos Ponce de León who in different ways contributed in encouraging me during these years.

Finally, I would like to acknowledge the Universidad de los Andes for giving to me the opportunity to do my studies abroad, and also the Cosejo Nacional de Investigaciones Científicas y Tecnológicas (CONICIT) for their financial support.

Table of Contents

CHAPTER 1

THEORY AND APPLICATIONS OF ULTRAMICROELECRODES

CHAPTER 1

THEORY AND APPLICATIONS OF ULTRAMICROELECTRODES

1.1. *Introduction*

An ultramicroelectrode is defined as an electrode with at least one dimension small enough for its properties e.g. transport regime, to be a function of its size [1]. In practice electrodes ranging from 1 to 50 μm fall into this category. This kind of device was first developed for use *in situ* and *in vivo* electrochemical studies in biological tissues [2,3]. They were used 50 years ago for determining oxygen in animal tissue [2]. They are ideal as sensors in biological systems because their small size minimises damage to the surrounding tissue, and allows local concentrations to be examined. Until the early 1970s, most of the ultramicroelectrode voltammetric literature was related to the determination of oxygen in biological tissues and fluids. It was during that decade that ultramicroelectrodes began to be applied to the *in vivo* voltammetric determination of specific compounds present in the brain, called neurotransmitters [3]. Although the advantageous properties of these small devices were recognized for many years, research in this area did not become very active until the late 1970s. Research carried out in the field of electronics, especially in the measurement of very small currents and the development of microstructural materials, have been important for construction and use electrodes of small dimensions. Fleischmann et al. at the University of Southampton [4,5], were interested in understanding electrode mechanisms under conditions of high current density, and they initiated and developed some theoretical aspects of the application of ultramicroelectrodes.

Ultramicroelectrodes with different geometries are widely described in the literature [6-9]. The shape is an important factor in determining the properties of an electrode. Table I summarises the common types and **figure 1.1** shows their diffusion geometries in the steady state. Smaller ultramicroelectrodes with dimensions less than 1μm are being increasingly used in areas as diverse as

scanning tunneling microscopy (STM) [9], chemical kinetics [10], and electrophysiology [11]. However characterisation of the size, shape and configuration of these ultrasmall electrodes is more difficult [12].

Table I

Type of ultramicroelectrode	Critical dimensions	Geometry of diffusion field
sphere	radius	spherical
hemisphere	radius	spherical
disc	radius	spherical
wire	radius	cylindrical
line	width	cylindrical
ring	width	cylindrical

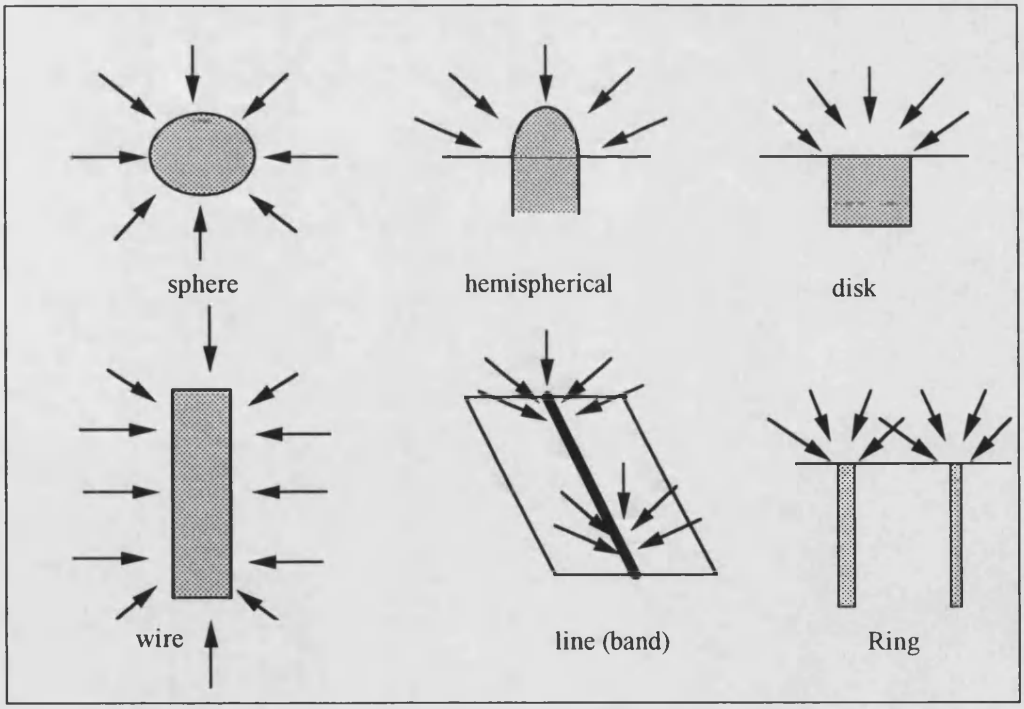

Figure 1.1. Different types of electrodes with their respective diffusion geometries.

The properties of ultramicroelectrodes, which have been exploited in many areas of the electrochemistry are:

1.- High steady state rates of diffusion. This behaviour permits the study of rapid electron transfer and fast coupled chemical reactions, using steady state techniques [13,14].

2.- Low iR drop, which allows the use of highly resistive media and very high speed cyclic voltammetry [15-17].

3.- Small RC time constant. When an ultramicroelectrode is used, the uncompensated resistance of the electrochemical cell will be inversely proportional to the radius of the ultramicroelectrode. Since, the capacitance is proportional to the area of ultramicroelectrode, the product RC will be proportioanal to the radius. The smaller r is, the smaller the RC time constant will be. This behaviour permits the study of fast electron transfer processes at short times.

4.- Small size. This property has already been mentioned at the beginning of this section, with its application in the area of electrophysiology [2,3]. Due to the small size advantages are also obtained in investigations of adsorption, conformational changes and kinetics at the molecular level, e.g. studies of the nucleation and growth of a single nucleus under well defined experimental conditions [18,19].

1.2. *Diffusion to disk ultramicroelectrodes*

In this section the properties of disk ultramicroelectrodes will be explained in more detail, because this type of ultramicroelectrode was predominantly used in the present work. The popularity of disk ultramicroelectrodes arises from their easy construction, but a disadvantage is the difficulty in making theoretical predictions of their electrochemical behaviour, though this problem has been solved for some experimental conditions.

To explain the diffusion process when these disk ultramicroelectrodes are used, it is first necessary to explain the behaviour observed at planar and spherical electrodes. During electrolysis, mass transfer from the bulk solution to the electrode surface takes place. The electrochemical response of the electrode will

therefore depend on the modes of mass transport that are operative. Unless the electrolyte is stirred or the electrode is rotated, the dominant mode of mass transfer will be diffusion. In the case of ultramicroelectrodes, the flux due to diffusion is large [20], so the effects of convection are less apparent than at electrodes of conventional size. Mass transport to ultramicroelectrodes is enhanced by the radial component [21] which is dependent on the geometry of the ultramicroelectrode.

In the following discussion, the simple electron transfer reaction:

$$O + ne^- \longrightarrow R \qquad (1.1)$$

will be analysed, for the case of chronoamperometry under well defined conditions, where the current is limited only by diffusion of species to the electrode. Diffusion control is obtained by applying an overpotential, at which the electrolysis rate is limited by the rate of diffusion of the species O to the electrode surface (i.e. for $t > 0$, $C_O = 0$ at the electrode surface). Initially $C_O = C_O^\infty$ and $C_R = 0$ throughout the solution, where C_O, C_R are the concentrations of species O and species R respectively in bulk solution.

1.2.1. *Semi-Infinite planar disk electrode*

In the simplest case of a semi-infinite planar electrode, derivation of the current-time response requires solution of Fick's laws of diffusion under the appropriate boundary conditions. According to Fick's 1st law, and considering the case of linear (one dimensional diffusion), the flux of species O at the electrode surface is given by the following equation:

$$-J_O = D_O \frac{\partial C_O(x)}{\partial x} \qquad (1.2)$$

where D_o is the diffusion coefficient of the species being electrolysed.

When the reaction rate is equal to the rate of linear diffusion at the electrode surface, the flux of species O is related to the current density **j** by:

$$J_O = \frac{j}{nF} \tag{1.3}$$

Here n is the number of electrons per molecule oxidised or reduced, F is Faraday's constant and j is the current density.

Combining (1.2) and (1.3), gives:

$$\frac{j}{nF} = -D_O \frac{\partial C_O(x)}{\partial x} \tag{1.4}$$

According to Fick's 2nd law, for a linear diffusion process:

$$\frac{\partial C_O}{\partial t} = D_O \frac{\partial^2 C_O}{\partial x^2} \tag{1.5}$$

Solving equations (1.4) and (1.5), with the initial condition: at $t = 0$, $C_O = C_O^\infty$ for all values of x; and boundary conditions, for $t > 0$, $C_O = 0$ at $x = 0$ and $C_O = C_O^\infty$ at $x = \infty$, the current transient for a large potential step is obtained (Cottrell equation [22]):

$$j = nFD^{1/2}C_O^\infty(\pi t)^{-1/2} \tag{1.6}$$

1.2.2. *Spherical electrode*

For a spherical electrode mass transfer occurs in a spherical diffusion field. The boundary conditions for the reduction of species O, of bulk concentration C_O^∞, are:

$$\begin{aligned} &\lim_{r\to\infty} C_O(r,t) = C_O^\infty \\ &C_O(r,0) = C_O^\infty (r > r_O) \\ &C_O(r_O,t) = 0 (t > 0) \end{aligned} \tag{1.7}$$

where r_O is the radius of the sphere, and r is the distance from the center of the electrode. The faradaic current density evaluated for this process, is a function of the concentration gradient at the electrode surface. From Fick's 1st law:

$$\frac{j}{nF} = -D_O\left[\frac{\partial C_O(r_O,t)}{\partial r}\right] \tag{1.8}$$

Applying Fick's 2nd law to the process of spherical diffusion gives:

$$\frac{\partial C_O(r,t)}{dt} = D_O\left[\frac{\partial^2 C_O(r,t)}{dr^2} + \frac{(2/r)\partial C_O(r,t)}{dr}\right] \tag{1.9}$$

Solving equation (1.8) and (1.9) with the appropriate boundary conditions gives the following relationship for the current-time profile:

$$j = \frac{nFD_OC_O^\infty}{(\pi t)^{1/2}} + \frac{nFD_OC_O^\infty}{r_O} \tag{1.10}$$

In contrast to the planar electrode, the current is given by the sum of two terms. From equation (1.10), it can be seen that when the radius of the electrode is small, the second term is large, and the behaviour of the electrode will be independent of time. At short times, the behaviour of the current will be equivalent to the behaviour on a planar electrode (dependent on $t^{1/2}$).

1.2.3. *Inlaid disk ultramicroelectrodes*

In this type of electrode the current-time response is due to a combination of both planar and radial diffusion. The process of diffusion is more complex than for an infinite planar or a spherical electrode. The disk is not a uniformly accessible electrode. The flux of material reacting at the surface is unequal across the electrode surface because the electrolysis that occurs at the outer circumference of the disk diminishes the flux of material to the central portion of the disk [20]. The

radial diffusion near the edge of an ultramicroelectrode has a considerable effect, which makes the mathematical treatment more complicated. The determination of the current-time behaviour of the disk electrode requires the solution of the following partial differential equation:

$$\frac{\partial C_O}{\partial t} = D_O \frac{\partial^2 C_O}{\partial r^2} + \frac{D_O}{r} \frac{\partial C_O}{\partial r} + D_O \frac{\partial^2 C_O}{\partial z^2} \qquad (1.11)$$

where z is the perpendicular distance from the electrode surface. Different solutions to this equation have been obtained, using simulation or numerical methods [23-28]. Aoki and Osteryoung have reviewed the development of the theory of microdisk electrodes and have provided a general solution for the i-E response for reversible reactions [23], Shoup and Szabo considered the influence on the i-t response of the insulation geometry of a microdisk and concluded that the infinite plane model is useful as long as the radius of the insulation is at least twice that of the electrode [24]. An algorithmic method was described by them for obtaining results for the chronoamperometric response at a finite microdisk electrode [25]. Aoki et al. presented a mathematical description of i-E curves at stationary finite microdisk electrodes for quasi-reversible and irreversible reactions, and the results were compared with those predicted for hemispherical electrodes [26]. Solutions to the problem of steady-state transport to an inlaid disc electrode subject to control by diffusion, thermodynamics, or kinetics, or any combination of these three constraints, were also presented by Bond and Oldham [27]. Zoski, Bond, Oldham and co-workers also developed new analysis methods for linear-steady state voltammograms [28]. Often, however, it is assumed that inlaid disc ultramicroelectrodes behave electrochemically in a similar way to the more theoretically tractable microhemispherical electrodes [29]. Although, there is a similarity between, the steady state current obtained for a spherical electrode of radius $2r_O/\pi$, and the steady state current obtained for a disc ultramicroelectrode of radius r_O, it is necessary to keep in mind that the current density over the sphere is

uniform while on the disc ultramicroelectrode, the current density decreases from the edge to the centre of the ultramicroelectrode [30].

At long times, the current density at a microdisc electrode reaches a steady state, which is given by:

$$j = \frac{4nFDC_O^{\infty}}{\pi r_O} \qquad (1.12)$$

where r_O is the radius of the disc ultramicroelectrode. From this equation it is seen that the steady state current density is inversely proportional to the radius of the disc ultramicroelectrode. The larger the ultramicroelectrode, the longer it takes to reach a steady state. Since a high rate of steady state diffusion is obtained when ultramicroelectrodes are used, because of the radial diffusion operating near to the edge of the microsurface, the cyclic voltammetric curves at ultramicroelectrodes are different from those obtained at a macroelectrode. At low scan rates, a sigmoidally shaped curve is found, because radial diffusion to the surface is the dominant diffusion process. However at fast scan rates, a peak shaped voltammogram is obtained. This behaviour is attributed to linear diffusion control on this time scale. The use of ultramicroelectrodes, under conditions of steady state diffusion, offers an exciting opportunity for the accurate measurement of the kinetics of fast electrode reactions.

1.3. *iR drop*

When very small electrodes are used, little iR distortion of the data is observed. This permits experiments in extreme conditions (e.g. at high potential scan rates or using poorly conducting media). When conventional size electrodes are employed, it is necessary to use a three electrode cell arrangement **(figure 1.2)**. In this arrangement, the current is passed between the working electrode and a counter electrode, and the working electrode potential is measured using a reference electrode at zero current. However, taking this arrangement of three

electrodes, not all the iR drop is removed completely. This is due to a fraction of the total iR remaining between the reference electrode and the working electrode. This fraction is called iR_u, where R_u is the uncompensated solution resistance **(figure 1.3)**.

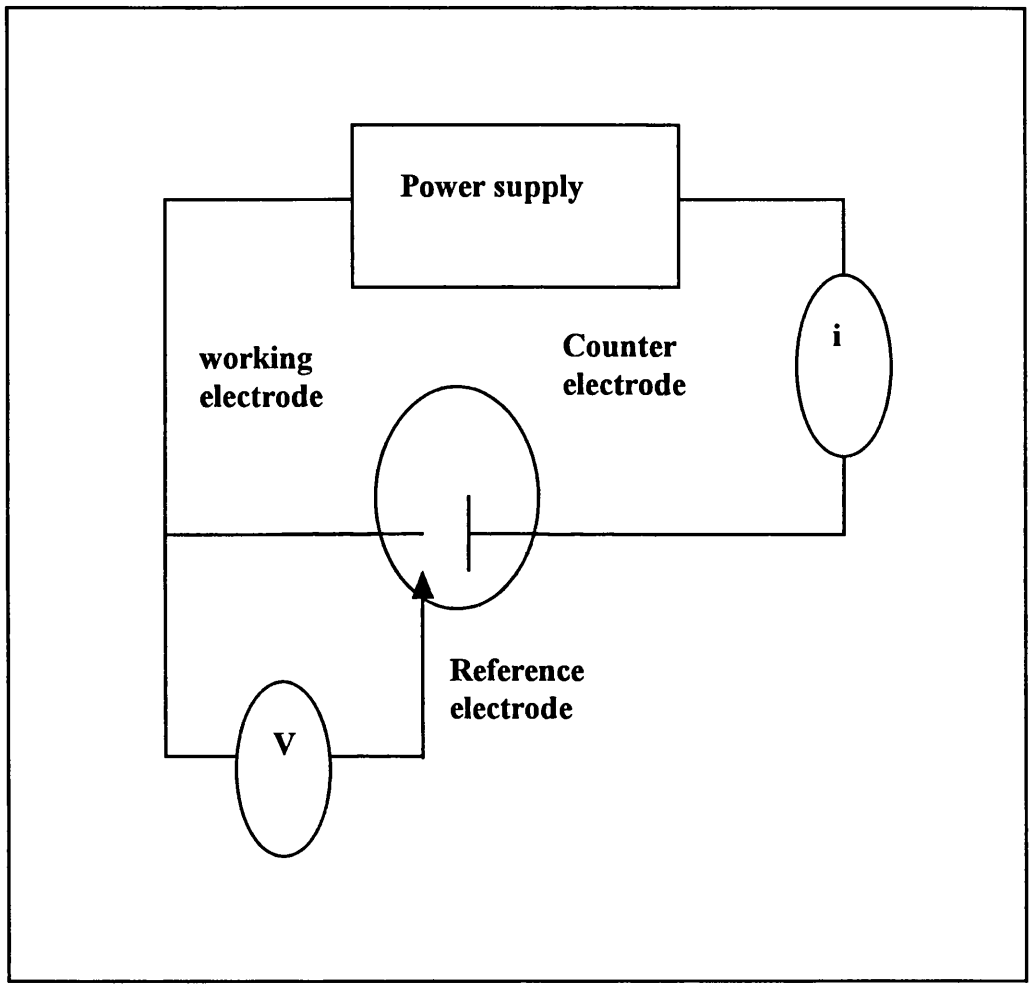

Figure 1.2. Diagram of a three electrode cell arrangement

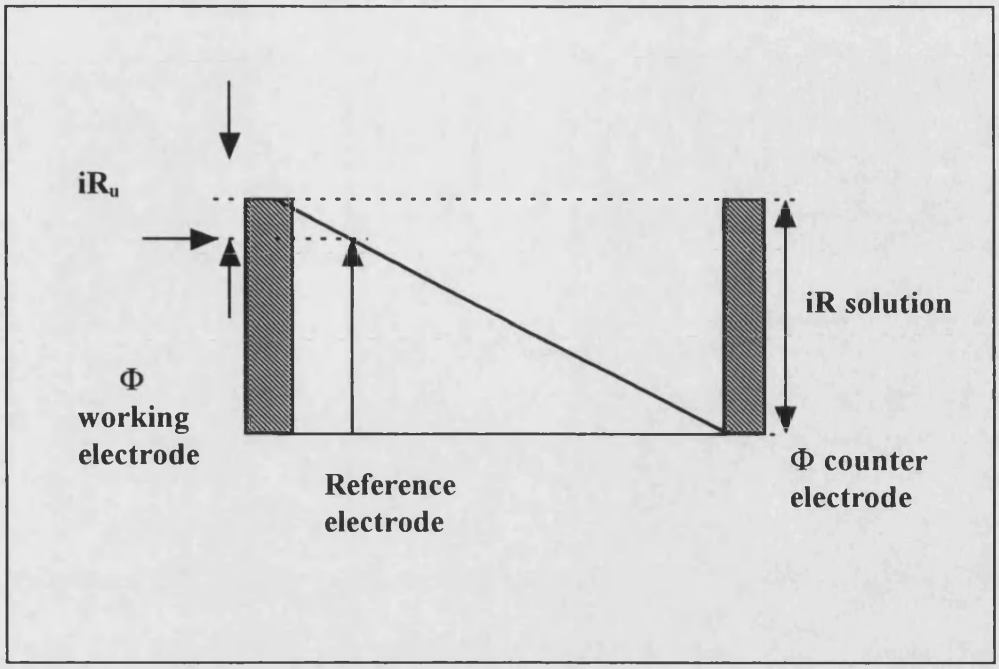

Figure 1.3. Potential drop between working an counter electrodes in solution and iR_u measured at reference electrode

A capillary tip reference electrode placed very close to the working electrode, is often used to decrease this uncompensated solution resistance. For a planar electrode with uniform current density across its surface, R_u is determined by the following equation:

$$R_U = \frac{x}{\kappa A} \qquad (1.13)$$

where x is the distance of the capillary tip from the working electrode, A is the electrode area, and κ is the solution conductivity.

On the other hand, when a ultramicroelectrode is used, a two electrode cell arrangement is often adequate **(figure 1.4)**. In this system the working ultramicro-electrode can be considered as a microhemisphere of radius r_0 and the reference electrode as a larger sphere at distance d **(figure 1.5)**.

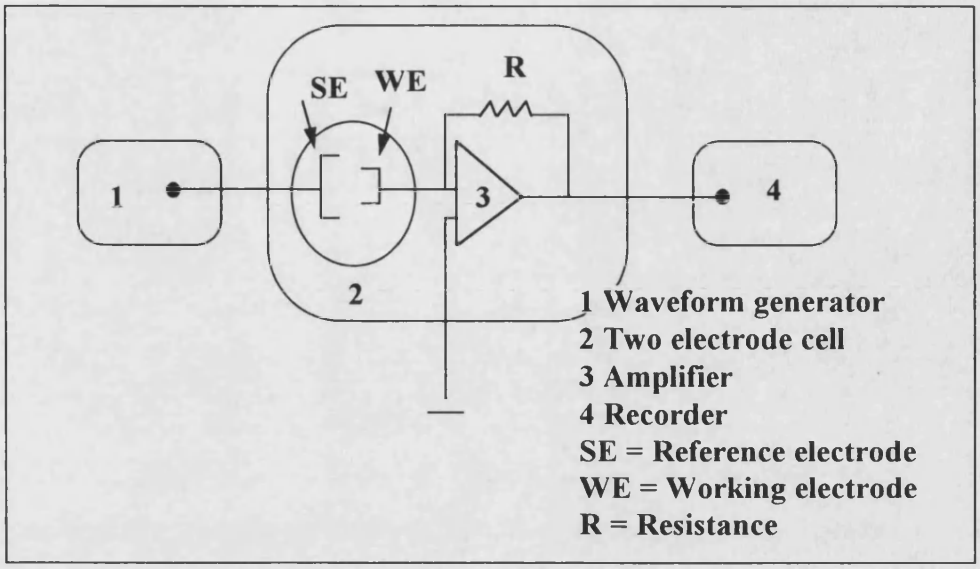

Figure 1.4. Diagram of a two electrode cell arrangement

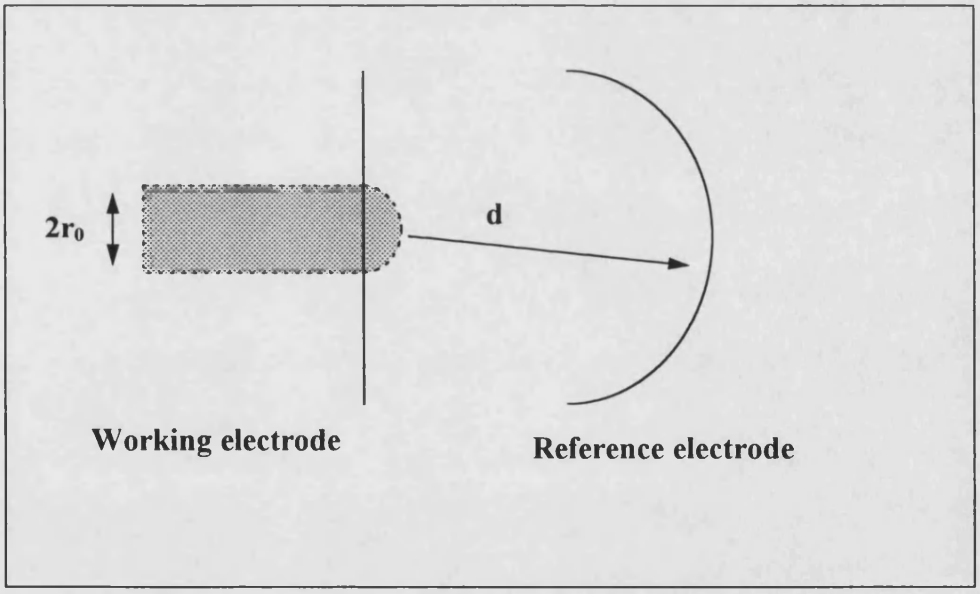

Figure 1.5. Two electrode cell consisting of a hemispherical ultra-micro electrode of area $2\pi r_O^2$, where the distance between WE and RE is d, with $d \gg r_O$

The effective resistance or uncompensated resistance under these conditions is calculated by integrating the series resistances of an infinite number of

infinitesimally thick shells; the resistance of a typical shell at a distance *d* from the coordinate origin being $dr/2\pi r^2\kappa$. Hence:

$$R = \int_{r_O}^{d} \frac{dr}{2\pi r^2 \kappa} = \frac{1}{2\pi\kappa}\left(\frac{1}{r_O} - \frac{1}{d}\right) \tag{1.14}$$

For $d \gg r_O$, $R \Rightarrow \frac{1}{2\pi\kappa r_O}$ (1.15)

At short times, the current at a microdisc is proportional to the electrode area,and is given by:

$$i_d = \frac{nFD^{1/2}C^{\infty}A}{\pi^{1/2}t^{1/2}} \tag{1.16}$$

The iR drop can be estimated, by combining equations (1.15) and (1.16), taking into account that the area of a microdisc is equal to πr^2. Hence:

$$iR \approx \frac{nFD^{1/2}C^{\infty}r_o}{2\pi^{1/2}t^{1/2}\kappa} \tag{1.17}$$

This equation shows that in a microdisc, under these circumstances, where non-steady state conditions apply, the iR drop decreases as the radius of the ultramicroelectrode decreases.

In steady state conditions, the limiting current for a disc ultramicroelectrode will be proportional to the radius r_O, according the following equation:

$$i_{ss} = 4nFD_OC^{\infty}r_O \tag{1.18}$$

Under these conditions the iR drop will be independent of the dimensions of the ultramicroelectrode, according to the following equation:

$$iR \approx \frac{4nFD_O C^{\infty}}{2\pi\kappa} \qquad (1.19)$$

1.4. *RC constant*

The use of ultramicroelectrodes permits experiments at short times, where the charging current with conventional size electrodes would limit meaningful measurements of faradaic currents. For studying the kinetics of fast reactions, fast sweeps, short pulses, or high frequencies are needed. When conventional size electrodes are used, this would mean large capacitive currents which would make measurement of the faradaic current unreliable. However, when ultramicro-electrodes are used, this problem is minimised. For a potential step experiment, using ultramicroelectrodes, the behaviour of the charging current, i_{dl} with time, t, when a potential step of magnitude E is applied, will be given by the following relationship:

$$i = \frac{E}{R} e^{-\frac{t}{RC_{dl}}} \qquad (1.20)$$

where R is the electrochemical cell resistance and C_{dl} is the double layer capacitance. According to equation (1.15), R will be proportional to $1/r_O$, and the double layer capacitance will be proportional to the area (i.e. $C_{dl} \propto r_O^2$).

Since the product of RC_{dl} is the time constant of the cell, it is seen that this time will be proportional to r_O, and will decrease when the radius of the ultramicroelectrode is decreased. This means that the charging time of the double layer is also greatly reduced. This prediction of decreased charging current time is important, since this parameter determines the shortest time at which meaningful measurements of faradaic current can be made [31]. For example, for a 6 μm disc ultramicroelectrode, the double layer should be 99% charged within 5 μs, assuming a 100 $\mu F/cm^2$ double layer capacitance and a cell resistance of 10 kΩ. This behaviour combined with the small iR distortion should permit the use of very fast

transient techniques. Fast cyclic voltammetry experiments can be carried out using ultramicroelectrodes without distorting the electrochemical response of the system studied [32].

1.5. *Small size*

The small size of ultramicroelectrodes, makes them very suitable as sensors in biological systems. When they are used in *in vivo* biomedical research, they cause less damage to the surrounding tissues. Once the ultramicroelectrode is implanted in the brain, it is considered to be lying in a pool of extracellular fluid. This interpretation of the relationship between the ultramicroelectrode and the brain tissue relates to their relative sizes. Neuronal tissues have dimensions varying from nanometers in the case of synapses to micrometers for cell bodies. In comparison, the tip of the ultramicroelectrode can have a diameter varying from 8 μm (carbon fiber) to 1 μm (gold or platinum) [2,33]. It follows that a ultramicroelectrode can be used for detecting electroactive compounds dissolved within the extracellular fluid immediately surrounding it. However, small ultramicroelectrodes having dimensions in the nanometer range scale, could offer opportunities to explore phenomena that occur near the synapses.

At the same time, this property (small size) has allowed measurements to be performed under purely diffusive conditions, that is without any involvement of convection. The concentration of the electroactive species is only perturbed by electrolysis for very small distances from the ultramicroelectrode surface (approximately six times the radius under totally steady state conditions) [31]. For this reason the diffusion layer in these devices is very thin compared to the typical thicknesses of hydrodynamic boundary layers so the behaviour of ultramicro-electrodes is independent of the motion of the bulk liquid phase.

Due to the small size of ultramicroelectrodes, electrochemical nucleation and growth studies can be carried out more easily. When large electrodes are used, the process of electrocrystallisation is often controlled by progressive nucleation and growth, and overlap of the centres for growth or overlap of the diffusion zones, make the study more complicated. However, when ultramicroelectrodes are

employed, the birth and growth of individual centres can be observed, which makes the study of the nucleation and growth rates easier [17,18]. The formation of single centres on ultramicroelectrodes, which can act as sub-microscopic electrodes, offers the possibility of determining the exchange current for a well defined redox system, using a simple steady state procedure [18].

Interesting applications regarding to the physically small size of the ultramicroelectrodes have also been developed in scanning electrochemical microscopy (SECM) [34].

1.6. *Applications of ultramicroelectrodes*

Because of the properties described in the last section, the applications of ultramicroelectrodes have increased considerably in the last fifteen years in many areas of research. They have had an impact on applied electrochemistry, because of their high immunity to ohmic drop phenomena, even under conditions where no significant faradaic information may be found using classical electrodes, and because steady state behaviour is obtained more easily, which permits measurements under purely diffusive conditions with no interference from convection phenomena. The applications of ultramicroelectrodes will be considered in more detail in the following section, taking into account some important areas of electrochemistry, such as electroanalysis, electrosynthesis, electrochemical kinetics, electro-crystallisation and bioelectrochemistry.

1.6.1. *Applications in electroanalysis*

When ultramicroelectrodes are used, mass transfer to the microsurface is enhanced. This permits the rapid determination of trace heavy metals by anodic stripping voltammetry [35]. The process of preconcentration is achieved quickly, without the need for forced convection. Experimental and theoretical advances in anodic stripping voltammetry (ASV) continue to be reported. Mercury ultramicroelectrodes have been used for the determination of heavy metals in wines rain water, and sea water [36].

With the use of these small area devices, the analysis can be carried out at natural pH and without added supporting electrolyte [35,36]. Recently a sensor array consisting of thin-film noble metal ultramicroelectrodes has been developed for simultaneous stripping analysis of trace metals [37], and square wave anodic stripping voltammetry has been used for lead and cadmiun speciation studies in river waters [38].

In recent years, interest in using ultramicroelectrodes in the analysis and control of food has appeared. Food analysis generally requires a specialist laboratory. Ultramicroelectrodes provide an easier solution because they can be used with minimum sample preparation. The use of gold microband and gold microdisk electrodes for the electroanalysis of ascorbic acid (vitamin C) in foodstuffs has been reported [39,40]. Cylindrical carbon fiber ultramicroelectrodes (8 μm in diameter) have been used for determining the phenolic antioxidants in samples of dehydrated potato flakes [41].

On the other hand, the freedom from convection effects makes the ultramicroelectrodes suitable for use in flowing streams (e.g. high performance liquid chromatography and flow injection analysis) [42,43]. Amperometric detection in flowing streams has proved to be a viable technique for many analytical problems demanding high sensitivity and selectivity. The separation and electrochemical detection of ferrocene derivatives with ultramicroelectrodes in a capillary-flow system has been reported [43], and enzyme ultramicroelectrodes for the analysis of neurotransmitters like choline and acetylcholine have been used in microflow injection and micro liquid chromatographic analyses [44].

Ultramicroelectrodes have also extended the boundaries of electrochemistry from the solution phase to the gas phase, as detectors in gas chromatography [45], and even for monitoring solid phase reactions [46].

Recently the electrochemical behaviour of a single molecule has been observed by trapping a small volume of a dilute solution of the electroactive species between a nanoultramicroelectrode tip with a diameter of ~15 nanometers and a conductive substrate [47].

1.6.2. *Applications in electrosynthesis and electrochemical kinetics*

Although high concentrations of supporting electrolyte are normally used in order to lower the solution resistance and to suppress the migration current whenever charged species are under study, it is known that the high ionic strength of the system can alter the voltammetric and thermodynamic properties. The mechanism and kinetics of the system can change in low ionic strength media [48]. Studies in the absence of supporting electrolyte are difficult to carry out with electrochemical techniques using large electrodes, due to the effects of ohmic drop and the migration produced. The iR drop is especially minimised when ultramicroelectrodes are used in voltammetry. It is independent of the size and shape of the ultramicroelectrode under diffusion limited by steady state conditions, according to equation (1.19). This has allowed these devices to be used in solutions containing low concentrations of supporting electrolyte [15,31], in the absence of supporting electrolyte [49,50], in highly resistive organic solvent [51] and in supercritical fluid conditions [52].

Electrochemical studies at high potentials where the supporting electrolyte would be decomposed, can be carried out when ultramicroelectrodes are employed without supporting electrolyte [53]. Inert species such as N_2, and Ar have been oxidised in aprotic solvents in the absence of added electrolyte [54,55].

Ultramicroelectrodes also permit voltammetric measurements on a much more rapid time scale than with electrodes of conventional size [15]. They have been found advantageous in high speed applications because the cell time constant and the ohmic drop are both much smaller than with large electrodes [56]. Rates and mechanisms of very fast chemical reactions accompanying the heterogeneous electron transfer can be elucidated. They have been found of crucial importance in measuring the kinetics of radical anion isomerizations [57]. Several investigators, have published work on non-steady state and ac behaviour at ultramicroelectrodes [6,58].

Similar advantages are found in the study of heterogeneous electron transfer under steady state conditions. Numerical expressions for the kinetic parameters for reversible, irreversible and quasi-reversible reactions have been

developed [59, 26-28]. In the steady state there is no charging current, and no characteristic time either. For studying the kinetics of fast electrode reactions under these conditions, it is necessary for the method of investigation to operate on a time scale comparable to the 'kinetic time scale', $D/(k^0)^2$ of the reaction, where D is the diffusion coefficient ($cm^2\ s^{-1}$), and k^0 is the standard rate constant, which is the rate constant at $E=E^{0'}$, where $E^{0'}$ is the formal potential, dependent on the medium since it includes the logarithmic activity coefficient terms (γ_i) as well as the standard electrode potential (E^0), according to the following relationship:

$$E^{0'} = E^0 - \frac{RT}{nF}\sum \nu_i \ln \gamma_i \qquad (1.21)$$

When ultramicroelectrodes are used, the 'kinetic time scale' can be considered as a 'kinetic distance scale', D/k^0, which is small for fast reactions (e.g about 10^{-6} m for $k^0= 10^{-3}$ $m.s^{-1}$ and typical diffusivities) [60]. Under these conditions, kinetic parameters like α, k^0 and the thermodynamic parameter $E^{0'}$ may be determined more accurately. On the other hand, the reduced iR drop permits the study of the kinetics and mechanisms of systems where the electroactive species are present in high concentrations. Such situations occur with real systems in industry, both in electrosynthetic reactions and electroplating baths [61,62]. For higher concentrations, the measured current and the ohmic drop are too large for electrodes of conventional size. Uncharged species can be present in excess of 1 mol dm^{-3} concentration, or if liquid as 100% pure solvent. Ciszkowska and Stojeck [63], demonstrated that methanol, ethanol and propanol as pure solvents give well defined waves at platinum microdisc electrodes with radii in the range 5-12.5 μm. However it is necessary to point out that some supporting electrolyte is required to prevent too much iR distortion. Studies at low temperatures (below -180°C) in combination with ultramicroelectrodes provide an excellent technique for cryogenic electrochemical experiments [64]. Application of low temperature voltammetry with microelectrodes has been described in the area of electrode kinetics [65], and reviewed with respect to the elucidation of electrode mechanisms [66].

Ultramicroelectrodes have also been utilized to study ultrafast reactions at conducting polymer like polyaniline at low temperatures [67].

1.6.3. *Applications in electrocrystallisation studies*

It is known that the electrocrystallisation process under kinetic control conditions is influenced by a number of factors, one of them being the overlap of growth centres when a large electrode is used. The application of electrodes with small areas (micro or ultramicroelectrodes) can restrict growth to one or a few centres on the timescale of the experiment. Several studies of electrocrystallisation on ultramicroelectrodes have been reported [4,18,19,68]. When these devices are used, the analysis of experimental data is simplified greatly if the overlap problem is eliminated. However, there are problems with edge effects that need to be considered. The characterisation of the size and shape of the centre or centres formed is generally carried out using scanning electron microscopy. These studies of electrocrystallisation on ultramicroelectrodes can be carried out straight-forwardly with the application of a single potential step. The reduced value of the double layer capacity does not affect the process of electrocrystallisation and the decrease in the frequency of nucleation ensures that the charging of the double layer occurs before the onset of nucleation and growth. Formation of small single centres on ultramicroelectrodes has also permitted another application of these devices, i.e. determination of the exchange current for redox couples using these small deposited centres as ultramicroelectrodes [19]. Li et al. [68] have carried out studies with carbon, platinum and lead ultramicroelectrodes, related to electro-crystallization reactions relevant to lead-acid battery electrochemistry. They have found that a combination of kinetic and electron microscopy measurements at ultramicroelectrodes permit information of the reaction mechanisms that cannot be derived from observations at electrodes of conventional size. At the moment, there is interest in understanding the influence of the particle size of a catalyst on its catalytic properties. By permitting the generation of one or a few catalytic centres,

ultramicroelectrodes could allow a study of the effect of size on the oxidation or reduction of molecules of importance in the field of fuel cell research.

1.6.4. *Applications in Bioelectrochemistry*

The applications of ultramicroelectrodes in this field have increased considerably in recent years. The area of electron transfer reactions involving proteins and mediators continues to dominate the bioelectrochemistry review literature [69-72]. The use of ferrocene and ferrocene derivatives as mediators for direct and indirect electron transfer represents a new generation of biosensors [69]. Immobilisation of glucose oxidase at a nanometer sized ultramicroband gold electrode has been used for detecting glucose without a mediator in solution [70]. Deposition of enzymes using electrochemically aided adsorption with glutaral-dehyde has permitted spatially well ordered protein layers to be formed on ultramicroelectrodes [71].

Platinized carbon ultramicroelectrodes have also been constructed as glucose biosensors [72]. Copper microwires coated with a thin film of borosilicate glass have been used for studying the electrochemical behaviour of glycine which represents an example of a biologically important molecule [73]. Investigation of adsorption and kinetics at the molecular level has been carried out [1] using small microelectrodes (radii <10μm). The adsorption of individual molecules like DNA has been studied [1].

Various approaches to the production of miniaturised chemical sensors for *in vivo* applications in neurochemical investigations of dynamic events have been carried out [2,3,32,74]. The cathecolamines, dopamine (DA) and noradrenaline (NA), and their metabolites are essential participants in the neurotransmission process [75]. Accordingly, they are frequently implicated in neurological diseases of the brain [76]. Advances in the treatment of such diseases have resulted from the study of these amines and their metabolites in the central nervous system. The potential applicability of voltammetric techniques together with the use of microelectrodes has permitted analytical and mechanistic characterisation of these compounds in the brain [11]. However, the specificity of the response of these

microelectrodes is affected by the presense of other compounds which have similar oxidation potentials. This is an important consideration and markedly affects the interpretation of *in vivo* electrochemical signals. Carbon fiber microelectrodes coated with Nafion®, a cation exchange polymer, have been found more selective to some neurotransmitters [77]. The polymer can exclude anions from the microelectrode surface and thus impair their detection. DA and NA are cations at physiological pH, and the metabolites and the important brain substance ascorbic acid are anions or neutral at pH 7.4. Although Nafion® provides increased selectivity, it may distort the temporal response of the sensor. Diffusion coefficients of the cations in the polymer tend to be greatly reduced compared with solution values. Modification of microelectrodes with functional composite monolayers, where these monolayers can act as nanoporous molecular recognition membranes, could be the way to prepare selective microelectrodes for certain neurotransmitters without problems of the distortion of the temporal response of these devices as sensors. The framework component of these composites could prevent probe-molecule penetration through the monolayer membrane, and the template component could induce defect sites within the inert framework which can be used for the probe-molecule penetration.

1.7. *Disadvantages of microelectrodes*

Apart from the more complex mathematical analysis required for describing the radial diffusion behaviour present when microelectrodes are used, other factors have meant that these devices have not had a wider impact on electrochemical research. However, some of them have been overcome in recent years. In the following section these factors will be mentioned, and the way some of them have been overcome will also be described.

1.7.1. *Instrumentation required to measure low currents*

In general, the small surface area of these devices means that low currents must be measured and recorded. When techniques such as high frequency *a.c.* impedance are applied using microelectrodes, small currents (typically 10^{-12} to

10^{-9} A) need to be measured on a short time scale, which requires relatively sophisticated and costly instrumentation. With very small electrodes, extremely low currents have to be measured, imposing serious constraints on the instrumentation needed. However, under some experimental conditions, where the shape and dimensions of the support which is used for holding the microelectrode do not play an important role in the measurements (as would be the case *in vivo* measurements inside living brain tissue), the current response can be increased by using ensembles of microelectrodes (arrays of band, circular or irregularly shaped microelectrodes, assembled in a number of possible ordered or disordered patterns) [1]. The advantages summarised at the outset for microelectrodes can be retained for an array of identical microelectrodes with the added advantage of a higher level of total current response. For N identical microelectrodes in a uniformly dispersed array, the total current signal will be N times the value at a single microelectrode, provided depletion zones for neighbouring electrodes do not intersect.

1.7.2. *Characterisation and fragility*

The surface state of an ultramicroelectrode is difficult to control, and when a submicron-sized ultramicroelectrode is used, its geometry may differ significantly from that of an ideal inlaid disk, ring or hemisphere, which makes characterisation of size, shape, and configuration more difficult [78]. At the same time, microelectrodes are difficult to obtain with high quality. Microelectrodes are usually constructed by sealing metal or carbon in an insulating matrix such as glass or polymers. If the seal between the conductor and matrix is not good, the electrolyte solution may enter the gap and increase the apparent capacitance of the microelectrode. This may of course happen with macroelectrodes as well, but the effect is more noticeable in microelectrodes because of their larger edge-area ratio. The gap between the conductor and insulating matrix, with its resulting impedance, is a critical characteristic of these small devices for a variety of applications. The charging current can be the major component of the background current making the interpretation of the results difficult. Furthermore, stray capacitance generated by the contact between the microelectrode and the instrument becomes important

when the electrode area becomes very small. Thus, stray capacitance, rather than electrochemical capacitance (or electrochemical noise), ultimately limits the precision of the measurement. The fragile nature of such small devices means that they have a short working life before electrical contact is weakened or broken. However this problem can be overcome using ensembles of microelectrodes as was described above.

1.7.3. *Poisoning of the microsurface*

From the applications summarised in this chapter, it is apparent that ultramicroelectrodes may be used for rapid anodic stripping voltammetry because of the high steady state flux given by radial diffusion to the edges of the microelectrode. However, this high steady state flux is also a disadvantage when impurities are present in the solution being studied. Minor impurity effects, surface fouling, or inadequate polishing are also serious problems with these small devices. The problems can be minimised by using microelectrodes which are very well sealed to avoid the collection of impurities in the cracks. An ultrasonic bath can be used to remove polishing debris from the surface.

The difficulty of maintaining clean electrode microsurfaces in the presence of surfactants or adsorbing materials is a problem that becomes more severe as the electrode size decreases. It follows that the biggest drawback in analytical studies with microelectrodes is the surface fouling that occurs with real industrial or enviromental samples. However, the advantages described in this chapter, together with the ability of microelectrodes to be used in so many electrochemical media where the use of conventional macroelectrodes is a problem, has led to their increasing use in the last ten years.

1.7.4. *Changes in the physicochemical characteristics.*

When ultramicroelectrodes with at least one of their dimensions approaching the molecular level are used, several physical features modify their physicochemical characteristics. For example, the thickness of the double layer may be comparable to or larger than the electrode dimensions. Under these conditions,

the capacitance of these devices will vary with their radius rather than their surface area [79]. At the same time, the dimensions of diffusion layers may be close to those of double layers. For all these reasons, new theories will be required to describe processes in which diffusion and migration are taking place within the double layer [80].

References (Chapter 1)

1. M.I. Montenegro, M.A. Queiros, J.L. Daschbach (eds.), "*Microelectrodes: Theory and applications*", Proceedings of NATO ASI (1990) Kluwer, Dordrecht
2. P.W. Davies, F.Brink, Jr.Ru.Sci.Instum., **13**, (1942), 524
3. F.Gonon, M. Buda, R. Cespuglio, M. Jonvet, J.F. Pujol, Nature (London), **286**, (1980), 902
4. P. Bindra, M. Fleischmann, J.W. Oldfield, D. Singleton, Faraday Disc. Chem. Soc., **56**, (1973), 180
5. S. Pons, M. Fleischmann, Anal. Chem., **59**, (1987), 1391A
6. S. Pons, M. Fleischmann, J. Electroanal. Chem. Interfacial Electrochem., **250**, (1988), 257
7. J.M. Davis, F.R.F. Fan, A.J. Bard, J. Electroanal. Chem. Interfacial. Electrochem, **239**, (1987), 9
8. R.M. Penner, M.J. Heben, N.S. Lewis, Anal. Chem., **61**, (1989), 1630
9. M.J. Heben, R.M. Penner, N.S. Lewis, M.M. Dovek, C.F. Quate, Appl. Phis. Lett., **54**, (1989), 1421
10. J.S. Jaworski, Polish Journal of Chemistry, **68**, (1994), 1917
11. R.M. Wightman, L.J. May, A.C. Michael, Anal. Chem., **60**, (1988), 769A
12. M.V. Mirkin, F.R.F Fan, A.J. Bard, J. Electroanal. Chem., **328**, (1992), 47
13. M. Fleischmann, F. Laserre, J. Robinson, D. Swan, J. Electroanal. Chem., **177**, (1984), 97
14. J.E. Baur, E.W. Kristensen, L.J. May, D.J. Wideman, R.M. Wightman, Anal. Chem., **60**, (1988), 1268
15. J.O. Howell, R.M. Wightman, Anal. Chem., **56**, (1984), 524
16. A.M. Bond, M. Fleischmann, J. Robinson, J. Electroanal. Chem., **172**, (1984), 11
17. K.B. Oldham, J. Electroanal. Chem., **250**, (1988), 1
18. G. Gunawardena, G. Hills, B. Sharifker, J. Electroanal. Chem., **130**, (1981), 99

19. G. Hills, A.K. Pour, B. Scharifker, Electrochim. Acta, **28**, (1983), 891
20. R.M. Wightman, D.O. Wipf, Electroanal. Chem., **15**, (1989), 267
21. S. Pons, M. Fleischmann, Anal. Chem., **59**, (1987), 1391 A
22. F.G. Cottrell, Z. Physik. Chem., **42**, (1902), 385
23. K. Aoki, J. Osteryoung, J. Electroanal. Chem., **160**, (1984), 335
24. D. Shoup, A. Szabo, J. Electroanal. Chem., **160**, (1984), 27
25. D. Shoup, A. Szabo, J. Electroanal. Chem., **199**, (1986), 437
26. K. Aoki, K. Tokuda, H. Matsuda, J. Electroanal. Chem., **235**, (1987), 87
27. A.M. Bond, K.B. Oldham, C.G. Zoski, J. Electroanal. Chem., **245**, (1988), 71
28. C.G. Zoski, A.M. Bond, C.I. Colyer, J.C. Myland, K.B. Oldham, J. Electroanal. Chem., **263**, (1989), 1
29. K.B. Oldham, J. Electroanal. Chem., **122**, (1981), 1
30. J. Cassidy, J. Ghoroghchian, F. Sarfarazi, J.J. Smith, S. Pons, Electrochim. Acta, **31**, (1986), 629
31. R.M. Wightman, Anal. Chem., **53**, (1981), 1125A
32. C. Amatore, L. Lefron, J. Electroanal. Chem., 324, (1992), 33
33. A. Meulemans, B. Pounlain, G. Baux, L. Tauc, D. Henzel, Anal.Chem., **59**, (1986), 2088
34. A.J. Bard, G. Denuault, C. Lee, D. Mandler, D.O. Wipt, Acc. Chem. Res., **23** (1990), 357
35. K.R. Wehmeyer, R.M. Wightman, Anal. Chem., **57**, (1985), 1989.
36. S. Daniele, M.A. Baldo, P. Ugo, Mazzocchin, Anal. Chim. Acta, **219**, (1989), 9
37. A. Uhlig, M. Paeschke, M. Schnakenberg, R. Hintshe, H.J. Diederich, F. Scholz, Sensor and Actuators B- Chemical, **25**, (1995), 899
38. M.L. Tercier, N. Parthasarathy, J. Buffle, Electroanalysis, **7**, (1995), 55
39. D.H. Craston, C.P. Jones, N. Mun, D.E. Williams, Talanta, **38**, (1991),17
40. A.M. Farrington, N. Jagota, J.M. Slater, Analyst, **119**, (1994), 233
41. M.L. Agni, A.J. Reviejo, P. Yanezsedeno, J.M. Pinganon, Analytical Chemistry, **67**, (1995), 2195

42. O. Niwa, Electroanalysis, **7**, (1995), 606
43. F.M. Matysik, A. Meister, G. Werner, Analytica Chimica Acta, **305**, (1995), 114
44. K. Kano, K. Morikage, B. Uno, Y. Esaka, M. Goto, Analytical Chimica Acta, **299**, (1994), 69
45. J.T. Lu, C.H. Tian, J. Electroanal. Chemistry, **345**, (1993), 27
46. M. Watanabe, M.L. Longmire, R.W. Murray, J.Phys Chem., **94**, (1990), 2614
47. F.R.F. Fan, A.J. Bard, Science, **267**, (1995), 871
48. G.N. Kamau, J.F. Rusling, J. Electroanal. Chem., **292**, (1990), 187
49. C. Lee, F.C. Anson, J. Electroanal. Chem., **323**, (1992), 381
50. B. Cooper, A.M. Bond, K.B. Oldham, J. Electroanal. Chem., **331**, (1992), 877
51. S.M. Drew, R.M. Wightman, C.A. Amatore, J. Electroanal. Chem., **317**, (1991), 117
52. E.F. Sullenberger, S.F. Dresman, A.C. Michael, J. Phys. Chemistry, **98**, (1994), 5347
53. J. Cassidy, S.B. Khoo, S. Pons, M. Fleischmann, J. Am. Chem. Soc., **89**, (1985), 3933
54. T. Dibble, S. Bandyopadhyay, J. Ghoroghchian, J.J. Smith, F. Sarfarazi, M. Fleischmann, S. Pons, J. Phys. Chem., **90**, (1986), 5275
55. C. Jehoulet, A.J. Bard, Angew. Chem. Int. Ed., **30**, (1991), 836
56. D.O. Wipf, R.M. Wightman, Anal. Chem., **60**, (1988), 2460
57. W.J. Bowyer, E.E. Engelman, D.H. Evans, J. Electroanal. Chem., **262**, (1989), 67
58. L.M. Abrantes, M. Fleischmann, L.M. Peter, S. Pons, B.R. Scharifker, J. Electroanal. Chem. Interfacial Electrochem., **256**, (1988), 229
59. M. Fleischmann, S. Pons, J. Electroanal. Chem., **222**, (1987), 107.
60. B. Oldham, J.C. Myland, C.G. Zoski, A. M. Bond, J. Electroanal. Chem., **270**, (1989), 79

61. A. Malmstan, C. P. Smith, H.S. White, J. Electroanal. Chem., **215**, (1986), 223

62. P.E. Skinner, Platinum Metals Reviews, **33**, (1989), 2

63. M. Ciszkowka, Z. Stojek, J. Electroanal. Chem., **344**, (1993), 135.

64. J.J. MeDevitt, S. Ching, M. Sullivan, R.W. Murray, J. Am. Chem. Soc., **111**, (1989), 4528.

65. L. Safford, M.J. Weaver, J.Electroanal.Chem., **331**, (1992), 857

66. V.V. Strelets, Soviet Electrochem., **28**, (1992), 399

67. M. Vuki, M. Kalaji, L. Nyholm, L.M. Peter, J. Electroanal. Chem., **332**, (1992), 315

68. L. J. Li. M. Fleischmann, L. M. Peter, Electrochim. Acta, **34**, (1989), 475

69. J.E. Frew, H.A.O. Hill, Eur. J. Biochem., **172**, (1988), 261

70. C.X. Cai, H.X. Ju, H.Y. Chen, Acta Chimica Sunica, **53**, (1995), 281

71. D.J. Struke, N.F. Derooi, M. Koudelkahep, Biosensors & Bioelectronics, **10**, (1995), 61

72. E.R. Reynolds, A.M. Yacynych, Electroanalysis, **5**, (1993), 405

73. A.M. Bond, K.Z. Brainina, M. Koppenal, Electroanalysis, **6**, (1994), 275

74. R.M Wightman, L.J. May, A.C. Michael, Anal. Chem., **60**, (1988), 769A

75. D.M. Paton, Pharmacology, **21**, (1980), 85

76. S.H. Snyder, S.P. Barrarjee, H.I. Yamamura, D. Greenberg, Science, **184**, (1974), 1243

77. E.N. Navera, M. Suzuki, E. Tanuya, T. Takeuchi, I. Karube, Electro-analysis, **5**, (1993), 17

78. F.F. Fu- Ren, A. J. Bard., Science, **267**, (1995), 871.

79.- A.J. Bard, L.R. Faukner, Electrochemical methods, Wiley, New York,1980

80.- J.D. Norton, H.S. White, S.W. Feldberg, J. Phys. Chem., **94**, (1990), 6772

CHAPTER II

PREPARATION AND CHARACTERIZATION OF ULTRAMICROELECTRODES

CHAPTER 2

PREPARATION AND CHARACTERISATION OF MICROELECTRODES

2.1. *Preparation of ultramicroelectrodes*

2.1.1. *Introduction*

As was indicated in the first chapter, the use of ultramicroelectrodes in different areas of electrochemistry has dramatically increased over the past 20 years [1-5]. A major reason for this is the beneficial characteristics that result from the small physical dimensions of these devices. Most of them have been fabricated by insulating carbon fibers or metal wires with different kinds of materials [3,4]. Recently ultramicroelectrodes with diameters on the order of 1-5 μm [6], 0.1-1 μm [7], 5 nm [8], and 1 nm [9] have been fabricated. However, it is necessary to point out that for devices in the nanometer to Ånstrom range, characterization is difficult with respect to size, shape and configuration. Also, the technical difficulty in achieving the mandatory perfect seal between the material used as electrode and the insulating substrate increases as the electrode size decrease. Cracks or other imperfections in the seal may cause severe problems, particularly when solution leaks into the cracks. From a fundamental electrochemical point of view, the small dimensions of ultramicroelectrodes provide a considerable improvement in the quality of the electrochemical information (greater sensitivity of the measurement, enhanced mass transport, increased temporal resolution, and decreased influence of the solution resistance due to the small current).

A series of factors must be considered when an ultramicroelectrode is fabricated. Parameters like geometry, electrode material and insulating material, are the main factors that control the fabrication of these devices. A very good geometry is required to obtain a well defined diffusion field around the ultramicrosurface. The choice of the electrode material depends on its suitability

and selectivity for the required electrochemical reactions. Moreover the electrode material and the insulating material must be stable in the electrolyte media used.

One of the most popular shapes of these devices is the circular disc surrounded by an insulator material, which is coplanar with the electrode. The popularity of these inlaid disc electrodes arises from their ease of construction [2]. When these kinds of devices are used, it is often assumed that they behave electrochemically like the theoretically more tractable microhemispherical electrodes [10].

Different materials have been used as insulator material around carbon fibre and metal wires. The most common of these materials has been glass. This type of material has been successfully used due to its mechanical strength which protects fragile metal wires and because it permits polishing of ultramicroelectrode to reproducibly form a clean smooth ultramicrosurface. Moreover, glass materials are stable in most electrolytes, which is an advantage for maintaining a very clean ultramicrosurface. The seal between the electrode material and the glass is generally obtained by melting the glass around the electrode material. The method for doing this depends on the melting point of the electrode material.

Other insulator materials like epoxy resin are formed around the electrode material without need to use high temperatures for obtaining the seal. These type of insulating materials are much softer than glass materials. When the electrode material is harder than the epoxy resin, the epoxy material may be smeared over the ultramicrosurface during polishing, which can produce changes in the electrochemical response. Also, epoxy resins can contaminate the ultramicro-electrode surface because impurities can be leached out. Moreover, they can be unstable in some electrolytes, where they can dissolve causing contamination of the electrolyte, and deterioration of the seal.

With respect to the electrode materials used for preparing ultramicro-electrodes, platinum and carbon have been utilised more than gold and other metals like silver and nickel. The quality of the seals between the electrode materials and the insulating materials depend on the difference of thermal expansion coefficient between them, this difference must be small or zero, so that the electrode material

does not shrink away from the insulating material as the assembly cools. The formation of air bubbles around the interface, between the electrode material and the insulating material can affect the quality of the seal. For that reason, the process of sealing is generally carried out under vacuum when glass materials are used as insulators.

Information about the quality of the seal between the material used as microelectrode and the insulating material and the shape of the microdisk can be obtained by micrographs of the surfaces of the disc and the boundaries of the interface between the electrode material and the insulating substrate. Scanning electron microscopy (SEM) is particulary useful for mapping the morphology of the microelectrode surface. The quality of the seal may be also evaluated by capacitance measurements.

Ultramicroelectrodes are usually polished mechanically and sometimes etched in acid media. For obtaining successful mechanical polishing it is necessary to take into account the characteristics of the material used as electrode and the material used as insulator. Differences in the hardness of these materials can produce protuberances and recessions during the process of polishing with different grades of alumina. Electrochemical treatment of ultramicroelectrodes inmediately prior to the measurement is generally necessary. The simplest procedure is to polarise the electrode with a series of pulses into the potential ranges where the formation of oxide and the evolution of hydrogen occurs. However, it is necessary to point out that potential cycling can substantially increase the roughness of the ultramicrosurface.

Determination of the true surface area of the electrodes is essential in any electrochemical study, since electrochemical measurements such as electrode capacitance and current need to be normalized before meaningful comparison with theory can be made. Generally, an electrode that is macroscopically characterized by a smooth surface actually contains many steps and other microscopic irregularities. The real (physical) electrode surface is thus larger than the geometric surface and the ratio of the real and geometric surface areas is termed the roughness factor, $f_R=A_{real}/A_{geometric}$. In the present work, some *in situ* and *ex situ*

methods have been utilized for the characterization of microdiscs fabricated from carbon fibre, platinum and gold wires.

2.1.2. *Carbon ultramicroelectrodes*

A. Properties of carbon

When carbon is used there is a severe problem with the reproducibility of the physical properties of the material itself. Electrochemical reactions are normally slower at this substrate than at metallic electrodes, electron transfer kinetics being dependent on structure and surface preparation [11]. This material exists in various forms such as graphite, and glassy carbon, which can be superficially oxidized by chemical or electrochemical treatment. Graphite is the thermodynamically most stable form of elemental carbon below approximately 2600 ° K at 100 Mpa. This kind of carbon is anisotropic in electrical conductivity. Large single crystals of graphite are rare, and for this reason, it is utilized in polycrystalline form (solid block, paste electrodes, suspensions, etc). However, the so-called highly oriented pyrolytic graphite (HOPG), formed from ordinary pyrolytic graphite by heat treatment under simultaneous compressive stress (stress annealing) around 3500 °C, matches the properties of graphite single crystals. The faces parallel to the plane of carbon hexagons (100), called basal planes, present chemical and electrochemical properties significantly different from those of the perpendicular (edge) planes (110), which contain unsaturated carbon atoms that are highly active for reacting with oxygen, by chemical and electrochemical treatment. It is usually assumed that the surface functional groups generated during the activation process are phenolic, quinonic, carboxylic, carbonylic and epoxidic-like [12].

On the other hand, glassy carbon is the most popular carbon material for electrochemistry. This kind of carbon is prepared by pyrolysis of suitable polymers, e.g. polyfurylalcohol of phenolic resins. Glassy carbon has some amorphous characteristics. It is, in contrast to graphite, isotropic in electrical conductivity and physical-chemical properties. Its structure is characterized by randomly oriented strips (lamellae) of pseudo-graphitic layers of carbon hexagons. It has been found that on glassy carbon (GC), the electron transfer rates of several redox couples are

much higher than on HOPG. This has been attributed to either the lack of specific chemical sites on the basal plane or the low density of electronic states exhibited by low-defect HOPG [13].

The use of carbon fibres permits the construction of microelectrodes which are mechanically stable, with surfaces easily modified by chemical reaction. The choice of the right carbon fibre is an important first step in the fabrication of a carbon microdisc. The mechanical properties and chemical reactivity of these fibers depends very much on the type and orientation of the precursor material as well as the details of the heat treatment (e.g. duration, temperature range, temperature profile, extent of stretching during heat treatment). The mechanical and chemical properties may differ drastically from one carbon fibre to another. Carbon fibers of the highest possible stiffness are recommended as they are more grafitized and thus may yield better electrochemical results.

The following scheme shows the cross section of the highly orientated carbon fibers used for the preparation of these devises:

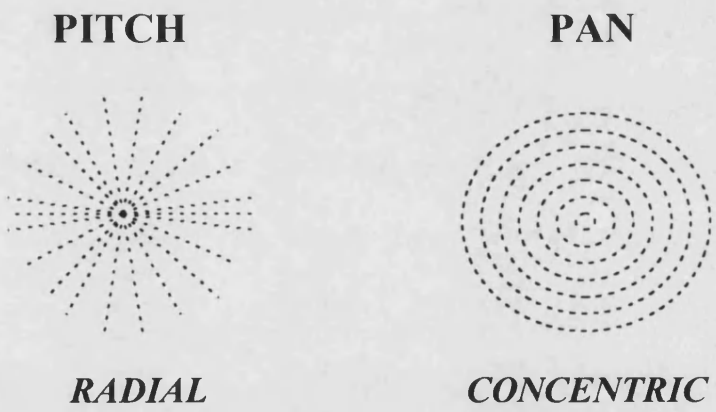

Figure 2.1. Typical schematic cross sections of highly oriented carbon fibres (after ref. [14])

Pitch fibres are characterized by a radial arrangement of the graphitic layers with high stiffness. This kind of fibre usually shows a star shaped cross section after electrochemical or chemical etching. The PAN fibres, formed by pyrolysis of polyacrylonitrile are characterized by a circular cross section and onion peel arrangement of the graphitic layers, with high tensile strength or high stiffness. The mechanical properties, morphological aspects and fabrication procedures for these fibres have been discussed elsewhere [14,15]. Different reaction products may be formed after anodic oxidation of carbon fibres with high stiffness in aqueous solutions [16]. Graphite intercalation compounds (GIC), may be formed according to the following reactions:

$$(C_n) + (1+x)HA \leftrightarrow (C_n)^+ A^- (HA)_x + H^+ + e^- \qquad (2.1)$$

$$(C_n) + (1+x)HA + yH_2O \leftrightarrow (C_n)^+ A^- (HA)_x (H_2O)_y + H^+ + e^- \qquad (2.2)$$

During the process of intercalation of graphite the interlayer spacing is increased, which produces some deterioration and loss of mechanical stability. However, this kind of fibre can still be handled easily.

Bulk graphite oxides (GO) are formed by hydrolysis of GICs according to the following reaction:

$$(C_n)^+ A^- (HA)_x + H_2O \leftrightarrow (C_n)OH + (1+x)HA \qquad (2.3)$$

For this kind of fibre, the interlayer spacings are highly dependent on the degree of solvation. They have been used as precursors for chemically modified electrodes [17].

Surface oxides (SO) differ from bulk graphite oxides not so much in their atomic composition as in their chemical and electrochemical properties. Like bulk oxides, surface oxides prepared by anodic oxidation are acidic. The functional

groups are situated at plane edges or at other defects in the graphite layers [18]. By contrast, in bulk oxides most of the oxygen is situated between the carbon layers.

B. Preparation of ultramicrodiscs from carbon fibre

Although, from a fundamental electrochemical point of view, the small dimensions of ultramicroelectrodes offers considerable improvements in the quality of electrochemical information, the quality of the results is highly dependent on the seal between the carbon fibre or metal wire with the insulator material. Under steady state conditions the radial diffusion at the edges of the ultramicrodisc can be affected by imperfection of the seal.

Also, the minimal ohmic loss and the low capacitance charging current are advantageous for fast scan voltammetric experiments with applications for heterogeneous and homogeneous kinetic measurements. However, imperfections in the seal can produce an increase in the apparent capacitance of the ultra-microelectrode, which can interfere with this kind of experiment. Different approaches have been used to obtain a good seal between the substrate and insulator. The most common method for sealing carbon ultramicrodiscs with diameters in the range of 10-20 μm is to encase the carbon fibre in a glass capillary, reduce the thickness of the glass support around the fibre with a capillary puller, and seal the tip with epoxy. Other methods include the electrochemical deposition of a thin insulating polymer coating [19] or heat sealing the carbon fibre in a polymer matrix [20]. Recently, the chemical vapor deposition of silica from a $SiCl_4$, H_2, and O_2 gas phase precursor system directly on a resistively heated fibre substrate [21], has been used, and a good quality seal between the carbon fibre and the silica film was obtained. In the present work, the carbon fibres were treated chemically in different acid media, before fabicating the seal with glass. It was found that when the carbon fibres were chemically treated in concentrated nitric acid for a period of 2-3 hours, the ultramicroelectrodes obtained after sealing with glass and after electrochemical treatment in acid media exhibited capacitances values less than 300 $\mu F/cm^2$. These capacitance values are high with respect to the values reported in the literature [22]. However, a porous and hydrated film has

been confirmed by ellipsometric by Kepley and Bard [23] after electrochemical treatment of glassy carbon (GC). Barbero et al. [24] have also reported that an electrochemical treatment in 1 mol dm^{-3} H_2SO_4, produce the formation of a multilayer porous film on GC. Considering that carbon fibre was treated chemically and electrochemically in acid media, the high value of capacitance obtained could be attributed to the formation of this kind of porous oxide film.

In the present work, PAN-based carbon fibres (radius 4 μm), were used for making ultramicrodiscs according to the following procedure:

1.- the carbon fibre was inserted into a soft glass tube, and then the tip was sealed with a flame.

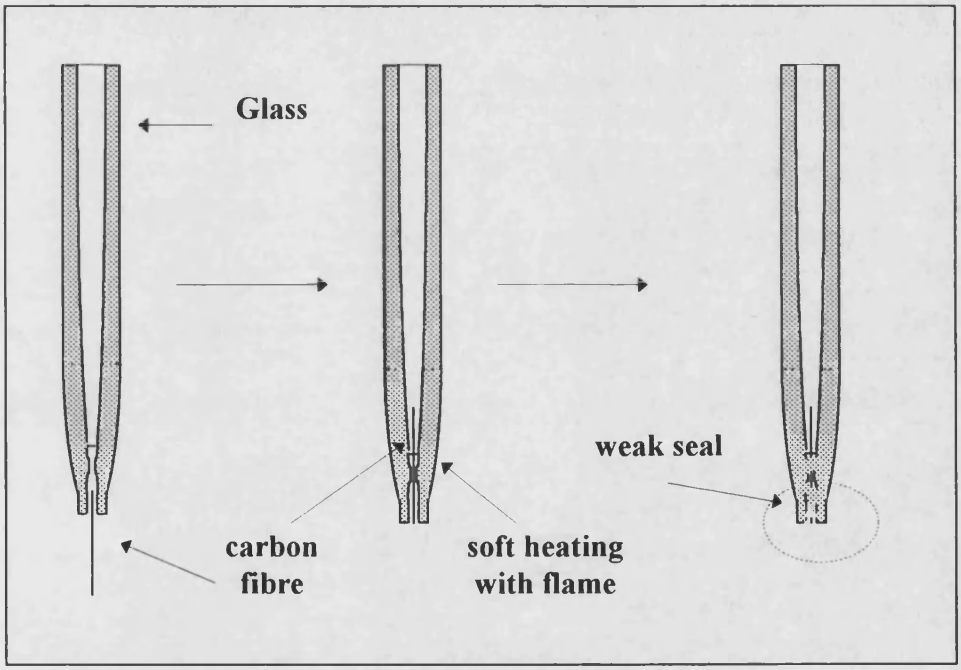

Figure 2.2

2.- A *v*acuum was applied to the capillary tube to remove the oxygen present and the tip was heated with a flame until the glass collapsed. It was necessary to take care that the fibre did not become completely covered by glass.

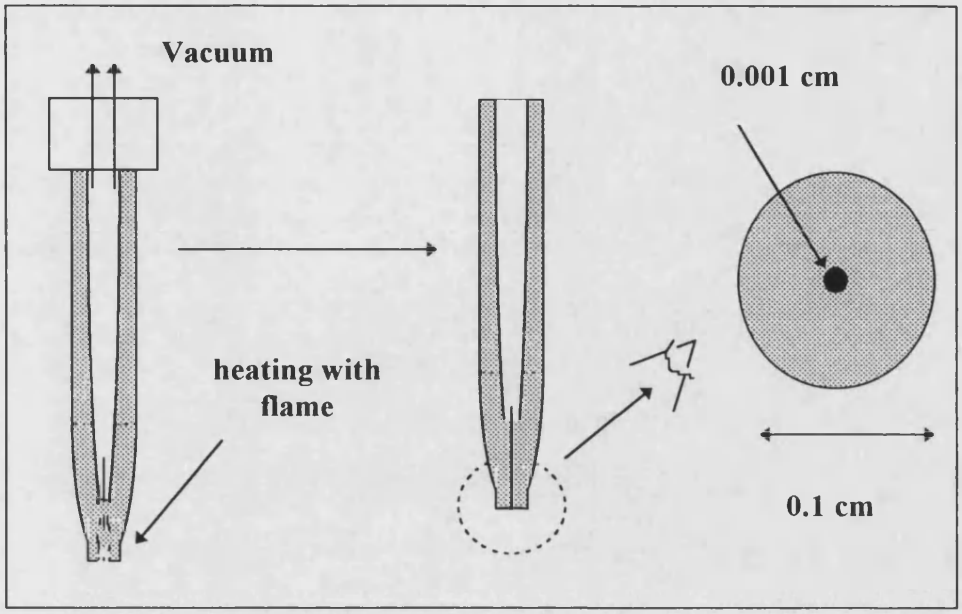

Figure 2.3

3.- The tip was cut to obtain an ultramicrodisc, and the ultramicroelectrode was filled with mercury. A nickel wire was inserted to make the electric contact and epoxy was used to fix the nickel wire in the glass. It was observed that using this procedure the electrical contact is sometime lost. It was found that this occurs due to the presence of air between the nickel and the mercury pool. To avoid this problem, vacuum was applied and the nickel wire was sealed in the glass by heating with a flame.

The electric contact was tested by carrying out a steady state measurement of the oxidation of $Fe(CN)_6^{4-}$. This method also permits the characterization of the apparent radius of the ultramicroelectrode.

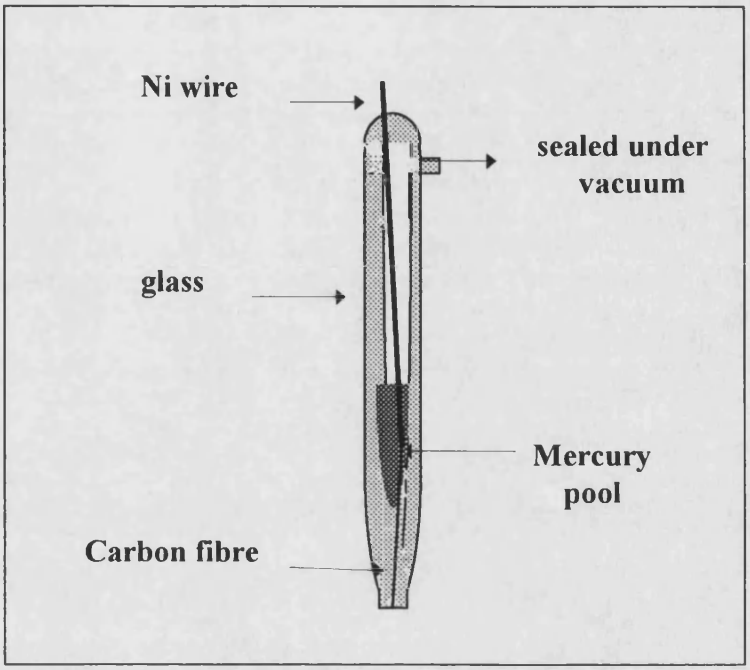

Figure 2.4

4.- The ultramicrodiscs were cleaned by polishing with fine grades of aluminium oxide sheet (Lapping Film, 3M; 30 and 3 μm) and with 0.3 μm alumina (Buehler), using ultrapure water as lubricant. After this cleaning procedure, they were rinsed and sonicated during few seconds in ultrapure water to remove alumina from the surface of the microelectrode. These ultramicroelectrodes were used for studying the electron transfer kinetic of ferrocene and some of its derivates, as well as for studying the oxygen reduction reaction.

2.1.3. *Platinum ultramicroelectrodes.*

Platinum has historically been the most important electrode material used. It is a d-band metal in the third row of the transition elements and is considered as a noble metal. It exhibits relatively high chemical inertness and electrocatalytic properties and it is extremely resistant to corrosion. Hot aqua regia (1/1 mix of nitric and hydrochloric acids) is one of the few aqueous solutions which can dissolve Pt due to the formation of a platinum complex. However, platinum is not completely inert electrochemically in aqueous solutions, where reactions involving oxygen and hydrogen may occur. In aqueous solution Pt is quickly covered, according to the polarization voltage, either with adsorbed hydrogen or a surface oxide, and only in a narrow potential range (from 0.4 to 0.8 V versus NHE), the so-called double layer region, may the Pt surface be considered almost free from adsorbed or chemisorbed species. In practice, it has been found that anions and organic impurities may be adsorbed even in this potential region. However, a potential window is obtained where there is a comparatively small steady-state faradaic current. This potential window is the interval from about 0 to1.6V versus NHE in acidic aqueous electrolytes. In the present work, the platinum microelectrodes used were fabricated at the University of Southampton. These ultramicroelectrodes were utilised for studing the oxygen reduction reaction.

2.1.4. *Gold disk ultramicroelectrode.*

Similar to Pt, gold is considered a noble metal, and it has been widely used for preparation of electrodes. In aqueous electrolyte, Au is covered with an oxide film over a large potential range. Hydrogen adsorption-desorption peaks are absent on the cyclic voltammograms of a gold electrode in aqueous solutions, and the electrocatalytic activity for many charge transfer reactions is lower than on platinum. It is the last of the sp metals in the periodic classification of the elements, close to the d-metals. The properties of this metal are between those of sp and d metals. Interaction of organic molecules with Au is stronger than with other sp metals, but weaker than with d-metals. Adsorption processes on Au usually have a reversible character. In contrast to other sp metals, adsorption is dominated by the metal-adsorbate rather than by the metal-solvent interaction [25]. The use of Au substrates is important to the

molecular self assembly process of thiols, which produce high quality films on its surface [26].

Gold was selected in the present work for investigating the influence of the concentration of supporting electrolyte on the electron transfer kinetics of the system $Fe(CN)_6^{4-}/Fe(CN)_6^{3-}$.

A. Preparation of gold ultramicroelectrodes.

The fabrication of gold ultramicroelectrodes proved to be a difficult task. Several attempts were made using different types of glass and epoxy to obtain a good seal between the gold and the insulator material. The main difficulty for reproducing a good seal stems from the relatively large difference between the thermal expansion coefficients of the gold and glass, which produces a large gap at the gold-glass interface. A mix of soft glasses was employed to obtain a material with a thermal expansion coefficient near to the metal ($14.2x10^{-6}$ m/m °C). However, this method was not successful when gold wire of 0.01 mm were used. It was found that using a composite of Araldite™ CY1301 + Hardener HY 1300 from Ciba-Geigy Plastic, very good seals between the gold and the composite could be obtained. Gold discs were then fabricated using gold wires of 0.01 mm and 0.06 mm diameter, 99.99% (Goodfellow Metal). The following procedure was used for fabrication:

1) The gold wires were cleaned chemically with 1:1 concentrated H_2SO_4/H_2O_2. This solution reacts violently with most organic materials and must be handled with extreme care. The wires were rinsed with ultrapure water and dried in an oven for 30 min.

2) Each gold wire was then soldered to a nickel wire and threaded through a glass pipette until the gold projected out of the pipette tip by at least 2 mm. The composite was then added to the pipette. The epoxy was allowed to harden at room temperature during 24 hours and then in an oven at 70°C for 5 hours.

3) The glass tube was cut flat to obtain the gold ultramicrodisc. The ultramicro-electrode was polished with different grades of alumina following the same procedure used for polishing carbon ultramicroelectrodes. **Figure 2.5**, shows a scheme of the procedure used.

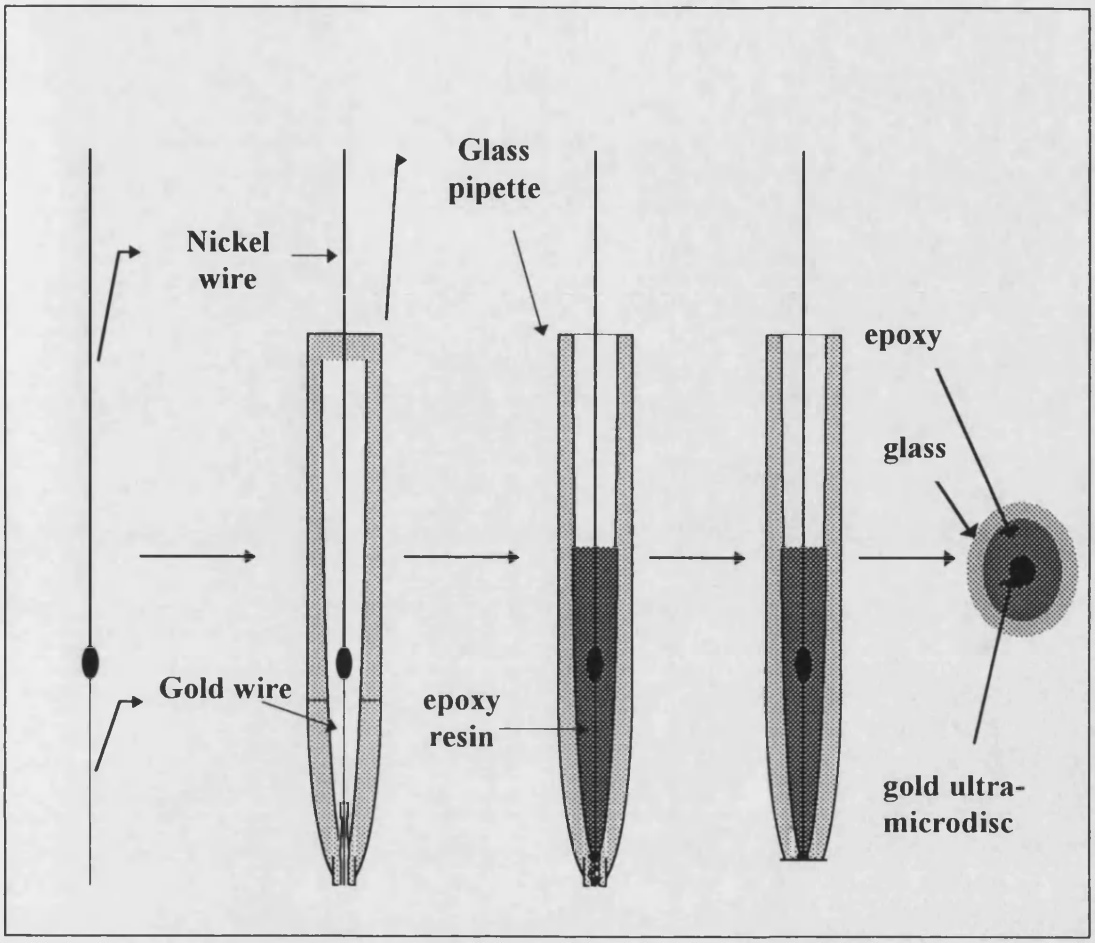
Glass
pipette
Nickel
wire
epoxy
glass
Gold wire
epoxy
resin
gold ultra-
microdisc

Figure 2.5

2.2. *Experimental section*

2.2.1. *Chemicals.*

Reagent grade concentrated 70% $HClO_4$, $K_4Fe(CN)_6$, ferrocene, and tetrabutyl- ammonium perchlorate were obtained from Aldrich, and Fluka. H_2SO_4 Aristar® grade from BDH. All these chemical were used as received, except acetonitrile, which was dried with aluminium oxide (Avocado, neutral 50-160 μm, 99%), which was activated by drying in a oven at 150 °C for 15 hours under vacuum. Water was purified by a Milli-Q filtering system (Millipore 18 MΩ). Sulphuric acid solutions were treated with activated granular charcoal for gas adsorption (particle size 0.85-1.70 mm) from BDH, to eliminate organic impurities which can interfere with the determination of kinetic parameters. Gaseous N_2 was passed through the system describe in **figure 2.6**, before passing through the solution contained in the electrochemical cell. This procedure was applied for 15 min before carrying out the experiment.

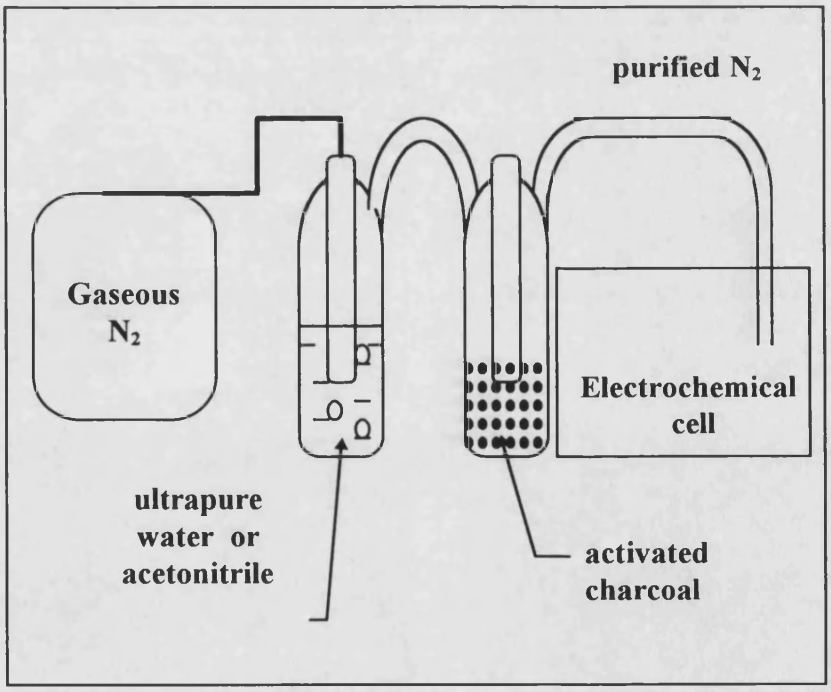

Figure 2.6

2.2.2. *Electrochemical cell*

Electrochemical experiments were carried out using a single compartment cell with a two electrode configuration. The cell was cleaned by using a solution of H_20/H_2S0_4 (1/1), and rinsing with ultra pure water to remove residual organics. A saturated calomel electrode (SCE), model K4040 from Radiometer Electrodes, a platinum quasi-reference electrode, and a reversible hydrogen electrode (RHE) were used as reference electrodes in different experiments. The platinum quasi-reference electrode was flamed each time before carrying out an experiment. The RHE was fabricated according to the following procedure:

A) A platinum wire spiral was cleaned in 1/1 H_2SO_4/H_2O_2 solution, rinsed with plenty of water, and dried in an oven at 70 °C.

B) The platinum wire spiral was sealed into a pipette tube, and the pipette was filled with 1 mol dm^{-3} H_2SO_4 solution. A potential where H_2 evolution occurs was applied. The H_2 produced displaces the solution, leaving a space where only the gas was in contact with the platinum wire. Under these conditions the electrode behaves like a reversible hydrogen electrode (**Figure 2.7**):

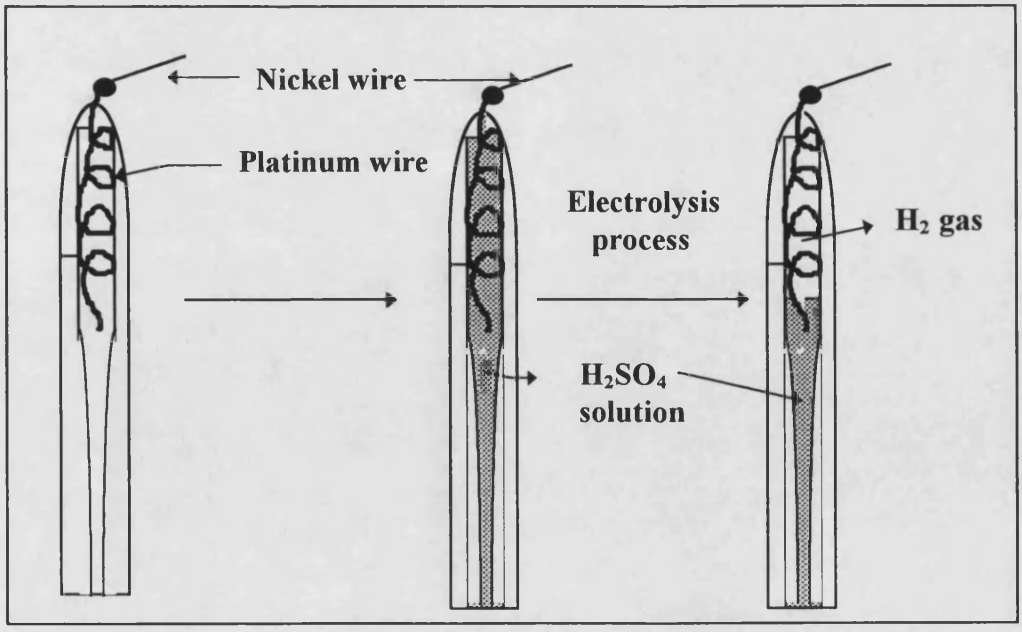

Figure 2.7

This kind of reference electrode was found to be stable for long periods of time. The use of this reference electrode instead of saturated calomel electrode, for example, avoids contamination of the solution under study.

2.2.3. *Electronic equipment*

Cyclic voltammetry experiments were carried out using a waveform generator (Hitek Instruments) coupled to a current amplifier with a low pass filter (sensitivity of $0.01\mu A\ V^{-1}$), built in house. The circuit diagram of this device is shown in **figure 2.8a**. The amplifier and the cell were placed in an earthed metal Faraday box (**figure 2.8b**). All experiments were carried out at room temperature.

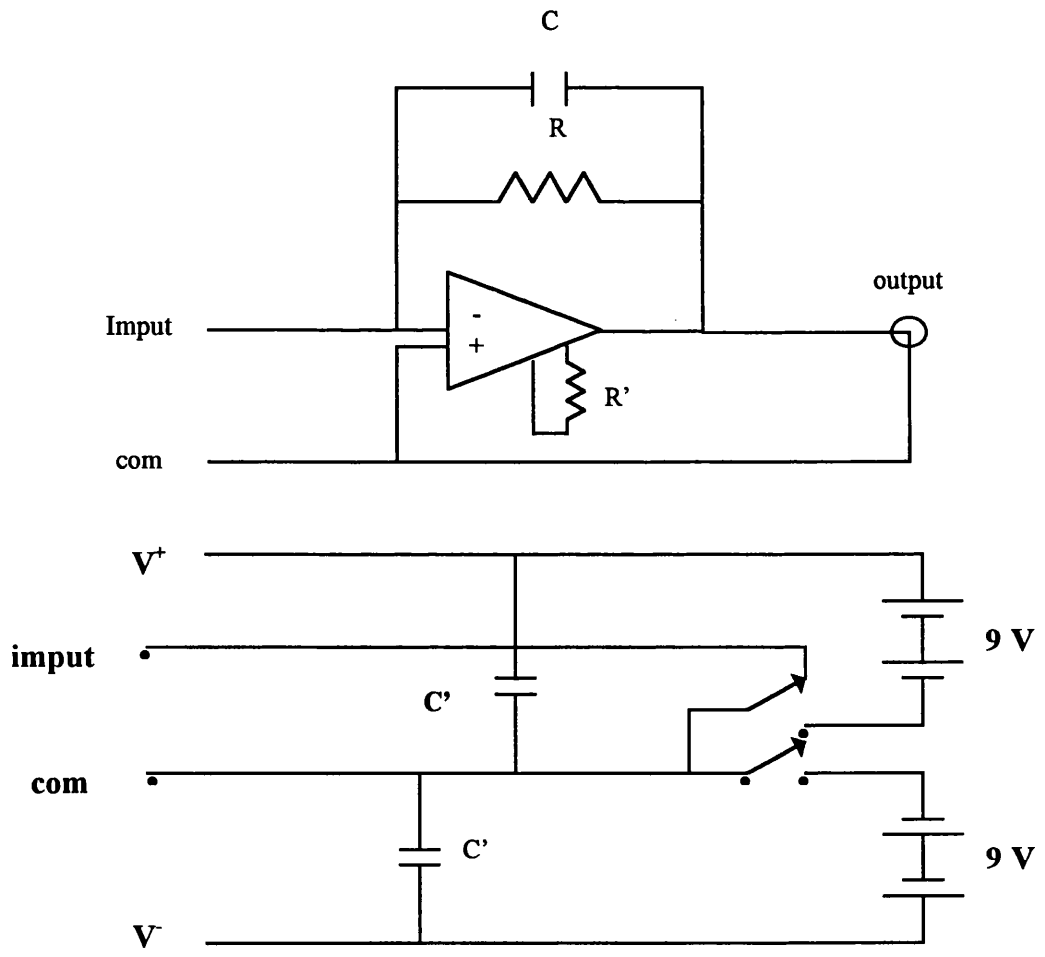

Figure 2.8a. Circuit diagram of the amplifier used

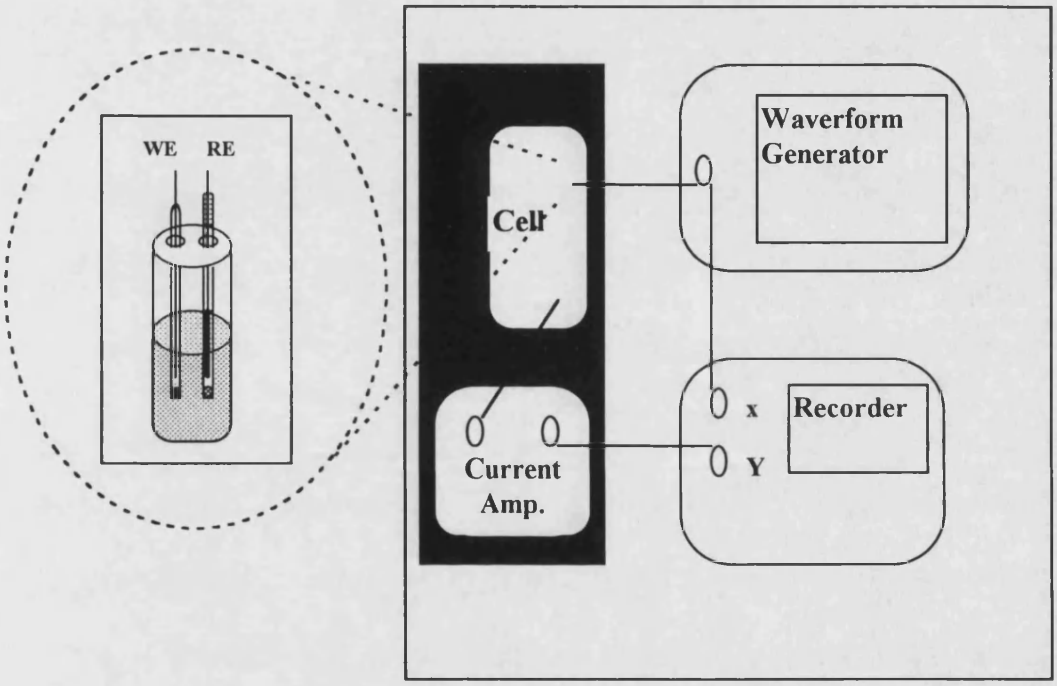

Fig 2.8b. Instrumental arrangement for voltammetric experiments with ultamicroelectrodes

2.3. *Characterisation of ultramicroelectrodes*

Characterization was carried out using physical and electrochemical measurements. The quality of the seal between the electrode material and the insula

tor material, as well as the shape of the microdisc were investigated by scanning electron microscopy. Capacitance measurements were also used to check the quality of the seal and steady state voltammetric measurements were used for determining the real surface area of these devices.

2.3.1. *Characterisation of carbon ultramicroelectrodes*

The quality of the seal between the carbon fibre and the glass was investigated by capacitance measurements, using cyclic voltammetry. Before carrying out the experiment, the microelectrode was repolished with 0.3 μm alumina and rinsed and sonicated in ultrapure water. After that, it was electrochemically treated by cycling between -0.3 and 1.4V vs SCE in the electrolyte medium used for the experiment, until reproducibility of the voltammogram was obtained. **Figures 2.9a**, and **2.9b** show the voltammmograms recorded in different aqueous media using the carbon microelectrodes fabricated under the conditions described in the section 2.1.2., and **Figure 2.9c** the comparison between a very well sealed ultramicroelectrode with a leaking ultramicroelectrode. The values of capacitance were calculated from the relationship:

$$C_{dl} = \frac{j_{dl}}{\upsilon} \qquad (2.4)$$

where j_{dl} is the current density in the the double layer region. The values of capacitance obtained show in a qualitative way the quality of the seal between the carbon and the glass. According to these values and the shape of the voltammograms obtained, the ultramicroelectrodes fabricated were classified into two groups. The first group of ultramicroelectrodes with values of capacitance less than 300 $\mu F/cm^2$, exhibited very flat voltammograms, the second group, in which

the values of capacitance are higher than 1 mF/cm^2, gave voltammograms that were tilted indicating that solution was penetrating between the carbon and the glass.The rather high values of capacitance obtained in the first group can be attributed to either the contribution of pseudocapacitance by redox surface groups present in the carbon microsurface or to the roughness of the surface due to the electrochemical treatment which can produce a porous multilayer film.

The apparent radii were calculated from the limiting current obtained from steady state voltammograms, according to the equation:

$$r = \frac{i_{diff}}{4nFD_oC^{\infty}} \qquad (2.5)$$

where, i_{diff} is the radial diffusion controlled current, C is the bulk concentration of the electroactive species, n is the number of electrons transferred during the electrochemical reaction, r is the radius of the microdisc, and D is the diffusion coefficient of the electroactive species (the diffusion coefficients were determined experimentally and the method used is explained in chapter 4). **Figures 2.10a**, and **2.10b** show the voltammograms obtained in different electrolyte media. The radius of the carbon ultramicroelectrode calculated from the plateau currents for a set of experiments was 3.8± 0.2 μm, which is in good agreement with the geometric value of 3.6 μm, determined by SEM.

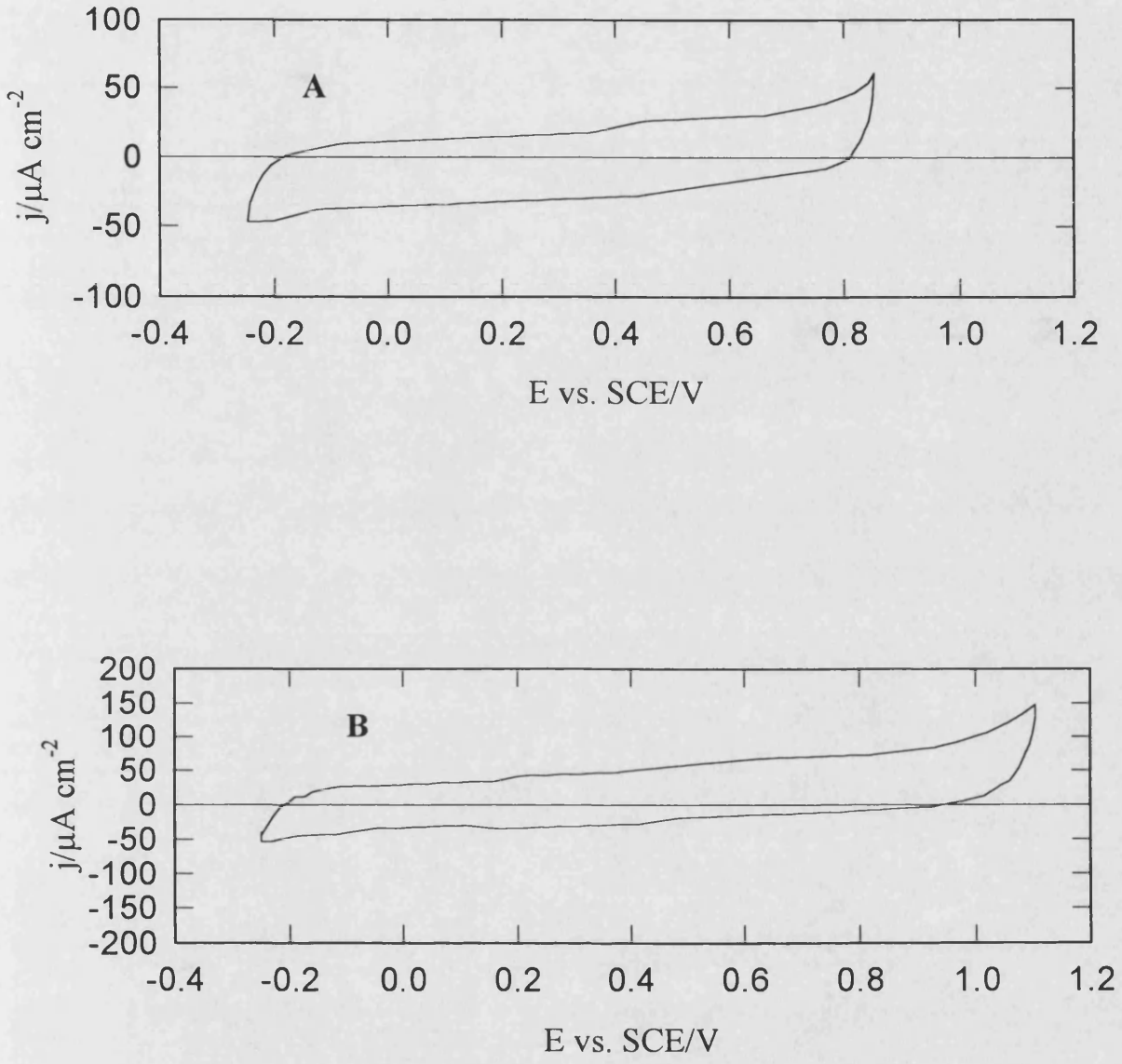

Figure 2.9 Cyclic voltammograms for a carbon ultramicroelectrodes of the first type (non-leaking): A) 1 mol dm^{-3} HCl; B) 1 mol dm^{-3} H_2SO_4; v=80 mV s^{-1}

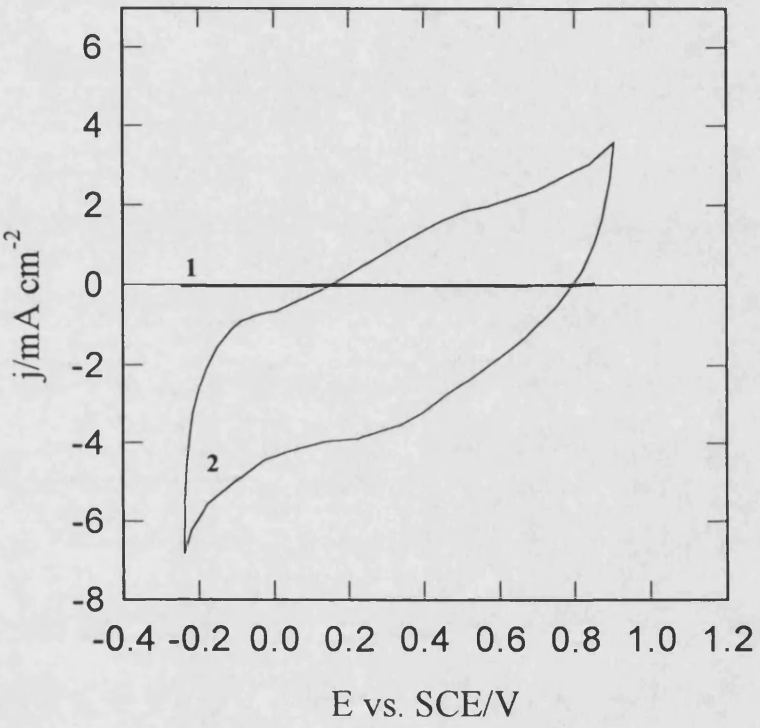

Figure 2.9c. Cyclic voltammograms for a carbon ultramicroelectrodes: 1) without leaking (data from figure 2.9a); 2) with leaking; solution 1 mol dm^{-3} HCl; ν=80 mV s^{-1}

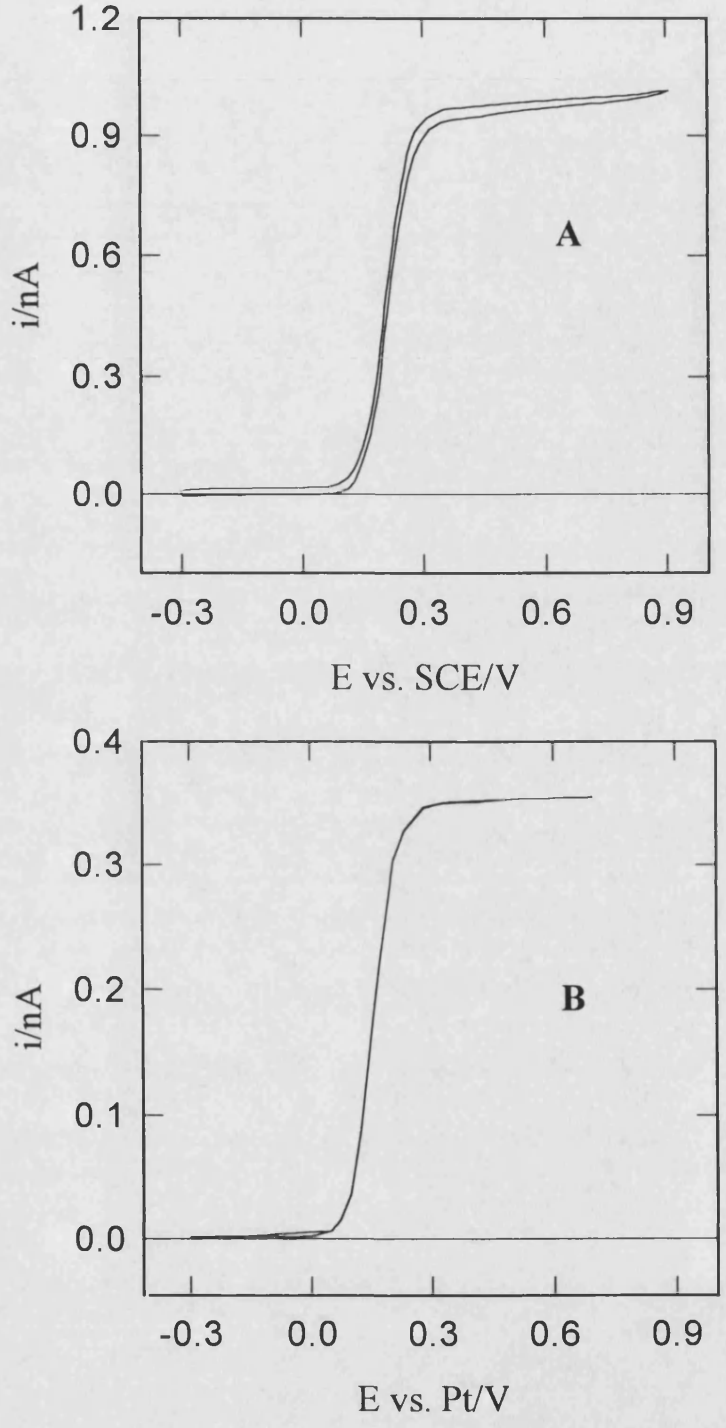

Figure 2.10. Voltammograms obtained at a carbon microelectrode for the: A) oxidation of $1x10^{-3}$ mol dm^{-3} $Fe(CN)_6^{4-}$ in 0.1 mol dm^{-3} KCl and B) oxidation of $1x10^{-4}$ mol dm^{-3} ferrocene in $1x10^{-3}$ mol dm^{-3} TBAP/ acetonitrile; v= 10 $mV.s^{-1}$

2.3.1.2. *Scanning electronmicroscopy (SEM)*

Scanning electron microscopy (SEM) was employed for the characterization of the quality, shape and size of the ultramicroelectrodes fabricated. At the simplest level an SEM can be thought of as providing images of external morphology rather similar in appearance to those formed by the eye. However it is necessary to point out that one of the main features of the SEM is that, in principle, any radiation from the specimen or any measurable change in the specimen, may be used to provide the signal to modulate the cathode ray tube (CRT) and thus provide contrast in the image. Each signal is the result of some particular interaction between the incident electrons and the specimen, and may provide us with different information about the specimen. **Figure 2.11** shows schematically some of the signals which may be obtained in the SEM:

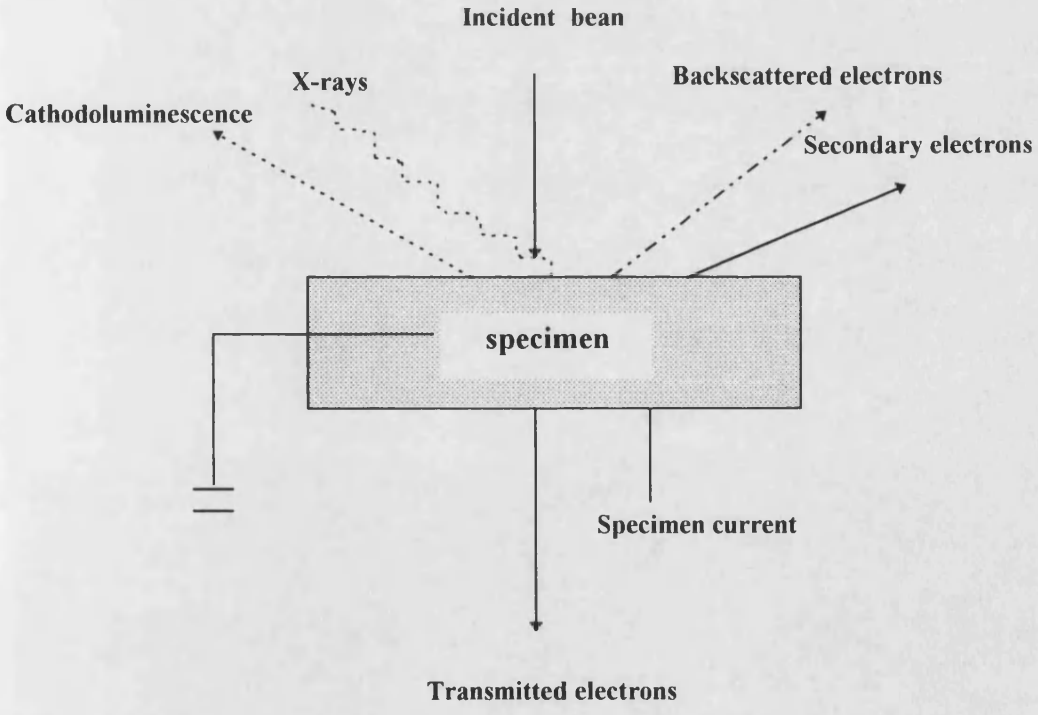

Figure 2.11. Some of the signals which may be obtained in the SEM

In the SEM, a beam of electrons is directed at the specimen and normally only secondary electrons are used to form the image of the surface. These secondary electrons are described as those electrons which escape from the specimen with energies below about 50 eV. These electrons are emitted from the outer electron orbits, which present the highest energy electrons (i.e those with the lowest binding energies). This emission is the result of inelastic collisions between the atoms in the sample and the incident electrons. These secondary electrons are first accelerated by a high voltage to impinge upon a scintillator, then the light produced passes down a light pipe to a photomultiplier where it is converted to an electric current for subsequent amplification and display on a cathode ray tube. The image formed is then taken by a mounted camera to provide a permanent record. The surface in some cases is coated with a thin conducting layer of gold by sputter coating. This is done to avoid charging of the surface by the electron beam.

Figures 2.12a, and 2.12b show the scanning electron microscopy photographs taken of the a carbon ultramicroelectrode fabricated with a carbon fiber without chemical modification (**figure 2.12c**). This ultramicroelectrode exhibed high capacitance values (>1000 $\mu F/cm^2$), and the voltammogram obtained was tilted. Similar behaviour was observed with other ultramicroelectrodes fabricated using carbon fibers without chemical modification. According to these results, when a large gap between the carbon and glass is observed by SEM, it can be assumed that the ultramicroelectrode will give a high capacitance value due to leakage of solution at the carbon-glass interface.

Figure 2.13 shows the SEM photograph obtained of a carbon fiber which was treated chemically with conc. HNO_3 for 3 hours. Grooves are observed along the fiber, when this treatment is used. The morphology of the modified carbon fiber is completely different to the structure observed when the carbon fiber has not been modified (**figure 2.12c**). It appears that during the chemical treatment, the outer shell of the carbon fiber is removed and oxidation takes place along the carbon fiber. On the other hand, during this oxidative process the radius of the carbon fibre is decreased. Most of the ultramicroelectrodes fabricated using these chemically modified carbon fibers gave capacitance values less than 300 $\mu F/cm^2$, and the

voltammograms were completly flat. **Figure 2.13b** shows the SEM picture of a carbon ultramicrodisc, which was fabricated using a carbon fiber that had been modified chemically. The surface was coated with a thin layer of gold by sputter coating. The boundary between the carbon and glass is very narrow (**figure 2.13c**). This mean that a very good seal has been formed between the carbon and glass. In some case, high capacitances values (>500 $\mu F/cm^2$), were obtained. The SEM pictures showed that in these cases that small air bubbles were trapped at the carbon-glass interface (**figure 2.14a and 2.14b**). The presence of these small bubbles produces a gap between the carbon-glass, which is reflected in the capacitance measurements.

2.3.2. *Characterisation of platinum ultramicroelectrodes.*

The characterisation of Pt ultramicroelectrodes was carried out using cyclic voltammetry in order to determine the real area of the microelectrode. In acidic aqueous electrolytes, at least two well-defined peaks for hydrogen adsorption-desorption on platinum must be observed at low sweep rate. This behaviour is characteristic of a clean solution and a clean platinum microelectrode. The real surface area was calculated from the charge due to hydrogen adsorption assuming 210 $\mu C/cm^2$. The area under the adsorption or desorption (A_d) hydrogen peaks was determined, and the double layer charging contribution was subtracted. This determination involve the assumption of considering that the double layer capacitance is constant in the hydrogen adsorption and desorption region.
The experimental charge associated with hydrogen adsorption or desorption was determined from the following equation:

$$Q_{exp} = A_d \frac{S_i x S_v}{\upsilon} \qquad (2.6)$$

where S_i and S_v are the current and voltage sensitivities for the respective axes on the cyclic voltammogram, and ν is the sweep rate. The real surface area was then calculated from the ratio:

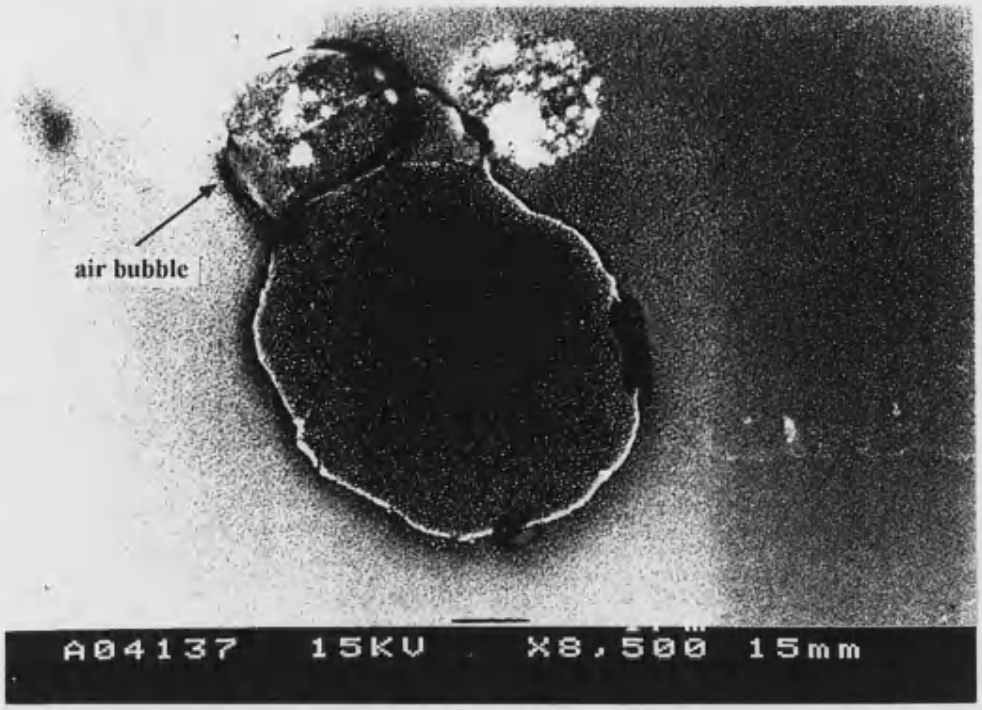

Figure 2.12a. SEM photograph of a carbon ultramicrodisk fabricated with a carbon fiber without chemical modification

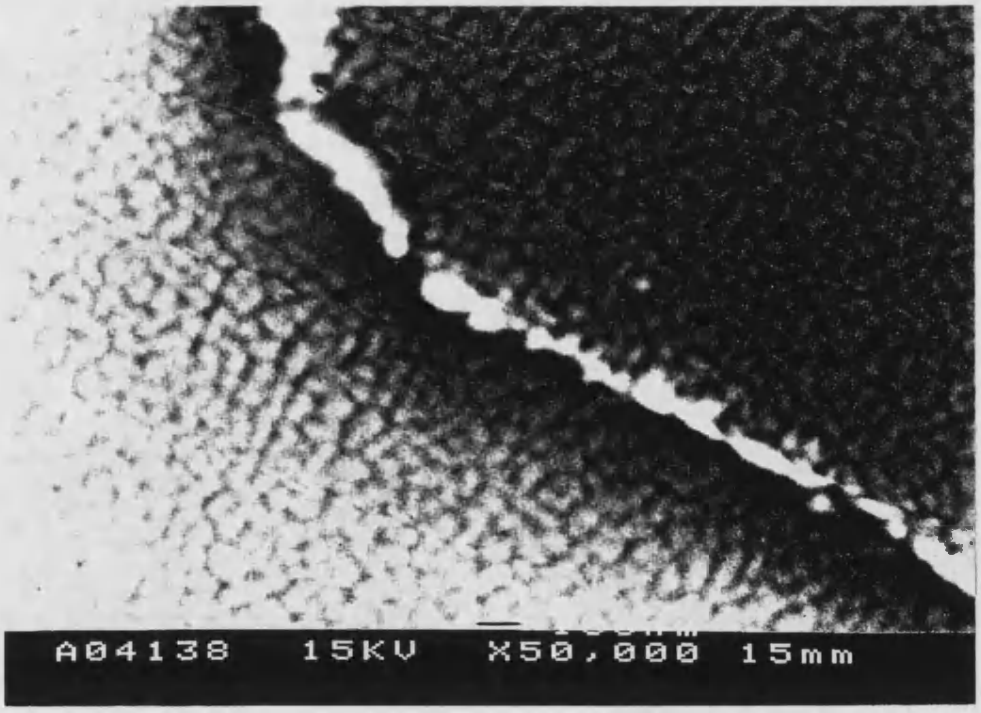

Figure 2.12b. Carbon-glass interface of a carbon ultramicrodisk prepared using a carbon fiber without chemical modification.

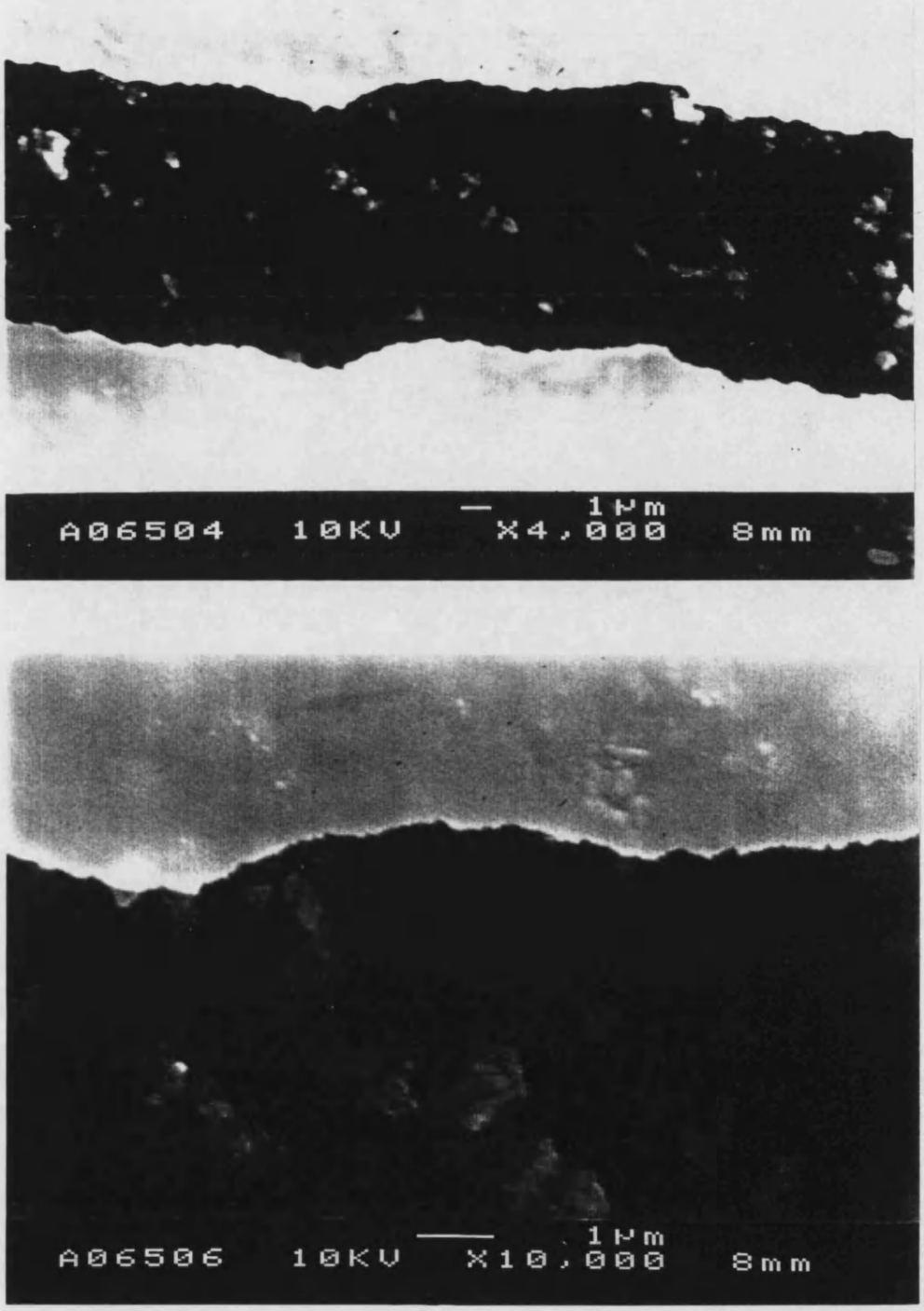

Figure 2.12c. SEM photograph of a carbon fiber without chemical modification

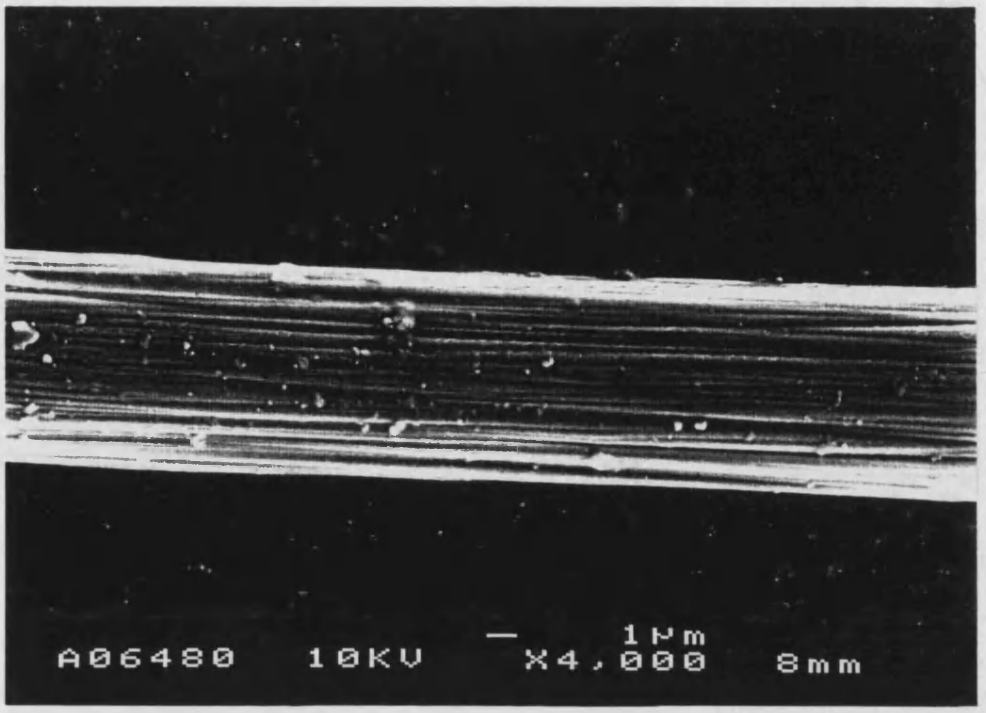

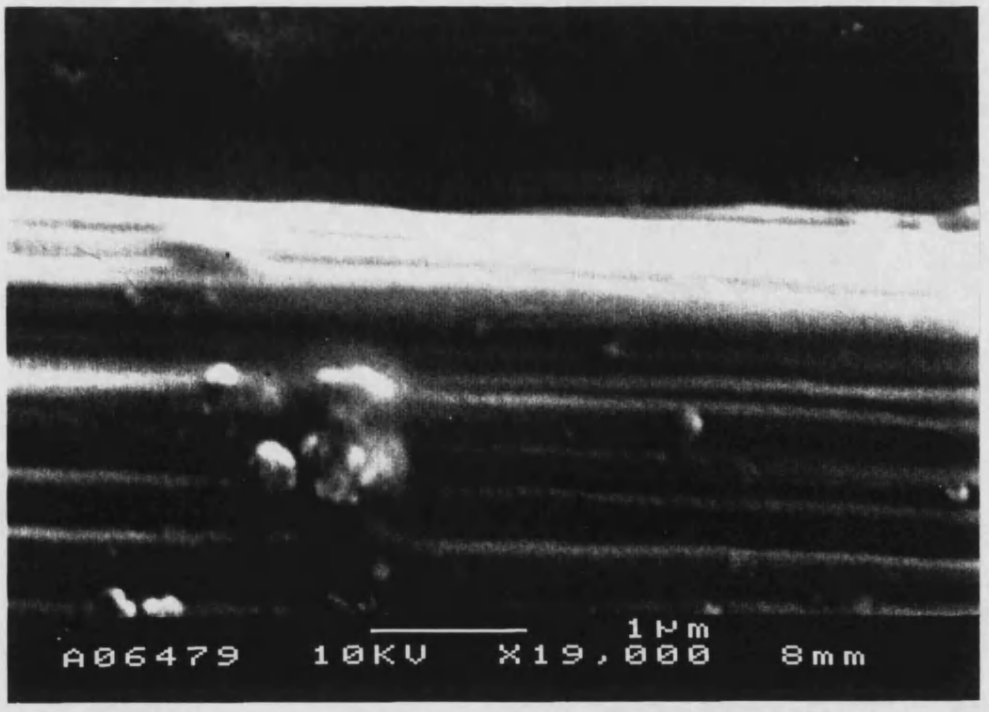

Figure 2.13a. SEM photograph of a carbon fiber with chemical modification in concentrated HNO_3

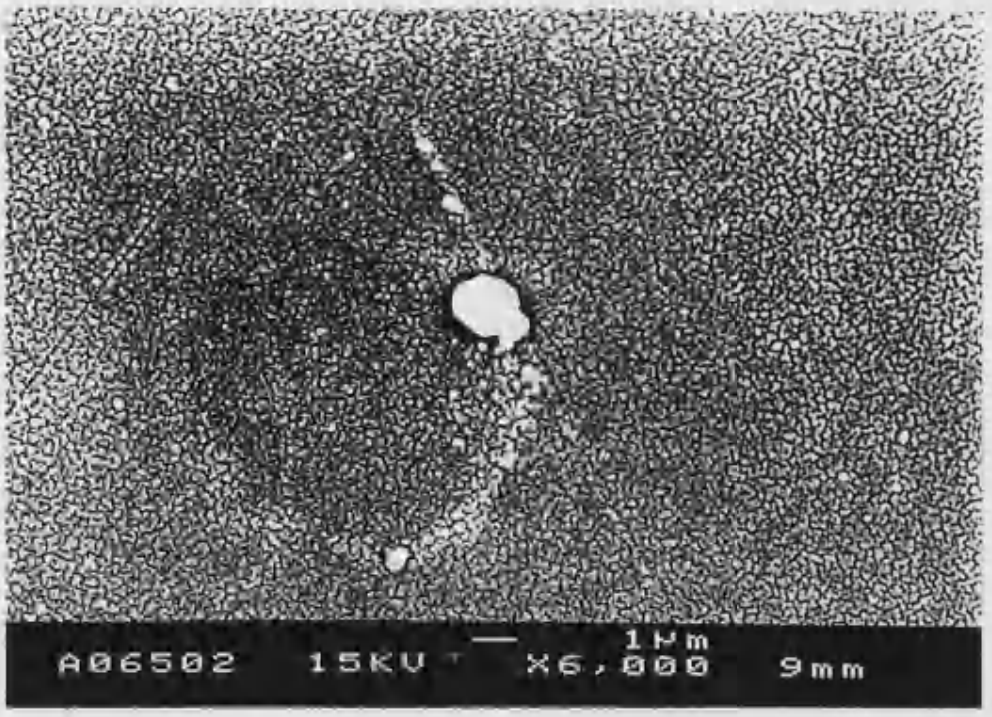

Figure 2.13b. SEM photograph of a carbon ultramicrodisk fabricated with a carbon fiber modified chemically with concentrated HNO_3

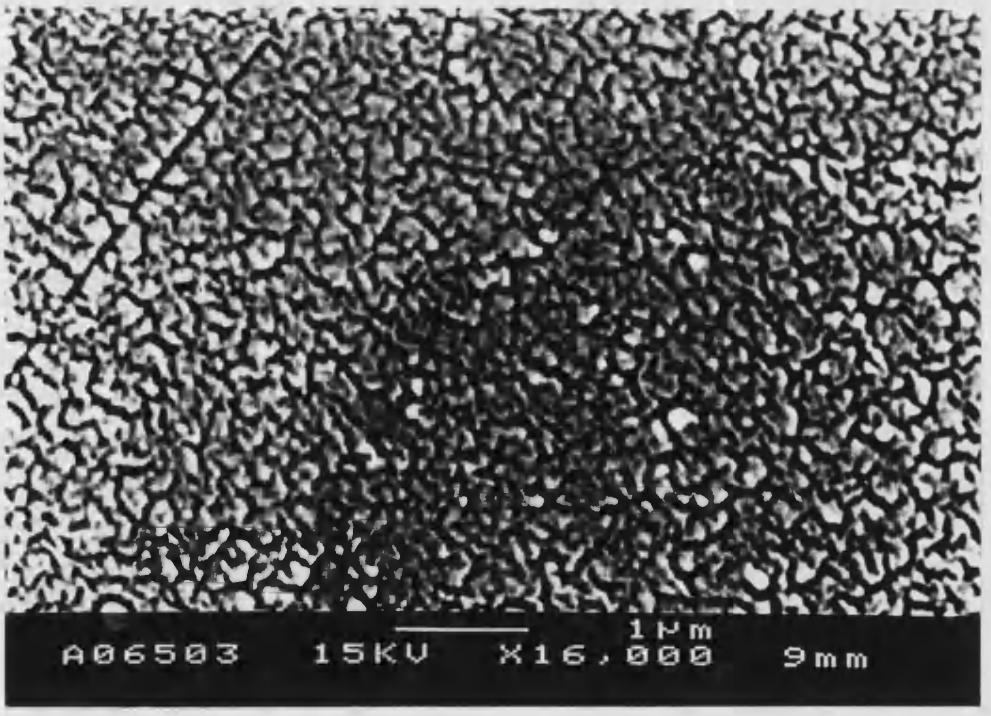

Figure 2.13c. Carbon-glass interface of a carbon ultramicroelectrode prepared using a carbon modified chemically with concentrated HNO_3

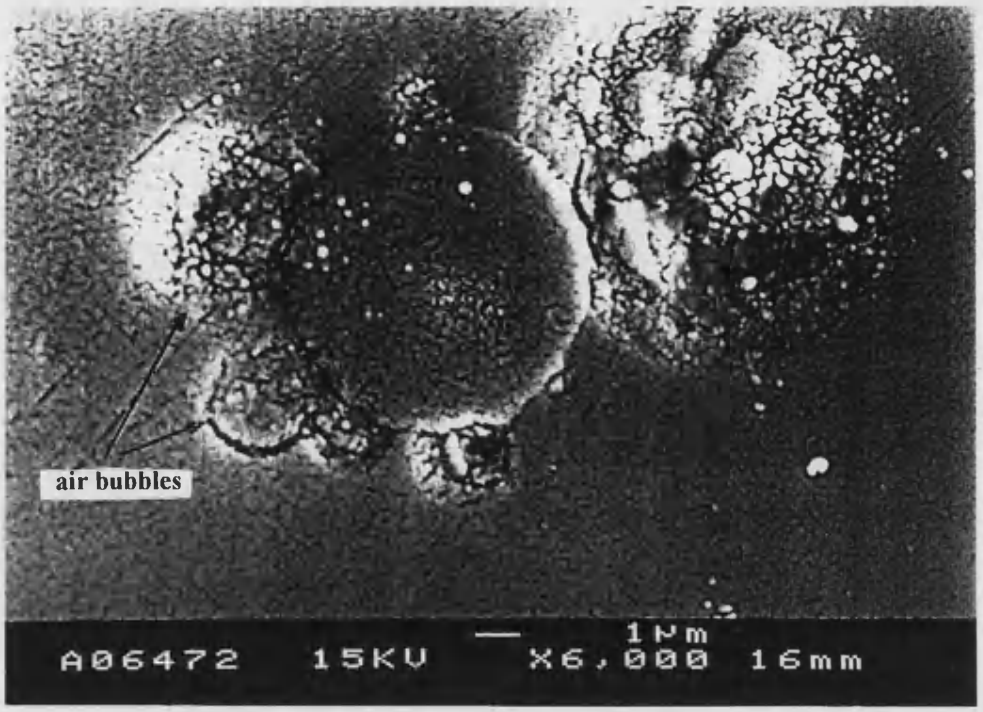

Figure 2.14a. SEM photograph of a carbon ultramicrodisk fabricated with a carbon fiber modified chemically with conc.HNO_3 (where air bubbles were trapped at the carbon-glass interface).

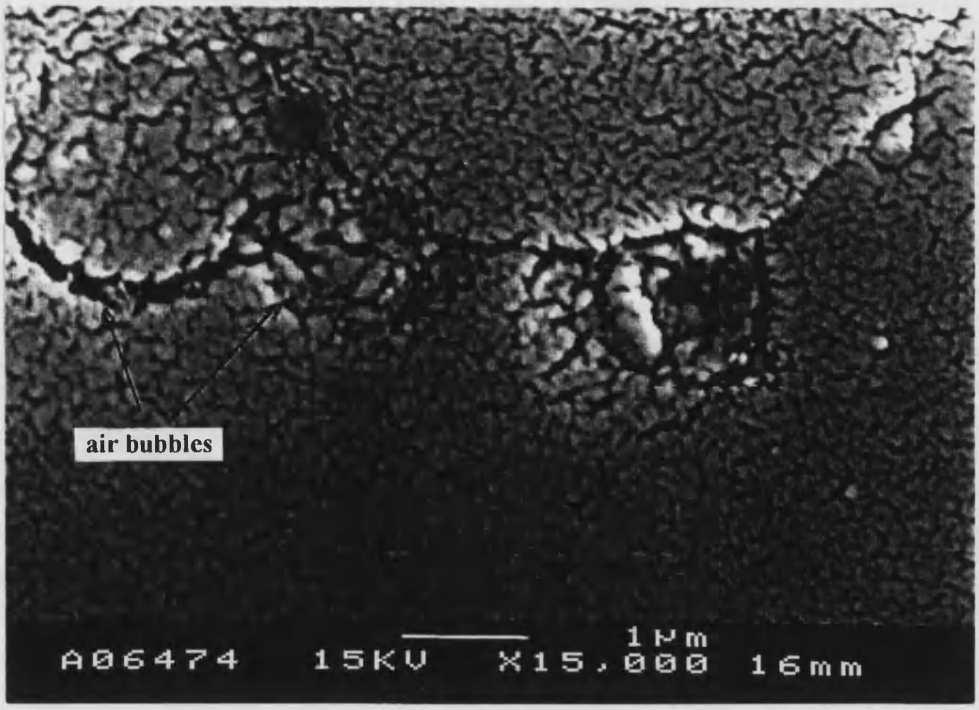

Figure 2.14b. Carbon-glass interface in the place where air bubbles were formed. The carbon ultramicroelectrode was prepared using a carbon fibre modified chemically with concentrated HNO_3

$$A_{real} = \frac{Q_{exp}}{Q_{theo}} \qquad (2.7)$$

According to Woods [27], on the the polycrystalline platinum surface, there is an equal distribution of the three low index planes, (100), (111), and (110). However the value taken as standard is that of the (100) surface, the median of the three planes in terms of surface atom density. Considering the packing structure of platinum as a face-centred cubic:

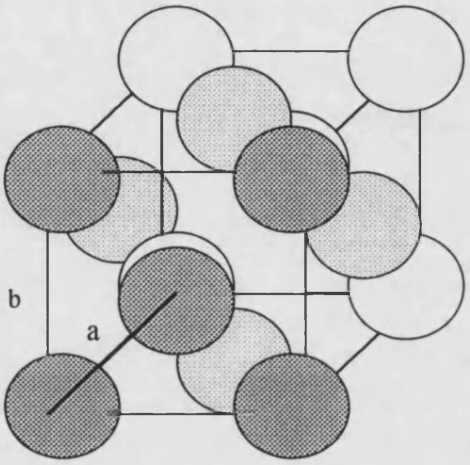

Figure 2.15. Face-centred cubic (fcc 100) unit cell for platinum, a= 3.91 Å, and b= $\sqrt{2}a^2$.

the charge (Q_{theo}) corresponding to a monolayer coverage with hydrogen is determined by considering the hydrogen atoms adsorbed on both, the first layer (dark shaded) and the second layer (light shaded). With these assumptions, a value of approximately 210 $\mu C/cm^2$, is predicted, which was the value used at the present work as Q_{theo}.

Before carrying out an experiment, the platinum ultramicroelectrodes were cleaned. The first step was the same as the procedure utilized for cleaning the carbon microelectrodes. After that, they were soaked in conc. HNO_3, and then they were rinsed with plenty of ultrapure water before being placed in the electro-chemical cell. Electrochemical treatment was carried out by cycling between 0 to

1.4V vs RHE at 100 mV/s, until reproducibility of the voltammogram was obtained. **Figure 2.16** shows the voltammogram obtained at a platinum micro-electrode (radius 5 μm) in 1 mol dm^{-3} H_2SO_4 solution, after passing N_2 gas for 30 min. In this experiment, the potential sweep began at E=0.0 V vs RHE, where the surface is covered with a layer of adsorbed hydrogen. When the potential is shifted to a more positive value, the adsorbed hydrogen is oxidized, giving rise to two anodic peaks in the range 50 mV to 250 mV vs RHE. In the potential range between 300 mV and 800 mV, no electrode process was observed. In this region only the current for electrode charging flows through the system. At potentials of E> 800 mV, the adsorption of oxygen begins to occur, being characterized by a drawn-out wave. When the direction of polarization was reversed at 1.4 V, the reduction of the oxide layer is observed at a more negative potential than the anodic process. When the potential is driven more negative between 300 and 50 mV, the one electron reduction of hydrogen ions results in a growing monoatomic layer of adsorbed hydrogen on the platinum surface, as indicated by the two cathodic peaks observed in the voltammogram in the cathodic direction. The two well-defined reversible hydrogen adsorption/desorption peaks have been attributed to a different kind of adsorption of hydrogen. Most authors choose to refer to the peak at about 250 mV as strongly bound hydrogen, and the peak at around 120 mV as weakly bound hydrogen. According to UV/visible reflectance spectra reported by Bewick and Tuxford [28,29], the two peaks arise from hydrogen adsorption with different coordination numbers at the surface. They reported that the strongly adsorbed hydrogen penetrates into the surface and the weakly adsorbed hydrogen behaved like a chemisorbed species. However it is necessary to point out that two more peaks can appear at the voltammogram [30]. These peaks have been attributed to different adsorption sites on the crystal face [31,32].

From the area calculated, roughness factors between 1.57 to 2 were determined. Most of the Pt ultramicroelectrodes used in the present work did not leak because the platinum and glass have similar thermal expansion coefficients. The roughness factors of 1.5 to 2 were attributed to the electrochemical treatment used in the present work.

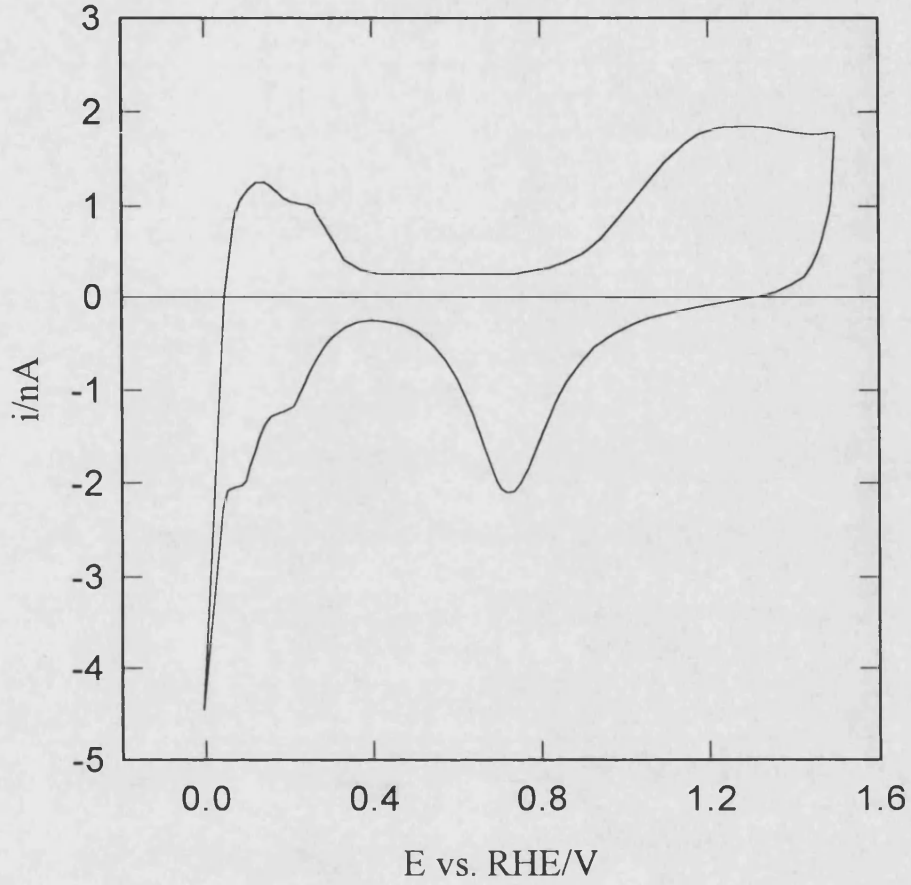

Figure 2.16. Cyclic voltammogram at a platinum ultramicroelectrode of 5 μm in radius in 1mol dm^{-3} H_2SO4 at 25 °C, in the absence of oxygen; sweep rate = 100 mV s^{-1}.

2.3.3. *Characterisation of gold ultramicroelectrodes.*

In the present work, the gold ultramicrodisks were characterized by capacitance measurements and oxygen adsorption from acid solutions, SEM and by underpotential deposition of lead on their microsurfaces. The method used to calculate the real area and the apparent radius from underpotential deposition data will be discussed in chapter 3.

Figure 2.17, shows the cyclic voltammogram recorded using a gold ultramicroelectrode, for a blank solution of 0.2 mol dm^{-3} $HClO_4$. The double layer capacitance was determined, using equation (2.4). The value of about 50 $\mu F/cm^2$ is in agreement with the values reported in the literature [33].

A. Oxygen adsorption method.

By using the oxygen adsorption method, it is assumed that oxygen is chemisorbed in a monoatomic layer prior to O_2 evolution with a one to one correspondence with surface metal atoms. Knowing that gold has well-developed regions for oxide monolayer formation and reduction [34], this method may be used to determine surface areas. However, the cleanliness of the surface of the ultramicrodisc and the solution must be ensured. During adsorption (positive potential sweep), the anodic measured charge may include oxidizable impurity effects and some charge associated with oxygen evolution. On the other hand the charge measured during adsorbed oxygen reduction may correspond to multilayers (oxide film) of undefined stoichiometry.

The successful application of this method entails a careful selection of the limits of the potential range where the charge corresponding to oxidation or reduction should be determined. Different methods of cleaning the ultramicroelectrodes were tested and extreme care was taken when preparing the solution. The gold ultramicroelectrodes were repolished with 3 and 0.3 alpha alumina, followed by rinsing and sonicating with ultra pure water for 1 min. Then they were electrochemically treated by cycling in acid media in the potential range where the formation of gold oxide and its reduction occurs. In experiments carried out in 0.5 mol dm^{-3} H_2SO_4, the onset of the formation of gold oxide and its reduction are

shifted to more positive potentials than in 0.2 mol dm^{-3} aqueous solutions of $HClO_4$. This behaviour has also been reported by Kozlowska et al. [35], and it has been attributed to the sulphate ion which is adsorbed more strongly than the perchlorate ion. On the other hand, when the ultramicroelectrode is cycled at high sweep rate in the potential range where the formation of gold oxide and its reduction occur, the voltammogram changes after the first cycle, and it was found that the roughness of the microsurface increases with cycling time.

Following these results, the characterization of these ultramicroelectrodes was performed using $HClO_4$ as supporting electrolyte because the range of potential where oxide formation and its reduction occur can be reduced, hence increased surface roughening avoided. **Figure 2.18** shows the voltammogram obtained at a gold ultramicroelectrode in $HClO_4$ aqueous solution. The potential scan includes the double layer region (0.1 to 1 V vs SCE), as well as the region of oxide formation (1 to 1.4 V). In the double layer region, an electrode process is observed around 0.65 V. This shoulder is attributed to the adsorption of the ClO_4^- anion [35]. In the region of oxide formation, replacement of the adsorbed anions by OH^- occurs and two peaks are observed. The first peak at 1.25 V is attributed to formation of the first sublattice of OH^- deposited in between adsorbed anions [35]:

$$\left[M_xA^-\right]M + H_2O \rightarrow \left[M_xA^-\right]MOH + H^+ + e^- \qquad (2.8)$$

The second peak at 1.35 V has been attributed to the deposition of OH^- accompanied by desorption of the anions [32].

$$M_xA^- + H_2O \Leftrightarrow M_{x-1} + MOH + A^- + H^+ + e- \qquad (2.9)$$

A peak is observed on the cathodic side of the voltammogram between 0.85 to 0.9 V vs SCE, which corresponds to the reduction of adsorbed oxygen (oxide stripping).

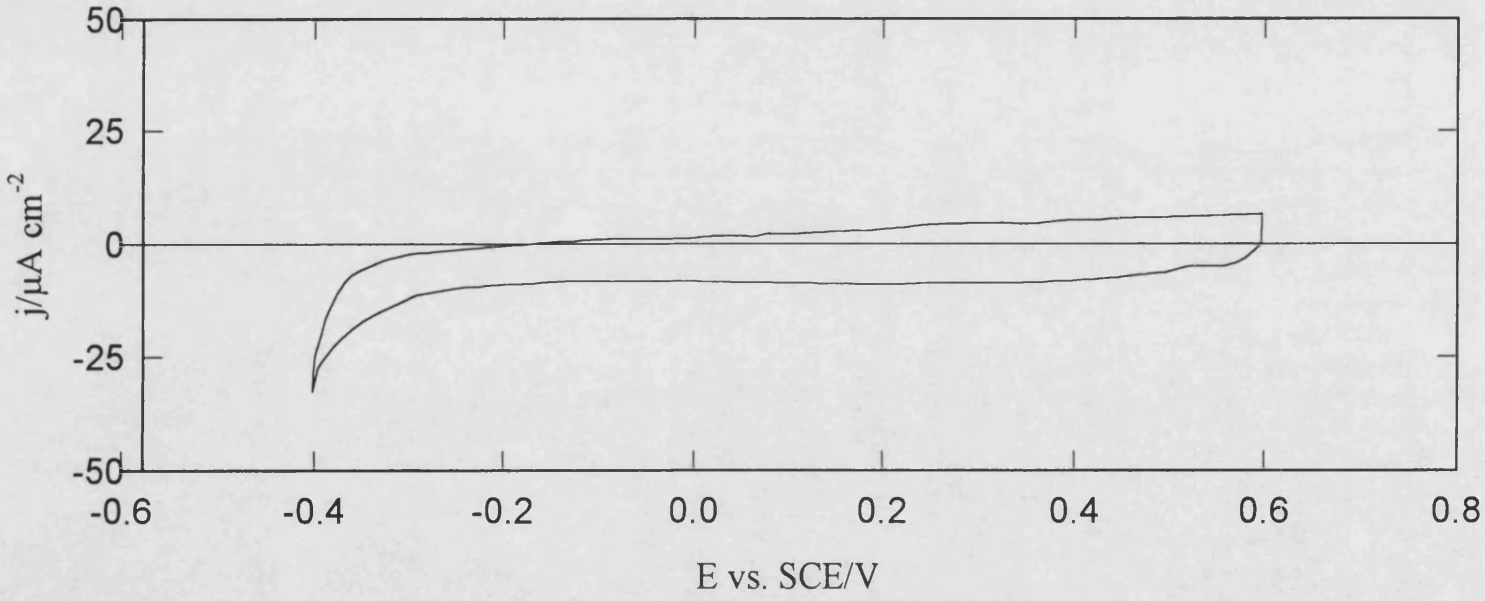

Figure 2.17. Cyclic voltammogram at gold ultramicroelectrode in in 0.2 mol dm^{-3} $HClO_4$; ν = 60 mV.s^{-1}.

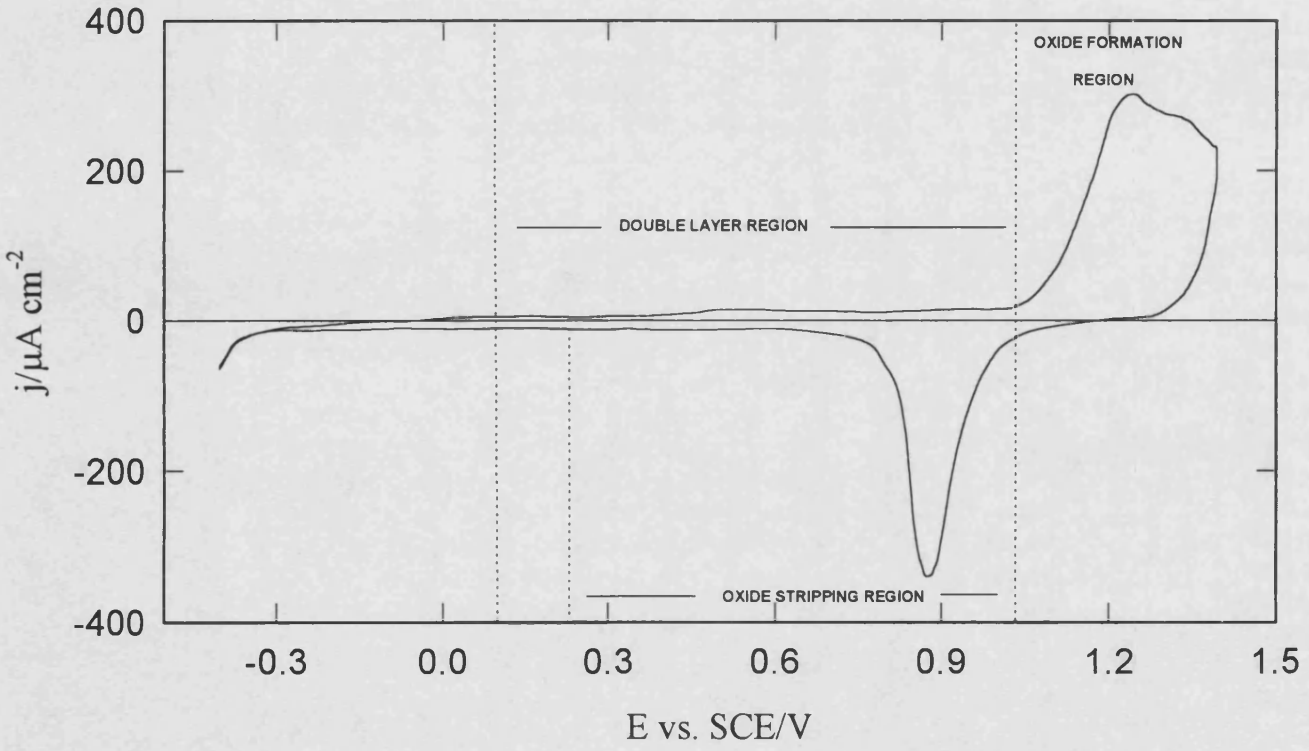

Figure 2.18. Cyclic voltammogram at a gold ultramicroelectrode of 5 μm radius (sealed in epoxi composite), in 0.2 mol dm^{-3} $HClO_4$; $\nu = 70\ mV.s^{-1}$.

The shape of the voltammogram is similar to that reported for polycrystalline gold [34]. The effective area of the gold ultramicroelectrode was calculated taking into account that the cathodic charge in aqueous solutions of $HClO_4$ increases almost linearly with the applied potential above 1.2 V vs SCE and that this charge is independent of pH [36]. The charge value (Q_B) used was taken from the curve cathodic charge vs anodization potential reported by Brummer et.al. [36]. This value and the charge obtained experimentally by integration of the oxide stripping peak (**figure 2.19**), were used to calculate the real area of the microdisc from the radio:

$$A_{real} = \frac{Q_{exp}}{Q_B} \tag{2.10}$$

The apparent radius was calculated by assuming the ultramicroelectrode is an ideal disk:

$$r = \sqrt{\frac{A_{real}}{\pi}} \tag{2.11}$$

For a series of experiments carried out at 60 mV/s, using gold wires of 10 μm diameter, the values of apparent radius obtained was 4.80 ± 0.13 μm. This value corresponds closely to the nominal value of 5 μm.

Figures 2.20a and **2.20b**, show the SEM photographs obtained for a transverse section of a 10 μm diameter gold wire surrounded by epoxy. It is necessary to point out that all photographs were taken without performing the complete cleaning procedure reported in the section *2.1.4.*

Figures 2.21a and **2.21b**, show the SEM photographs for a gold ultramicroelectrode (60 μm diameter) sealed in glass which exhibited an anomalously high capacitance value. Again, the SEM showed that the high capacitance arises from leakage due to an air bubble trapped at the gold-glass interface, which produces a gap at the interface. However, it is seen that the boundary between the epoxy and gold is very sharply defined, indicating a good

quality seal. From these pictures, it is also observed that the diameter of each disk is about 10 and 60 μm respectively.

Figure 2.22a shows a family of voltammograms obtained on a gold ultramicroelectrode of 10 μm diameter, with sweep rates from 10 to 100 mV/s. Since the peak heights are linearly dependent on the sweep rate (**figure 2.22b**), it was concluded that the electrode processes responsible for the peak are surface processes and not diffusion of some electroactive species from the solution. **Figure 2.23a** shows a family of voltammograms with an anodic limit increasing in 50 mV steps from 1.25 to 1.45 V. It is observed that the area under the oxide stripping peak increases with the increase in anodic potential limit. **Figure 2.23b** shows the behaviour of the cathodic charge calculated, from the area under the stripping peak. It is seen that the variation of the cathodic charge with the potential is almost linear.

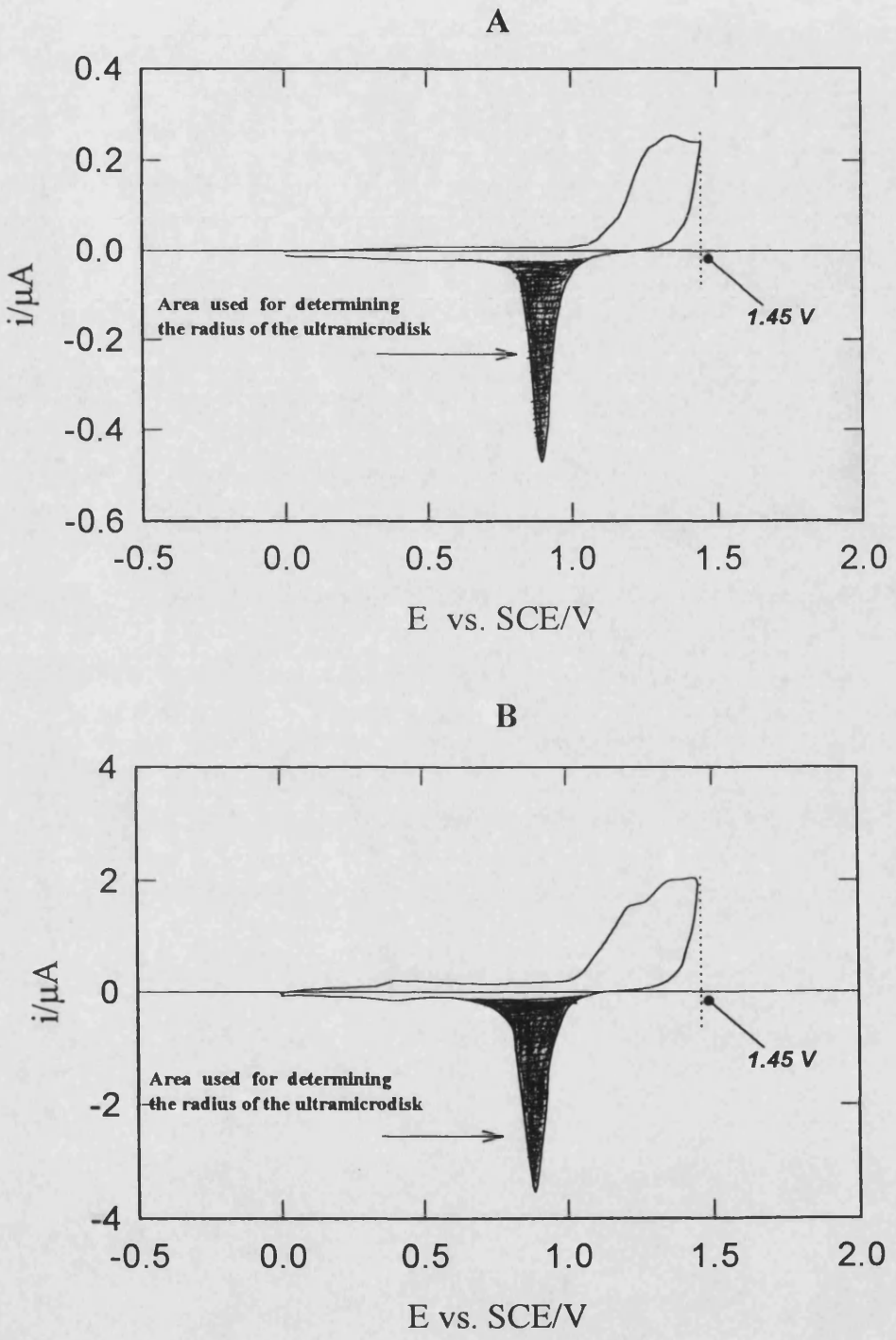

Figure 2.19. Cyclic voltammograms at: A) a gold ultramicroelectrode sealed in epox (10 μm diameter); B) a gold ultramicroelectrode sealed in glass (60 μm diameter) for the system $HClO_4$ 0.2 mol dm^{-3}; ν = 60 mV/s

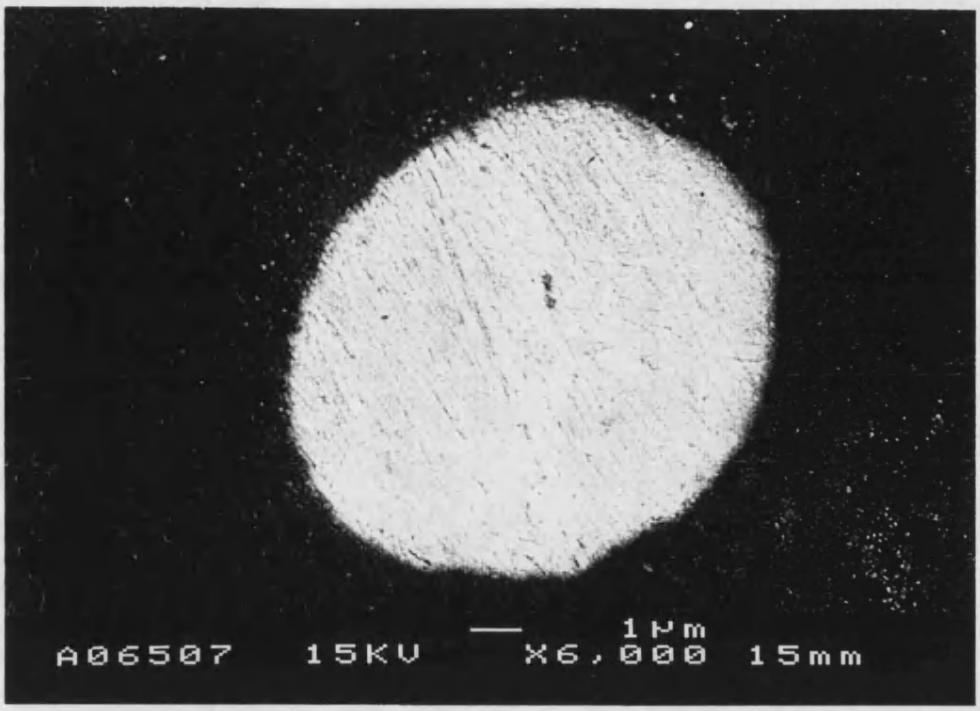

Figure 2.20a. SEM photograph of a gold ultramicroelectrode fabricated with gold wire (10 μm diameter), sealed with epoxy

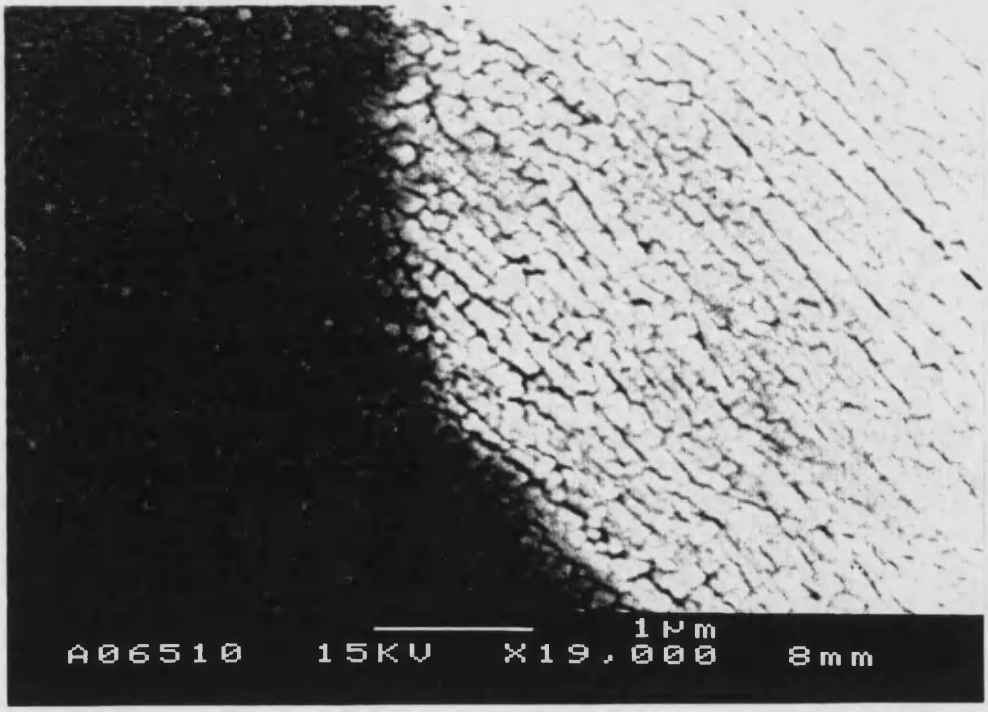

Figure 2.20b. gold-epoxy interface of a gold ultramicroelectrode prepared using a gold wire (10 μm diameter)

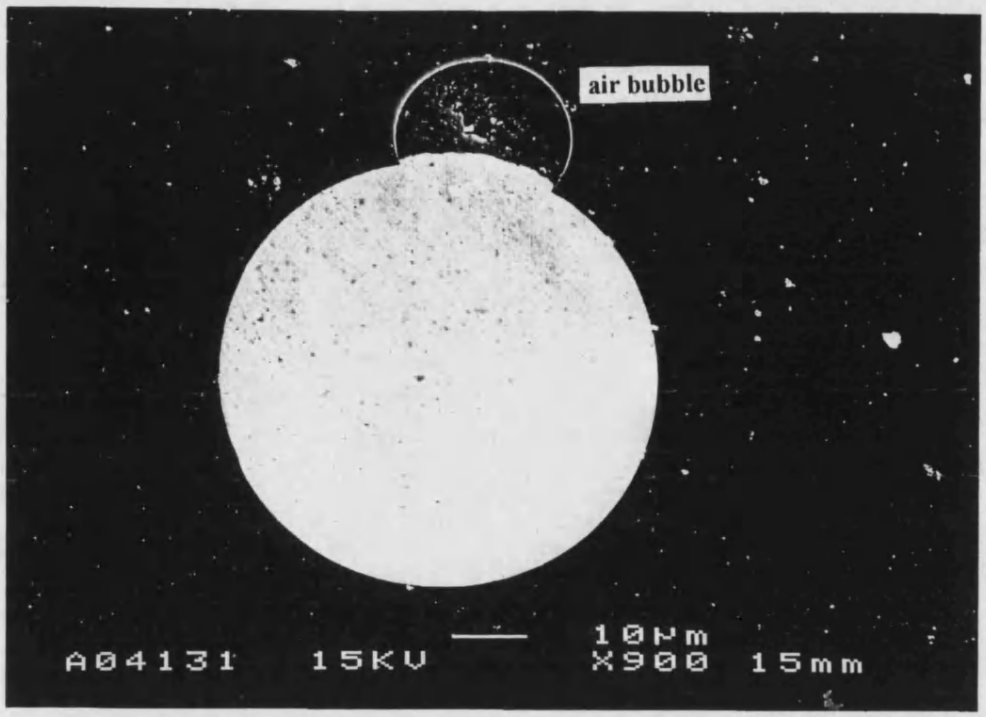

Figure 2.21a. SEM photograph of a gold microelectrode fabricated with gold wire (60 μm diameter), sealed in soft glass, showing bubble formation

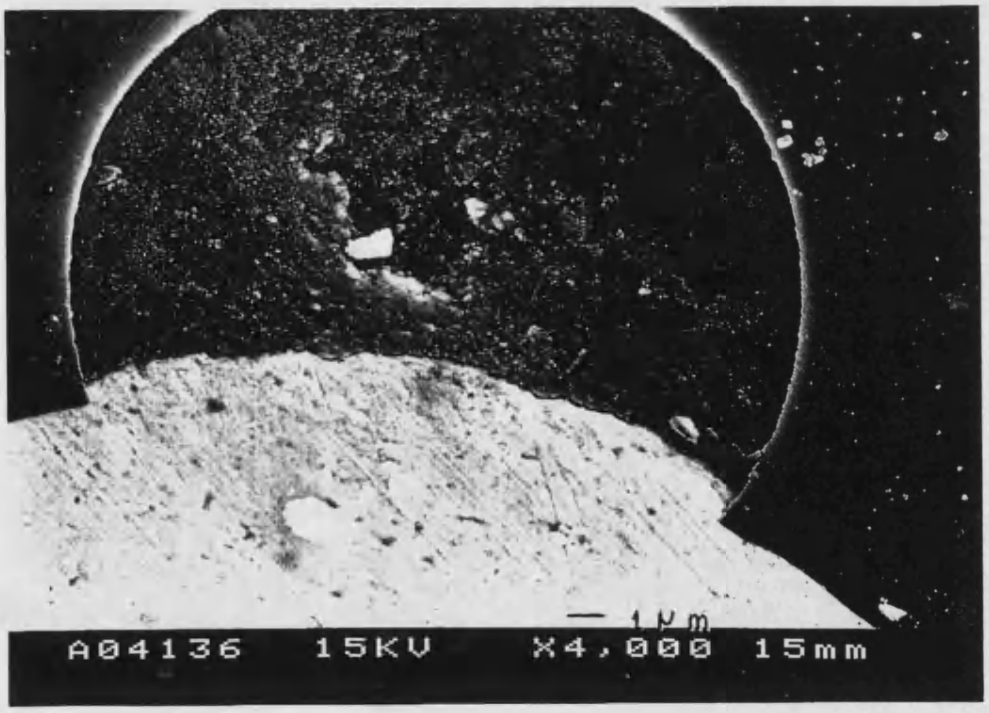

Figure 2.21b. gold-glass interface of a gold microelectrode prepared using a gold wire (60 μm diameter), showing bubble formation

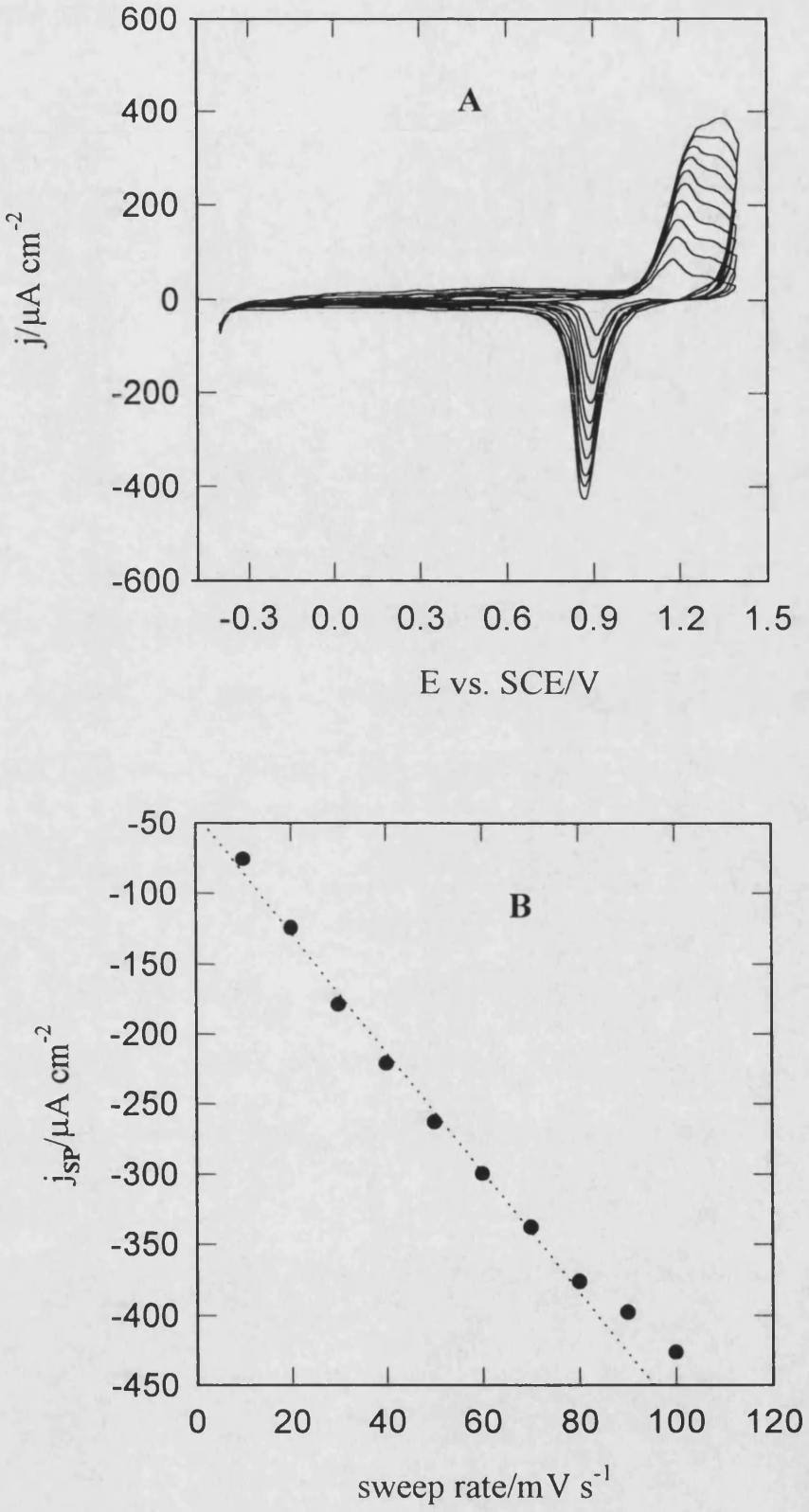

Fig 2.22. A) Cyclic voltammograms recorded at a gold ultramicroelectrode sealed i epoxy; 0.2 mol dm^{-3} $HClO_4$; υ=10, 20, 30, 40, 50, 60, 70, 80, 90, 100 mV s^{-1}; B) Current density (stripping peak) versus sweep rate plot from data in A.

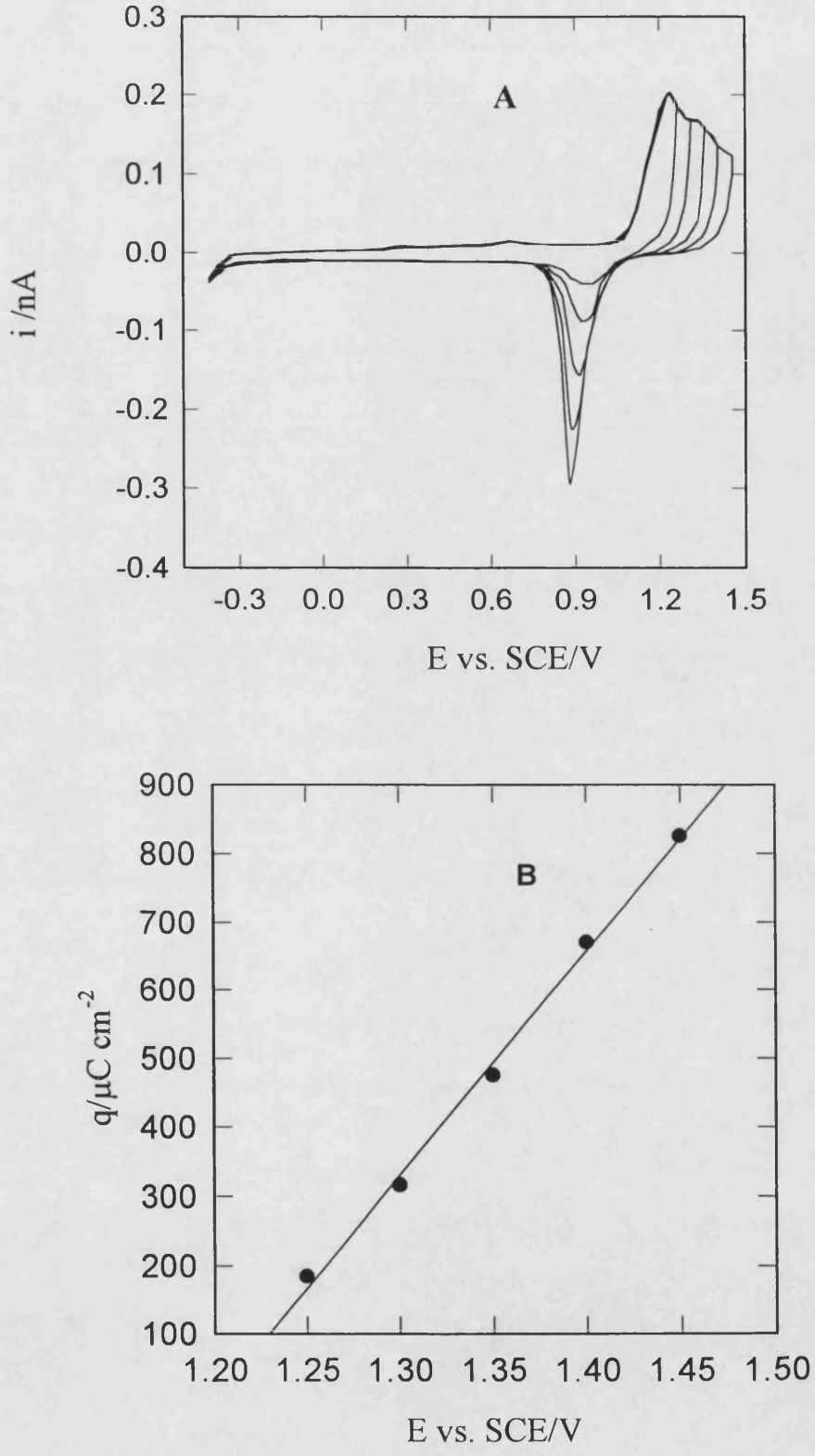

Figure 2.23. A) Cyclic voltammograms recorded at a gold microelectrode sealed in epoxy; ν=60 mV s^{-1}; B) Charge vs. potential plot from data in A.

2.4. *Conclusions.*

Electrochemical techniques for characterisation of the real area, and apparent radius of ultramicroelectrodes must be accompanied with scanning electromicroscopy measurement, for determining the real shape of the surface, and for obtaining complete information about the quality of the seal at the electrode material-insulator material interface.

Carbon fibres chemically modified in conc. HNO_3, can be used for the fabrication of carbon ultramicrodiscs with a good quality seal. This type of modification offers some advantages over other methods, in particular the absence of an organic-based epoxy or polymer coating permits its use without concern of electrode degradation or contamination of the system being studied.

The electrochemical characterization of platinum ultramicroelectrodes using the adsorption and desorption hydrogen method should be carried out at low scan rate (< 200 mV/s). At low scan rate, contamination of the solution due to very small amount of impurities can be detected, as a loss of the well defined hydrogen adsorption and desorption peaks. When, high sweep rate are employed (~100 V/s), the presence of these impurities is not readily detected.

The reproducible construction of well sealed gold ultramicroelectrodes using glass materials is not an easy task, because glass has a lower thermal expansion coefficient than gold. The use of an epoxy resin, which has a higher thermal expansion coefficient than glass appears to offer a simple, low cost and highly successful method for preparing gold ultramicroelectrodes.

References (Chapter 2)

1. R.N. Adams, Anal. Chem., **48**, (1976), 1126A
2. R.M. Wightman, Anal.Chem., **53**, (1981), 1125A
3. S. Pons, M. Fleischman, Anal.Chem., **59**, (1987), 1391A
4. R.M. Wightma, D.O. Wipf, *In Electroanalytical Chemistry*, Bard A.J., Ed; Dekker: New York, (1989), **15**, 267
5. P.A. Broderick, Electroanalysis, **2**, (1990), 241
6. R.M. Penner, M.J. Heben, N.S. Lewis, Anal. Chem., **61**, (1989), 1630
7. C. Lee, C.J. Miller, A.J. Bard, Anal. Chem., **63**, (1991), 78
8. N. Casillas, S.R. Snyder, H.S. White, J. Electrochem. Soc., **138**, (1991), 641
9. R.M. Penner, M.J. Heben, T.L. Longin, N.S. Lewis, Science, **250**, (1990), 1118
10. K.B. Oldham, J. Electroanal. Chem., **122**, (1981), 1
11. E. Katz, J.Electroanal.Chem., **291**, (1990), 257
12. M.L. Bower, J. Hefter, D.L., Digger, R. Wilson, Anal. Chim. Acta, **248**, (1991), 27
13. K.R. Kneten, R.L. McCreery, Anal. Chem., **64**, (1992), 2518
14. A. Oberlin, M. Guigon in: *Fibre Reinforcements for Composite Materials, Composite Material,s* Series Vol. 2, A.R. Bunsell (ed.), Elsevier, Amsterdam 1988, p.149
15. S.M. Lee (ed.), International Encyclopedia of Composites, Vol. 1, VCH Publishers, New York 1990, pp. 187-253
16. M. Irene Montenegro, M. Arlete Queirós and John L. Daschbach, *Microelectrodes: Theory and Applications*; Nato ASI Serie,1990, pp. 191
17. E. Theodoridou, J.O. Besenhard, H.P. Fritz, J. Electroanal. Chem., **124**, (1981), 87
18. R.E. Panzer, P.J. Elving, Electrochim. Acta, **20**, (1975), 635
19. T.G. Strein, A.G. Ewing, Anal. Chem., **64**, (1992), 1368
20. L. Nyholm, G. Wikmark, Anal. Chim. Acta, **257**, (1992), 7

21. G. Zhao, D.M. Giolando, J.R. Kirchhoff, Anal. Chem., **67**, (1995), 2592
22. K.K. Cline, M.T. McDermott, R.L. McCreery, J. Phys. Chem., **98**, (1994), 5314
23. L.J. Kepley, A.J. Bard, Anal. Chem., **60**, (1988), 1459
24. C. Barbero, J.J. Silber, L. Sereno, J. Electroanal. Chem., **248**, (1988), 321
25. J. Lipkowski, L. Stolberg, *in Adsorption of molecules at metal electrodes*, (Edited by J. Lipkoswki, and P.N. Ross), UCH, New York (1992).
26. M.D. Porter, T.B. Bright, D.L. Allara, C.E.D. Chidsey, J. Am. Chem. Soc., **109**, 1987, 3559
27. R. Wood, Electroanal. Chem., **9**, (1976), 1
28. A. Bewick and A.M. Tuxford, Symp. Farad. Soc., **4**, (1970), 114
29. A. Bewick and A.M. Tuxford, J. Electroanal. Chem., **47**, (1973), 255
30. J. Clavilier, J. Electroanal. Chem., **107**, (1980), 211
31. B.E. Conway, H.A. Kozlowska, Acc. Chem. Res., **14**, (1981), 49
32. H.Q.A. Laitinen, S.M. Chao, J. Electrochem. Soc., **108**, (1961, 726
33. W.R. Fawcett, Z. Kovacova, A.J. Motheo, C.A. Foss Jr., J. Electroanal. Chem., **326**, (1992), 91
34. James P. Hoare, J. Electrochem. Soc., **131**, (1984), 808
35. H. Angerstain-Kozlowska, B.E. Conway, Electrochim. Acta, **31**, (1986), 1051
36. S.B. Brummer, A.C. Makrides, J. Electrochem. Soc., **111**, (1964), 122

CHAPTER 3

ULTRAMICROELECTRODE STUDIES OF UNDERPOTENTIAL DEPOSITION

CHAPTER 3

ULTRAMICROELECTRODE STUDIES OF UNDERPOTENTIAL DEPOSITION

3.1. *Introduction.*

In the present work the underpotential deposition (*upd*) of lead on gold was used to characterise the real surface area of gold ultramicroelectrodes, prior to their use in kinetic studies. This chapter is concerned with the mechanism of the underpotential deposition and details how more information was obtained about the process using ultramicroelectrodes.

The deposition of metal atoms on a foreign metal electrode at a potential positive of the reversible bulk potential has been known for a long time [1]. The potential difference between the oxidation potential of a monolayer of metal deposited on an inert foreign metal substrate and the reversible Nernst potential (E_N) of the depositing metal in the same electrolyte, is called the underpotential shift, and the process itself, underpotential deposition. Different approaches have been described in the past for trying to explain the thermodynamics of underpotential deposition [2]. An activity of less than unity for the underpotential deposited phase has been considered in some cases to explain this process. The most important and direct thermodynamic information one obtains from experiments is that the chemical potential of the first monolayer (μ_{ML}), is markedly different from that of the bulk metal (μ_{metal}). The difference between these chemical potentials represents a direct measure of the difference in binding energies between a metal adatom (at a certain coverage) on the substrate and the same atom on the parent surface. This difference is independent of the metal ion concentration. To establish a quantitative description of underpotential deposition, the peak potentials of monolayer and bulk stripping peaks have been considered as the most suitable values for the difference in chemical potentials of monolayer and bulk deposits [2]. In the case of multiple peaks in the corresponding I-E curve, the position of the

most anodic (low coverage) peak is chosen as the stripping potential of the monolayer (E_{MLS}). The potential difference between bulk and monolayer stripping peaks is termed the underpotential shift or underpotential range, and it is defined as:

$$\Delta U = E_{MLS} - E_{bulk} \geq 0 \qquad (3.1)$$

This difference in chemical potentials between the monolayer and bulk metal has been related to work function differences between the two dissimilar metals [2]. The work function Φ of the metal is the energy required to remove an electron from the metal to charge free vacuum. According to experimental observations [2], the work function of the substrate must be higher than that of the adsorbate metal for *upd* to occur. In cases where the underpotential effect is not observed, the differences in work function are relatively small. Another closely related model of the adatom-substrate bond is that the charge transferred from the adatom to the substrate is proportional to the difference in their electronegativities. A linear correlation exists between Pauling's electro-negativity (χ_M) of a metal atom and the work function (Φ) of the same metal. The empirical formula is:

$$\chi_M = 0.5\Phi - \text{constant} \qquad (3.2)$$

where the constant value is 0.29 for sp metals and 0.55 for transition metals [3]. From the fact that differences in the electronegativities are linearly related to the work functions, the underpotential shift (ΔU) has been found to change linearly with the difference in work functions for the bulk substrate and bulk deposited metals [2]. This behaviour suggests that the covalent part of the adatom-substrate bond does not differ appreciably from the bond strength between the adatom and the surface of the same metal [2]. However it is necessary to point out that this good linear correlation between substrate and monolayer exists as long as no complications, such as alloy formation, arise.

The *upd* process extends from a few millivolts to several hundred millivolts, depending on the strength of adsorbate substrate interactions, i.e. on the system studied. The so-called underpotential range (ΔU) has been demonstrated to depend strongly on the crystallographic orientation of the substrate, and thus the underpotential deposition of metals on foreign metal surfaces has a multiple-state character [2].

Upd is a complex process consisting of several phenomena. The first of these is transport of the metal ions from the bulk of the solution to the substrate surface. The second is charge transfer, and finally the adsorption of the discharged metal on one or more adsorption sites of the substrate metal surface. However, the adsorption step may precede charge transfer. Adsorption of the metal ions on the substrate, where chemical or physical bonds can be formed between the ions, the surrounding solution components and the metal lattice of the substrate, can take place in the *upd* region [2,4,5] before charge transfer occurs. In aqueous solutions, the ions of the depositing metal (M^{Z+}) penetrate into the double layer to make direct contact with the substrate metal (S) [5]. During this process adsorbed water molecules are removed from the surface of the substrate metal, and the solvation shell of the depositing ions will be partly or completely destroyed [5]. Depending on the chemical nature of the interaction between adsorbent (S) and adsorbate (M^{Z+}), a purely physical bond or a much stronger chemical bond is formed. It has also been found that the *upd* of a foreign metal on a well defined substrate is strongly affected by the type of solvent and supporting electrolyte utilised. The use of solvents of low dielectric constant produces different cyclic voltammetric curves in the *upd* region for a specific foreign metal on a specific substrate [6]. This behaviour has been attributed to extensive ion pairing both at the interface and in the bulk solution.

The presence of anions like Cl^- and SO_4^{2-} in the supporting electrolyte has a strong effect on the potential region where deposition/stripping of the foreign metal occurs and on the reversibility of the reaction [7,8]. This behaviour has been attributed to the coadsorption of these anions together with the foreign metal. This coadsorption may also influence the number of atoms deposited [9] as well as the

charge transferred to the deposited foreign metal [9,10]. If a chemical bond is formed, a partial charge transfer of λ electrons will take place from the substrate metal to the depositing ions [11]. According to the formalism originally introduced by Schultze and Vetter [5], *upd* in aqueous solutions may be described by the following equation:

$$\nu S - OH_2 + M^{z+}.aq + \lambda e^- \leftrightarrow S_\nu - M_{ads}{}^{(z-\lambda)+} + \nu H_2O.aq \qquad (3.3)$$

where M^{Z+}.aq is a metal (M) ion of charge z^+ solvated by solvent (aq) molecules; S are adsorption sites covered with solvent molecules, ν is the number of surface sites occupied by one metal ad-ion, λe^- is the charge transferred from the electrode to the species M^{Z+} upon adsorption. This formal analysis suggests that the magnitude of (z-λ) will modify the state of solvation of the adsorbed metal species and therefore the overall energetics and kinetics of the *upd* process. The partial charge transferred is defined by the difference between the ionic charge of the adsorbing ions (z) and the actual charge of the deposited metal atoms (z_{ads}), according to the following equation:

$$\lambda = z - z_{ads} \qquad (3.4)$$

The partial charge on adsorbed metal atoms is usually small and cannot be determined experimentally [5]. When a physical bond is formed and the ionic charge on the adsorbed metal atoms is low ($z_{ads} \approx 0$), the adsorption behaviour of M^{Z+} can be described by Nernst equation:

$$E = E_o + \frac{RT}{zF} \ln \frac{a_m{}^{z+}}{a(\Gamma)} \qquad (3.5)$$

where the activity of the M_{ads} adsorbate (a(Γ)) represents the system-specific type of isotherm as a function of Γ only, where Γ is the surface coverage.

It has been found that some metals can undergo partial discharge on the electrode surface in the *upd* region [4,6]. Some hint of a macroscopic partial charge for adsorbates like Pb^{2+} on gold substrates has been reported in the past [12,13]. This behaviour may produce changes in the solvation characteristics of the adsorbed species as was mentioned before. However, Conway et.al [14] have found very small differences for the *upd* of Pb on polycrystalline gold electrodes in water, methanol and acetonitrile solutions, which means that the *upd* of Pb on Au is largely independent of the nature of solvents with high dielectric constants. The following schemes (**figure 3.1 and figure 3.2**) summarise the phenomena involved in the *upd* process, taking into account chemical bonding, physical bonding and coadsorption of anions from the supporting electrolyte

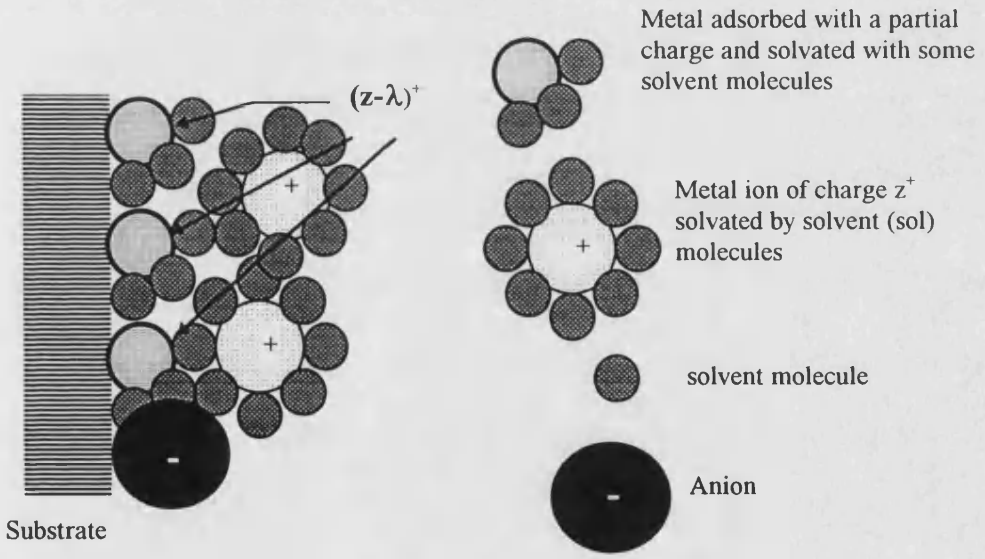

Figure 3.1. Schematic representation of the *upd* process when a chemical bond is formed between the metal ion and the substrate.

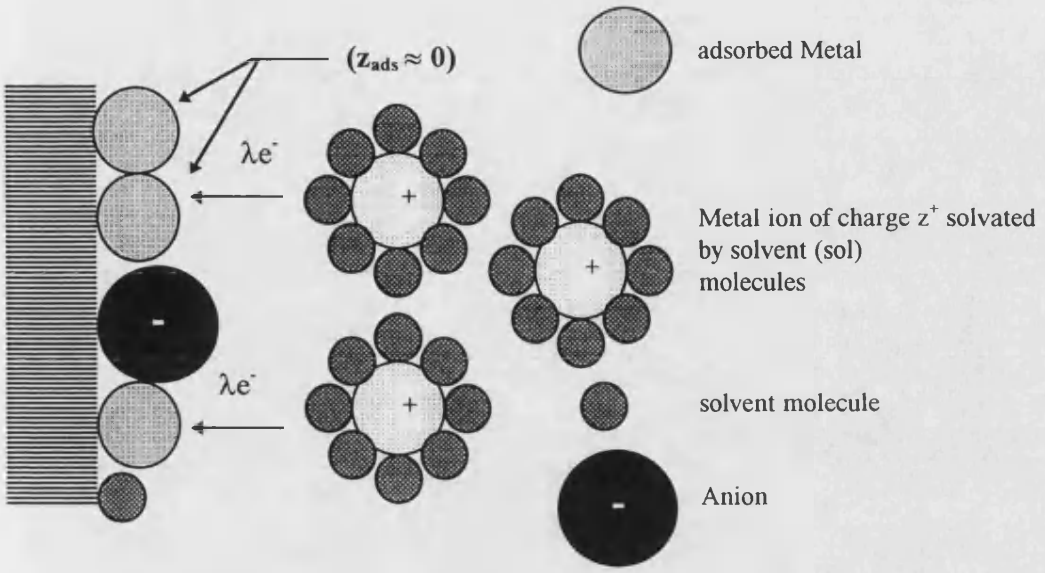

Figure 3.2. Schematic representation of the *upd* process when a physical bond is formed between the metal ion and the substrate and $Z_{ads} \approx 0$.

The description of the *upd* process is complicated by the fact that when chemical bonds are formed between the substrate and adsorbate, changes in the state of charge of the adsorbed species can occur when the potential is driven to more negative potentials. Surface diffusion of M_{ads} as well as electrostatic repulsion between adsorbed atoms is another phenomenon which can play an important role in *upd*.

Although there has been considerable research on the *upd* of different systems, several crucial problems remain to be resolved. There is no clear agreement on the extent of the partial charge on the deposited atoms, nor has it been clearly established whether a two-dimensional phase is formed at any stage in the deposition process. Moreover, there is still a controversy regarding the mechanism of the *upd* process in some systems [15,16].

Different techniques have been used for studying the *upd* of metals. An abundant literature exists for the investigation of the structure and structural transformation of the metal deposited by using electrochemical [15,17,18], and *in*

situ surface techniques [19-22]. It has been known for a long time that the modification of electrode surfaces by using *upd* to produce a monolayer of a foreign metal [2,23] may increase reaction rates for oxidation and reduction of small molecules. *Upd* monolayers or submonolayers of Pb adatoms, act as catalysts for the electroreduction of both H_2O_2 and O_2 to H_2O in both acid and basic environments [24,25].

The formation of adsorbed metal monolayers on foreign metal substrates is usually carried out in very dilute solutions of the ions to be deposited, so that mass transport has a profound effect on the kinetics of the *upd.* The main characteristic of *upd* processes is that the formation or desorption of the monolayer occurs in a number of usually easily resolvable stages over a potential range characteristic of both the adsorbate and adsorbent. This behaviour can in principle be used to determine the active surface of the electrode. The amount of metal deposited at a certain potential can be obtained from the corresponding charge by scanning the potential positive and integrating the current caused by oxidative desorption of the deposit, with subtraction of the contribution due to double layer charging. In the present work it was envisaged that this behaviour could be employed for determining the real surface area of an ultramicroelectrode.

One of the simplest and yet most powerful techniques often used for *upd* studies is cyclic voltammetry, utilising electrodes of conventional size and rotating ring disk electrodes [17,26]. Potentiostatic or galvanostatic pulse measurements have also been used for studying the kinetics of *upd* [16,27].

The use of gold ultramicroelectrodes in *upd* studies has not previously been reported in the literature. Although it is obvious that measurements of monolayer coverage charges on a polycrystalline surface have the disadvantage of representing an average over all bonds formed on a rather heterogeneous surface, large atoms can form a close packed monolayer at high coverage [2], with a surface concentration independent of the substrate structure. Atomic scale analysis of the Pb *upd* process by surface X-ray scattering (SXS) measurements [28], showed that the *upd* of Pb forms a hexagonal close packed monolayer. The *upd* literature for Pb on gold is somewhat contradictory. Some authors [29,30], have reported that Pb

does not form an alloy with gold, while other authors [31] have found that the formation of an alloy is possible in the *upd* region. As was mentioned in the first and second chapters, the *iR* drop when ultramicroelectrodes are used is very small and the charging current is negligible, which permits a study of *upd* at low concentrations of the metal to be deposited. It follows that the use of these small electrodes can contribute to a more detailed understanding of the mechanism of the *upd* of Pb on gold. In the present work, the *upd* of Pb on gold ultramicrodisks (10 μm diameter) was investigated by cyclic voltammetry and chronoamperometry, using dilute solutions of Pb^{2+} in 0.2 mol.dm^{-3} $HClO_4$.

3.2. *Experimental.*

Gold ultramicroelectrodes were prepared according to the method explained in chapter 2. The cyclic voltammetry and chronoamperometry experiments were carried out with the electronic equipment also reported in chapter 2. The *upd* of Pb on gold was investigated using different concentrations of Pb^{2+} in 0.2 mol.dm^{-3} $HClO_4$. Before carrying out each experiment, the solution was deoxygenated by passing N_2 gas for 15 min and the ultramicroelectrodes were electrochemically treated by cycling between 0 and 1.45 V in 0.2 mol dm^{-3} $HClO_4$. The experiments were started at a potential which was positive of the underpotential region but negative of the oxygen chemisorption region. Electrode potentials were measured vs. SCE. All experiments were carried out at room temperature in an earthed Faraday box.

3.3. *Results and discussion.*

3.3.1. *Cyclic voltammetry experiments*

Several experiments were carried out in an attempt to obtain reproducible voltammograms in the *upd* region under well-defined experimental conditions. It was found that the experimental behaviour is considerably affected by the method used to clean the ultramicroelectrode surface. It was also clearly observed that the experimental behaviour of the *upd* of Pb is strongly influenced by the concentration of Pb^{2+} cations present in the bulk solution. **Figure 3.3** shows the cyclic

voltammograms obtained at two different concentrations of Pb^{2+}. Different stages of the process of adsorption and desorption of the monolayer are observed when the concentration of Pb^{2+} is changed from $8x10^{-6}$ to $8x10^{-5}$ mol dm^{-3}. A shift of the monolayer stripping peak (A') towards a more positive potential is observed when the concentration is raised from $8x10^{-6}$ to $8x10^{-5}$ mol dm^{-3}. **Figure 3.4** shows the family of voltammograms obtained for a solution of $8x10^{-5}$ mol dm^{-3} Pb^{2+} in 0.2 mol dm^{-3} $HClO_4$, when the cathodic potential limit is changed in 50 mV steps from -0.4 to -0.65V vs SCE, using a sweep rate of 60 mV/s.

The inhibition of the hydrogen evolution reaction by Pb^{2+} *upd* is observed in this figure when a comparison is made with the voltammogram obtained for the supporting electrolyte alone. The different peaks observed are labeled A, A', B, B', C, C' and D. When the cathodic potential is decreased to values more negative than -0.4V, another peak (peak D) begins to appear in the anodic direction and rises quickly with potential. This peak was attributed to the oxidation of the bulk lead deposit. The difference between the bulk (D) and monolayer (A') stripping peaks is 0.40V. This value is in agreement with the value reported by Bruckenstein [26] and Schmidt [32]. The peaks B' and C' could be related to changes in the structure of the adsorbed atoms to allow the accommodation of more Pb on the Au microsurface [2]. However *upd* studies carried out in aqueous solutions of Pb^{2+} with conventional electrodes or rotating disk electrodes have attributed the peak observed between -0.35 and -0.25V vs SCE in the anodic direction to a phase transition attended by a change in the state of charge within the adsorbed layer, which produces condensation into patches of predominantly metallic character. This behaviour is characterised by quite a sharp peak in both directions (cathodic and anodic) in the voltammetry curves which also proves that the process is not under diffusion control [7]. This was not found in the present study using a gold ultramicroelectrode. The characterisation of the real surface area of the gold ultramicroelectrode was carried out by assuming that the Pb atoms, being large, can form a close packed monolayer at high coverage, with a surface concentration independent of the substrate structure [2]. The quantity of Pb(0) which constitutes a monolayer coverage on polycrystalline gold was calculated assuming a hexagonal

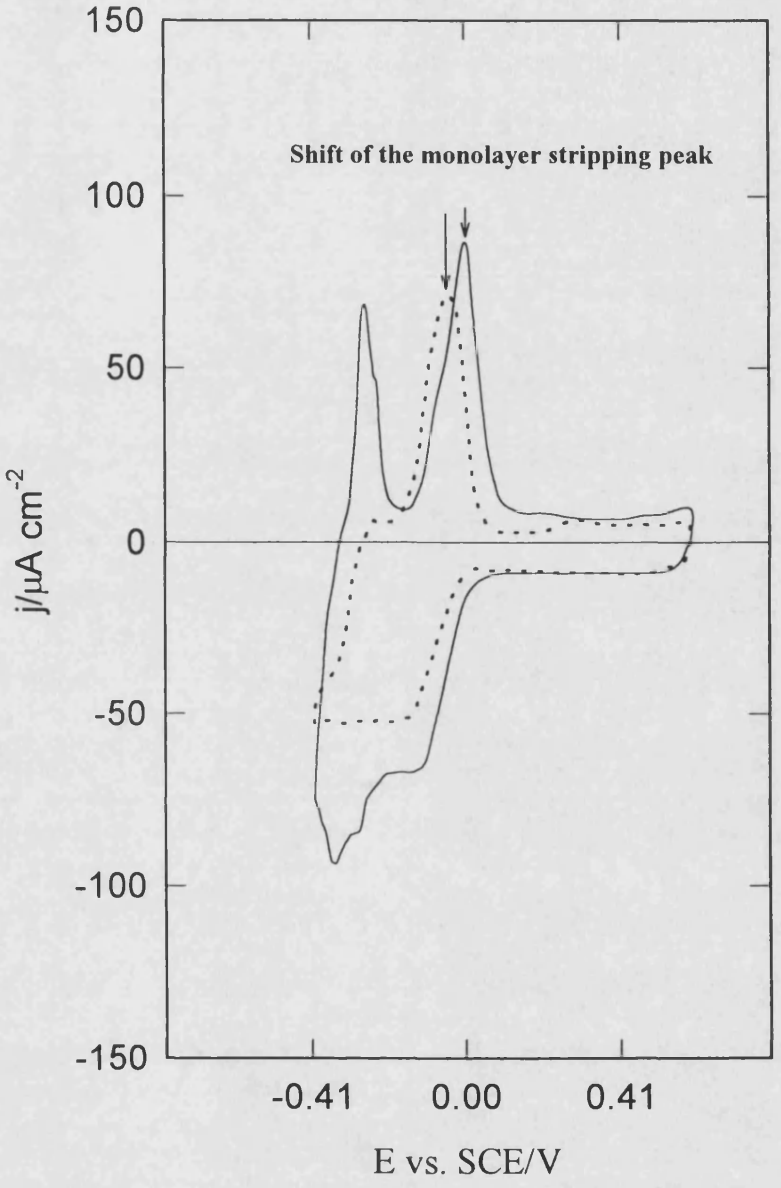

Figure 3.3. Cyclic voltammograms recorded at a gold ultramicroelectrode sealed in epoxy (10 μm diameter) from 0.6 V to the *upd* region in ---- $8x10^{-6}$ mol dm^{-3} $Pb(NO_3)_2$ and — $8x10^{-5}$ mol dm^{-3} $Pb(NO_3)_2$ + 0.2 mol dm^{-3} $HClO_4$; ν =60 mV s^{-1}

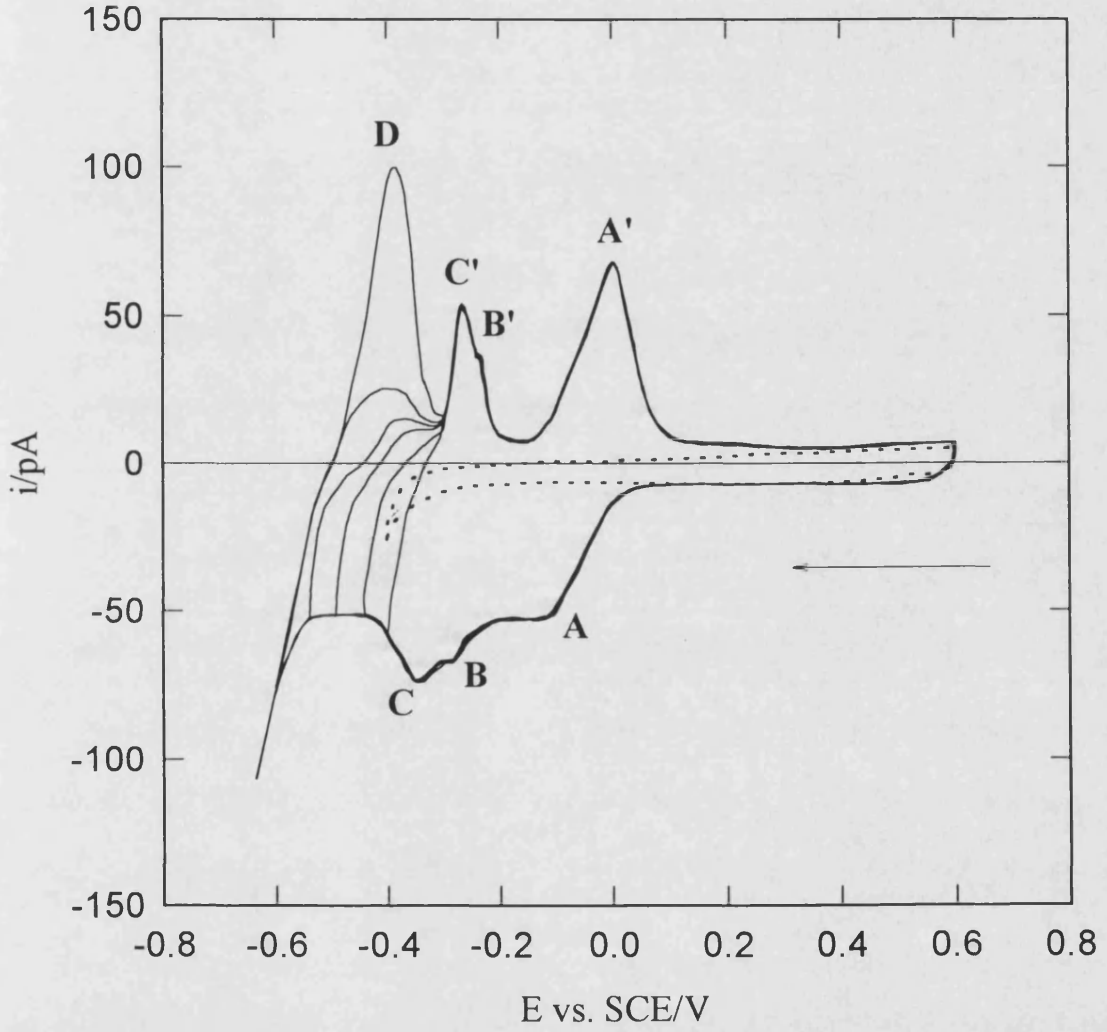

Figure 3.4. Family of voltammograms recorded at a gold ultramicroelectrode from 0.6 V to more negative potentials in the *upd* region:— Solution $8x10^{-5}$ mol dm^{-3} $Pb(NO_3)_2$ + 0.2 mol dm^{-3} $HClO_4$; ----- only supporting electrolyte; ν = 60 mV s^{-1}.

close packed structure, **(figure 3.5)**:

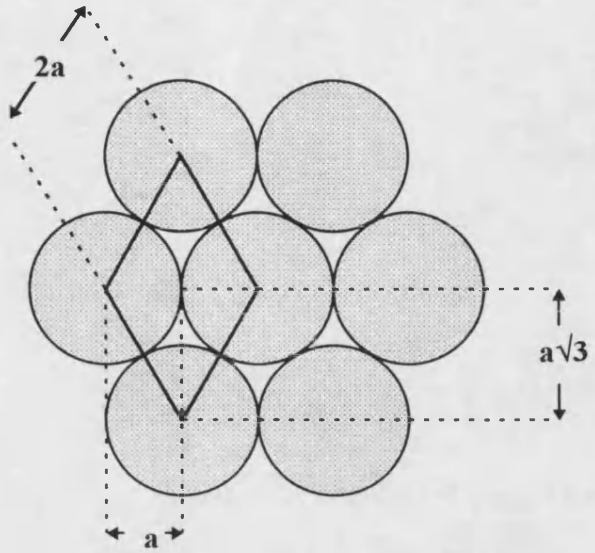

Figure 3.5. Hexagonally close-packed monolayer of Pb on a gold substrate.

In this figure, it is seen that each Pb atom has six other Pb atoms touching it. The area occupied by 1 atom corresponds to the area of the parallelogram shown in figure 3.5, and is given by:

$$A_{atom} = 2a^2\sqrt{3} \tag{3.6}$$

where, a is the Pb metallic radius, which equals 1.75 Å [33]. Assuming 2 electrons per atom, the charge per unit area of lead monolayer will be:

$$Q_{monolayer} = \frac{2xq}{A_{atom}} = 302\mu C / cm^2 \tag{3.7}$$

where q is the elementary charge of an electron. The experimental charge was determined by integration of the i vs E curve, with allowance for double layer charging. The real area of the gold ultramicroelectrode was then calculated using the equation:

$$A_{real} = \frac{Q_{exp}}{Q_{monolayer}} \qquad (3.8)$$

where Q_{exp} is expressed in μC. The electrode area was found to be (7.0± 0.2) x10^{-7} cm^2 for a series of experiments in which Q_{exp} was determined from the anodic charge. This experimental charge was determined in the potential range of -0.4 to 0.6 V vs. SCE. The roughness factor was always less than 1. When the electrode area was determined using the cathodic charge a value of (9.3 ± 0.4)x10^{-7} cm^2 was found. This represent a roughness factor of 1.14 ± 0.01. It was observed that the anodic charge/cathodic charge ratio was 0.77 in most of the experiments carried out where the concentration of Pb^{2+} was 8x10^{-5} mol dm^{-3}. This value shows that other processes may be taking place which hinder the stripping.

Experiments carried out in aqueous solutions of Pb^{2+}, with concentrations ≤1x10^{-5} mol.dm^{-3} show a broad plateau in the cathodic direction and two broad peaks in the anodic direction in the underpotential region. **Figure 3.6** shows the voltammogram obtained under these conditions. In the potential region between 0 and -0.4V vs SCE, a well defined mass transfer limited plateau is observed in the cathodic direction and two peaks, one at -0.04V (peak A'), and another at -0.25V (peak B') in the anodic scan. The steady state diffusional plateau observed was used for determining the radius of the gold ultramicrodisc, according to equation (2.5). Although the value obtained in some experiments was in good agreement with the value of 5 μm as specified by the manufacturer, lack of reproducibility of these experiments suggest that alloy formation is taking place.

Figure 3.7 shows the family of voltammograms obtained when the anodic scan rate was maintained constant and the cathodic sweep rate was decreased from 100 to 5 mV/s. It was observed that charge under peak B' increases faster than the charge under peak A' and a new peak, F, starts to grow when the cathodic sweep rate is < 20 mV/s. The increase of peak B' could be attributed to two different factors. First, when the cathodic sweep rate is low, the surface concentration of Pb^{2+} is higher because more Pb^{2+} cations can reach the microdisk when the experimental time for the potential scan is longer. Consequently, there is an increase in the coverage of the microsurface

with Pb^{2+}, which can produce changes in the structure of the adsorbed atoms to allow more Pb to be accommodated on the surface. These changes in the structure could be accompanied by changes in the state of charge within the adsorbed layer permitting condensation into patches of predominantly metallic character. If this is the case, the *upd* of Pb^{2+} is controlled by the rate of diffusion of Pb^{2+} to the microdisc. However, the unequal cathodic and anodic charges, the lack of a reproducibility of the experiments and the appearance of the peak F could be attributed to the formation of alloys in the *upd* region. If alloy formation is occurring, it should be enhanced at low sweep rates. Different Pb/Au alloys formed during the cathodic scan can then be dissolved in the anodic direction, and the increase of peak B and the appearance of the peak F at a more positive potential than the stripping monolayer potential, when the scan rate is decreased to < 20 mV/s, could be attributed to the stripping of one type of alloy formed below the lead monolayer.

Figure 3.8 shows the $Q_{anodic}/Q_{cathodic}$ charge ratio vs. sweep rate $_{anodic}$/ sweep rate $_{cathodic}$ ratio from the data in **figure 3.7**. It was observed that when the cathodic sweep rate is decreased whilst maintaining the anodic sweep rate constant, the $Q_{anodic}/Q_{cathodic}$ charge ratio decreases. This behaviour shows that the cathodic charge is inversely proportional to sweep rate which indicates that alloy formation is enhanced under these conditions.

3.3.2. *Potential step experiments.*

Current-time curves were obtained for a single potential step from an anodic starting potential to the *upd* region. Experiments were carried out at different concentrations of Pb^{2+}. The transients show a shoulder superimposed on the falling curve when the potential was stepped into the *upd* region.

Figures 3.9a and **3.9b** show the behaviour of the current vs time when the concentration of Pb^{2+} was $8x10^{-6}$ mol.dm^{-3} and $8x10^{-5}$ mol dm^{-3} respectively. When the potential is decreased between the underpotential range the formation of a Pb monolayer is enhanced. It was observed that the shoulder appears at longer times when the concentration of Pb^{2+} is lower. In the case of a metal adsorbate, the appearance of non-monotonic flux-time transients under potentiostatic step polarisation conditions has been attributed to a two dimensional nucleation growth mechanism [34,35], or to

nucleation-free adsorption controlled by diffusion and/or charge transfer only [36]. The relative rates of mass transport, surface diffusion or bulk diffusion, and lattice growth are important factors in determining the behaviour of the shoulder observed in these transients. The appearance of the shoulder in the transients recorded under the experimental conditions mentioned before could be attributed to the formation of a monolayer of Pb(0). A complete monolayer of Pb atoms on gold is equivalent to 302 $\mu C/cm^2$, when this metal forms a hexagonal closed packed monolayer. Figures **3.10a** and **3.10b** show a family of charge vs time plots obtained from data in figure **3.9a** and **3.9b**. It is seen that a complete monolayer is formed just when the shoulder appears in the transients of current density vs. time. The appearance of the shoulder at different times in the transients when the concentration of the Pb^{2+} ions is changed can be explained if it is considered that the *upd* process is controlled by diffusion of the Pb^{2+} ions to the surface. A monolayer is formed more quickly when the concentration of Pb^{2+} ions is increased.

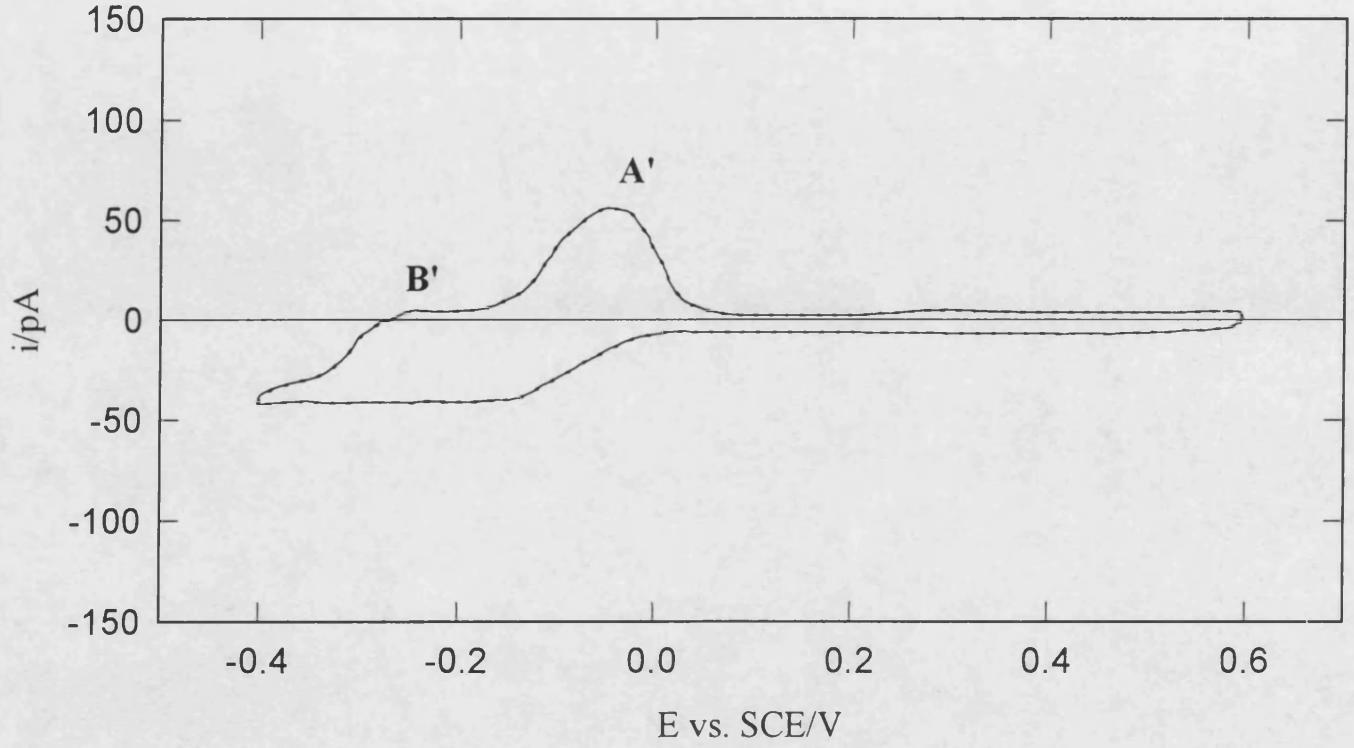

Figure 3.6. Cyclic voltammogram recorded at a gold ultramicroelectrode sealed with epoxy (10 μm diameter) from 0.6 V to the *upd* region in $8x10^{-6}$ mol dm^{-3} $Pb(NO_3)_2$ + 0.2 mol dm^{-3} $HClO_4$; ν =60 mV s^{-1}

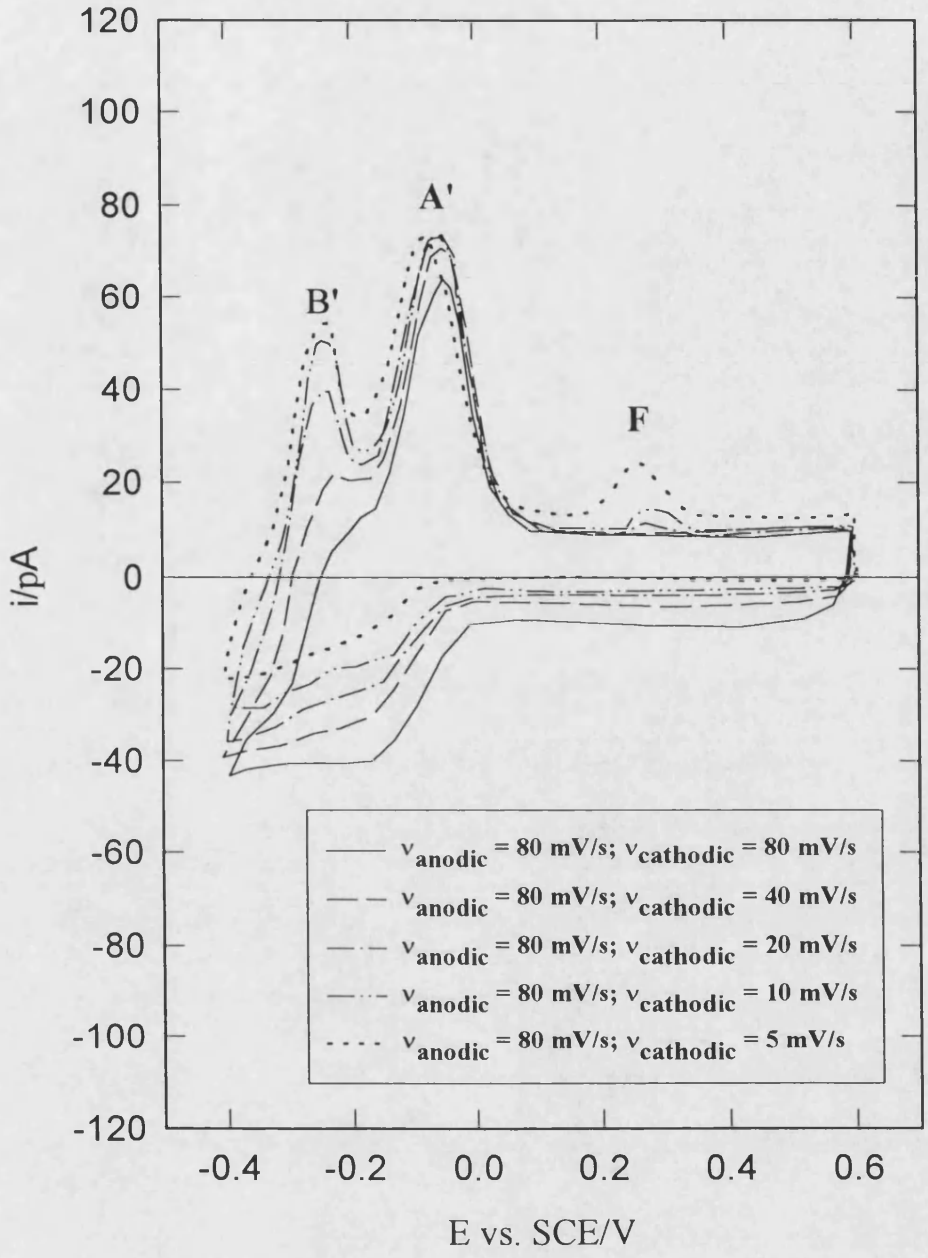

Figure 3.7. Cyclic voltammograms recorded at a gold ultramicroelectrode changing the cathodic sweep rate but with a constant anodic sweep rate; Solution $8x10^{-6}$ mol dm^{-3} $Pb(NO_3)_2$ + 0.2 mol dm^{-3} $HClO_4$

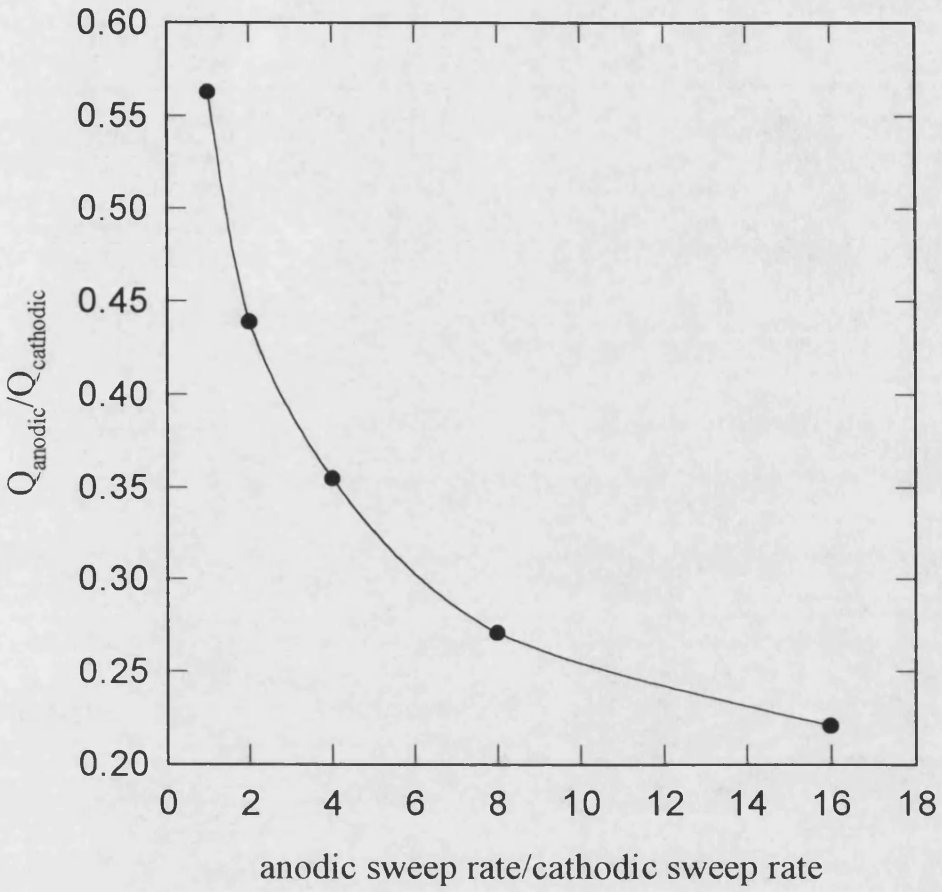

Figure 3.8. $Q_{Anodic}/Q_{Cathodic}$ vs. sweep rate $_{anodic}$/sweep rate $_{cathodic}$ from data figure 3.7

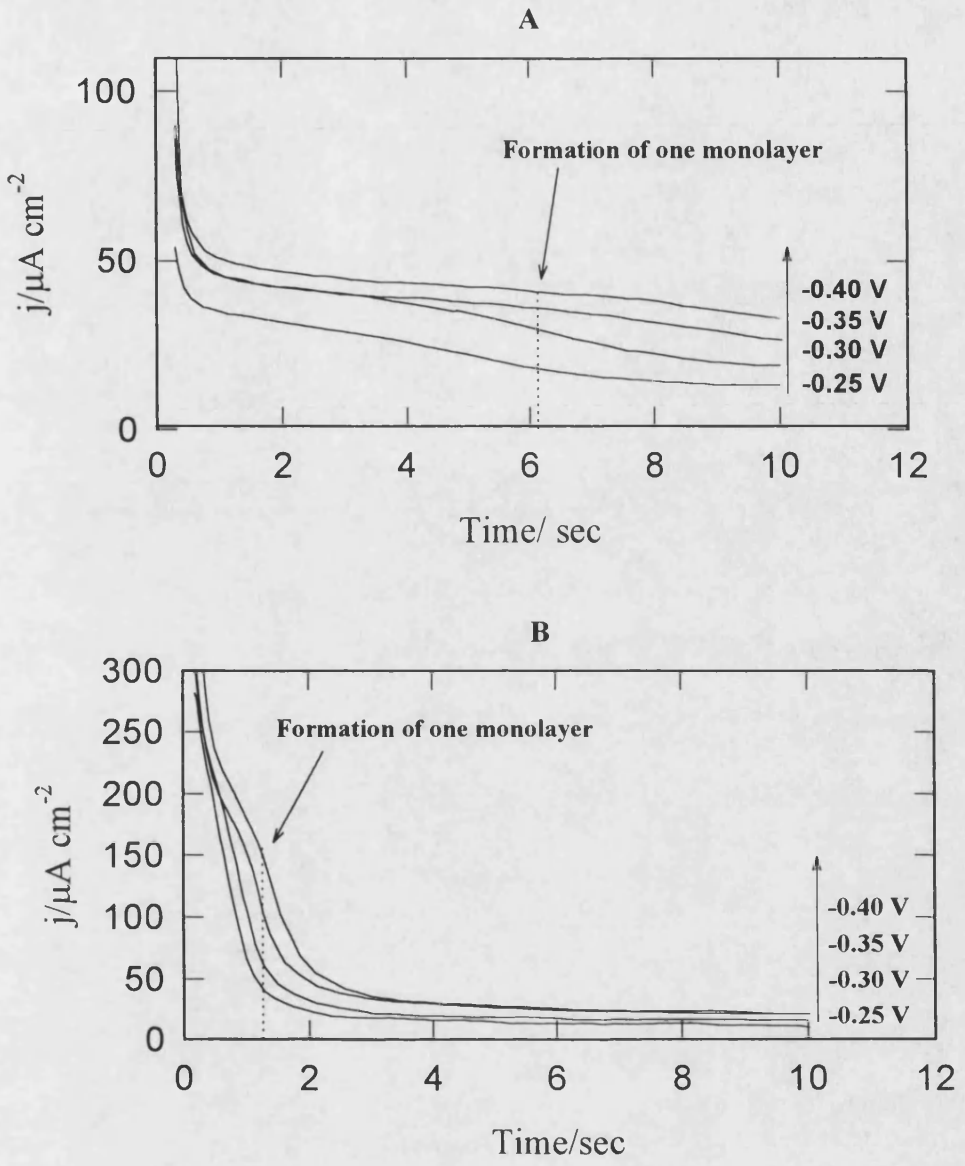

Figure 3.9. Current density vs time plots in the underpotential deposition (upd) region for: A) $8x10^{-6}$ mol dm^{-3} Pb^{+2}; B) $8x10^{-5}$ mol dm^{-3} Pb^{+2} in 0.02 mol dm^{-3} $HClO_4$ using a gold ultramicroelectrode.

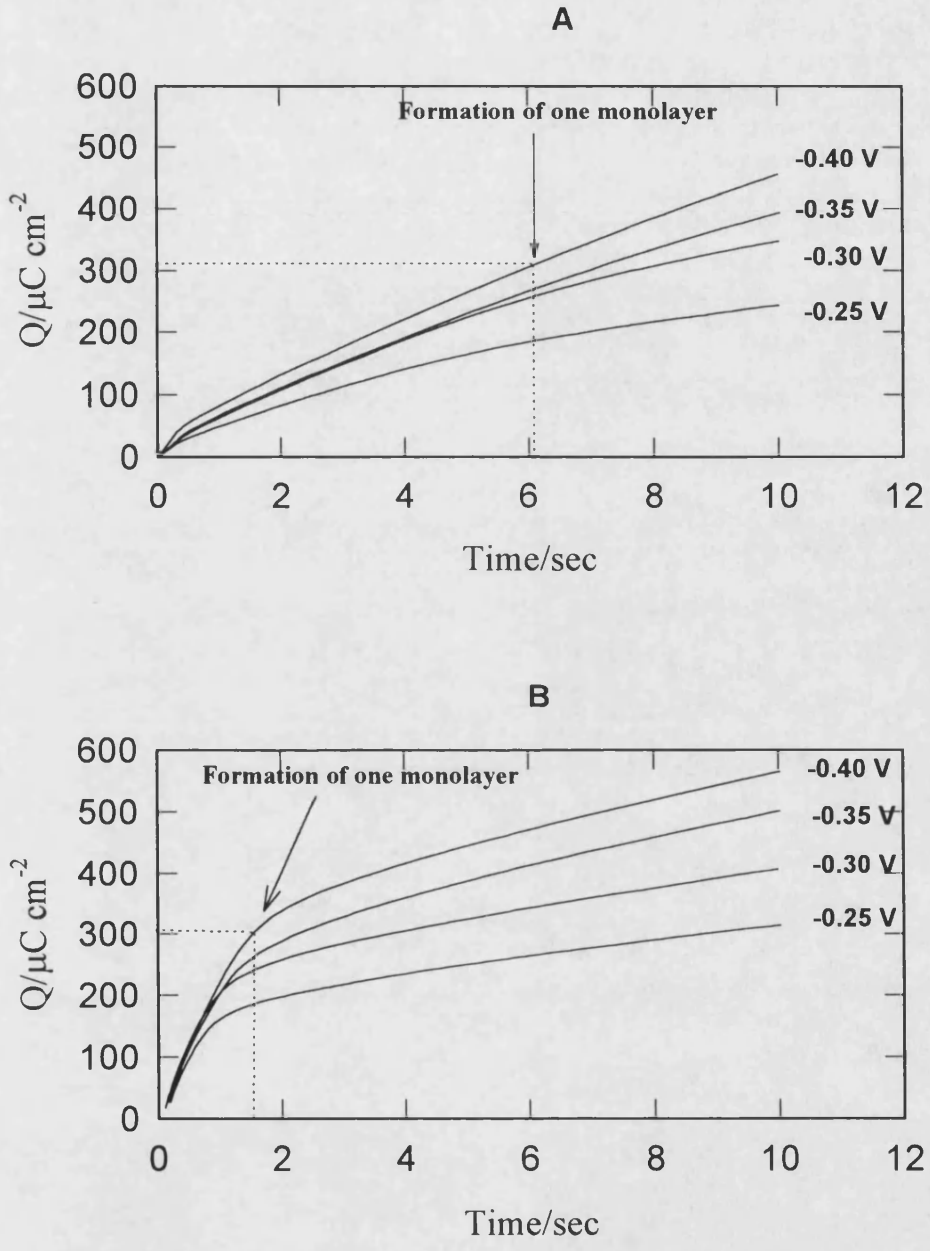

Figure 3.10. Charge density vs time plots in the underpotential deposition (upd) region for: A) $8x10^{-6}$ mol dm^{-3} Pb^{+2}; B) $8x10^{-5}$ mol dm^{-3} Pb^{+2} in 0.02 mol dm^{-3} $HClO_4$ using a gold ultramicroelectrode.

3.4. *Conclusions.*

The underpotential deposition (*upd*) of Pb(0) on gold occurs between 0V>E>-0.4V vs SCE.

Determination of real surface area of the gold ultramicroelectrodes from the charge of the monolayer deposited in the *upd* region or from the mass transfer limited plateaus is hindered by the formation of alloys.

The results show that a monolayer of lead and Au-Pb alloys are formed simultaneously in the *upd* region. When the concentration of Pb^{2+} is $\geq 8x10^{-5}$ $mol.dm^{-3}$, the formation of a monolayer of lead on the gold ultramicroelectrode occurs faster than when $C_{Pb}^{2+} \leq 8x10^{-6}$ $mol.dm^{-3}$. This shows that the formation of *upd* is controlled by diffusion. Under conditions where $C_{Pb}^{2+} \leq 8x10^{-6}$ $mol.dm^{-3}$, the formation of alloys is enhanced. Holding the ultramicroelectrode at potentials anodic of the equilibrium reduction potential for the metal/metal ion couple for a long time enhances the alloy formation.

The results of the chronoamperometry experiments demonstrate that the formation of a complete monolayer can be related to the appearence of a non-monotonic current-time transient. Formation of a second monolayer may also occur. However, due to the complications associated with formation of the alloy, further work would be required to characterise the system fully.

References (Chapter 3)

1. M. Haissinsky, J. Chim.Phys., **30**, (1933), 27
2. D.M. Kolb, *in Advances in Electrochemistry and Electrochem. Engineering* (Edited by H. Gerischer and C.W. Tobias), Wiley, New York (1978), Vol 11, p125
3. S. Trasatti, J. Electroanal. Chem., **33**, (1971), 351
4. G. Salie, K. Bartels, Electrochim.Acta, **39**, (1994), 1057
5. J.W. Schultze, K.J. Vetter, J. Electroanal. Chem., **44**, (1973), 63
6. X.K. Xing, I.T. Bae, D.A. Scherson, Electrochim. Acta, **40**, (1995), 29
7. G.M. Brisard, E. Zenati, H.A. Gasteiger, N.M. Marcovic, P.N. Ross, Langmuir **11**, (1995), 2221
8. G. Horanyi, J.Electroanal. Chem., **55**, (1974), 45
9. Z. Shi, J. Lipkowski, J. Electroanal. Chem., **365**, (1994), 303
10. P.N. Ross, N.M. Marcovic, Langmuir, **10**, (1994), 976
11. S. Szabó, Int. Rew. Phy. Chem., **10**, (1991), 207
12. R. Adzic, E. Yeager, B.D. Cahan, J. Electrochem. Soc., **121**, (1974), 474
13. J. Harkans, B.D. Cahan, E. Yeager, J. Electrochem. Soc., **122**, (1975), 1585
14. B.G. Conway, K. Tellesfson, S. Marshall, *in Proceeding of the Symposium on the Chemistry and Physics of Electrocatalysis*, E CS, Princeton, N.J., 1984, p15
15. A. Bewick, B. Thomas, J. Electroanal. Chem., **65**, (1975), 911
16. W.J. Lorenz, H.P. Hermann, N. Wuthrich, F. Hilbert, J Electrochem. Soc., **121**, (1974), 1167
17. M. Seo, M. Aomi, K. Yoshida, Electrochim. Acta, **39**, (1994), 1039
18. W. Vissher, A.P. Cox, Electrochim. Acta, **37**, (1992), 2245
19. R.J. Nichols, D.M. Kolb, R.J. Behm, J. Electroanal. Chem., **313**, (1991), 109
20. C.H. Chen, N. Washburn, A.A. Gewirth, J Phys. Chem., **97**, (1993), 9754
21. J.F. Rodriguez, D.L. Taylor, H.D. Abruna, Electrochim. Acta, **38**, (1993), 235
22. M.P. Green, K.J. Hanson, D.A. Scherson, Y. Xing, M. Richter, P.N. Ross, R. Carr, I. Lindau, J Phys. Chem., **93**, (1989), 2181

23. R. Adzic, *in Advances in Electrochemistry and Electrochemical Engineering*; (Edited by Gerischer H., Tobias C.W.), Eds., Wiley-Intercence: New York 1984; Vol 13, pp 159
24. R. Parsons, G. Picq, P. Vennereau, J. Electroanal. Chem., **181**, (1984), 267
25. M. Alvarez-Rizatti, K. Juttner, J. Electroanal. Chem., **144**, (1983), 351
26. V.A. Vicent, S. Bruckenstein, Analytical Chem., **45**, (1973), 2036
27. A. Bewick, B. Thomas, J. Electroanal. Chem., **85**, (1977), 329
28. R.R. Adzic, J. Wang, C.M. Vitus, B.M. Ocko, Surf. Sci., **293**, (1993), 876
29. E. Schmidt, H.R. Gygax, J. Electroanal. Chem., **13**, (1967), 378
30. H.J. Pauling, K. Juttner, Electrochim. Acta, **37**, (1992), 2237
31. H.J. Schmidt, V. Pittermann, H. Scheider, K.G. Weil, Analytical Chim. Acta, **273**, (1993), 561
32. E. Schmidt, N. Wuthrich, J. Electroanal. Chem., **34**, (1972), 377
33. E. Teatum, K. Gschneidner K., Waber J., " Compilation of calculated data useful in predicting metallurgical behaviour of the elements in binary alloy system ", (1960), LA-2345, Los Alamos Scientific Laboratory
34. A. Bewick, M. Fleischmann, H.R. Thirsk, Trans. Faraday Soc., **58**, (1962), 2200
35. M. Fleischmann, J.A. Harrison, H.R. Thirsk, Trans. Faraday Soc., **61**, (1965), 2742
36. K. Juttner, G. Staikov, W.J. Lorenz, E. Schmidt, J. Electroanal. Chem., **80**, (1977), 67

CHAPTER 4

STUDIES OF KINETIC PARAMETERS ON ULTRAMICROELECTRODES

CHAPTER 4

STUDIES OF KINETIC PARAMETERS ON ULTRAMICROELECTRODES

4.1. *Introduction*

Ultramicroelectrodes have become popular as a means of studying electron transfer kinetics, especially when they are used in conjunction with voltammetry [1-5]. The most striking feature of ultramicroelectrodes is that they have extremely small surface areas which enhance the effective rate of mass transport and reduce the potential drop in resistive solutions. Ultramicroelectrodes generally exhibit sigmoidal voltammograms at slow scan rates, giving a number of advantages over the more familiar transient voltammetry observed at macroelectrodes.

Kinetic measurements at ultramicroelectrodes can be carried out by using high speed cyclic voltammetry (e.g. sweep rates in the range 10^6 V/s may be used for ultramicroelectrodes about 10 μm in diameter [6,7]), slow steady state measurements with electrodes of submicrometer size [4,7,8] or ac voltammetry at frequencies where kinetic parameters can be determined [9]. The first method requires advanced electronic equipment and complicated algorithms for extracting kinetic information. Further, the electron transfer processes can be obscured by charging currents and by the slow response of electronic circuits. The second method, although limited by the ability to prepare and characterise sufficiently small ultramicroelectrodes allows measurements where there is virtually no capacitive current. This permits accurate measurements of the kinetics of fast electrode reactions.

The third method could be the most useful of those mentioned because it allows the determination of not only kinetic parameters but also the solution resistance, the double layer capacitance and the mass transport impedance from a single experiment. However, for the study of fast reactions, a high frequency a.c. impedance analysis is required, which normally results in high capacitive currents making the measurement of the faradaic current unreliable. It is also difficult to

measure small currents or voltages over a wide frequency range due to the effects of stray capacitance and bandwidth limitations of electronic instruments.

In this work, carbon ultramicroelectrodes (~8 μm diameter), gold ultra-microelectrodes (10 μm diameter), and gold microelectrodes (60 μm diameter), were used to study the electrochemical behaviour of ferrocene, some of its derivatives and the $Fe(CN)_6^{4-}/Fe(CN)_6^{3-}$ redox couple, at varying concentrations of supporting electrolyte.

4.2. *The electrode-solution interface*

Kinetic processes on electrodes are profoundly affected by the double layer structure at the electrode-solution interface. It is well known that the properties of this interface depend on the nature of the solvent and supporting electrolyte [10,11], as well as the electrode material [12]. The electrical potential difference developed as a result of the separation of charge of opposite sign across the electrochemical interface is known as the electrical double layer. At potentials where no charge transfer occurs across the interface, an ideally polarized electrode-electrolyte solution interface acts like a pure capacitor. The structure of the double layer [13] depends on different factors, such as the distribution of ions through the interphase region, the orientation of polar molecules and the formation of polar chemical bonds. The properties of the interfacial region play an important role in electrode kinetics. In general the double layer is considered divided into three regions where electrostatic interactions occur; the electrode surface itself, the compact layer and the diffuse layer. On the basis of this model, the overall differential capacitance, C_d, for a system without specific adsorption, results from two capacitances in series, one corresponding to capacitance of the Helmholtz layer (C_H) and the other to the capacitance of the Gouy-Chapman diffuse double layer C_{GC} [13,14]:

$$\frac{1}{C_d} = \frac{1}{C_H} + \frac{1}{C_{GC}} \qquad (4.1)$$

Most of the studies of the structure of the double layer have been carried out on the mercury electrode, which has almost ideal properties. When a solid electrode is considered, the study of the structure of the double layer is hindered by several factors. Electrode contamination, geometrical reproducibility, interference by electrode reactions and in aqueous solutions the formation of adsorbed films of hydrogen and oxygen, represent some of the experimental difficulties that arise. Experimental studies of the structure of the double layer asociated with the gold-solution interface have been reviewed by Hamelin recently[15].

4.2.1. *Potential of zero charge on solid electrodes*

The gold-aqueous solution interface has been studied by a number of workers [15-20]. However there is considerable disagreement regarding the value of the potential of zero charge (E_{pzc}). This potential is considered as the potential where the excess charge on the metal and in the solution phase are zero hence the amount of cationic surface excess at the solution side of the interface $\Gamma+$ equals the anionic excess $\Gamma-$. The wide range of E_{pzc} values reported indicates that the double layer structure on gold electrodes in aqueous solutions may be complicated by oxide films or adsorption of solution species. Also, a well known problem with capacity measurements at polycrystalline gold electrodes is the frequency dispersion observed [18]. This phenomenon has been attributed to surface inhomogeneity. Superficial defects on single crystal faces can affect the properties of the double layer. Moreover it is well established that the E_{pzc} of a metal in contact with a solution depends on the crystallographic orientation at the interface [4,15,21]. This behaviour has been attributed to the dependence of the work function on the atomic roughness of the crystal face. The E_{pzc} of a single crystal face is considered to be the potential of the capacitance minimum, E_c, in the absence of specific adsorption. For polycrystalline metal electrodes, the surface heterogeneity model [4,15,21], is used to describe the metal/aqueous solution interface. In this model each crystalline face has associated with it a localised charge density and a solution double layer consisting of a Helmholtz and diffuse layer capacitance, C_H and C_{GC} , in series. The capacitance of a polycrystal is given

by the parallel contribution from all the faces, and the potential of the capacitance minimum occurs at the potential where the total capacitance is a minimum.

One of the few techniques available for obtaining direct double layer information on solid metals is the capacity method. However, experimental difficulties are found when solid electrodes are studied. The main difficulties are frequency dispersion and pseudo-capacity. The former is minimised by using smooth electrodes or electrodes of single crystals and ac frequencies which do not coincide with the relaxation frequencies of the other processes which are not under investigation. The pseudo-capacity, which is related to the adsorption of reaction intermediates, can considerably affect the double layer capacitance. This problem is avoided by choosing a suitable potential range at which to work, as well as by choosing a suitable electrolyte and/or pH at which to work. By taking into account all these effects, the capacitance vs. potential curves can be used for determining the E_{pzc}.

Specific adsorption of F^- on gold has been reported to be very small [15,22]. For polycrystalline gold, the potential of the capacitance minimum on the C(E) curves is found close to the E_{pzc} of the (110) face (~ -0.05 ± 0.01 Vs SCE) [18]. Analysis of C(E) on this kind of electrode only can give a qualitative information because the effects of its crystallographic non uniformity are difficult to take into account. However, this kind of information can be used to give an indication of the nature of the electrode and interpret other types of electrochemical measurements.

4.3. *Interpretation of electrode kinetics*

Electrode reactions are heterogeneous processes with kinetics depending on the rates of charge transfer and mass transfer. The kinetics can also be affected by the rate of chemical reactions coupled with the charge transfer. Heterogeneous redox reactions involve the reorganization of the coordination and solvation spheres of the participating ions, which determines the kinetics of the overall electron transfer process because the electronic transition is a very fast event. Two types of mechanism for the redox process at the electrode-solution interface may

occur. According to Weaver and Anson [23], the reactant center or ion in a heterogeneous outer sphere electron transfer reaction is located in the outer Helmholtz plane, while heterogeneous inner sphere redox reactions proceed through a common ligand and correspond to specifically adsorbed reactants.

The simplest conditions for the interpretation of the effect of double layer structure on electrode kinetics are obtained in the absence of specific adsorption of the supporting electrolyte, reactants and/or products.

At the equilibrium potential, the net current density is equal to zero and $\vec{j} = \overleftarrow{j}$. In the absence of specific adsorption, the net current is expressed as :

$$j = j_t^o e^{(\alpha n - z)f\phi_2}\left[e^{(1-\alpha)nf\eta} - e^{\alpha nf\eta}\right] \qquad (4.2)$$

where j_t^o is the true exchange current density, α is the cathodic transfer coefficient, z is the ionic valence of the oxidised species, $f = F/RT$, η is the overpotential equal to potential difference ($E-E_{eq}$), n is the number of electrons tranfered and ϕ_2 is the potential in the outer plane of closest approach. The term ϕ_2 appears because the concentration of the discharged species in the pre-electrode state, defined by Frumkin [24], is different from the bulk concentration and because the effective potential is not E but $E-\phi_2$, i.e. there is a potential drop through the diffuse layer (**figure 4.1**). These potential differences in the double layer have a considerable effect on the kinetics.

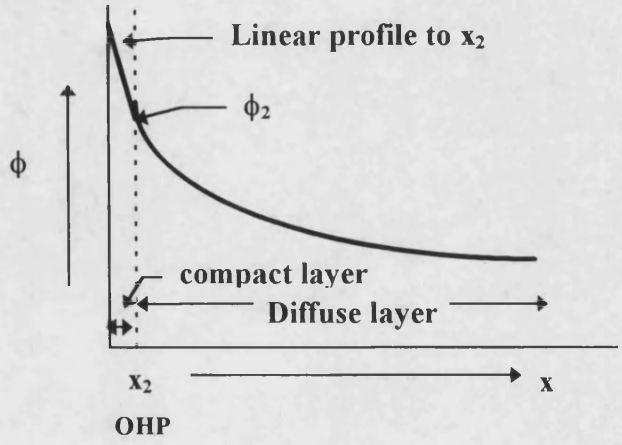

Figure 4.1. Potential distribution with distance x from the electrode surface

The interpretation of kinetic parameters requires knowledge about the type of electron transfer process occuring at the electrode-solution interface. Depending on whether the electron transfer process is fast, quasi-fast or slow with respect to the rates of mass transport, kinetic parameters may or may not be experimentally accessible. The experimental technique utilised needs to operate on a time scale comparable to the kinetic time scale, $D^o/(k^o)^2$, with some characteristic time, τ, which can be a drop time, a pulse width, a reciprocal frequency or the quantity $RT/nF\nu$, where ν is the sweep rate. For fast reactions, when large electrodes are used together with fast sweeps, short pulses or high frequency ac, the electrochemical behaviour can be affected by large charging currents that flow under such conditions.

Steady state experiments may be used to avoid the experimental difficulties mentioned above. Under these conditions, the role of the kinetic time scale is assumed by a kinetic distance scale D^o/k^o. When ultramicroelectrodes are used, very fast reactions can be studied. If the dimensions of the ultramicroelectrode sufficiently exceed this kinetic distance the process is controlled by mass transport and kinetic parameters are not measurable using steady state technique. However, it the inlaid disk electrode is sufficiently small compared with D/k^o, a mixed kinetic and mass transport control can be obtained and the kinetic parameter can be measured under steady state conditions without interference from charging currents.

The shape of a steady state voltammogram is also influenced by diffusion of the electroactive species from bulk solution to the ultramicroelectrode surface, electron transfer and the diffusion of the species produced on the surface to the bulk solution. The current measured is governed by these three processes. For the overall reaction:

$$O^{bulk} + ne^- \longrightarrow R^{bulk} \qquad (4.3)$$

the reactant O diffuses to the electrode with a diffusion coefficient of D^o:

$$O^{bulk} \xrightarrow{D^o} O^{surface} \qquad (4.4)$$

and then the electron(s) must be transfered:

$$ne^- + O^{surface} \underset{k_b}{\overset{k_f}{\rightleftharpoons}} R^{surface} \qquad (4.5)$$

Here k_f and k_b are the (potential dependent) heterogeneous rate constants. The product R must diffuse away from the surface:

$$R^{surface} \xrightarrow{D_R} R^{bulk} \qquad (4.6)$$

where D_R is its diffusion coefficient.

The experimental current observed will be determined by the slowest step. If step (4.4) is rate determining, then the overall reaction is controlled by the rate of diffusion of O to the electrode surface. According to this the current will be i_{dif}, as given by equation (2.5). However, if the charge transfer process is rate determining, then the reaction rate obeys the simple kinetic law:

$$\frac{j}{nF} = \text{rate} = k_b C_R^s - k_f C_O^s \qquad (4.7)$$

where j is the current density and C^S denotes a surface concentration. Here it is assumed that the diffusion of O and R impose no restriction on the current, in which case the surface concentration of O would have its bulk value, and the surface concentration of R is close to zero. It follows that the kinetic current is given by:

$$i_{kin} = \pi r^2 n F k_f C^s_O \qquad (4.8)$$

where πr^2 is the area of microdisk. On the other hand, if the diffusion of R from the electrode surface to the bulk solution is the rate determining step according equation (4.6), the current will be given by:

$$i = 4nFC^{s}_{R}D_{R}r \tag{4.9}$$

The surface concentration C^{S}_{R} can be established if it is assumed that the kinetic process is so fast that is maintained thermodynamic equilibrium between the two species at the electrode surface, so that:

$$C^{s}_{R} = \frac{k_f C^{s}_{O}}{k_b} = \frac{k_f C^{b}_{O}}{k_b} \tag{4.10}$$

where the concentrations of $C^{s}_{O}=C^{b}_{O}$, where C^{b}_{O} is the concentration of the O in the bulk solution. Combination of equations (4.9), and (4.10) give:

$$i_{t/d} = 4nFC^{b}_{O}\left(\frac{k_f}{k_b}\right)D_{R}r \tag{4.11}$$

where the term $i_{t/d}$ represents 'thermodynamic/diffusion' and reflects the fact that the current in this case is controlled jointly by the thermodynamics and the transport of species R by diffusion. It follows from this discussion that when the experimental current is controlled by all three processes a circuit of three impedances in series can be considered. If the current passed by each impedance on its own is known, then the current passed where all three are present is given by the reciprocal sum formula :

$$\frac{1}{i} = \frac{1}{i_{dif}} + \frac{1}{i_{kin}} + \frac{1}{i_{t/d}} \tag{4.12}$$

When the kinetics of reaction is so fast, the term $1/i_{kin}$ will be negligible, so that equation (4.12) can be expresed as:

$$i = \frac{i_{dif} i_{t/d}}{i_{dif} + i_{t/d}} = \frac{4nFC^{b}_{O}D_{O}r}{1 + \frac{D_O k_b}{D_R k_f}} \qquad (4.13)$$

k_f and k_b are large, the rates of the reaction (4.5) will be fast compared to (4.4), and (4.5) will appear to be in equilibrium. Under these conditions, the surface concentrations can be calculated using thermodynamic arguments. The ratio k_b/k_f of rate constants is the equilibrium constant of the electron transfer reaction, which can be related by Nernst's equation to the potential. It follows that:

$$i = \frac{i_{dif}}{1 + \frac{D_O}{D_R} \exp\left(\frac{nF}{RT}\left(E - E^{\circ}\right)\right)} \qquad (4.14)$$

This equation describes the shape of the sigmoidal curve under steady state condition when the electrochemical process is only controlled by mass transport at an ultramicrodisc. The difference between the standard and half-wave potential satisfies the relationship:

$$E^{\circ} - E_{1/2} = \frac{RT}{nF} \ln \frac{D_O}{D_R} \qquad (4.15)$$

For a process where the rates of mass transport and electron transfer are comparable, the shape of the voltammogram obtained using an ultramicrodisc has been investigated for Oldham et al [25-27]. They have introduced two dimensionless parameters κ and θ. κ is defined by:

$$\kappa = \kappa^{\circ} \exp\left[-\alpha n F\left(E - E^{\circ}\right) / RT\right] \tag{4.16}$$

where κ° is given by:

$$\kappa^{\circ} = \frac{\pi k^{\circ} r}{4D^{\circ}} \tag{4.17}$$

r is the radius of the ultramicroelectrode, k° is the standard rate constant rate. θ is defined by :

$$\theta = 1 + \left(\frac{D_O}{D_R}\right) \exp\left[nF\left(E - E^{\circ}\right) / RT\right] \tag{4.18}$$

With these parameters, the current-potential relationship for this process is given by:

$$i = \frac{i_d}{\theta}\left[1 + \frac{\pi}{\kappa\theta}\left(\frac{2\kappa\theta + 3\pi}{4\kappa\theta + 3\pi^2}\right)\right]^{-1} \tag{4.19}$$

This equation has been verified independently by Michael et al. [28]. Equation (4.19) can be written as:

$$\frac{1}{q\theta} - 1 = \frac{2(h+1)}{3h(2h+\pi)} \tag{4.20}$$

where, $q = i/i_d$ and h is a new parameter, proportional to the $\kappa\theta$ product and defined by:

$$h = \frac{2\kappa\theta}{3\pi} \tag{4.21}$$

For a process where the electron transfer is the determining step, the reduction wave is displaced negatively from the standard potential, which means

that the term exp[nF(E-E°)/RT] in equation (4.18) is negligible in comparison with unity, so that $\theta \rightarrow 1$ and equation (4.19) reduces to the form:

$$\frac{i}{i_d} = \left[1 + \frac{\pi}{\kappa}\left(\frac{2\kappa + 3\pi}{4\kappa + 3\pi^2}\right)\right]^{-1} \qquad (4.22)$$

4.4. *Low concentrations of electrolyte*

According to the classical Frumkin analysis of diffuse double layer effects on electrode processes [13], changes in the rates of the electrode reactions can be produced by changing the concentration of the supporting electrolyte. At the same time, a decrease of the solution electrical conductivity, by decreasing the concentration of electrolyte, produces an increase in the iR drop, which distorts the voltammetric curve, resulting in the calculation of erroneous values of the rate constant when macroelectrodes are used. This problem can be overcome by using ultramicroelectrodes because the iR drop will decrease with the radius of the ultramicroelectrodes [29,30,31,32]. However, distortions due to migration can ocurr when little or no electrolyte is used, because the migration of electroactive species becomes an important transport mechanism. A variation in steady state plateau currents when supporting electrolyte is removed from the solutions has been reported [33,34]. Amatore et al. [35] have studied the effects of migration on the diffusion limited current (i_{lim}) and $E_{1/2}$ for steady state voltammograms, without taking into account voltammetric distortions due to uncompensated resistance, while Oldam et al. [36], have studied such distortions taking into account iR drop and migration effects using a model based on the [electrolyte]/[analyte] ratio. Ways of using steady state voltammetry at disk ultramicroelectrodes to elucidate heterogeneous kinetics have been reported by the same authors [37]. A theoretical treatment has also been reported by Amatore et.al [38], which provides a reasonable estimate of the effects to be found in steady state experiments without supporting electrolyte under specific conditions.

4.5. *Electrochemical behaviour of the oxidation of ferrocene and its derivatives on ultramicroelectrodes.*

The oxidation of ferrocene to the ferrocenium cation:

$$(C_5H_5)_2Fe_{(soln)} \rightleftarrows (C_5H_5)_2Fe^{+}_{(soln)} + e^{-} \qquad (4.23)$$

has been considered as a standard one electron transfer process [39] for use in instrumental and reference potential calibration in organic solvents. The use of ferrocene as a standard implies that the rate of electron transfer is extremely fast so that the electrode process exhibits reversible behaviour. Voltammetric studies on the Fc^{+} /Fc couple have been reported in aqueous media [40] and nonaqueous solvents [41-43]. Strange behaviour has been observed for this compound in acetonitrile, in which the formation of a film on a Pt electrode of conventional size has been reported [44]. Similarly, distorted, quasireversible steady-state voltammograms were obtained at Pt ultramicroelectrodes of 12.5 μm radius, especially with ferrocene concentrations of ≥ 10 mM. By contrast little evidence of film formation was found for 1 μm radius ultramicroelectrodes in more dilute ferrocene solutions [44]. This behaviour is consistent with the lower sensitivity of microelectrodes to chemical reaction following charge transfer due to rapid diffusion of products away from the electrode. Studies carried out on platinum microelectrodes of sizes apparently approaching nanometer dimensions [45] have given the largest apparent heterogeneous rate constant for the oxidation of ferrocene in acetonitrile (220 cm s^{-1}). The differences between the values of apparent heterogeneous rate constants previously reported for this system on macroelectrodes, microelectrodes and nanoelectrodes have been attributed to a decrease of ohmic drop and an increase of the mass transport rate, when the size of the electrode is changed from macro → micro → nanometer scale. However, these differences could also be attributed to a blocking of the electrode surface by a film, which is formed more easily on large Pt electrodes. FTIR, Auger spectroscopy and electrochemical studies of ferrocene at Pt electrodes of different sizes [46], have

shown that ferrocene is oxidised at Pt electrodes in acetonitrile to form ferricinium ion, which then reacts to produce a film on the electrode surface.

Ferrocene and its derivatives have been widely studied using different physical methods [1,2]. With a view to advancing chemical sensor technology, modelling electron transfer processes in biological systems and producing new redox catalysts, the syntheses of these types of compounds have aroused considerable interest [47-49]. They are potential aids to the understanding of biological electron transfer. Their redox potential and kinetic parameters are helpful for selecting donor/acceptor couples for the establishment of membrane systems as well as for electrochemical recognition.

In the present work, carbon ultramicroelectrodes were selected for studying the electrochemical behaviour of the ferrocene and some of its derivatives. Steady state voltammetry was used for determining some electrochemical parameters, as well as for determining the diffusion coefficients of these compounds. Experiments at different concentrations of supporting electrolyte were carried out, and the observed behaviour was compared with a theoretical model.

4.6. *Electrochemical behaviour of the hexacyanoferrate couple*

Electrochemical studies of this system in solution without electrolyte have been carried out by Anson et al. [50] using carbon ultramicroelectrodes. They found that in the absence of KCl the reduction of $Fe(CN)_6^{3-}$ is suppressed completely. This suppression was attributed to a 'dynamic diffuse layer effect' in which the transport of charged reactants across the diffuse part of the double layer limits the rate of their electroreduction. However, other factors such as the kinetics of electron transfer at the surface could be involved. The influence of ion pair formation between the hexacyanoferrate couple and the alkali metal cations of the electrolyte on the rate and mechanism of the charge transfer has been established [51,52]. First order dependence of the rate constant on cation concentration of the electrolyte was found by Peter et.al. [52] for this couple over a wide range of electrolyte concentrations. It has been suggested that the hexacyanoferrate electrode transfer process can also be governed by other factors besides charge

transfer and diffusion [53,54]. Adsorption of ferrocyanide and ferricyanide on the electrode surface has been reported [55-57]. Wieckoswki et.al. [57] proposed a surface bonding scheme in which hexacyanoferrate is adsorbed on Pt through the nitrogen of the -C=N group:

$$Pt \leftarrow :N \equiv C - Fe(CN)_5^{n-} \qquad (4.24)$$

The nature of the adsorbed intermediate has been studied more directly by *in-situ* or *ex-situ* vibrational spectroscopy, infrared, Raman and electrochemically modulated infrared spectroscopy (EMIRS) [56,58,59]. Fleischmann et al. [58] studied this redox system in alkali chloride solutions using enhanced Raman spectroscopy (SERS) on Au. They found a C≡N stretching band of adsorbed ferrocyanide which was significantly dependent on the nature of the cation of the electrolyte. Beriet and Pletcher [60], have reported that the reduction of ferricyanide as well as the oxidation of ferrocyanide could be affected by surface poisoning. Stieble and Juttner [61] found that depending on the defined prepolarisation conditions, a partial blocking of the platinum electrode surface is observed when this couple is studied in presence of 0.5 mol dm^{-3} Na_2SO_4. However it is necessary to point out that the experiments carried out by Fleischmann et.al and Beriet and Pletcher were made using KCl as supporting electrolyte and it is known that chloride ions can be adsorbed at Pt and gold electrodes [62], altering the kinetic behaviour of the hexacyanoferrate redox system in solutions of low concentrations of supporting electrolyte. Although some authors have verified the presence of adsorbed species [56,57,61] on Pt electrodes, other authors have not found any evidence of specific adsorption [52] on gold electrodes. It is possible that platinum can induce decomposition of the hexacyanoferrate species due to its high catalytic activity.

Recently Campbell and Peter [63] found by a.c. impedance spectroscopy a minimum in the rate constant when this parameter was analysed as a function of the total potassium cation concentration present in the system. They showed that the minimum in k° coincides with the concentration value reported by Eaton et.al. [64],

at which the hexacyanoferrate anions becomes predominantly free from association with the potassium cation.

In the present work the hexacyanoferrate couple was studied in a range of different concentrations of KF as supporting electrolyte. The aim was to obtain information that will allow an understanding of the relative importance of the effects produced when much, little or no supporting electrolyte was used, as well as to obtain more information about the charge transfer kinetics of this system. The steady state response at a gold ultramicrodisc at different concentrations of hexacyanoferrate couple with high concentrations of electrolyte was utilised to determine the diffusion coefficients of both electroactive species.

4.7. *Experimental*

Reagent grade concentrated 70% $HClO_4$, KF, $K_3Fe(CN)_6$, $K_4Fe(CN)_6$, ferrocene, ferrocenecarboxylic acid, and ferrocenecarboxaldehyde > 98% (Fe) were obtained from Fluka; tetrabutylammonium perchlorate, was obtained from Aldrich. All these chemicals were used as received. Acetonitrile was dried with alumina, according to the procedure described in chapter 2. Supporting electrolyte solutions of KF were treated with purified active charcoal for gas adsorption (particle size 0.85-1.70 mm) from BDH to eliminate organic impurities, which can interfere with the determination of kinetic parameters. Gaseous N_2 was passed through the solution in the cell for 15 min before measurements were made, according to the procedure described in figure 2.6 (chapter 2).

In the present work, voltammetric measurements of ferrocene and some of its derivatives were carried out using the electrochemical cell described in chapter 2, with a carbon ultramicrodisc electrode as working electrode, and a wire platinum electrode as a quasi-reference electrode. Gold microdisc electrodes (60 μm diameter), and gold ultramicrodisc electrodes were used with a SCE in the electrochemical study of the hexacyanoferrate couple $Fe(CN)_6^{4-}/Fe(CN)_6^{3-}$.

Capacitance measurements were carried out using gold microelectrodes (60 μm diameter), sealed in glass or epoxy resin. These measurements were made after calibration using an equivalent circuit of a resistor and a capacitor in series. A three

electrode electrochemical cell was utilised. A SCE was used as the reference electrode, and a platinum wire was used as the counterelectrode. The differential capacity curves (C-E) were recorded by the application of a slow potential sweep (5 mV s^{-1}) to the working microelectrode plus a sinusoidal *ac* component of low amplitude (6 mV p/p) at 15 Hz, using a two-phase lock in amplifier (Bentham) coupled to a sine-square wave oscillator (Farnell-LFM4). Potentiostatic control was achieved using a home built potentiostat (sensitivity 1μA V^{-1}) and a waveform generator (Hitek Instruments). **Figure 4.2** shows the circuit diagram utilised for these measurements.

Impedance measurements were carried out using a two electrode electrochemical cell. A gold microelectrode (60 μm diameter), sealed in glass was used as the working electrode. The generator output and voltage analyser input of the frequency response analyser (Schlumberger-Solartron, model 1250) were connected to a platinum grid counter electrode (surface area c.a 1 cm^2), while the working gold ultramicroelectrode was conected to the current analyser input through a home built amplifier (sensitivity 10 $^{-7}$ A V^{-1}). **Figure 4.3** shows the circuit diagram utilised for these experiments.

The pretreatment of the carbon and gold ultramicroelectrodes was of prime importance for the present experiments. The carbon and gold ultramicroelectrodes were cleaned and polished according to the method described in chapter 2. In addition, the gold ultramicroelectrodes and gold microelectrodes were treated electrochemically by cycling between 0 and 1.45 V vs. SCE in 0.2 mol dm^{-3} $HClO_4$. The ultramicroelectrodes were rinsed with ultrapure water and transferred to the cell where the experiment was carried out, taking care to leave a drop of water on the electrode surface during the transfer, when gold ultramicroelectrodes were used.

The pH was measured with a digital pH meter (Orion, model 520A), which was calibrated with a buffer solution, pH 7, before carrying out the measurement. The quasi-reference Pt electrode was flamed each time before performing the experiment, and the solutions were deoxygenated before each experiment. All the experiments were carried out at 25 °C in an earthed metal Faraday box.

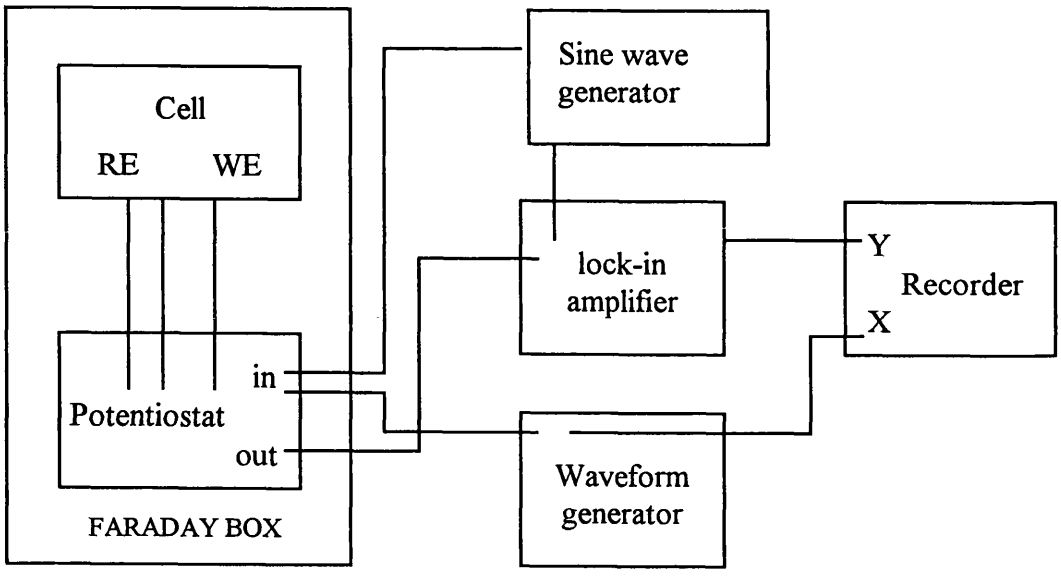

Figure 4.2 Instrumental arrangement for capacitance measurements

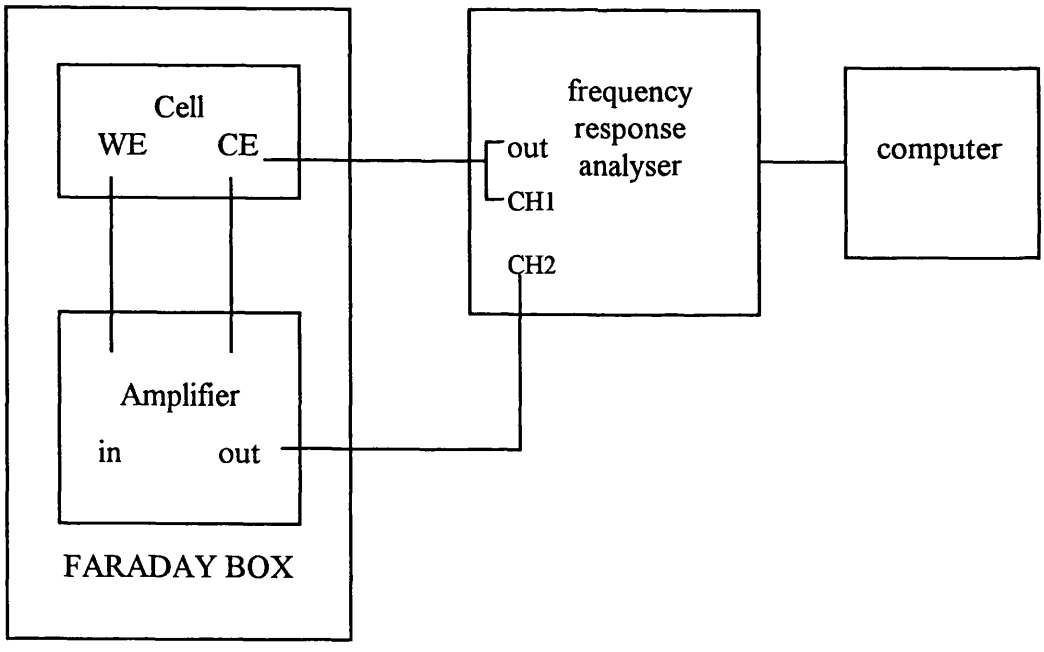

Figure 4.3. Instrumental arrangement for impedance measurements

4.8. *Electrochemical study of ferrocene and some of its derivatives*

4.8.1. *Diffusion coefficients*

Steady state voltammetry at a carbon ultramicroelectrode, sealed in glass, with different concentrations of electroactive species was carried out to determine the diffusion coefficients of ferrocene, ferrocenecarboxylic acid, and ferrocenecarboxaldehyde. **Figure 4.4a** shows the steady state voltammograms obtained when the concentration of ferrocene was increased from 10^{-5} to 10^{-4} mol dm^{-3}, in TBAP/acetonitrile at 25°C. Well defined steady-state voltammograms were observed, with diffusion currents proportional to the concentration (**figure 4.4b**). The diffusion coefficients of these species were determined from the slopes of plots of diffusion current vs. concentration of ferrocene (**figure 4.4b**) using the equation:

$$D^{\circ} = \frac{s}{4nFr} \qquad (4.25)$$

where s is the slope of the limiting current vs. concentration of the electroactive species plot, r is the radius of the ultramicroelectrode, and n is the number of electrons transferred in the oxidation process. For a series of experiments, the values obtained for the diffusion coefficient of ferrocene was $(2.46 \pm 0.1)\times10^{-5}$ cm^2 s^{-1}. This value agrees with that reported by Kadish et al. [65] of 2.46×10^{-5} cm^2 s^{-1}.

Plots of E vs. log[*(id-i)/ i*], show that the reversibility of the system was maintained (61.7 ± 2.3 mV) when the concentration of ferrocene was increased from 5×10^{-5} to 2×10^{-4} mol dm^{-3} (**figure 4.5**). The apparent half-wave potential ($E_{1/2}$) was observed to change little in the concentration range studied. The variation was not a function of concentration. Differences of ≤8 mV between the apparent half-wave potentials ($E_{1/2}$) determined from each voltammogram were observed. This behaviour could be attributed to changes in the quasi-reference Pt electrode utilised.

The quasi-reference Pt electrode could actually be behaving as a reversible electrode under the experimental conditions used. It was placed in the main

compartment where the electroactive species were present. The concentrations of the electroactive species were between $5x10^{-5}$ to $2x10^{-4}$ mol dm^{-3}, and small concentrations of the corresponding oxidised species could be present before starting the electrochemical oxidation process. For instance, for the ferrocene system, if a concentration of the oxidised species of about 10^{-7} mol dm^{-3} is present in the solution where the concentration of ferrocene is about 10^{-4} mol dm^{-3}, equilibrium between the ferrocene and ferrocinium may be established on the Pt electrode giving a reference potential of -177 mV vs. E^{θ} for the redox couple.

For the ferrocenecarboxylic acid and ferrocenecarboxaldehyde values of $(1.91 \pm 0.2)x10^{-5}$ $cm^2.s^{-1}$ and $(2.61 \pm 0.1)x10^{-5}$ cm^2 s^{-1} were found respectively for the diffusion coefficients. It is seen that the diffusion coefficient of the ferrocene and ferrocenecarboxaldehyde are similar in contrast to the ferrocenecarboxylic acid. From plots of $\log[(id-i)/i]$ vs. E, a slope of 70 ± 4mV was observed for the oxidation of ferrocenecarboxylic acid, while a slope of 63 ± 3mV was found for the oxidation of ferrocenecarboxaldehyde. The oxidation of ferrocenecarboxylic acid does not seem to be a process controlled only by mass transport. Differences <10 mV were observed between the values of $E_{1/2}$ potential determined for each system in the range of concentration considered. Table 4.1 shows the values of diffusion coefficient and half-wave potentials ($E_{1/2}$) for these three compounds.

Table 4.1

compound	diffusion coefficient (D^o) (cm^2 s^{-1})	$E_{1/2}$ (mV)
Ferrocene	$(2.36 \pm 0.1)x10^{-5}$	163 vs.QRE
Ferrocenecarboxylic acid	$(1.91 \pm 0.2)x10^{-5}$	533 vs. QRE
Ferrocenecarboxaldehyde	$(2.61 \pm 0.1)x10^{-5}$	581 vs.QRE

According to equation (4.15), if the diffusion coefficient of the reactant species is similar to that of the product formed during the oxidation process, the

value of $E_{1/2}$ for the oxidation of ferrocene could be considered as the standard potential.

For ferrocenecarboxylic acid and ferrocenecarboxaldehyde, *i-E* curves show that the forward and reverse scans differ, and changes in the $E_{1/2}$ from the values reported above were found when water was added to the system. For the oxidation of ferrocenecarboxylic acid, it was observed that $E_{1/2}$ shifts to more negative values when water is added. $E_{1/2}$ shifts about 30 mV when the % of water is doubled. **Figure 4.6 and 4.7** show the voltammograms and the *E* vs. log[(*id-i)/I*], plots obtained for this system. The pH of the solution of ferrocenecarboxylic acid in acetonitrile decreases from 6.9 to 6.2 when 8% of water is added. For the oxidation of ferrocene aldehyde, a different behaviour was observed with respect to the apparent $E_{1/2}$. The apparent $E_{1/2}$ increased a little when water was added to the system and the pH of the solution does not change on addition of water. **Figure 4.8** shows this behaviour. These results may indicate that specific interaction at the electrode-solution interface is taking place. It seems possible that these derivatives of ferrocene are reacting with the carbon surface through the substitutent groups when water is present in the electrolyte. It has been considered that a series of phenolic, quinonic, or carboxylic groups are bonded on the carbon surface [66].

4.8.2. *Voltammetry study in low concentration electrolyte solutions*

The oxidation of ferrocene and ferrocenecarboxylic acid was investigated in dilute solutions and in the absence of intentionally added supporting electrolyte. **Figure 4.9a** shows the family of voltammograms obtained for different ratios of [electrolyte]/ [ferrocene]. Plots of *E* vs. log[(*id-i)/ i*] show that the reversibility of the system is lost when the ratio between the concentration of supporting electrolyte and the concentration of ferrocene falls below unity (**figure 4.9b**). Knowing that inlaid disc ultramicroelectrodes produce an electrochemical response identical to hemispherical ultramicroelectrodes for reversible systems under steady-state conditions [27], the model developed by Oldham [36], which is based on the determination of the analyte and electrolyte concentrations at the surface of a hemispherical microelectrode, was used for testing the experimental results

obtained for different ratios of [ferrocene]/electrolyte]. **Figure 4.10** shows this comparison with the model proposed by Oldam, which is given by:

$$E = E^{\theta} + \frac{RT}{nF} \ln\left[\frac{D_O i}{D_R(i_{dif} - i)}\left(1 + \frac{D_O c_O}{4D_R\, c_{MX}} \frac{i}{i_{dif}}\right)\right] \qquad (4.26)$$

$$E_{1/2} = E^{\theta} + \frac{RT}{nF} \ln\left[\frac{D_O}{D_R}\left(1 + \frac{D_O c_O}{8D_R c_{MX}}\right)\right] \qquad (4.27)$$

Equation (4.26) permits the shape of the rising portion of the steady- state voltammeteric wave to be described in presence of little supporting electrolyte for the oxidation of O to R, O being a neutral species. Equation (4.27) allows the correction of the observed $E_{1/2}$. In these equations D_O and D_R represent the diffusion coefficient of these species, i and i_{dif} are the current and diffusion limited currents, and c_O and c_{MX} are the concentrations of the analyte and supporting electrolyte respectively. It is seen that the shape of the steady-state voltammogram for a reversible process on a carbon ultramicrodisc can be predicted successfully using Oldham's approach when the ratio [ferrocene]/[electrolyte] is >0.6 and assuming that D_O=D_R. The deviations observed when the ratio [ferrocene]/[electrolyte] is < 0.6 could be attributed to electrode kinetic effects, double layer effects or migration. Another factor which it is necessary to take into account is that generation of a cation on the electrode surface when oxidation occurs requires an anion for its neutralisation. When supporting electrolyte is absent the process of neutralisation could be taking place by autoprotolysis of the solvent (acetonitrile) or of water, if the latter is present in the system.

Norton et al. [67] showed that the diffuse double layer affects voltammetric behaviour only if its thickness is comparable with the dimensions of the ultramicroelectrode. According to Gouy-Chapman double layer theory, the thickness of the diffuse layer can be determined by:

$$d_H = \left(\frac{RT\varepsilon\varepsilon_o}{2F^2I}\right)^{1/2} \qquad (4.28)$$

where, ε is the relative permitivity of the solvent, ε_o is the vacuum permitivity, and I is the ionic strength of the solution. It was found that the thickness of the diffuse layer calculated taking into account the ionic strength at different ratios of [electrolyte]/[ferrocene] was less than 15 nm, much smaller than the radius of the ultramicroelectrode (~4 μm). For this reason double layer effects could be ignored in principle. However, when the supporting electrolyte concentration is decreased considerably, changes at specific adsorption sites on the carbon surfaces can be produced as the carbon surface contains phenolic, quinonic or carbonilic groups.

Figure 4.11 shows the behaviour observed for ferrocene-carboxylic acid in acetonitrile when the concentration of the supporting electrolyte was changed. It was observed that the oxidation process of this electroactive species does not fit well to Oldham's model in all the concentration range investigated. This behaviour is expected for systems in which mass transport cannot be considered as the determining step. This result also suggest that, specific interaction between the electroactive species and the electrode surface could be also taking place.

Despite the advantages in using ultramicroelectrodes in conditions where little or no supporting electrolye is present, carbon may not be the ideal material in the study of electrochemical systems under those experimental conditions. Different kinds of oxide can be present on the carbon surface and the electrochemical behaviour of electroactive species may be affected due to changes in the sites at which electron transfer occurs. The behaviour observed in the electrochemical oxidation of ferrocene when the ratio [electrolyte]/ [ferrocene] is less than 0.6 can probably be attributed to changes in active sites on the electrode. Clearly, more work is required to confirm these results.

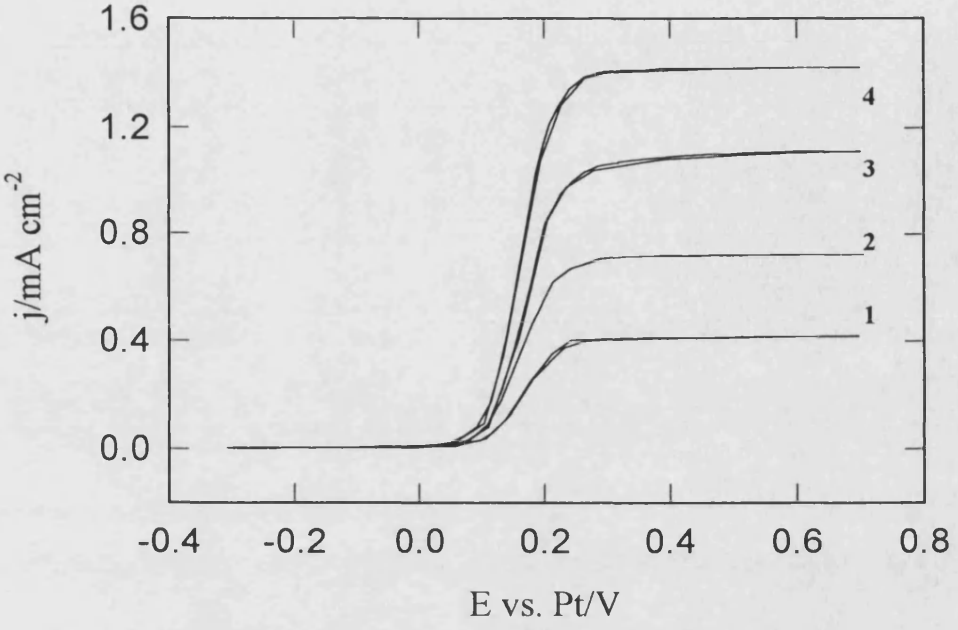

Figure 4.4a. Steady-state voltammograms obtained at a carbon ultramicroelectrode for different concentrations of ferrocene: 1) $5.7x10^{-5}$; 2) $1.0x10^{-4}$; 3) $1.50x10^{-4}$; 4) $1.92x10^{-4}$ mol dm^{-3} in $1x10^{-3}$ mol dm^{-3} TBAP/acetonitrile; $\nu = 10$ mV s^{-1}.

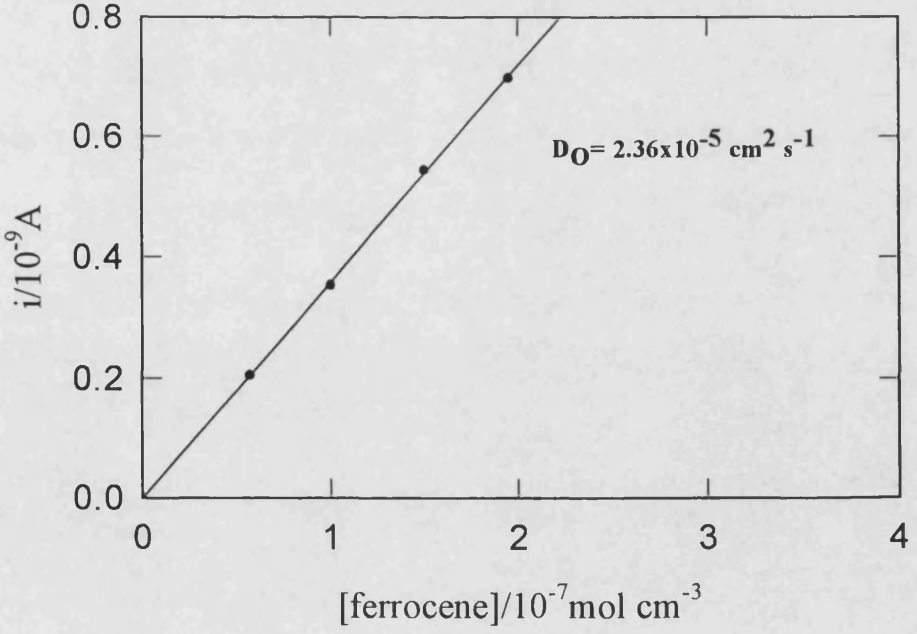

Figure 4.4b. Diffusion current vs. concentration of ferrocene in $1x10^{-3}$ mol dm^{-3} TBAP/acetonitrile; $\nu = 10$ mV s^{-1}.

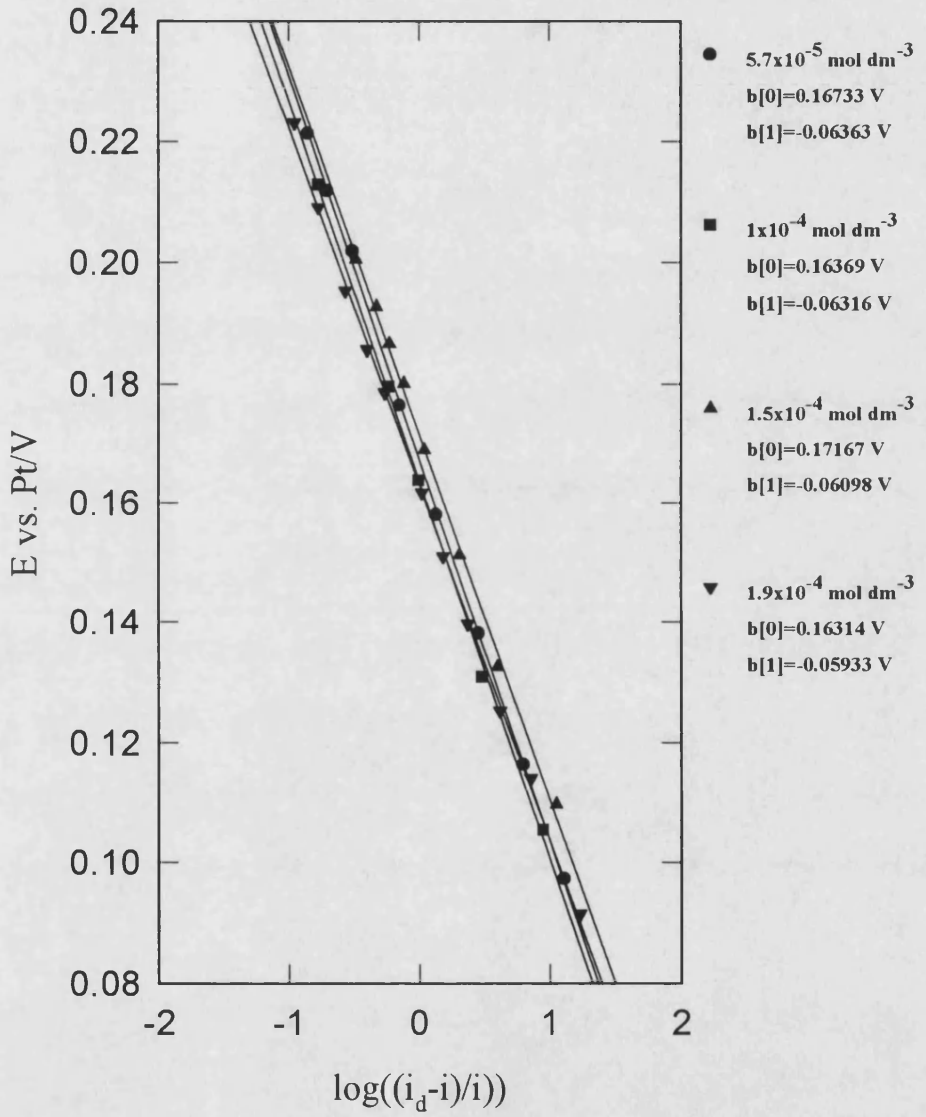

Figure 4.5. E vs. log(((i$_d$-i)/i)) plots at a carbon ultramicroelectrode for different concentrations of ferrocene in 1x10^{-3} mol dm^{-3} $HClO_4$; ν = 10 mV s^{-1}; b[0] is $E_{1/2}$ and b[1]= slope

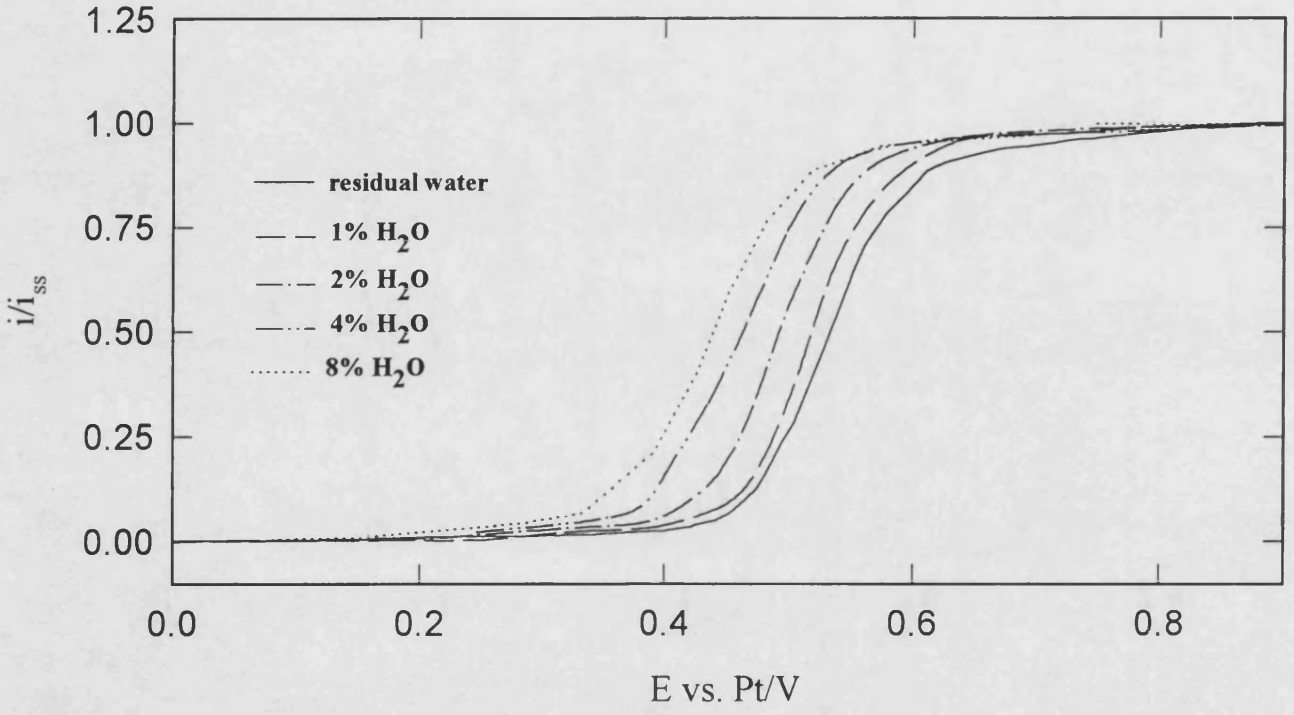

Figure 4.6. Steady-state voltammograms obtained at a carbon ultramicroelectrode when water was added to the system ferrocenecarboxylic acid + $1x10^{-3}$ mol dm^{-3} TBAP/acetonitrile; ν =10 mV s^{-1}

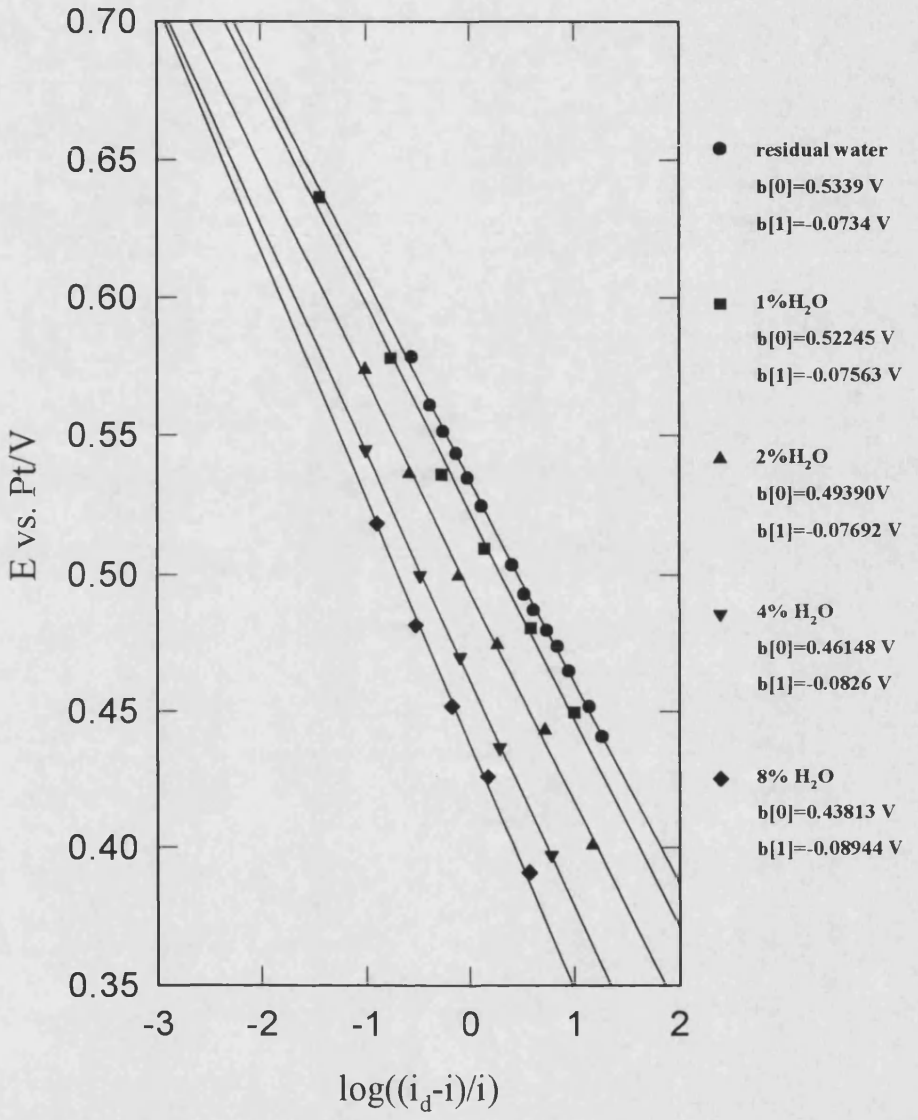

Figure 4.7. E vs. log($(i_d-i)/i$) plots obtained at a carbon ultramicroelectrode when water was added to the system ferrocenecarboxylic acid + $1x10^{-3}$ mol dm^{-3} TBAP/acetonitrile; ν =10 mV s^{-1}; b[0] is $E_{1/2}$ and b[1]= slope

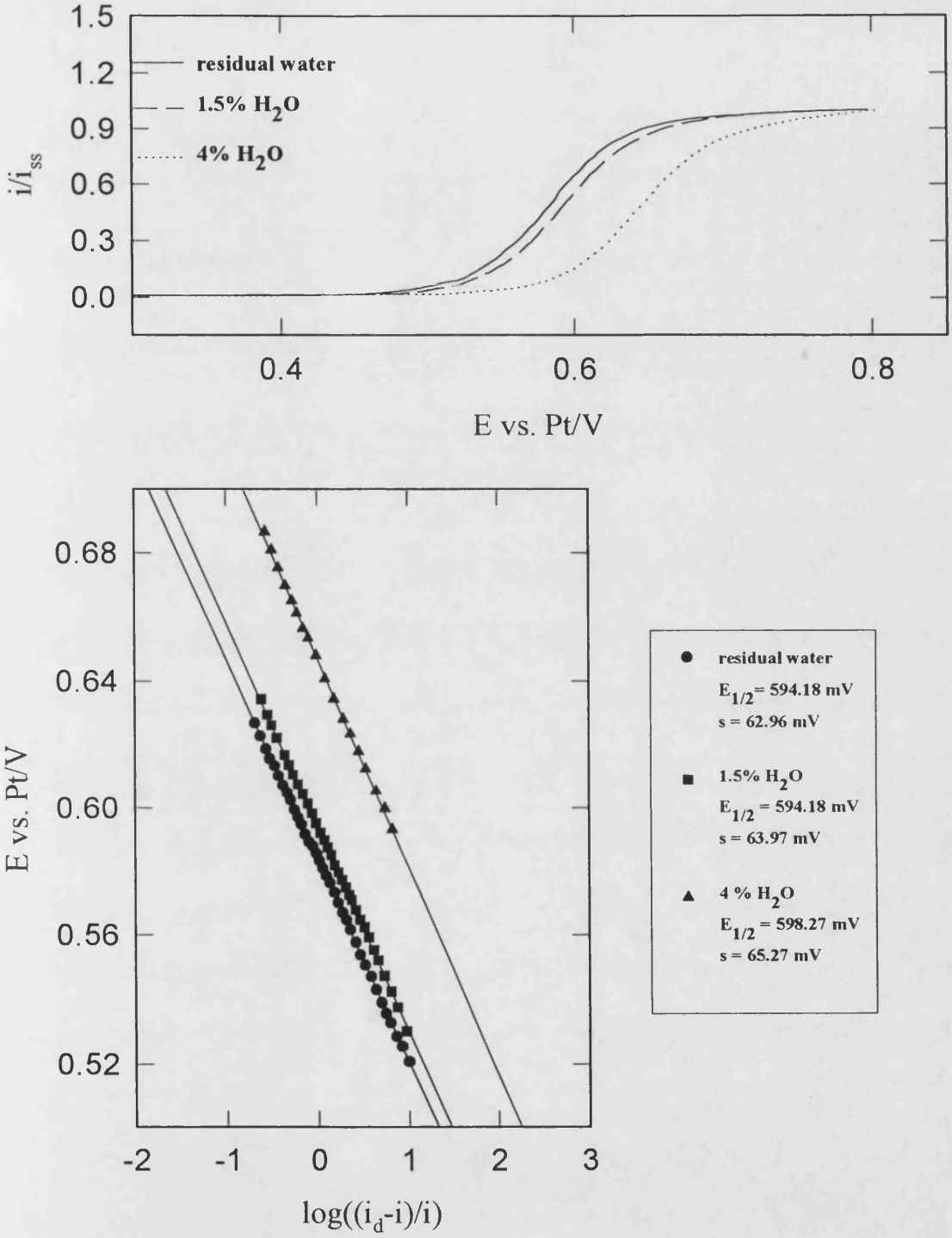

Figure 4.8. E vs. log($(i_d-i)/i$) plots obtained at a carbon when water was added to the system ferrocenealdehyde + $1x10^{-3}$ mol dm^{-3} TBAP/acetonitrile; ν= 10 mV s^{-1}

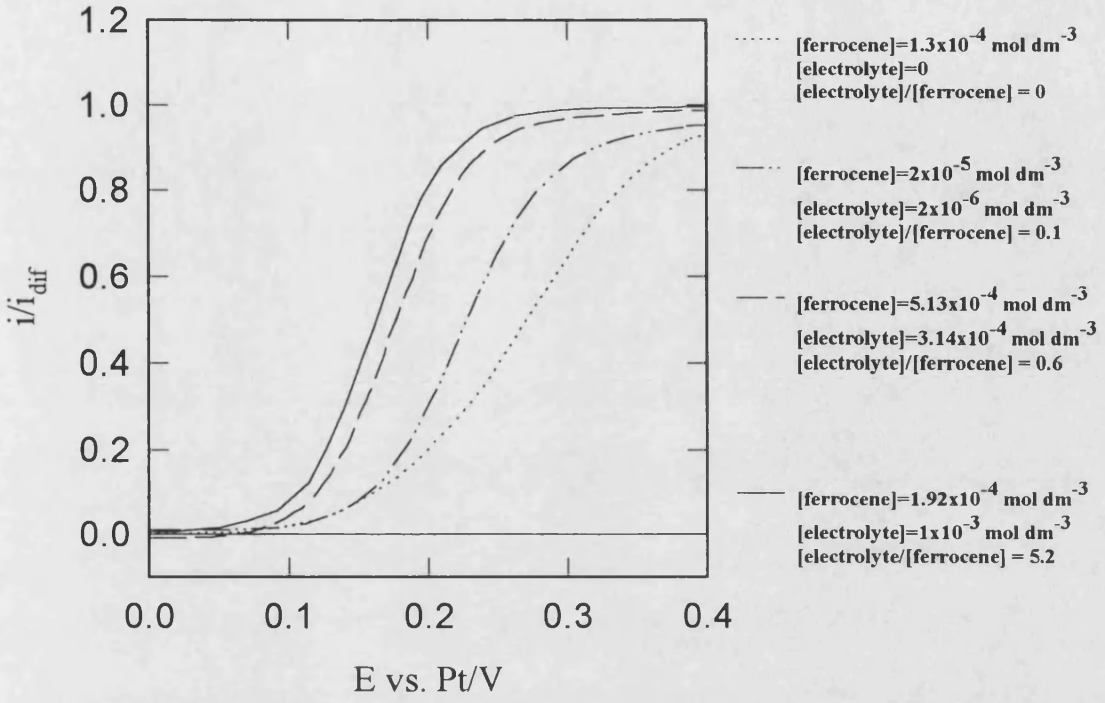

Figure 4.9a. Steady state voltammograms of ferrocene in acetonitrile at a carbon ultramicroelectrode (8μm diameter), where the ratio between [electroyte]/[ferrocene] was changed; ν=10 mV s^{-1}

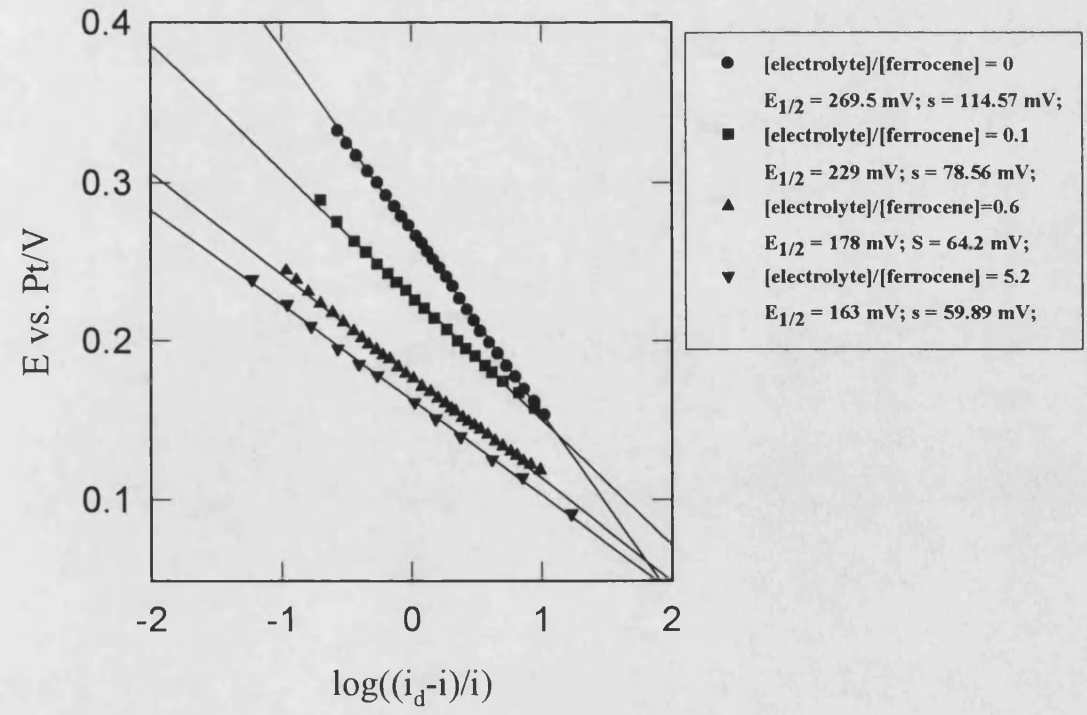

Figure 4.9b. E/Pt vs. log($(i_d$-i)/i) from data in figure 4.9a

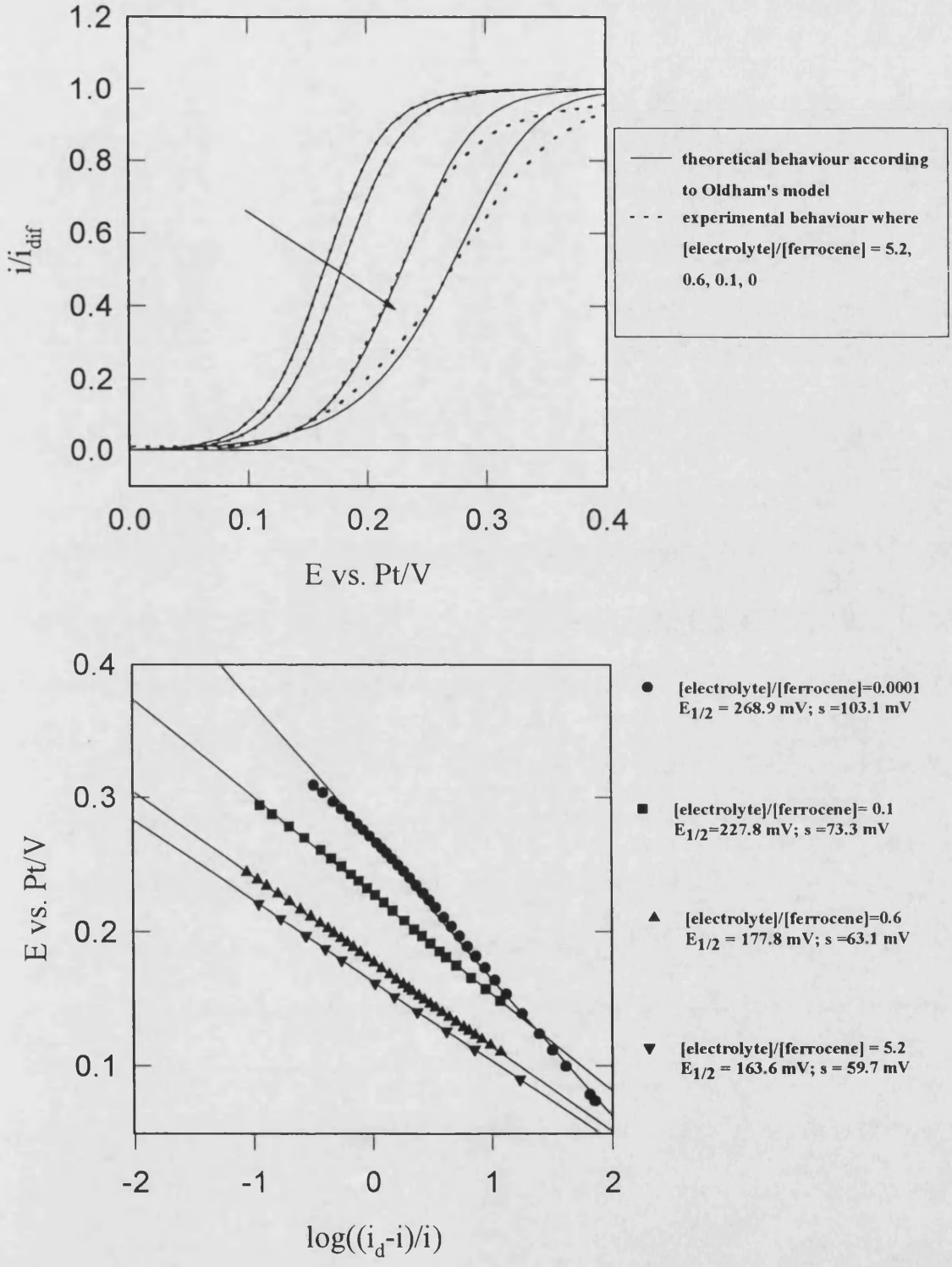

Figure 4.10. Steady state voltammograms and E vs. log((id-i)/i) plots according Oldham's model

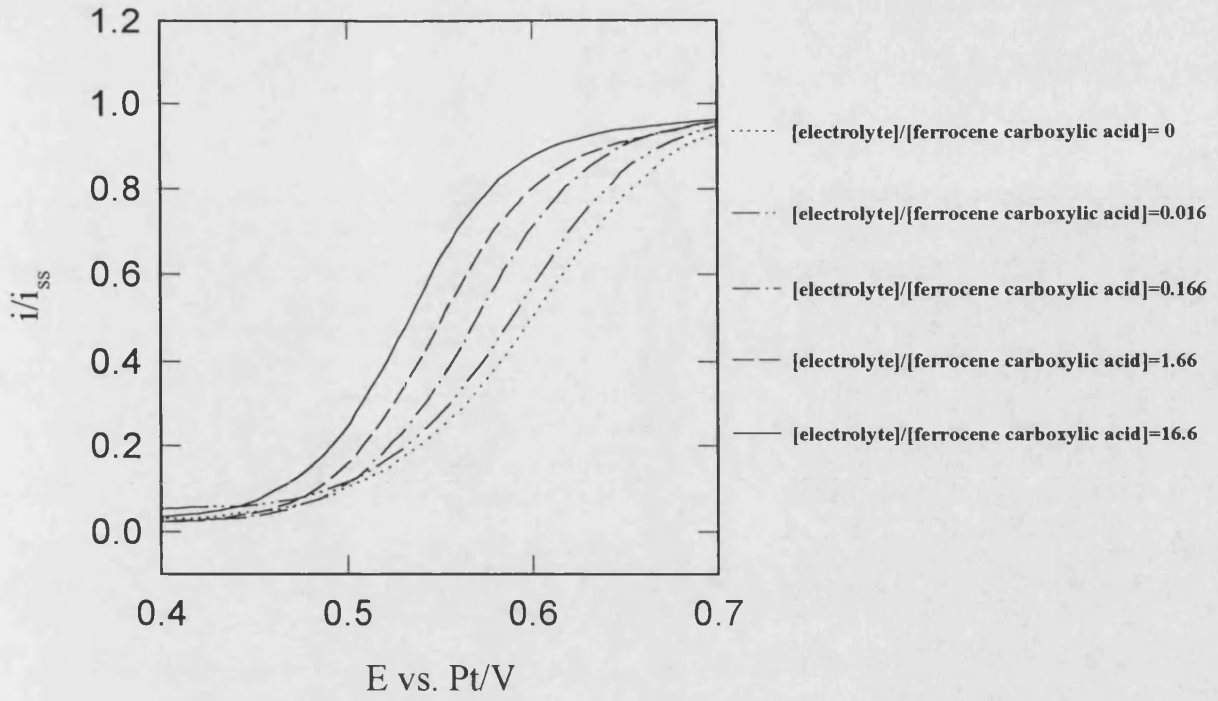

Figure 4.11a. Steady state voltammograms of ferrocene carboxylic acid at a carbon ultramicroelectrode (8μm diameter), where the ratio between [electrolyte]/[ferrocene carboxylic acid] was changed; The concentration of ferrocene carboxilic acid was $6x10^{-3}$ mol dm^{-3} and the concentration of supporting electrolyte was changed between:0, $1x10^{-6}$, $1x10^{-5}$, $1x10^{-4}$ and $1x10^{-3}$ mol dm^{-3}; ν=10 mV s^{-1}

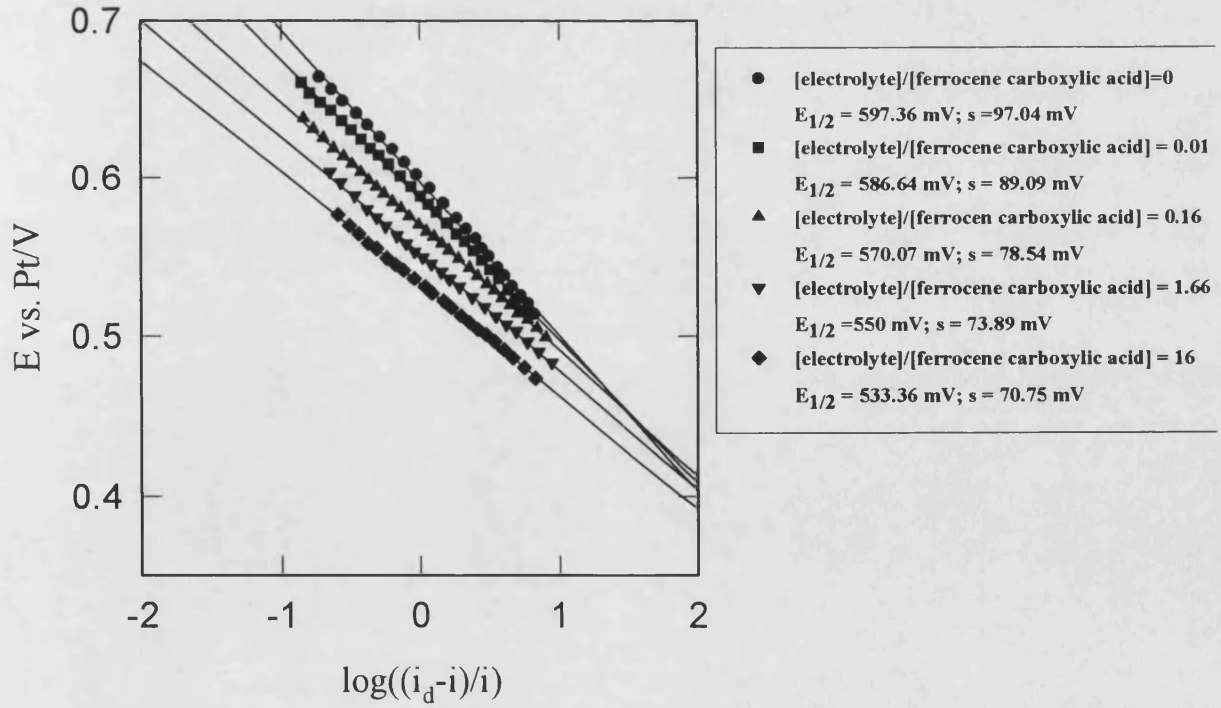

Figure 4.11b. E/Pt vs. log($(i_d-i)/i$) from data in figure 11.a

4.9. *Electrochemical study of redox couple $Fe(CN)_6^{4-}/Fe(CN)_6^{3-}$*

4.9.1. *Diffusion coefficients*

Steady state voltammetric studies of the hexacyanoferrate couple were performed using a gold ultramicroelectrode (10 μm diameter), sealed in epoxy. The solution was prepared keeping the concentrations of ferrocyanide equal to the concentration of ferricyanide. Different concentrations of the electroactive species were used to determine the diffusion coefficient of the oxidised and reduced forms. **Figure 4.12a** shows the steady state voltammograms obtained when the concentration of these species was increased in steps from $5x10^{-5}$ to $2.5x10^{-4}$ mol dm^{-3} in 0.5 mol dm^{-3} KF at 25 °C. In these experiments it was observed that the diffusion limited current was proportional to the concentration (**figure 4.12b**). The diffusion coefficients of the oxidised and reduced species were determined from the slope of plots of diffusion current vs. concentration (**figure 4.12b**), applying equation (4.25). The value obtained for the oxidised species was $(5.74 \pm 0.2)x10^{-6}$ cm^2 s^{-1} and the value for the reduced species was $(7.25 \pm 0.2)x10^{-6}$ cm^2 s^{-1}. These values agree with the values reported in the literature [70].

4.9.2. *Capacitance vs. potential measurements*

Capacitance experiments were carried out using a gold microelectrode (60 μm diameter) sealed in glass. Initially cyclic voltammetry was used to test the purity of the solution, the cleanness of the microelectrode surface and to establish if the microelectrode was not leaking. Measurements of capacitance vs. potential for different concentrations of supporting electrolyte (**figure 4.13**) showed a high capacity maximum in the vicinity of 0.3 V vs SCE, as well as, a poorly defined minimum between -0.1 V to -0.05 V vs. SCE, which could be attributed to the potential of zero charge. The maximun in the vicinity of +0.3 V vs. SCE increased and shifted to more negative potential when the concentration of the electrolyte KF was increased from $1x10^{-5}$ to $1x10^{-2}$ mol dm^{-3}. This maximum may be attributed to the adsorption of F^- anions. However, this behaviour may be masked by the presence of a small amount of oxide on the electrode as the experiments were made

between 0.8 V to -0.3 V vs. SCE. The p.z.c. cannot be assigned more accurately as the minimum of capacitance is not well defined. This behaviour is attributed to complications such as an adsorbed film of oxygen atoms or heterogeneity of the microelectrode surface.

4.9.3. *Supporting electrolyte dependence*

A very large number of experiments was carried out using different [electrolyte]/[hexacyanoferrate couple] ratios. It was clearly determined that the experimental response is strongly influenced by the cleaness of the ultramicro-electrode surface. The experimental results showed that the electrochemical behaviour of the oxidation and reduction of the hexacyanoferrate couple was also strongly affected by the concentration of the electrolyte. At high concentration of supporting electrolyte, it has already been demonstrated by Peter et al. [53] that there is a first order dependence of the apparent standard rate constant on the supporting electrolyte cation concentration. In solutions where the concentration of supporting electrolyte was > 0.1 mol dm^{-3}, a well defined steady-state behaviour was observed using a gold ultramicroelectrode (**figure 4.14**). The equilibrium potential of the hexacyanoferrate couple shifted to more positive potential as the concentration of supporting electrolyte was increased beyond 0.1 $mol.dm^{-3}$. Although the equilibrium potential had an unknown contribution from the liquid junction potential of the reference electrode (SCE), the changes observed seemed too large to be attributed to changes of liquid junction potential. The potential shift was attributed to the association of the K^+ cations and the hexacyanoferrate ions.

When the concentration of supporting electrolyte was < 0.1 mol dm^{-3} and the hexacyanoferrate couple concentration ≤ $1x10^{-3}$ mol dm^{-3}, steady state limiting currents were not observed (**figure 4.15**). Initially it was thought that this behaviour could be attibuted to poisoning of the gold surface by adsorption of Cl^- anions from the reference electrode (SCE) or by contamination from epoxy used for sealing the gold wire. However, experiments carried out using platinum as a quasireference electrode and gold ultramicroelectrodes sealed in glass (~ 60 μm diameter) gave the same results. According to Steven and Wightman (71),

electrochemical measurements performed when the electrolyte/analyte ratio is > 1 can give information which is not affected due to scavanging electrolyte in the diffuse layer. In a series of experiments the [electrolyte]/ [hexacyanoferrate couple] ratio was changed from 0 to 100, using a constant concentration of hexacyano-ferrate. However no steady-state behaviour was observed. If the absence of a limiting current is considered to result from migration effects, the ratio i_i /i_d (where i_i is the limiting current when supporting electrolyte is absent from solution and i_d is the diffusion controlled limiting current in the presence of excess supporting electrolyte) must be > 1 for the anion oxidation, according the equations developed by Amatore et al. [39] for the oxidation or reduction of multiply charged ions in the absence of supporting electrolyte. For this reason comparisons with this model can not be made. Moreover, this model has been developed by making several assumptions such as similar diffusion coefficients for products and reactant, no double layer effects, and no ion pairing. It was concluded that migration cannot be considered to be responsible for the experimental behaviour observed in the present system.

According to the results obtained by Campbell and Peter [64] for the system $Fe(CN)_6^{4-}$ /$Fe(CN)_6^{3-}$ on gold electrodes using impedance measurements and KF as supporting electrolyte, a minimum in the apparent rate constant is observed when the total concentration of K^+ cations is increased over the range $4x10^{-4}$ to 1 mol dm^{-3}. Experiments with different concentration of supporting electrolyte in the range where the total concentration of K^+ increases from $7x10^{-4}$ to 0.01 mol.dm^{-3} were carried out . Initially a lack of reproducibility was found. Different methods for cleaning the ultramicroelectrode surfaces were employed. It was found that when the ultramicroelectrodes were cleaned following the procedure described in the experimental section (4.6) and the scan initiated at the equilibrium potential, acceptable reproducibility was obtained. **Figure 4.16a**, shows Tafel plots under the experimental conditions mentioned above and **figure 4.16b** shows the behaviour observed when the supporting electrolyte concentration was ≥ 0.01 mol dm^{-3}. From these plots, the apparent exchange current i°_{app}, and the electron transfer coefficients were determined for both processes. It was found

that the sum of the electron transfer coefficients for the anodic and cathodic processes is less than one. These results agree with the values obtained by Peter et al. [53] using a coulostatic method.

Figure 4.17 shows $\log k^{\circ}_{app}$ vs. $\log [K^{+}]_{total}$ plots for the oxidation and reduction processes. k°_{app} was determined using the equation:

$$k^{\circ}_{app} = \frac{j^{\circ}_{app}}{nFC_{[Fe(CN)_6^{3-/4-}]_{total}}} \tag{4.29}$$

where j°_{app} is the exchange current density and $C_{[Fe(CN)_6^{3-/4-}]_{total}}$ is the total concentration of hexacyanoferrate couple. A minimum in the apparent rate constants k°_{app} is found when the concentration total of K^{+} is between $1x10^{-3}$ to $3x10^{-2}$ mol dm^{-3}. Effects of association of the K^{+} cation with the hexacyanoferrate couple or double layer effects on the rate of electron transfer could be responsable for the behaviour observed in this range. According to Eaton et al. [64] the association constants K_1 and K_2 for the equilibrium reactions:

$$K^{+} + Fe(CN)_6^{4-} \underset{\longleftarrow}{\xrightarrow{K_1}} KFe(CN)_6^{3-} \tag{4.30}$$

$$K^{+} + Fe(CN)_6^{3-} \underset{\longleftarrow}{\xrightarrow{K_2}} KFe(CN)_6^{2-} \tag{4.31}$$

are related to the thermodynamic association constant, K°, by the following equation:

$$\log K = \log K^{\circ} - \frac{NI^{1/2}}{\left(1 + 1.5I^{1/2}\right)} \tag{4.32}$$

based on the extended Debye-Hückel theory. Here the equilibrium constant $K=K_1$ and K_2, depending on the equilibrium studied and they are defined in terms of the molar concentration of the species present in the reaction. N is a constant; N=4.08

for reaction (4.30), and N=3.06 for the reaction (4.31) [64]; I is the ionic strength. From this equation, values of K were determined for a constant concentration of the hexacyanoferrate couple and different concentrations of supporting electrolyte. From these values, the concentrations of $KFe(CN)_6^{3-}$ and $KFe(CN)_6^{2-}$ were determined. **Figure 4.18** shows the change of ion-pair association with increasing total concentration of K^+ present in the system. Not surprisingly, it is observed that the ion association of the ferrocyanide anion is more appreciable than the association of the ferricyanide anion. When the total concentration of K^+ is $2.2x10^{-3}$ mol dm^{-3}, the extent of association is 24% for the ferrocyanide anion, while it is only 4% for the ferricyanide anion. When the concentration of the supporting electrolyte increases beyond 0.02 mol dm^{-3}, the [associated species]/[electroactive species] ratio becomes less steep (**figure 4.18a**). In any case beyond this concentration, equation (4.32) is not valid due to deviation from the extended Debye-Hückel theory.

From **figure 4.16a** it can be seen that the Tafel plot for the electrochemical process in absence of supporting electrolyte exhibits anodic and cathodic branches that are not symmetrical. The anodic branch is higher than the cathodic branch. This behaviour may be attributed to double layer effects. According to differential capacitance experiments (**figure 4.13**) it is seen that the potential of zero charge related to a capacity minimum appears at potentials negative of the equilibrium potential for the hexacyanoferrate couple. This means the charge on the metal surface (q_m) near the equilibrium potential is positive. This excess of positive charge on the metal will result in the concentration of ferrocyanide anions near to the electrode surface being higher than in a bulk solution and higher than the concentration of ferricyanide anions at the microelectrode surface. This difference in concentration means that the current density at potentials positive of the equilibrium potential will be enhanced.

The plots of ϕ_2 vs. q_M shown in **Figure 4.19a Figure 4.19b** were obtained using the relationship:

$$q^M = \pm\left[2RT\varepsilon\varepsilon_o \sum c_i^S \left(e^{-z_i F\phi_2/RT} - 1\right)\right]^{1/2} \qquad (4.33)$$

which is derived from the Gouy Chapman theory of the diffuse double layer [13]. The plots were calculated considering no association of the ferrocyanide and ferrycianide anions with the K^+ cations **(figure 4.19a)** and considering this association effect **(figure 4.20a)**. In this equation, c_i^S is the concentration of ions in bulk solution, and ϕ_2 is the potential at the outer-Helmholtz plane [13]. From these plots it is seen that when the electrode is charged positively, a high concentration of anions must be near to the electrode surface, which is reflected in the small values of ϕ_2. If association of these electroactive species with the cations from the supporting electrolyte is considered, the concentration of these species near to the electrode surface is less with respect to the situation where no association is considered. This behaviour is also observed in the values of ϕ_2 in **figure 4.19b**.

The charge on the metal electrode can be related to the potential by the equation:

$$q_M = \int_{E_{pzc}}^{E} C_{dl} dE \qquad (4.34)$$

If C_{dl} is considered constant in the potential range studied, the potential difference $E\text{-}E_{pzc}$ is given by:

$$\left(E - E_{pzc}\right) = \frac{q_M}{C_{dl}} \qquad (4.35)$$

Figure 4.20 shows the behaviour of ϕ_2 vs. $E\text{-}E_{pzc}$ calculated using this approximation and C_{dl} equal to 25 $\mu F\ cm^{-2}$.

Figure 4.21a shows the reported dependence of the formal potential for the hexacyanoferrate couple $1x10^{-4}$ mol dm^{-3} on the concentration of supporting electrolyte at 25 °C [71]. If the overpotential is calculated as $(E - E_{formal})$ and this data and ϕ_2 are taken from **figure 4.20**, the behaviour of the ratio between the current density and the true exchange current density can be evaluated for the hexacyanoferrate couple under conditions where supporting electrolyte is present

or absent using equation (4.2). **Figure 4.21b** shows this behaviour. It is seen that the theory predicts that the cathodic current should be considerably hindered by double layer effects even taking into account the formation of ion-pairs. Experimentally this effect was not as large as predicted; **figure 4.21b**. The ion-pair species may be reacting faster than the free ferricyanide anions present near to the electrode-solution interface. The association constant of formation of ion-pair species may be different in the double layer from the association constant of these species in the bulk solution. The concentration of the ion-pairs species in equilibrium with the free association species may be affected in the double layer region due to the potential difference developed in the electrode-solution interface.

Electrochemical and chemical reactions could be also occuring in parallel during the oxidation and reduction of the hexacyanoferrate couple, influencing the electrochemical response observed experimentally. The heterogenous rate constant of electron transfer of the ion-pairs species is expected to be higher than the heterogenous rate constant of electron transfer of the free electroactive species since the reorganization energy of the ion-pairs species may be smaller as the result of the lower charge.

According to the Marcus theory of electron transfer at electrodes [72], the heterogenous rate constant of the forward reaction in its simplified version is expressed by the equation:

$$k_f = Z\exp\left(-\frac{\Delta G_f^*}{kT}\right) \tag{4.36}$$

where Z is the thermal velocity of reacting particles $\approx (kT/2\pi m)^{1/2}$, k is Boltzmann's constant, T is the temperature, and m is the reduced mass of the reactant. $Z \sim 10^4$ cm sec^{-1}. ΔG_f^*, the free energy of activation of the forward reaction, is given by:

$$\Delta G_f^* = \frac{\lambda}{4} = \frac{\lambda_i + \lambda_o}{4} \tag{4.37}$$

where λ is reorganization energy of the atoms and molecules in the environment of the reactant from their positions at equilibrium to the positions occupied about the product species when it is at equilibrium. This reorganization energy is considered to be the contributions of two types of energies λ_i and λ_o. λ_i is the inner contribution which is related with the changes of bonds lengths and angles within the molecule, and λ_o is the outer contribution due to electrostatic effects, which in its simplest form can be related to the solvation energy determined by the Born equation considering the ion as a rigid sphere of radius r and charge *ze* immersed in a continuous medium of dielectric constant ε.

The reaction mechanism may be represented by the scheme of squares:

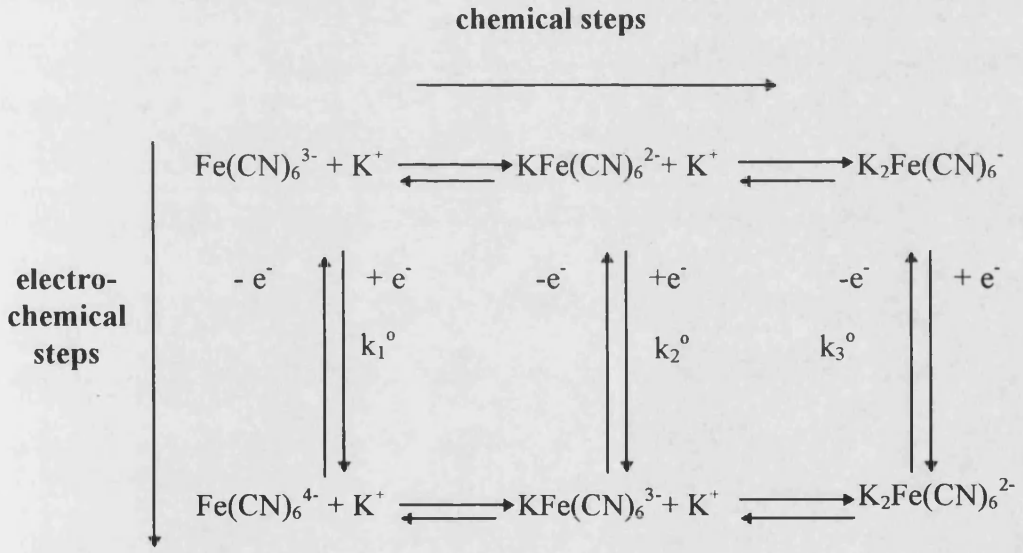

Figure 4.22. Schematic representation of squares for the electro-chemical and chemical reactions of the hexacyanoferrate couple

where $k_2^o > k_1^o$

When the supporting electrolyte is increased, and ion-pair species are formed, the electrochemical reaction of these species is considered to be more favourable than that of the free hexacyano ferrate ions. The outer contribution to the reorganization energy according to Marcus theory is independent of the charge

of the electroactive species. The theory was developed considering very diluted solutions where only the fluctuations from the equilibrium polarization of the dielectric around an ion were considered. However in concentrated solutions, where the formation of ion-pairs is taking place, electrostatic interactions between the different ions present in the solution should be taken into account. These strong interactions between ions may produce appreciable changes on the reorganization energy of the electroactive species during the electron transfer process.

4.9.4. *Impedance studies of the hexacyanoferrate couple.*

When an ultramicroelectrode is used, the a.c. response at lower frequencies is dominated by the diffusional impedance of the microdisc. It is characterised as a quarter circle with its origin displaced below the real axis in the complex plane [72]. This behaviour is attributed to the radial diffusion contribution to the edges of the electrode surface. This quarter circle due to diffusional impedance is less noticeable as the radius decreases. Under charge transfer control, the impedance of ultramicroelectrodes is similar to that of planar electrodes and the impedance is characterised by a semicircle in the complex plane.

Impedance measurements were carried out under the same experimental conditions as those employed in cyclic voltammetric studies using a gold micro-electrode (60 μm diameter). **Figure 4.22** shows the family of complex plane plots obtained. From these plots the charge-transfer resistance (R_{ct}) was calculated. This was achieved using the computer software package, ZVIEW. The capacitance (C_{dl}) was determined from the frequency value at the semi-circle maximum in the complex plane using:

$$\omega_{max} = \frac{1}{R_{ct}C_{exp}} \qquad (4.38)$$

When the concentration of supporting electrolyte was increased, the diameter of semi-circle decreased, indicating a smaller R_{ct}. This behaviour can be attributed to an enhancement of the electron transfer rate with the supporting electrolyte cation

concentration . The experimental capacitance was observed to increase from 11 to 29 $\mu F\ cm^{-2}$. This behaviour could be attributed to adsorption of F^- anions on the gold microsurface as was shown in **figure 4.13**. When the concentration of supporting electrolyte is higher than 0.05 mol dm^{-3} the kinetics of electron transfer of the hexacyanoferrate couple is faster and the diffusional impedance becomes more prominent relative to charge transfer impedance. A gold ultramicroelectrode (5μm radius) was used in an attempt to obtain a better defined semi-circle from which the charge transfer resistance could be determined. However, noise hindered the measurements.

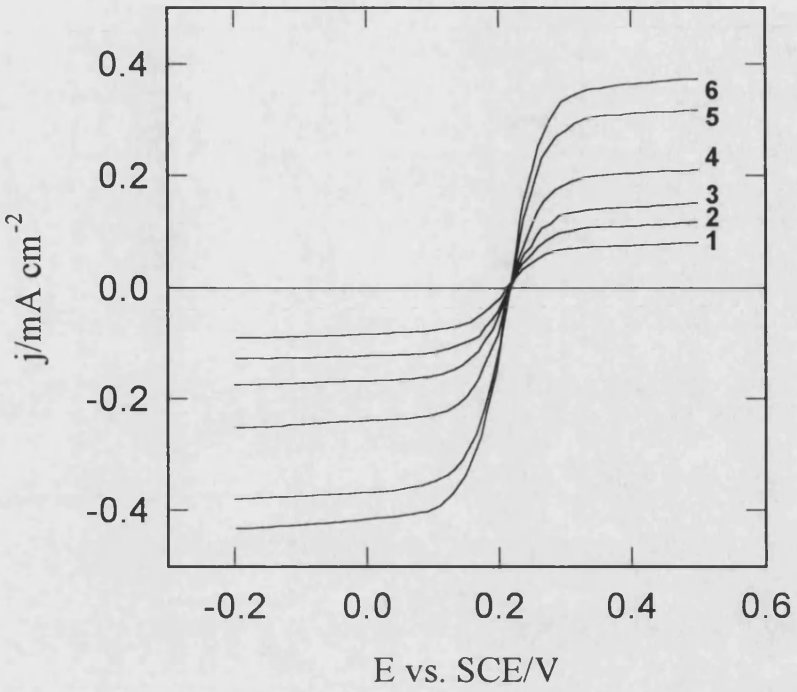

Figure 4.12a. Steady state voltammograms at a gold ultramicroelectrode (10 μm diameter) sealed in glass for different concentrations of hexa-cyano ferrate couple : 1) $5x10^{-5}$; 2) $7.3x10^{-5}$; 3)$1x10^{-4}$; 4) $1.4x10^{-4}$; 5) $2.1x10^{-4}$; 6) $2.5x10^{-4}$ mol dm^{-3} in 0.5 mol dm^{-3} KF; ν = 20 mV s^{-1}

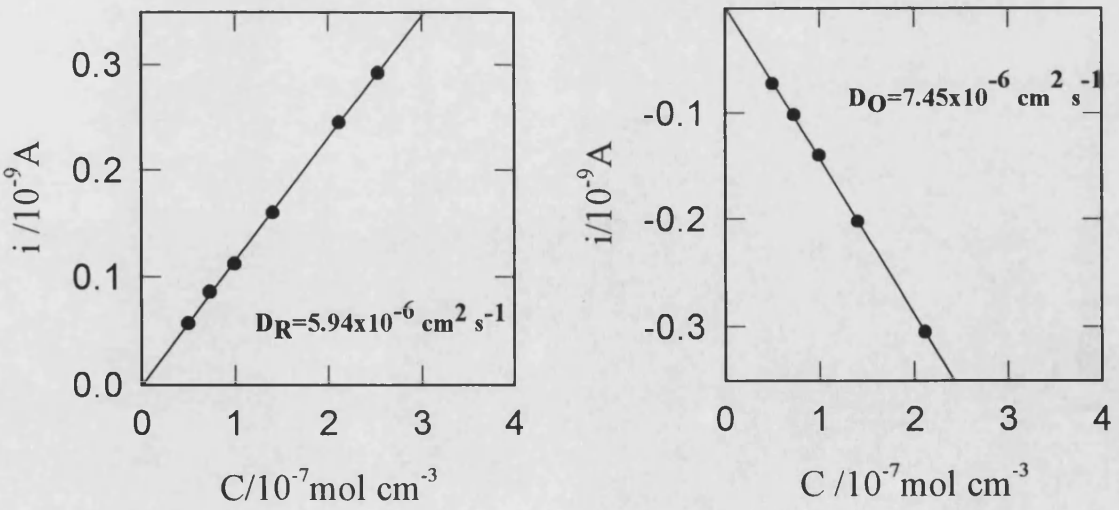

Figure 4.12b. Current vs concentration plots from data in figure 4.12a

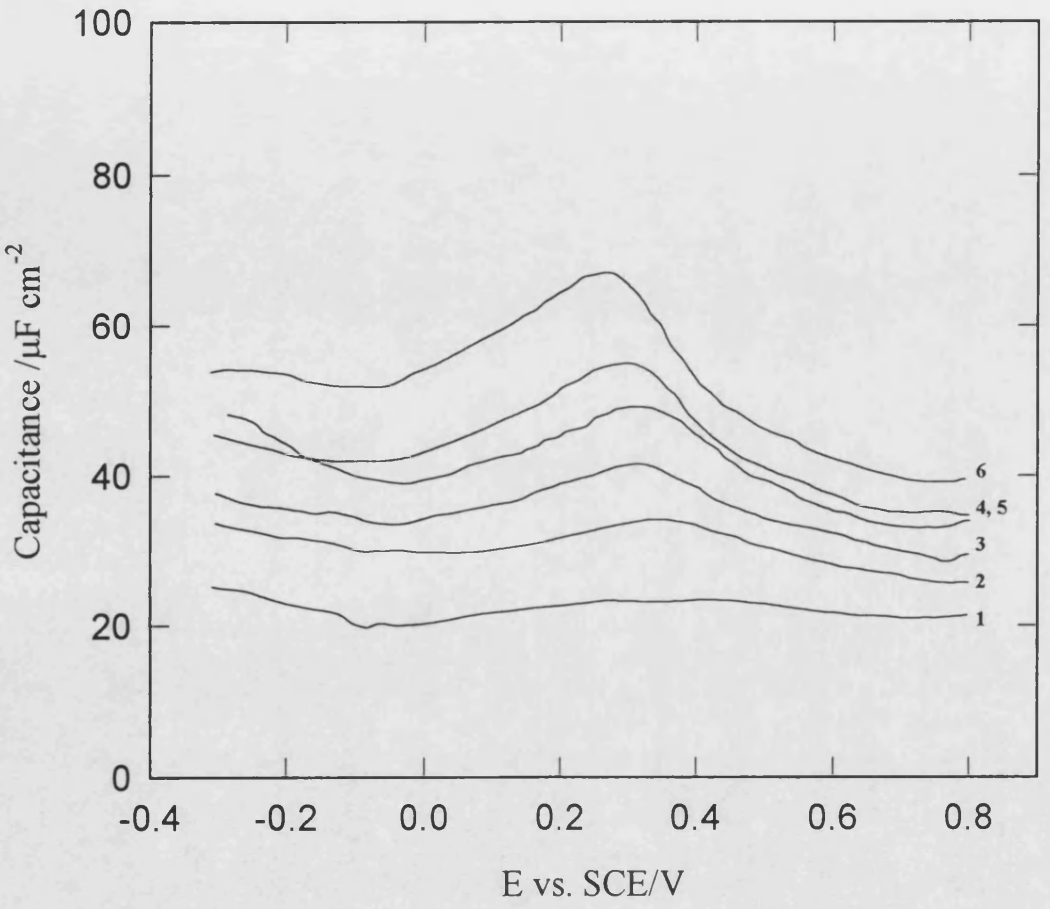

Figure 4.13. Capacitance vs. potential plots at a polycrystalline gold microelectrode (60 μm diameter) sealed in glass for different concentrations of supporting electrolyte:1) $1x10^{-4}$; 2) $5x10^{-4}$; 3) $1x10^{-3}$; 4) $5x10^{-3}$; 5) $1x10^{-2}$; 6) $1x10^{-1}$ mol dm^{-3} KF; ν = 10 mV s^{-1}; 15 Hz; 6 mV p/p

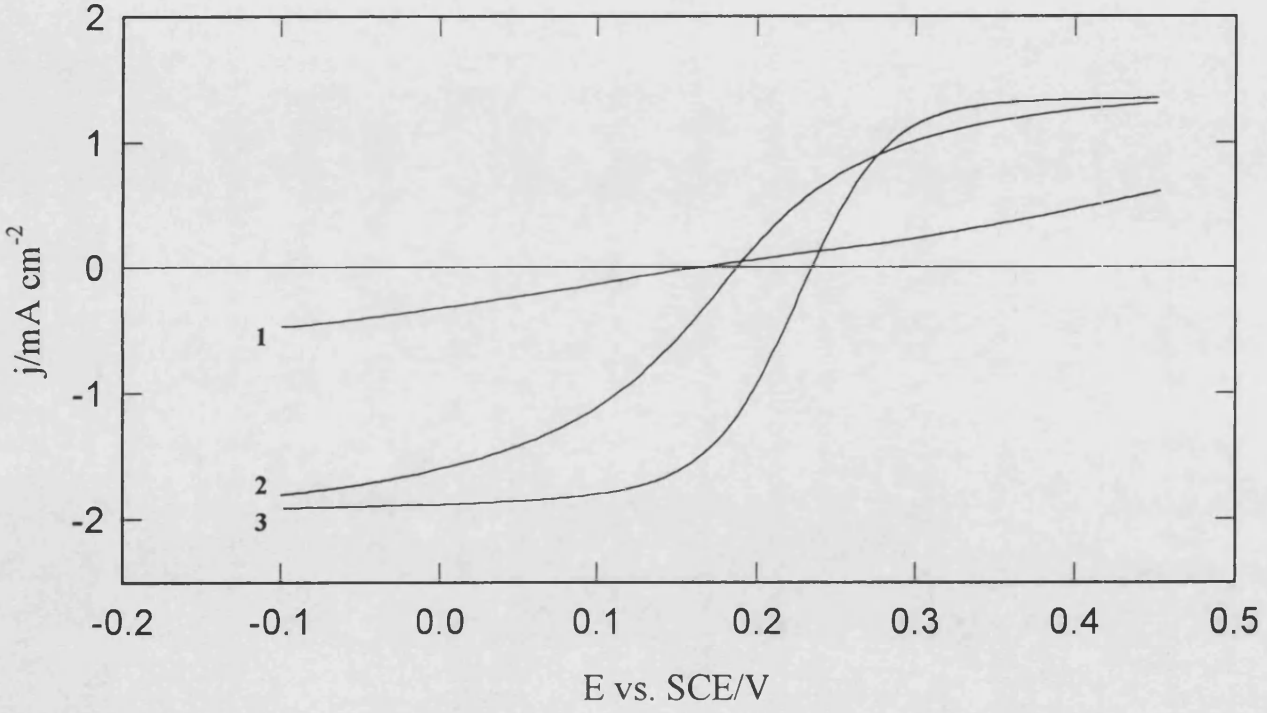

Figure 4.14. Voltammograms obtained at a gold ultramicroelectrode (10 μm diameter) sealed in epoxy for the system $Fe(CN)_6^{4-}/Fe(CN)6^{3-}$ $1x10^{-3}$ mol dm^{-3} in different concentrations of KF: 1)$1x10^{-2}$; 2) $1x10^{-1}$; 3) 1 mol dm^{-3}; $\nu = 5$ mV s^{-1}

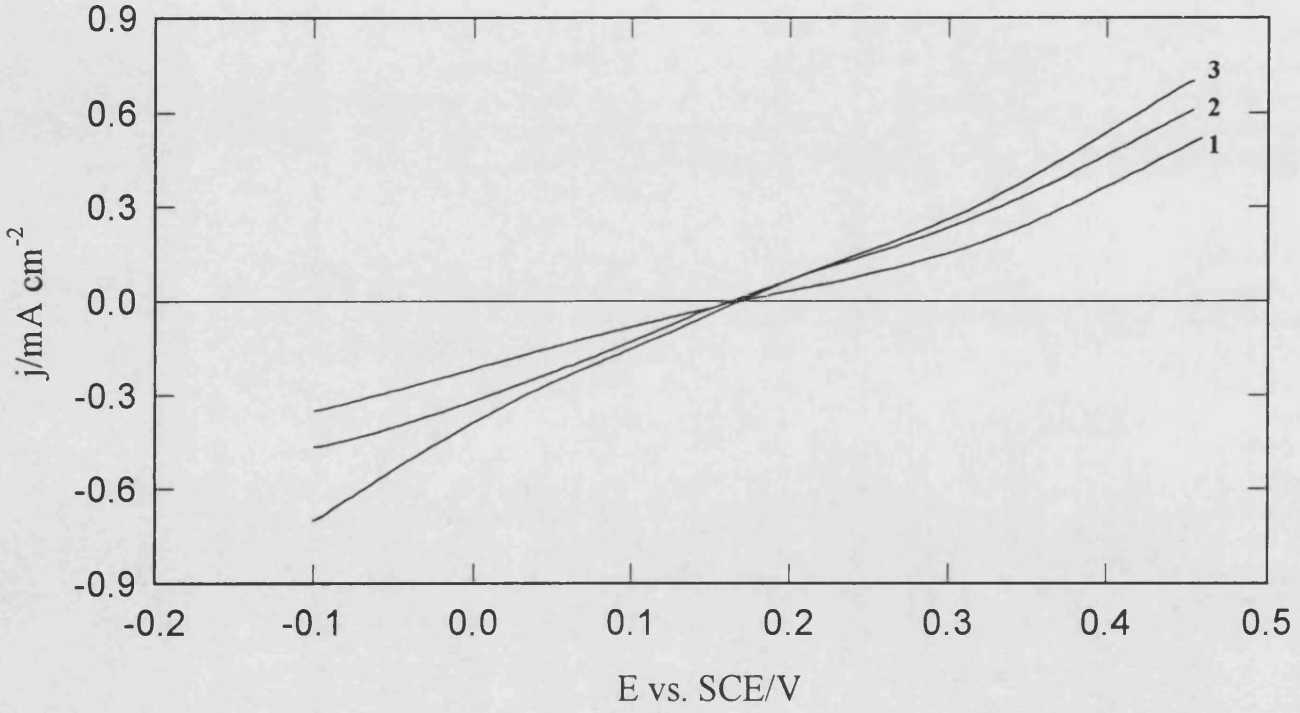

Figure 4.15. Voltammograms obtained at a gold ultramicroelectrode (10 μm diameter) sealed in epoxy for the system $Fe(CN)_6^{4-}/Fe(CN)6^{3-}$ $1x10^{-3}$ mol dm^{-3} for different concentrations of KF: 1) 0; 2) $1x10^{-3}$; $1x10^{-2}$ mol dm^{-3}

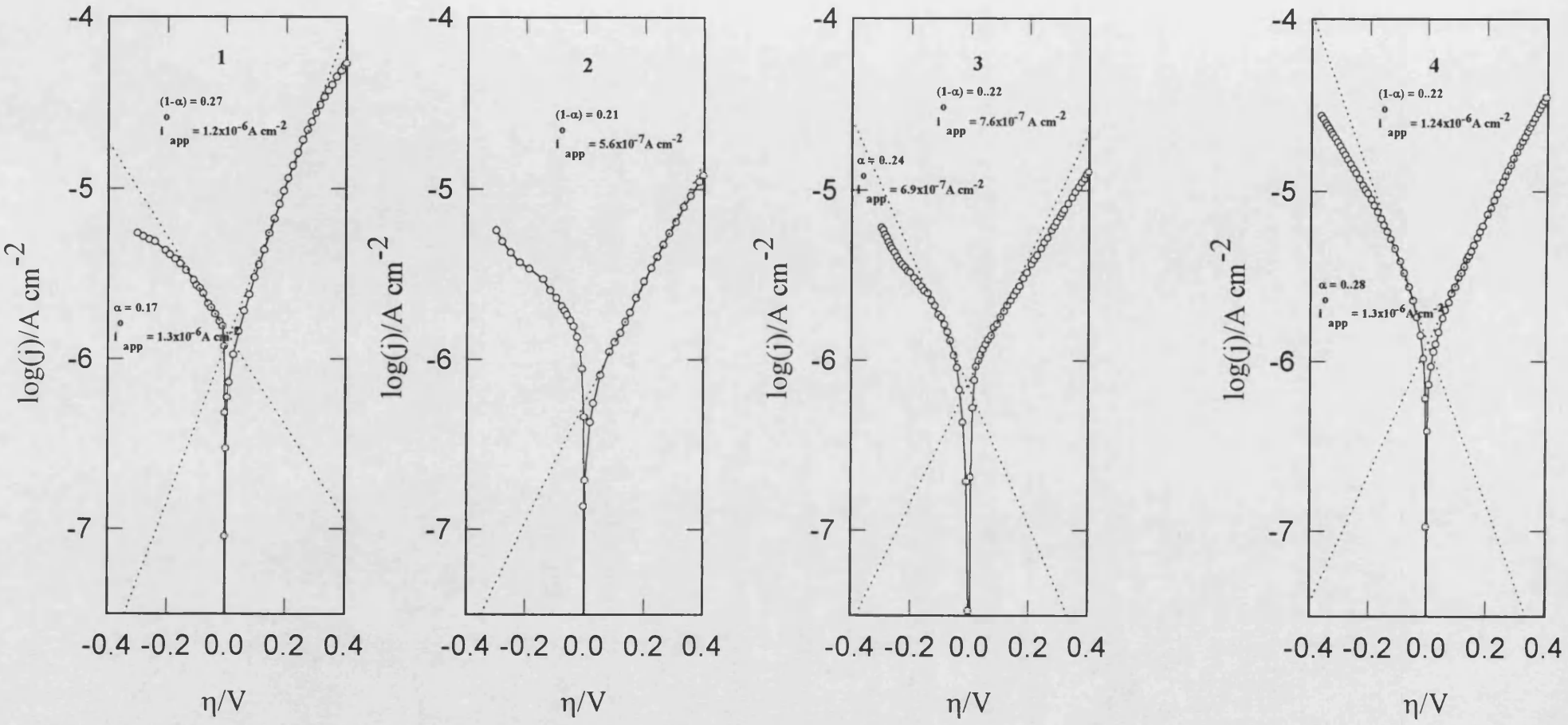

Figure 4.16a.Tafel plots at a gold ultramicroelectrode (10 μm diameter) for the system $Fe(CN)_6^{4-}/Fe(CN)6^{3-}$ 1x10^{-4} mol dm^{-3} for different concentrations of KF: 1) without supporting electrolyte; 2) 4x10^{-4}; 3) 1.5x10^{-3}; 4) 6.9x10^{-3} mol dm-3; ν=25 mV s^{-1}

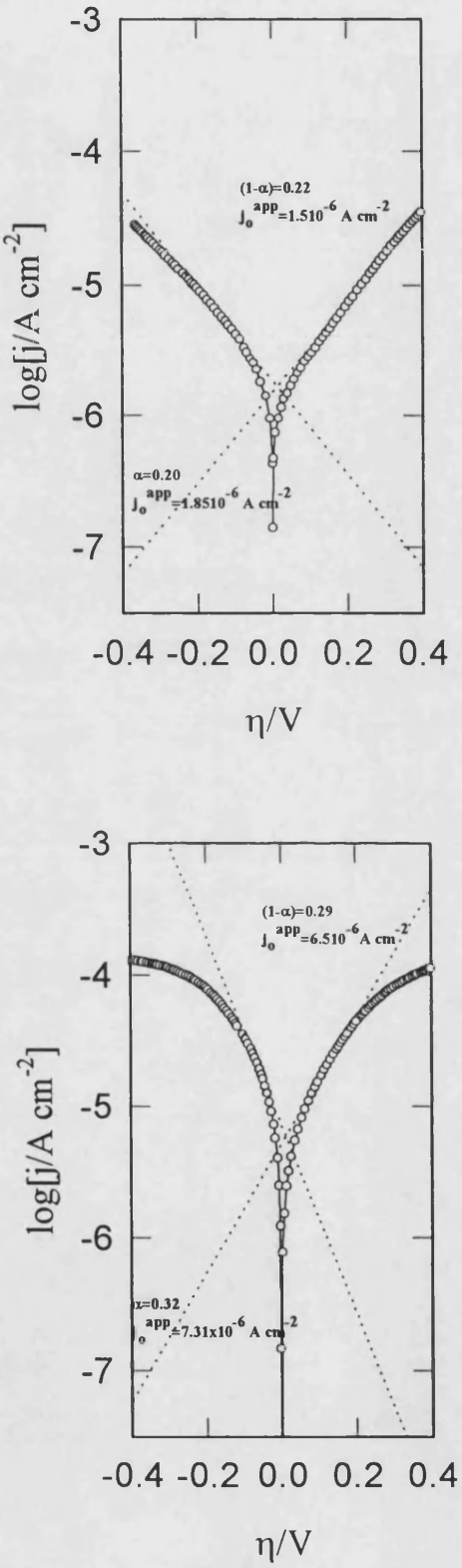

Figure 4.16b. Tafel plots at a gold ultramicroelectrode (10μm diameter) for the system $Fe(CN)_6^{4-}/Fe(CN)6^{3-}$ 1x10^{-4} mol dm^{-3} for different concentrations of supporting electrolyte: 5) 0.01; 6) 0.05 KF; ν = 25 mV s^{-1}

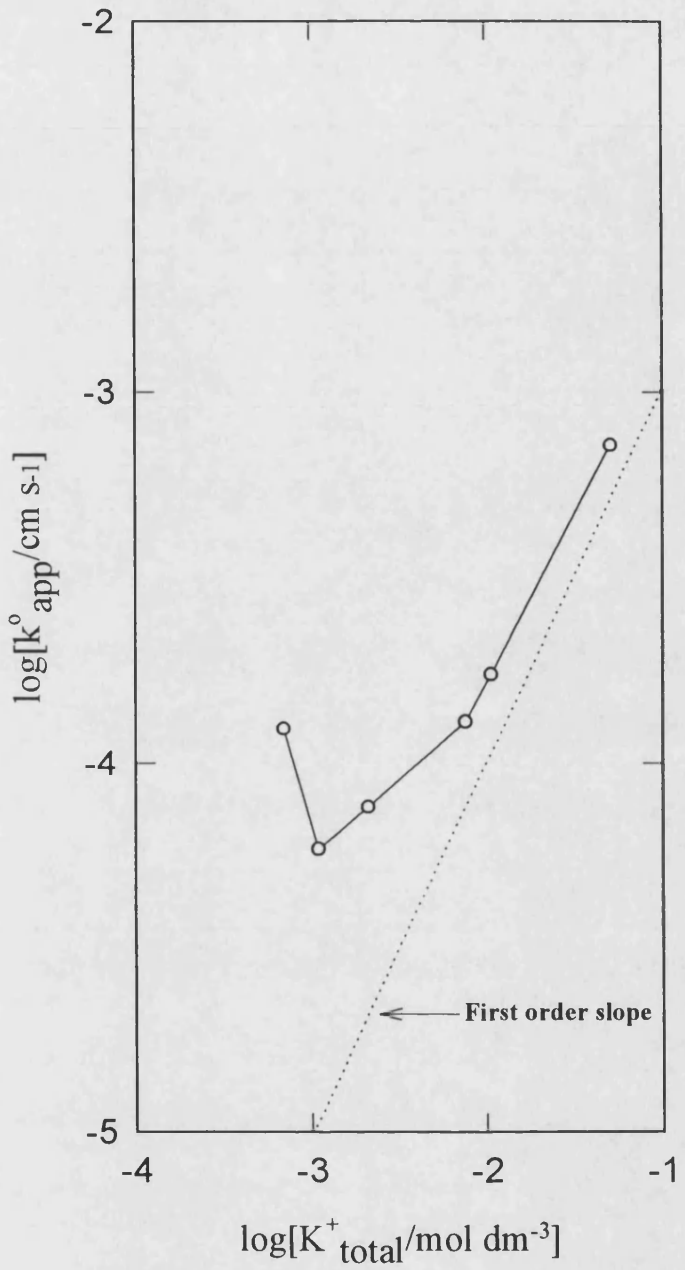

Figure 4.17. Log(k^{o}_{app}) vs. log($[K+]_{total}$) plot for the oxidation and reduction of the hexacyanoferrate couple at a gold ultramicroelectrode (10 μm diameter); ν = 25 mV s^{-1}

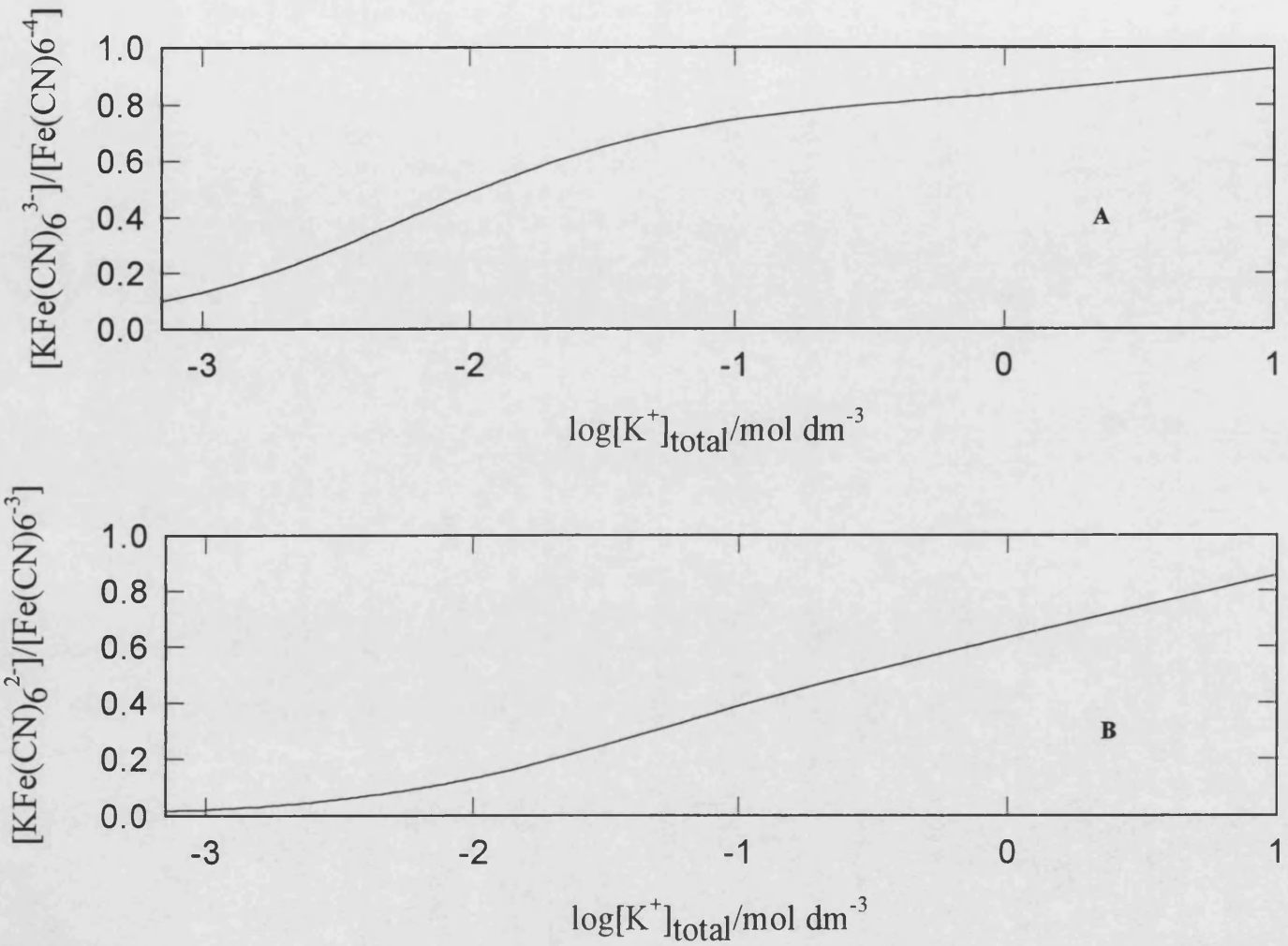

Figure 4.18. Ion-association behaviour calculated from equation (4.32) for the system $Fe(CN)_6^{4-}/Fe(CN)_6^{3-}$ $1x10^{-4}$ mol dm^{-3} when the total concentration of K^+ is increased

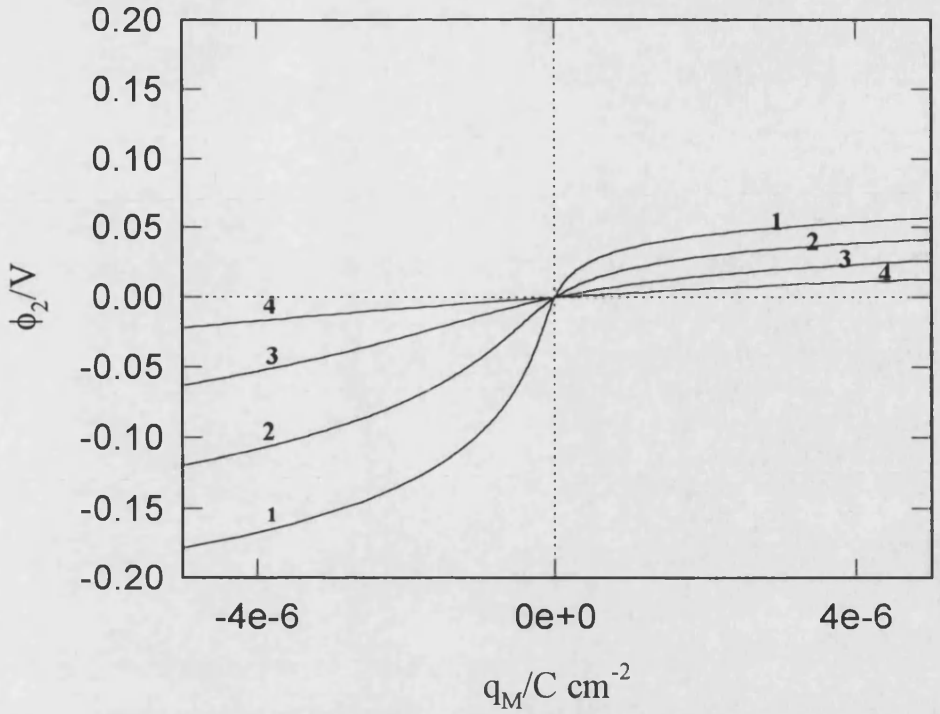

Figure 4.19a. Potential o_2 vs. q_M plots calculated from equation (4.33) without considering specific adsorption and association of the electroactive species with K^+ cations;concentration of $Fe(CN)_6^{4-}$ and $Fe(CN)_6^{3-}$: 1)$1x10^{-4}$; 2) $1x10^{-3}$; 3) $1x10^{-2}$; 4) $1x10^{-1}$mol dm^{-3}.

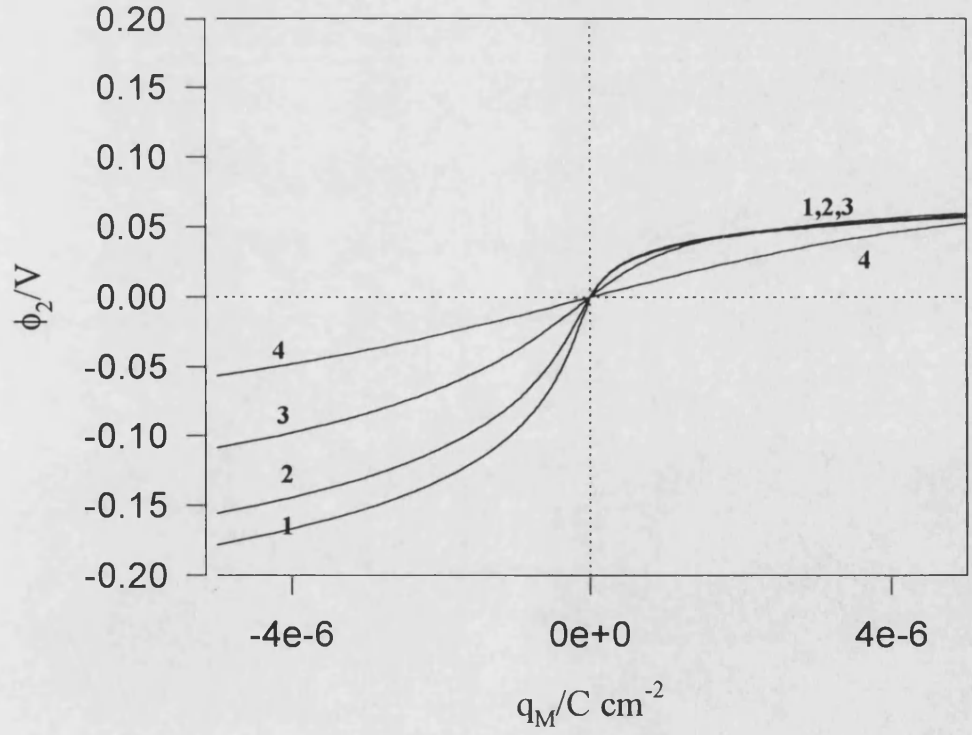

Figure 4.19b. Potential o_2 vs. q_M plots calculated from equation (4.33) without considering specific adsorption and taking into account association of the electroactive species with K^+ cations;concentration of $Fe(CN)_6^{4-}$ and $Fe(CN)_6^{3-}$:$1x10^{-4}$ mol dm^{-3}; 1) without KF; 2) $1x10^{-3}$; 3) $1x10^{-2}$; 4) $1x10^{-1}$ mol dm^{-3} KF

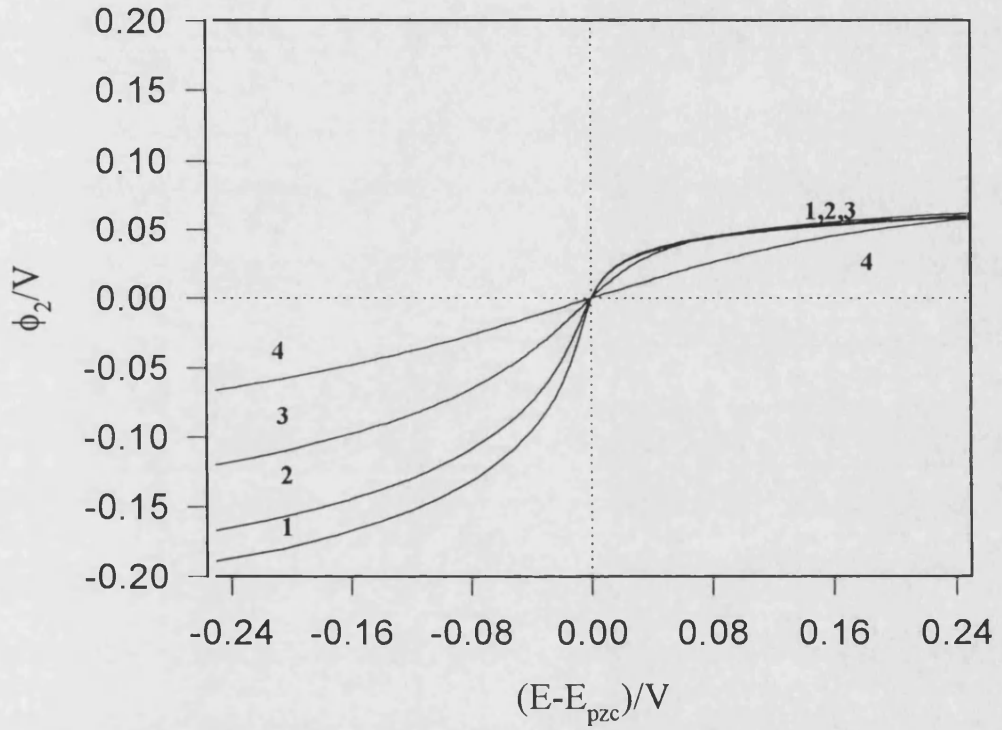

Figure 4.20. Potential o_2 vs. (E-E_{pzc}) plots from data in figure 4.19b; assuming C_{dl}= 25 μF cm^{-2} ; hexacyanoferrate couple concentration: $1x10^{-4}$ mol dm^{-3}; supporting electrolyte concentration variable: 1) without Kf; 2) $1x10^{-3}$; 3) $1x10^{-2}$; 4) $1x10^{-1}$ mol dm^{-3} KF.

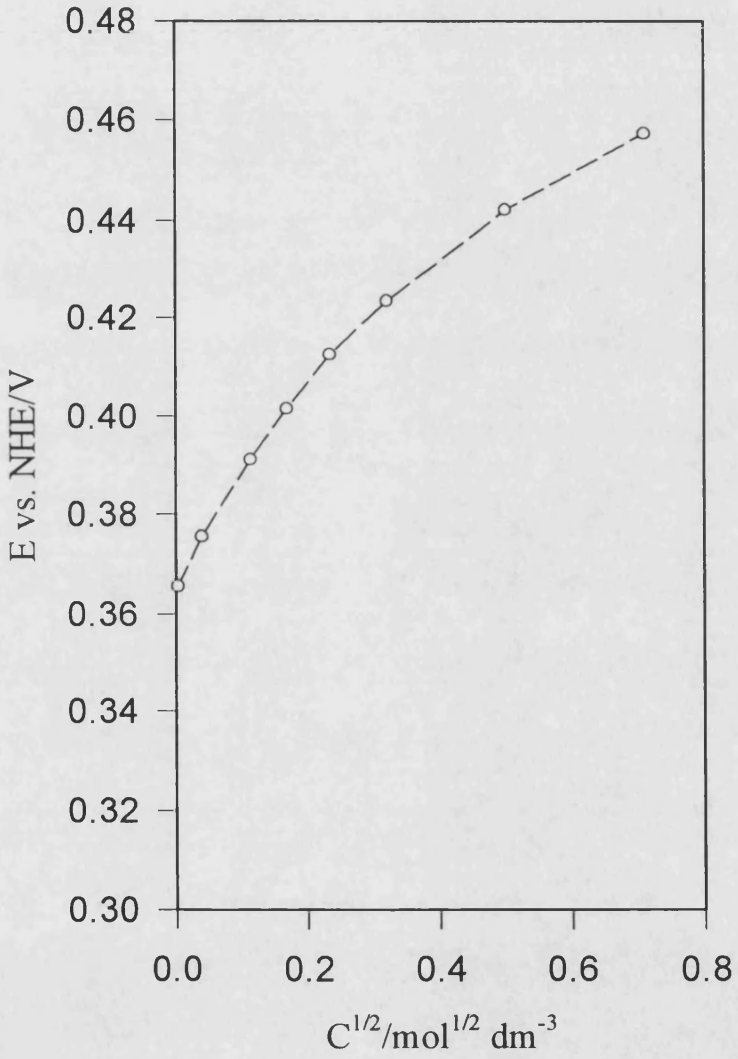

Figure 4.21a. Variation of measured formal reduction potential with the concentration of KBr; equal concentrations of $K_4Fe(CN)_6$ and $K_3Fe(CN)_6$; T=25°C; data taken from reference [71]

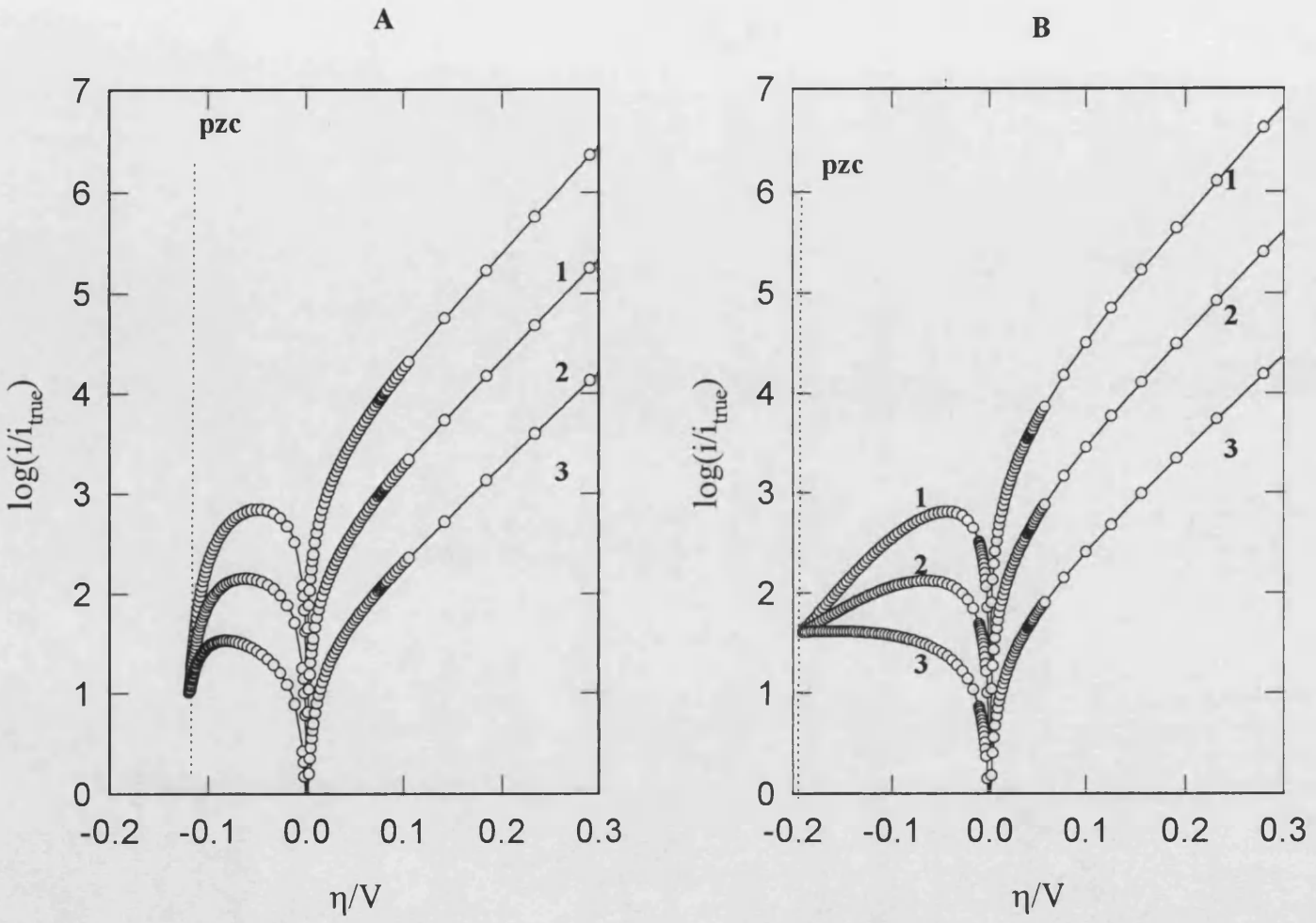

Figure 4.21b. $\log(j/j_{true})$vs. overpotential plots calculated from equation (4.2) taking data in figure 4.20a; considering the overpotential = $E-E_{formal}$,assuming that effective charge is 1) -3; 2) -2; 3) -1 assuming $\alpha = 0.5$; hexacyanoferrate concentration: $1x10^{-4}$ mol dm^{-3}; A) without supporting electrolyte; B) $1x10^{-2}$ mol dm^{-3} KF;

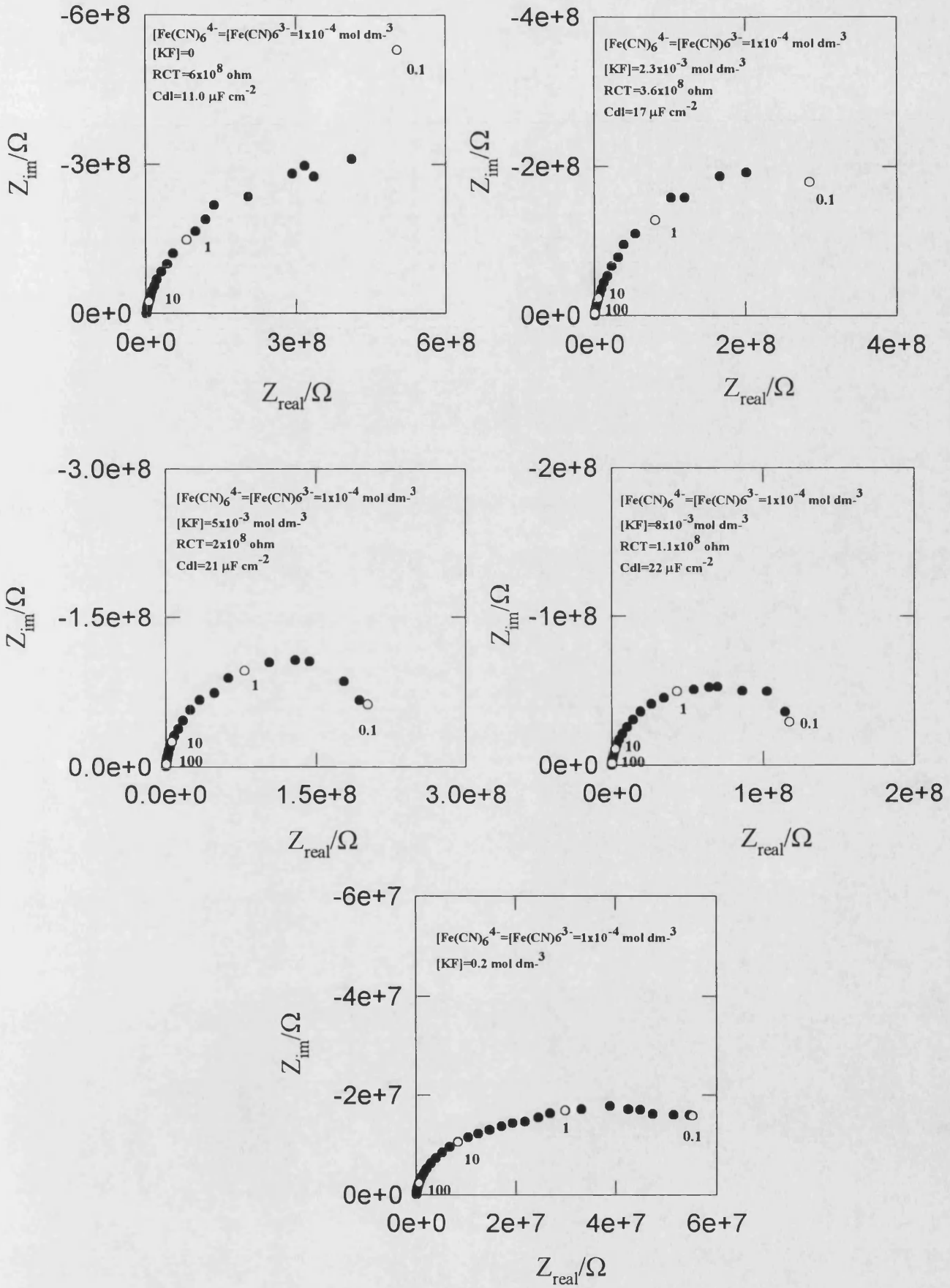

Figure 4.22. Complex plane plots obtained with a gold microelectrode (60 μm radius) for the hexacyanoferrate (II)/(III) couple for different concentrations of KF supporting electrolyte.

4.9.5 *Conclusion*

Microelectrode studies of the oxidation and reduction of hexacyanoferrate couple have shown that the electrochemical process is affected by the concentration of the KF supporting electrolyte. The experimental results show that a low concentration of potassium ion and overall ionic strength, the electrode kinetics become dominated by double layer effects. At higher concentration of potassium ion, the apparent rate constant increases approximately linearly with $[K^+]$ as has been reported previously [52]. Attempts to model the double layer effects on assuming that the reaction involves the free hexacyanoferrate ions showed that the predicted influence of the ϕ_2 potential was larger than that observed experimentally. This provide evidence that the main reacting species are ion pairs, even at these low ionic strengths. The reason for this apparent anomaly is that the rate constants for the ion pair species are considerably higher than those for the free ions. Therefore the electrode reaction proceeds via the ion pairs, even when they are minority species.

The experimental Tafel plots gave α and $(1-\alpha)$ values that do not sum to unity. This effect has been reported previously for measurements made by the coulostatic methods at much higher concentrations of KF [52]. The reason for this anomalous behaviour remains obscure. It is certainly not due to a preceding rate limiting chemical step involving ion pair formation, since this is expected to occur with a second order rate constant in excess of the diffusion controlled limit of 10^{10} dm^3 mol s^{-1}. The possibility that adsorption of hexacyanoferrate ions occurs cannot be ruled out, but it seems unlikely since the capacitance of the gold electrodes appeared to be unaffected by the presence of ions. Tafel plots predicted for taking into account the double layer effect show a large effect only on the cathodic branch. By contrast the anodic branch is largely unaffected because $\phi 2$ is small. It therefore seems unlikely that double layer effects are responsables for the observed values of α

The hexacyanoferrate system is often considered as a 'model' redox system. However this study has revealed that the system is extremely complex.

Comparisons of experimental rate constant with values predicted by Marcus theory [72] are clearly not justified because the reacting species are ion pairs and the apparent rate constant is sensitive to the total potassium ion concentration.

In conclusion, this study has shown that it appears impossible to determine the rate constants for the hexacyanoferrate couple for the free (unpaired) anionic species. Even at the lower concentrations and after correction for double layer effects, the reaction is still dominated by ion pair effects.

Appendix 4.1

Calculations of the concentrations of ion-pair using association constants

$$K^+ + Fe(CN)_6^{4-} \underset{}{\overset{\longleftarrow}{\xrightarrow{K_1}}} KFe(CN)_6^{3-} \qquad (4.29)$$

C'_1	C_2	0	(before equilibrium)
$C'_1 - x$	$C_2 - x$	x	(after equilibrium)

where $C'_1 = C_1 + 7C_2$ (being C_1 the concentration of cations from supporting electrolyte) and x is the concentration of the ion- pair formed. According to equation (4.31):

$$\log K_1 = \log K_1^{\circ} - \frac{NI^{1/2}}{\left(1+1.5I^{1/2}\right)} \qquad (4.31)$$

where N is a constant equal to 4.08 and I is the ionic strength which is represented by the follow equation:

$$I = \frac{1}{2}\sum_i z_i^2 C_i \qquad (4.33)$$

z_i is the ionic charge and C_i is the concentration of each ionic species present in the solution

K_1 was determined to different concentrations of supporting electrolyte considering $\log K^{\circ}$ equal to 2.35 according Eaton [64] and the concentration of ion-pair formed (x) was calculated from:

$$K_1 = \frac{x}{\left(C'_1 - x\right)\left(C_2 - x\right)} \qquad (4.34)$$

which give:

$$K_1 x^2 - \left(C'_1 K_1 + C_2 K_1 + 1\right)x + K_1 C'_1 C_2 - C'_1 K_1 = 0 \qquad (4.35)$$

The same procedure was used for determining the ion-pair concentration from the ferricyanide potassium considering N=3.06 and $\log K^{\circ}$= 1.46.

Appendix 4.2

Calculation of ϕ_2 vs. q_M for a solution containing equal concentrations of $K_4Fe(CN)_6$ and $K_3Fe(CN)_6$, without considering specific adsorption and association of the electroactive species with K+ cations.

The charge q on the electrode per unit area was determined by equation (4.32):

$$q^M = \pm\left[2RT\varepsilon\varepsilon_o \sum c_i^S \left(e^{-z_i F\phi_2/RT} - 1\right)\right]^{1/2}$$

assuming different values of ϕ_2.

Parameter:
M1=$(2RT\varepsilon\varepsilon o)^{1/2}$, where RT=$2.48*10^3$ J mol^{-1}; ε=78.49 at 25 °C;
ε_o=$8.85*10^{-14}$ F cm^{-1}; M1=$1.8566x10^{-4}$ C $cm^{-1/2}$ $mol^{-1/2}$

M2=ferrocyanide concentration/mol cm^{-3}
M2=$1*10^{-4}$; $1*10^{-5}$; $1*10^{-6}$, $1*10^{-7}$

M3=4f, where f=$38.92V^{-1}$; M3=$155.68V^{-1}$

M4=ferricyanide concentration/mol cm^{-3}
M4=$1*10^{-4}$,$1*10^{-5}$, $1*10^{-6}$, $1*10^{-7}$

M5=3f=$116.76V^{-1}$

M6=total concentration of K^+/mol cm^{-3}
M6=$7*10^{-4}$, $7*10^{-5}$, $7*10^{-6}$, $7*10^{-7}$

M7=f=38.92V

Variables:
y = theta=ϕ_2=(potential at outer Helthmonz layer in V)

Equations:
q_M=M1*(M2*(exp(M3*y)-1)+M4*(exp(M5*y)-1)+M6*(exp(-M7*y)-1)) $^{1/2}$

Appendix 4.3

Calculation of ϕ_2 vs. q_M for a solution containing equal concentrations of $K_4Fe(CN)_6$ and $K_3Fe(CN)_6$, without considering specific adsorption and taking into account association of the electroactive species with K+ cations.

The charge on the metal was determined using equation (4.32):

Parameter:
M1=$(2RT\varepsilon\varepsilon o)^{1/2}$, where RT=$2.48*10^3$ J mol^{-1}; ε=78.49 at 25 °C;
ε_o=$8.85*10^{-14}$ F cm^{-1}; M1=$1.8566x10^{-4}$ C $cm^{-1/2}$ $mol^{-1/2}$

M2=ferrocyanide concentration/mol cm^{-3} = $9.13x10^{-8}$, $8x10^{-8}$, $5x10^{-8}$, $2.63x10^{-8}$

M3=4f, where f=$38.92V^{-1}$; M3=$155.68V^{-1}$

M4=$KFe(CN)_6^{3-}$ concentration/mol cm^{-3}
M4=$8.75*10^{-9}$, $2*10^{-8}$, $5*10^{-8}$, $7.375*10^{-8}$

M5=3f; M5=$116.76V^{-1}$

M6=ferricyanide concentration/mol cm^{-3}= $9.88*10^{-8}$, $9.5x10^{-8}$, $8.63x10^{-8}$, $6x10^{-8}$

M7=$KFe(CN)_6^{2-}$ concentration/mol cm^{-3}
M7=$1.25*10^{-9}$, $5*10^{-9}$, $1.375*10^{-8}$, $4*10^{-8}$

M8=2f; M8=$77.84V^{-1}$

M9=total concentration of K^+
M9=$7*10^{-7}$, $1.7*10^{-6}$, $1.07*10^{-5}$, $1.007*10^{-4}$

M10=f; M10=$38.92V^{-1}$

M11=concentration of F^-
M11=0, $1*10^{-6}$, $1*10^{-5}$, $1*10^{-4}$

Variables:
y=theta=ϕ_2= (potential at outer Helthmonz layer in V)

Equations:
q_M=M1*(M2*(exp(M3*y)-1)+M4*(exp(M5*y)-1)+M6*(exp(M5*y)-1) +
M7*(exp(M8*y)-1)+M9*(exp(-M10*y)-1)+M11*(exp(M10*y)-1))^0.5

Appendix 4.4

The ratio between current density and the true exchange current density was determined by equation (4.2). The programme used for calculate this ratio is:

Parameter:
alfha=α=a; number electrons=n1; z=charge;
f1=38.92V^{-1}; a=0.5; n1=1; z=-3

Variables:
y=theta=ϕ_2 in V
n2= ($E-E_{formal}$)= overpotential

[Equations]
i/i_{true}=(exp(((a*n1)-z)*f1*y))*((exp((1-a)*n1*f1*n2))-exp(-a*n1*f1*n2))

REFERENCES (Chapter 4)

1. A.M. Bond, M. Fleischmann, J.Robinson, J. Electroanal. Chem., **168** (1984), 299
2. J.O.Howell, R.M. Wightman, J.Phys. Chem., **88**, (1984) 3915
3. M.F. Montenegro, D. Pletcher, J.Electroanal. Chem., **200**, (1986), 371
4. K.B. Oldham, G.G. Zoski, A.M. Bond, D.A. Sweigart, J. Electroanal. Chem., **248**, (1988), 467
5. L.K. Safford, M.J. Weaver, J. Electroanal. Chem., **331**, (1992), 857
6. C. Amatore, C. Lefron, J. Electroanal. Chem., **324**, (1992), 33
7. D.O. Wipf, E.W. Kristensen, R.M. Deakin, R.M. Wightman, Anal. Chem., **60**, (1988) 306
8. A.M. Bond, T.L.E. Henderson, D.R. Mann, T.F. Mann, W. Thormann, C.G. Zoski, Anal. Chem., **60**, (1988), 1878.
9. L.M. Abrantes, M. Fleischmann, L.M. Peter, S. Pons, B.R. Scharifker, J. Electroanal. Chem., **256**, (1989), 229
10. I.L. Cooper, J.A. Harrison, D.R. Sandbach, Electrochim. Acta, **23**, (1978), 527
11. X. Gao, H.S. White, J. Electroanal. Chem., **389**, (1995), 13
12. S. Trasatti, B.E. Conway and J.O'M. Bockris (Eds), *in Modern Aspects of Electrochemistry*, Vol 13, Plenum, New York, 1979
13. P. Delahay, *Double layer and Electrode Kinetics*, Interscience, New York, 1965, Ch.3,4,7,8,9
14. A.L. Bard, L.R. Faulkner, *Electrochemical methods: Fundamental and Applications*, John Wiley & Sons, Inc., 1980, pp500
15. A. Hamelin, *in Modern Aspects of Electrochemistry*, vol 16 (edited by B.E. Conway, R.E. White and J. OM Bockris, p.1, Plenum, New York (1985)
16. A. Hamelin, G. Valette, J. Electroanal. Chem.,**45**, (1973), 283
17. D.D. Bode, Jr.T.N. Andersen, H. Egring, J Phys.Chem., **71**, (1967), 792

18. J. Clavillier, C.N. Van Hnong, J. Electroanal. Chem., **80**, (1977), 101
19. A. Hamelin, T. Vitanov, E. Sevastyanov, A. Dopov, J.Electroanal. Chem., **145**, (1983), 225
20. K.M. Dickinson, K.E. Hanson, R.A. Fredlein, Electrochim. Acta, **37**, (1992), 139
21. J. Lecoem, J. Andro, R. Parsons, Surface Sci., **114**, (1982), 330
22. A. Hamelin, J. Electroanal.Chem., **138**, (1982), 395.
23. M.J. Weaver J.,F.C. Anson, Inorg. Chem., **15**, (1976) 1871
24. A.N. Frumkin, Z. Physik. Chem., **121**, (1933), 164A
25. A.M. Bond, K.B. Oldham, C.G. Zoski, J. Electroanal. Chem., **245**, (1988) 71
26. A.M. Bond, K.B. Oldham, C.G. Zoski, Anal. Chem.Acta, **216**, (1989), 177
27. K.B. Oldham, C.G. Zoski, J. Electroanal.Chem., **256**, (1988), 11
28. A.C. Michael, R.M. Wightman, C.A. Amatore, J. Electroanal. Chem., **263**, (1989), 163
29. J.O. Howell, R.M. Wightman, Anal. Chem., **56**, (1984), 524
30. A.M. Bond, M. Fleischmann and J.Robinson, J.Electroanal. Chem., **172**, (1984), 11
31. A.G. Ewing, B.J. Feldman, R.W. Murray, J. Phys. Chem., **89**, (1985) 1263
32. Z. Stojek, J. Osteryoung, Anal. Chem., **60**, (1988), 131
33. R.M. Morris, K.F. Fischer, H.S. White, J. Phys. Chem., **92**, (1988), 5306
34. B.D. Pendley, H.D. Abruna, J.D. Norton, W.E Benson, H.S.White,Anal. Chem., **63**, (1991), 2766
35. C. Amatore, R. Deakin, R.M. Wightman, J. Electroanal. Chem., **225**, (1987), 49
36. K.B. Oldham, J. Electroanal. Chem., **250**, (1988), 1
37. K.B. Oldham, J.C. Myland, C.G. Zoski, A.M. Bond, J. Electroanal. Chem., **270**, (1989), 79
38. C. Amatore, B. Fooset, M.R. Deakin and R.M. Wightman, J. Electroanal. Chem., **256**, (1988), 255

39. J. Niwa, K. Doblhofer, Electrochim.Acta, **31**, (1986), 439

40. D. Bauer, M. Breant, *in Electroanalytical Chemistry*, A.J. Bard , Ed.; Marcel Dekker: New York, 1975: vol 8

41. A.M. Bond, E.A. Malennan, R.S. Stojanovic, F.G. Tomas, Anal. Chem., **59**, (1987), 2853

42. K.M. Kadish, J.Q. Ding, T. Malinski, Anal. Chem., **56**, (1984), 1741

43. D. Dubois, G. Moninot, W. Kutner, M. Thomas Jones, K.M. Kadish, J. phys.Chem., **96**, (1992), 7137

44. J. Daschbach, D. Blackwood, J.W. Pons, S. Pons, J. Electroanal. Chem., **237**, (1987), 2699.

45.- P.M. Penner, M.J. Heben, T.L. Longin, N. Lewis, Science, 250, (1990), 118

46. G.N. Kaman, T.M. Saccucci, G.Gounilli, A.F. Nassar, J.F. Rusling, Anal. Chem., **66**, (1994), 994

47. M.P. Andrews, C. Blackburn, J.F. McAleer, V.D. Patel, J.Chem.Soc.Chem. Commun., (1987), 1122

48. M.P. Andrews, C. Blackburn, J.F. McAleer, V.D. Patel, J.Organometallic Chem., **350**, (1988), C15.

49. M.P. Andrews, C. Blackburn, J.F. McAleer, V.D. Patel, Inorganic Chemistry, **29**, (1990), 378.

50. Chongmok Lee, Fred C. Anson, J. Electroanal. Chem., **323**, (1992), 381.

51. D.J. Dieman, W.R. Fancett, J Electroanal.Chem., 34(1972)27

52. L.M. Peter, W. Durr, P. Bindra, H. Gerischer, J. Electroanal., Chem., **71**, (1976), 31

53. L. Muller, S. Dietzch, J. Electroanal. Chem., **121**, (1981), 255

54 . I.F. Hu, D.H. Karwerk, T. Kuwana., J. Electroanal. Chem., **188**, (1985), 59

55. S. Pons, M. Datta, J.F. McAleer, A.S. Hinman, J.Electroanal. Chem., 160, (1984), 369

56. J. Kawiak, T. Jedral, Z. Galus, J. Electroanal. Chem., **145**, (1983), 163

57. A. Wieckoswki, M. Szklarczyk, J. Electroanal..Chem., **142**, (1982), 157

58. M. Fleischmamn, P.R. Graves, J. Robinson, J. Electroanal. Chem., **182**, (1985), 87

59. K. Kunimatsu, Y. Shigematsu, K. Nosaki, A. Kita, J. Electroanal. Chem., **262**, (1989), 195

60. C.Beriet, D. Pletcher, J. Electroanal. Chem., **361**, (1993), 93

61. Z. Shi, S. Wu, J. Lipkowki, J. Electroanal. Chem., **384**, (1995), 171

62. M. Stieble, K. Juttner, J. Electroanal. Chem., **290**, (1990), 163

63. S.A. Campbell, L.M. Peter, J. Electroanal. Chem., **364**, (1994), 257

64. W.A. Eaton, P. George, G.I.H. Hanania, J. Phys. Chem., **71**, (1967) 2016

65. K.M. Kadish, J.Q. Ding, T. Malinski, Anal. Chem., **56**, (1984), 1741

66. L. Otero, N. Vettorazzi, C. Barbero, M.C. Miras, J.J. Silber, L. Sereno, J. Electroanal. Chem., **350**, (1993), 251

67. J.D. Norton, H.S. White, S.W. Feldberg, J. Phys. Chem., **94**, (1990), 6772

68. J.B. Cooper, A.M. Bond, K.B. Oldham, J. Electroanal. Chem., **331**, (1992), 877

69. J. Koryta, J. Duovak, L. Kavan, *Principles of Electrochemistry*, John Wiley & Sons, New York, 1993, pp116

70. S.M. Drew, R.M. Wightman, J. Electroanal. Chem., **317**, (1991), 117

71. G.I.H. Hanania, D.H. Irvine, W.A. Eaton, P. George, J.Phys.Chem., **71**, (1967), 2021

72. J.M. Hale, *Reactions of molecules at electrodes*, N.S. Hush, Ed.; Wiley-Interscience, 1971, pp 229

CHAPTER 5

MICROELECTRODE STUDIES OF ELECTROCATALYSIS

CHAPTER 5

MICROELECTRODE STUDIES OF ELECTROCATALYSIS

5.1. *Electrocatalysis*

Materials which provide an alternative route for an electrode reaction that has a lower energy of activation than that of the same process in their absence are considered as a electrocatalysts. For practical applications, these materials need to be stable in the electrolysis medium where the electrode reaction is carried out. Moreover, it is often fundamental in industrial processes that the catalyst acts specifically only on one reaction, e.g. it is a prerequisite for an anode for a chlorine cell to oxidize chloride ion at a low overpotential but it must also inhibit oxygen evolution, since this is the thermodynamically preferred reaction. Electrocatalysts are frequently expensive, and they are usually coated or dispersed on cheaper, inert substrates, using techniques such as electroplating, spraying, and vacuum sputtering. These procedures allow high surface areas to be obtained and the crystallite size to be controlled in order to enhance the catalytic activity. Characterisation of these small particles and their distribution on the inert substrate used for constructing the electrodes has been carried out using X- ray diffraction [1], scanning electron microscopy (SEM) [2], and transmission electron microscopy (TEM) [3].

Some electrode reactions, such Cl_2, O_2 and H_2 evolution involving adsorbed species play an important role in electrochemical technology. These industrial processes are summarised in **table I**.

Table I

Process	Importance	Applications
Water electrolysis	Production of very pure hydrogen and oxygen	- In processes where high purity is essential (e.g. for foodstuffs or where catalyst poisoning is problem)
Chlor-alkali industry	Production of Cl_2, sodium hydroxide and hydrogen	Synthesis of many organic and inorganic compounds; pulp and paper manufacture.
Fuel cells	High efficiency in conversion of chemical energy into electrical energy	Large-scale power generation; vehicle traction; energy recovery in the chemical industry.

5.2. *Fuel cell*

In a fuel cell, chemical energy is converted directly to electrical energy. One of the main features of such systems is that a higher fuel to electricity conversion efficiency can be obtained in comparison to thermal combustion processes. Moreover fuel cells offer a method of energy conversion free from the problem of pollution (i.e. thermal power stations and car engines).

An intense research effort has been directed at improving the anodic oxidation of certain hydrocarbons, as well as the cathodic reduction of oxygen in conditions where cost can be reduced and lifetime of the anodes and cathodes extended [4-6].

Different kinds of fuel cell have been developed for terrestrial and space applications. They have been classified according to the type of electrolyte used. Table II shows a summary of these fuel cells.

Table II

Type of fuel cell	electrolyte, oxidant, fuel and working temperature	electro de matrix and catalyst
(PAFC) [7] phosphoric acid fuel cell	electrolyte: conc. H_3PO_4 oxidant: air (without CO_2) fuel: pure H_2; 150 to 220°C	Pt on carbon black substrate
(AFC) [7] alkaline fuel cell	electrolyte: KOH conc.oxidant: pure O_2 + H_2O (without CO_2); fuel: pure H_2; 200 to 240 °C	anode: Ni electrodes cathode: Ni oxide
(MCFC) [7] molten carbonate fuel cell	electrolyte: it is usually combination of alkali carbonates retained in a ceramic matrix of $LiAlO_2$; oxidant: air + CO_2;fuel: hydrocarbons; 600-700°C	Ni-Cr anode; NiO cathode
(SOFC) [7] solid oxide fuel cell	oxidant:air; fuel: hydrocarbons; 900 to 1000°C	ceramic oxide electrodes
(PEFC) [7] polymer electrolyte fuel cell	oxidant:pure O_2; fuel: pure H_2; <120°C	Pt on carbon black substrate

In PAFC and PEFC, the oxygen reduction reaction is enhanced using highly dispersed Pt on a substrate that is chemically inert in the electrolyte medium utilised. Carbon has been found to be an ideal substrate for obtaining highly dispersed platinum catalysts [8]. Chemically it is reasonably inert in most electrolytes, even at high temperatures, it exhibits good electrical conductivity and it is cheap. Many aspects of metal/carbon electrocatalysts have been studied, such as the effects of metal particle size [9] and the effects of the treatment of the carbon support before deposition of the metal [8]. However, there is still a poor understanding of the electronic properties of the dispersed small particles on the substrate.

5.3. *Electrocatalytic oxygen reduction reaction*

The oxygen reduction reaction is a complicated electrode reaction from the point of view of mechanistic investigation. The reaction is very irreversible in aqueous media at room temperatures. Even with platinum, which is considered the best electrocatalyst for this reaction, the theoretical reversible oxygen-electrode potential has rarely been established. In spite of many years of experimental and theoretical research, it is still not possible to predict a priori the properties of potential electrocatalysts. The key to overall reversibility on good catalytic surfaces is the breaking of the O-O bond in one of the intermediate steps in the overall process.

A point of controversy in the literature concerning oxygen electroreduction is whether oxygen is reduced to water without the formation of hydrogen peroxide as a stable intermediate [11,12], or whether it reduces first to hydrogen peroxide [13], which then, partially at least, either reduces electrochemically to water, decomposes or escapes to the bulk solution. The following mechanisms may be used to describe this behaviour:

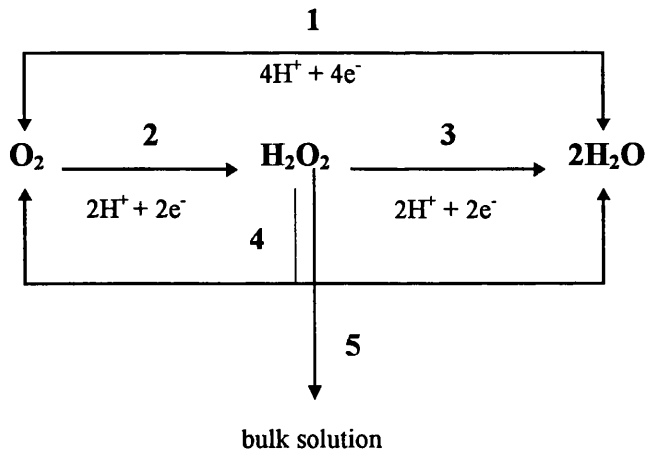

The 4-electron reduction to H_2O, step (1), is generally observed on clean platinum and silver [12-14] in acid media. On electrode materials like carbon, graphite and gold [15-17], the 2-electron reduction of oxygen predominates in acid and alkaline

solutions. In alkaline solutions, steps (1,2,3) can occur in parallel on Pt electrodes [18].

The formation of hydrogen peroxide has been detected using the rotating ring-disk electrode in alkaline solution [18]. When Pt ultramicroelectrodes were used in alkaline and neutral solutions, it was found that the final product from oxygen reduction depended on the the mass transport conditions. When the radius of the ultramicroelectrode is decreased hydrogen peroxide becomes the major product of the reduction of oxygen [19], since diffusion of H_2O_2 away from the electrode (step 5) competes effectively with reduction to water (step 3).

During the last decade, electrodes covered with a thin layer of a proton-exchange membrane (PEM) have been found suitable for improving the kinetics of oxygen reduction [2,20,21]. It was found that the use of a very thin layer of a proton exchange membrane (Nafion®) considerably enhanced the energy efficiency and power density of the fuel cell at lower temperatures. This polymer has negligible anion adsorption effects due to the sulfonate sites within the polymer structure are fixed and they do not cause anion adsortion problems as with the liquid electrolytes. The use of relatively thin membranes of Nafion® permits to minimize ohmic drops in the PEM fuel cells. Different techniques have been developed to increase the three dimensional electrochemically active surface area [22-25] of platinum in the proton exchange membrane fuel cells. High surface area Pt deposits on Nafion® have been achieved via chemical [26] or electrochemical reduction of Pt salts [25].

It has been reported that the oxidation of small molecules like methanol and formic acid as well as hydroquinone, is enhanced on an electrode/conducting polymer substrate compared with bulk electrodes [27,28]. This was attributed to a drastic decrease in the poisoning effect of the adsorption of subproducts formed during the reaction process. Electromodulated Infra-Red Reflectance Spectroscopy (EMIRS) studies showed no significant CO(ads) signal, which is attributed in most cases to the formation of a subproduct which poisons the electrode surface during the oxidation of methanol [27].

Deposition of small metal particles into the conducting polymer, has been shown to increase the catalytic effect for certain reactions [29-32]. Different methods have been used for incorporating small metal particles into these polymers, either dispersed or chemically bound to the polymeric matrices. One method for the generation of catalytically active sites is via covalent bonding of molecules containing the catalytic sites to the monomer before polymerisation [33].

Other methods are occlusion of colloidal suspensions or electrostatic incorporation of the active component during polymer synthesis [34], and electrodeposition of catalyst onto the polymer matrix [35]. Controversies have appeared in the literature regarding the catalytic properties of polymer-dispersed metal particle systems [36-38]. Jacobs et.al [36] have found that oxygen easily permeates through the polymer and that reduction occurs at the polymer/electrode interface. However, Holdcroft et.al [37] have found that with Pt particles dispersed in polypyrrole films of various thicknesses, the catalytic current density for oxygen reduction was strongly limited by oxygen permeation through the polymer matrix. Studies carried out by Vork et.al [38] on the oxygen reduction reaction on Pt particles electrodeposited onto polypyrrole, have shown that when the electrodeposition is made at high current density, the Pt particles exhibit a larger accessible area, and higher oxygen reduction rates to water are observed. When the electrodeposition is performed at lower current densities, reduction is slower, and hydrogen peroxide is obtained. This behaviour shows that the characteristics of the electrodeposition play an important role in determining the catalytic properties of the electrode.

Polyaniline might allow use of thicker coatings of polymer and higher catalyst loading, owing to its higher conductivity. This polymer has been used as a support for catalysts for the reduction of CO_2 [39], O_2 [29] as well as the oxidation of small organic molecules such as methanol [30].

The electrodeposition of small particles of catalyst on ultramicroelectrodes allows the particle size effect to be studied and accurate data to be obtained in the absence of resistive effects, which can hinder the real behaviour of these small particles as catalysts. In the present work, electrodeposition of platinum on carbon

ultramicroelectrodes and on platinum ultramicroelectrodes modified with Nafion®, and polyaniline was carried out, and the electrocatalytic effect on the oxygen reduction reaction was investigated.

5.4. *Experimental*

The H_2SO_4, Aristar grade from BDH, H_2PtCl_6, K_2PtCl_4, Nafion® from Johnson-Matthey, and aniline from Fluka, were used as received. The platinum salt solutions and H_2SO_4 solutions were prepared using ultrapure water (18 MΩ). The electrochemical cell, as described in chapter 2, was cleaned with H_2SO_4/H_2O_2 1/1, and rinsed with plenty of ultrapure water. The platinum disk ultramicroelectrodes with a nominal diameter of 10 μm, and carbon ultramicroelectrodes of 8 μm diameter, were characterised according to the method described in chapter 2. The purity of the solutions as well as the cleanness of the ultramicroelectrodes were investigated as described in chapter 2. In the present work, a reversible hydrogen electrode (RHE) was prepared according to the method given in chapter 2.

5.4.1. *Pt and carbon ultramicroelectrodes modified with Nafion.*

A drop of Nafion® solution was placing on the surface of carbon ultra-microelectrodes with a micropipette. The 2% Nafion solution was prepared by dilution of a 5% Nafion® solution in ethanol. The solution spread over the flat glass surface surrounding the microdisk up to the edge of the electrode. The ultramicroelectrode was positioned inverted on a rotator. The solvent was evaporated at room temperature with rotation at 100 r.p.m. for 15 min, and was then air dried overnight. The modified ultramicroelectrodes were rinsed with plenty of ultrapure water and then introduced into the electrochemical cell. The ultramicroelectrode was left in contact with the solution for 15 minutes before the experiment was carried out.

5.4.2. *Electrodeposition of Pt on platinum substrates modified with Nafion® or polyaniline.*

The electrodeposition of Pt on carbon ultramicroelectrodes and Pt ultramicroelectrodes modified with Nafion® or polyaniline, was carried out from dilute solutions of $5x10^{-5}$ mol.dm^{-3} K_2PtClO_4 using a thermostated cell (connected to a water bath thermostat at 30 °C). The electrodeposition was carried out by cyclic voltammetry and chronoamperometry.

5.4.3. *Pt ultramicroelectrodes modified with polyaniline.*

Pt ultramicroelectrodes were modified with polyaniline by electro-polymerisation of 0.1 mol dm^{-3} aniline in 1 mol dm^{-3} H_2SO_4. The ultramicro-electrode was cycled from -0.2 to 0.8V vs. SCE. The thickness of the deposited film was calculated by determining the charge passed, corresponding to the oxidation of the polymer at 20 mV s^{-1} from 0.05 to 0.75V vs RHE and related with the value of 1 mC cm^{-2}, which corresponds to a film thickness of 318Å [40].

5.5. *Results and Discussion.*

5. 5.1 *Experiments on platinum as substrate.*

Cyclic voltammetric experiments were carried out in the absence and presence of oxygen in 1 mol.dm^{-3} H_2SO_4 at 25 °C. **Figure 5.1** illustrates the diffusion current from the oxygen reduction reaction when a naked Pt ultramicroelectrode was utilised. In the voltammogram recorded in the presence of oxygen the current on the anodic scan is larger than the current on the cathodic scan, in the potential range of 0.4V to 0.7V vs RHE. This behaviour can be attributed to the oxide-free state of the Pt surface up to 0.7V during the anodic scan, while the Pt surface is partly covered with oxide during the cathodic scan down to 0.4V. This behaviour was taken into account for checking the purity of the electrolyte solution used. When the solution was contaminated, the current in the anodic scan was lower than the cathodic current.

The reduction of O_2 at a Pt ultramicroelectrode was also investigated with a slow potential scan (10 mV/s), starting from 1.3 V in the cathodic direction and reversing the scan at 0.3 V. **Figure 5.2** shows the sigmoidal-shaped current-voltage curve obtained under these conditions. The same characteristic feature obtained in **figure 5.1** is observed, i.e. the current in the anodic (reverse) scan is larger than the current in the cathodic scan, over the potential range of 0.65 to 0.9V vs. RHE.

The concentration of oxygen present in a air saturated solution was determined by using Henry's law:

$$P^{o}_{O_2} = x_{O_2\,(solution)} K_H \qquad (5.1)$$

where P^o is the partial pressure of oxygen, x_{O2} is the mole fraction and K_H is Henry's constant for oxygen in water at 25°C (3.3×10^7 Torr). The partial pressure of oxygen was determined from:

$$P^{o}_{O_2} = x_{O_2\,(air)} P_t \qquad (5.2)$$

where P_t was taken equal to 1 atm (760 torr) and the oxygen mole fraction in air is 0.2094 [41]. From equations (5.3) and (5.4):

$$x_{O_2(solution)} = \frac{n_{O_2}}{n_{O_2} + n_{H_2O}} \approx \frac{n_{O_2}}{n_{H_2O}} = \frac{P^{o}_{O_2}}{K_H} \qquad (5.3)$$

where n_{H2O} is 55.55 mol if 1 kg of solution is considered. According to this equation the molality of O_2 in an aqueous solution saturated with air is 2.6765×10^{-4} mol kg^{-1} and the molar concentration is 2.6765×10^{-7} mol cm^{-3}.

The number of electrons which appear to be involved in the reduction of oxygen was determined from the steady state current, using the equation:

$$n_{app} = \frac{i_{ss}}{4FDCr} \qquad (5.4)$$

where i_{SS} is the steady state current, F is the Faraday constant, C is the concentration of oxygen dissolved in the solution, r is the radius of the ultramicrodisk and D is the diffusion coefficient. An average value of 2.32×10^{-5} cm^2 s^{-1} for D was calculated from the values reported by other authors [19,42] in aqueous solutions at 25 °C. From a set of experiments, a value of $n = 1.8 \pm 0.2$ was found for the apparent number of electrons transferred during the oxygen reduction reaction These experiments were repeated several times to test this result. This behaviour can be explained if it is assumed that the final product of the oxygen reduction is H_2O_2, which diffuses away from the ultramicroelectrode surface before further reduction occurs.

Potential step experiments were carried out to study the oxygen reduction reaction in acid media at 25 °C. The potential scheme employed consisted of a cyclic potential sweep from 0V to 1.4V to 0V, followed by a potential step from E_1=1.1V vs. RHE to E_2, where E_2 ranged from 0.3V to 0.95V. Under these conditions the electrode surface is considered to be free of contamination following

the anodic sweep, While the amount of platinum oxide formed is considered to be small.

Diffusion is enhanced at an ultramicrodisc, which can mean that the surface will be poisoned easily. This could change the mechanism of the oxygen reduction reaction. When an ultramicrodisc is used in potential step experiments, and the final potential applied is in the mass transfer limited region, a steady state plateau current at long times must be obtained. This current represents the steady state current due to radial diffusion to the electrode surface. When the experiments were carried out in conditions where the solution was contaminated, a rapid decrease of the current with time was observed at long times. This behaviour is attributed to a process which is kinetically controlled. Contamination of the electrode surface is hindering the charge transfer process. **Figure 5.3** shows the response obtained for the oxygen reduction when a high purity solution was employed. The constant current value observed at long times was used to determine the number of electrons transfered during the electrochemical process using equation (5.6). For a set of experiments a value of 2.2± 0.1 was found for the apparent number of electrons transferred during the oxygen reduction reaction. This result confirms that the final product of the oxygen reduction is H_2O_2 in acid solutions. The H_2O_2 produced during the oxygen reduction reaction escapes easily from the electrode surface due to the rapid mass transport present on the Pt ultramicroelectrode. Formation of H_2O_2 as product of the reduction of oxygen has been reported on rotating disk electrode [18], and on ultramicroelectrodes [19] using alkaline and neutral solutions. The present work shows clearly that H_2O_2 ia also formed in H_2SO_4 solutions.

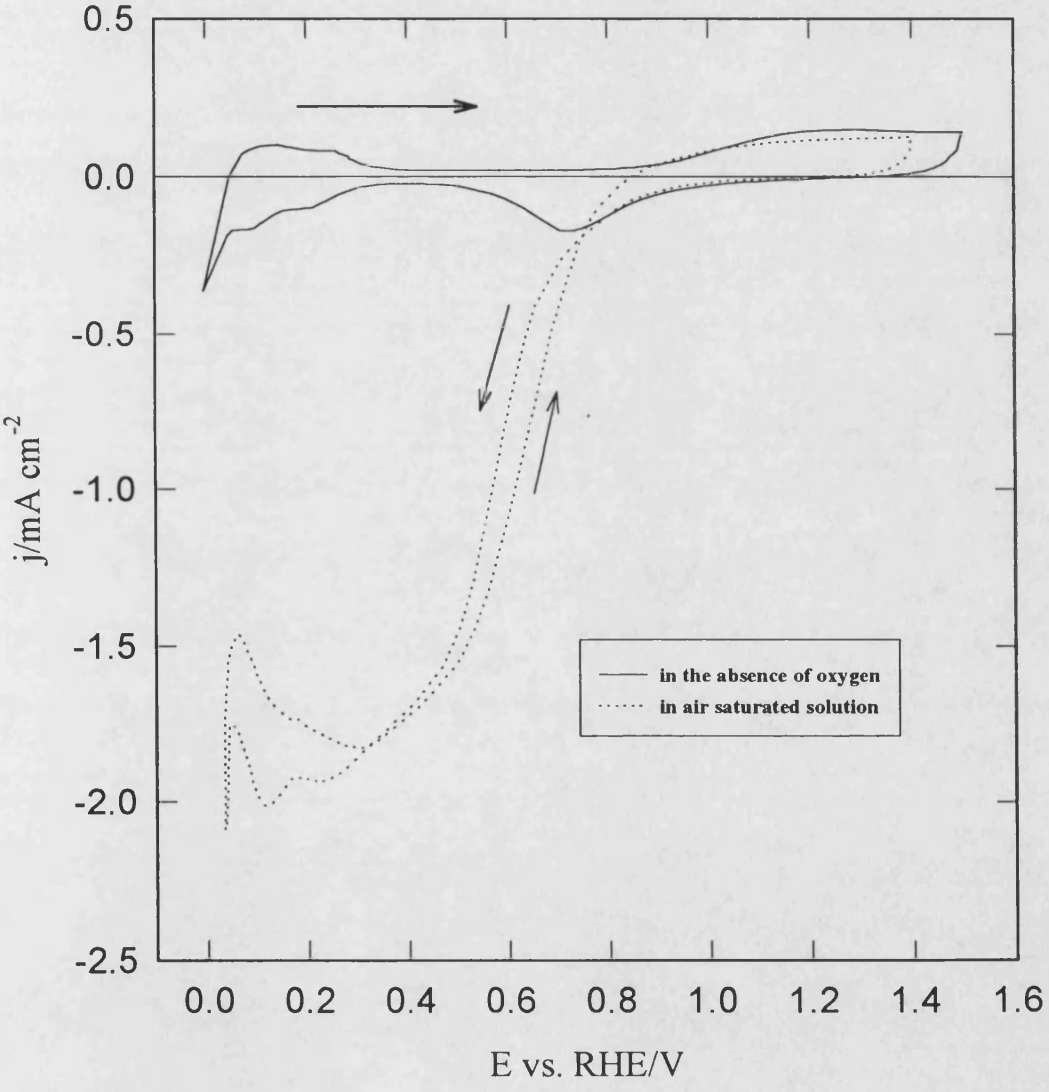

Figure 5.1. Cyclic voltammograms of a platinum microelectrode of 5 μm in radius in 1mol dm^{-3} H_2SO_4 solution at 25°C in the absence of oxygen and in air saturated solution. Roughness factor= 1.57; sweep rate= 100 mV s^{-1}.

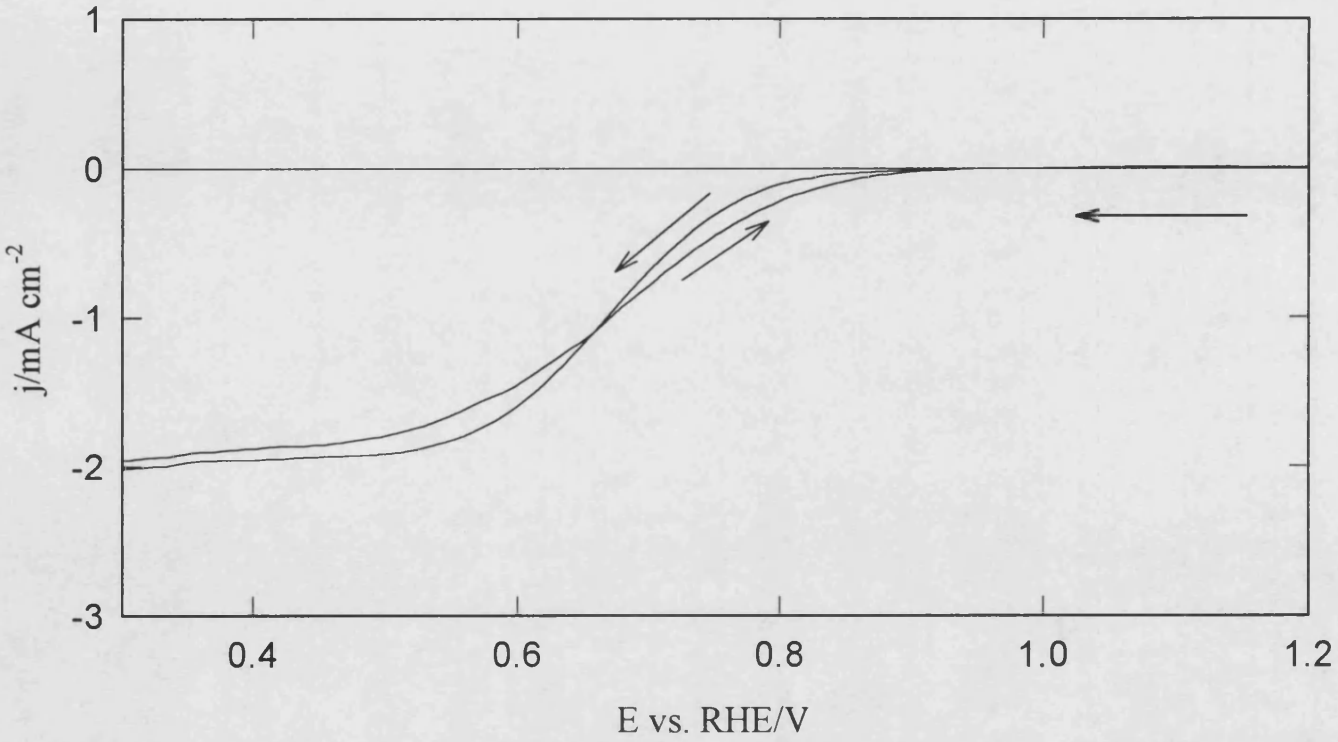

Figure 5.2. Steady state voltammogram recorded on a platinum microelectrode (5 μm radius) in an air saturated solution 1 mol.dm^{-3} H_2SO_4 at 25 ^{o}C; Roughness factor = 1.67; sweep rate = 10 mV s^{-1}.

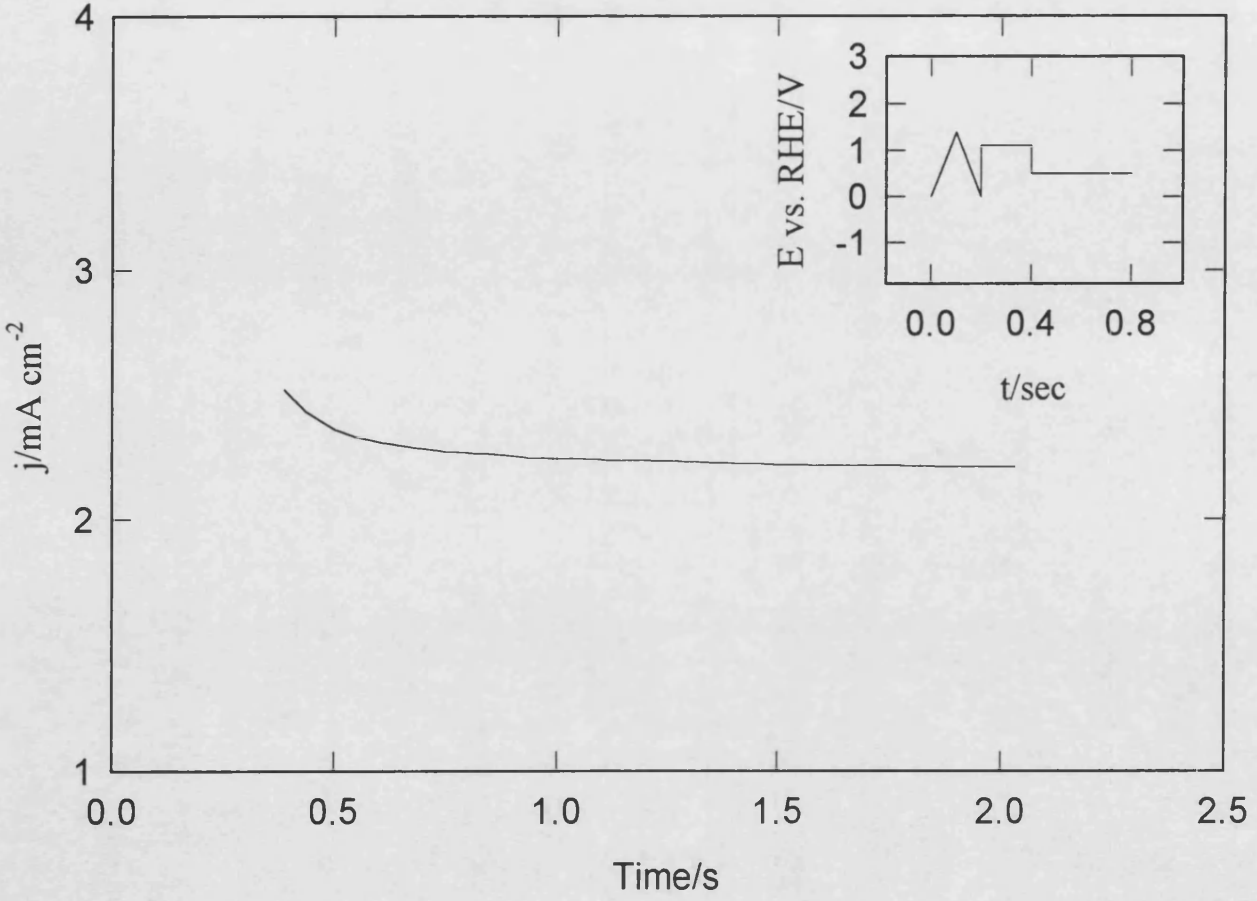

Figure 5.3. Current density vs. time plot for oxygen reduction reaction at a Pt ultramicroelectrode (5 μm radius) in air saturated solution 1 mol dm^{-3} H_2SO_4 at 25 °C. Roughness factor =1.57; Inset: potential program used during the experiments.

5.5.2 *Experiments on platinum ultramicroelectrodes modified with Nafion®*

Platinum ultramicroelectrodes (5 μm radius) were modified with Nafion® using the method described earlier. In previous experiments [3] on conventional electrodes, profilometric measurements have been used to determine the thickness of the dry polymer. In this work, the thickness of the film was difficult to determine because the electrode is so small. However, it is thought that under the experimental conditions employed, a 4-5 μm thick film is formed [3]. After modification, the ultramicroelectrodes were soaked in a nitrogen-purged solution of 1 mol dm^{-3} H_2SO_4 and then cycled between 0 and 1.5V vs. RHE in the same solution.

The initial cyclic voltammogram did not show well defined adsorption and desorption hydrogen peaks. After 4-5 cycles, the electrochemical features characteristic of platinum were established and the shape of the voltammogram remained constant. During the first few cycles, the film is cleaned, and the interface is maintained in an activated state. However some differences were found with respect to the voltammogram recorded using a naked Pt ultramicroelectrode. **Figure 5.4** shows these features. This behaviour can be explained if it is assumed that hydrophobic domains of the polymer are blocking active sites present on the metal surface, or that some organic impurities formed from the recast ionomer can be electrooxidised during cycling as indicated by the larger anodic current in the case of the modified ultramicroelectrode between 1V and 1.5V vs. RHE.

When the solution was saturated with air a noticeable difference was observed between the cathodic current response for the oxygen reduction on the naked ultramicroelectrode and on the modified ultramicroelectrode. **Figure 5.5** shows this behaviour when the experiment was carried out at 100 mV s^{-1}. It is observed that the oxygen reduction kinetics are affected by the Nafion® film. Experiments carried out at low scan rate showed that the limiting current decreased when the Pt ultramicroelectrode was modified with the polymer. Although the modified ultramicroelectrode was cycled several times between 1.3V and 0.1V at a scan rate of 10 mV s^{-1}, the current observed in the anodic scan was always lower

than the current in the cathodic scan. However when the experiments are carried out at a sweep rate >50 mV s^{-1} the current in the anodic scan was larger than the current in the cathodic scan in the potentials range between 0.55V to 0.7V (**figure 5.5**).

The effect of Pt particle size was investigated by electrodeposition of Pt onto the polymer film. A K_2PtClO_4 solution was used and the potential stepped from 1V to 0.5V vs RHE according to the method described in section *5.5.2*. A very dilute solution of K_2PtClO_4 ($5x10^{-5}$ mol.dm^{-3}) was used to attempt to deposit Pt particles only inside or near the top of the Nafion® film. **Figure 5.6a** shows the electrochemical behaviour observed during electrodeposition and figure **5.6b** shows the cyclic voltammogram obtained following platinum deposition.

Attempts to characterise the film with electrodeposited Pt particles using scanning electron microscopy (SEM) and transmission electron microscopy (TEM) were unsuccessful. The amount of metal deposited per square centimeter (W), was determined by the charge passed during the electrodeposition (Q1), assuming 100% current efficiency, subtracting the charging current determined under the same experimental conditions using a blank solution, and employed the following equation:

$$W = \frac{Q1xAr}{2FA_{geometric}} \qquad (5.5)$$

where Ar is the relative atomic mass of platinum (195); F is the Faraday constant and $A_{geometric}$ is the geometric surface area the Pt ultramicroelectrode ($7.85x10^{-7}$ cm^2).

The real surface area (A_{real}) of the exposed Pt was determined from the anodic charge for the desorption of hydrogen in 1 mol dm^{-3} H_2SO_4 at 25 °C, assuming 210 μC cm^{-2} and a roughness factor was calculated using the equation:

$$R = \frac{A_{real}}{A_{geometric}} \qquad (5.6)$$

Figure 5.7a shows the behaviour observed for the steady state current for the oxygen reduction process at the naked and modified ultramicroelectrodes. The steady state current at the Pt/Nafion/Pt ultramicroelectrode (R=15.8) is larger than the steady state current observed on the naked Pt ultramicroelectrode (R=1.57). If it is considered that the product of diffusion coefficient and concentration of the oxygen at the Pt/nafion/Pt microelectrode is equal to the product of these terms when a naked Pt ultramicroelectrode is used, the number of electrons transferred was calculated to be aproximately 3, according to equation (5.4).

Figure 5.7b shows the Tafel plots obtained using the naked and modified ultramicroelectrodes. Similar slopes were observed, but the current density was lower on the Pt/Nafion/PT than on the naked Pt ultramicroelectrode. This behaviour may be explained if it is considered that the Pt surface is not totally available for the oxygen reduction reaction, i.e. the real active surface of Pt for this reaction is lower than for adsortion or desorption of hydrogen. The schematic representation (**figure 5.8**) shows the structure of Pt/nafion/Pt ultramicroelectrode proposed to explain this behaviour:

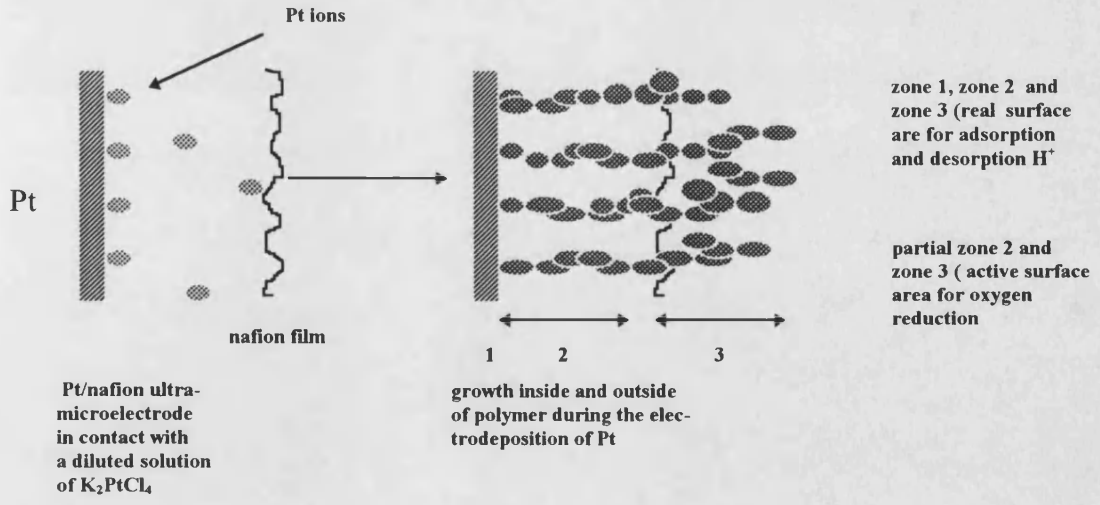

Figure 5.8. Schematic representation of the proposed structure of Pt/Nafion/Pt ultramicroelectrode

Table III presents a summary of the results obtained with Pt, Pt/Nafion and Pt/Nafion/Pt ultramicroelectrodes:

Table III

ultramicro-electrode	Q_1 (C)	W ($\mu g\ cm^{-2}$)	Q_H (C)	R	n_{app}
(1)Pt	-	-	$2.6x10^{-4}$	1.57	~2
(2)Pt	-	-	$3.1x10^{-4}$	1.88	~2
Pt/Nafion	-	-	$3.0x10^{-4}$	1.85	*
Pt/Nafion/Pt	$2x10^{-9}$	2.6	$2.6x10^{-3}$	15.8	~3

Q_1= Total charge passed in Pt electrodeposition

W= Amount of Pt deposited per unit area (geometric area)

Q_H=Charge measured for the oxidation of adsorbed hydrogen in 1 mol dm^{-3} H_2SO_4

R= Roughness factor: Real surface area of Pt/geometric area of ultramicro-electrode

* A well defined steady state current was not observed, and the current was lower than the current obtained on the naked Pt ultramicroelectrode.

From these results, it seems likely that Pt is deposited inside and outside the Nafion film. Pt particles probably grow three-dimensionally from the electrode surface throughout the polymer and outside of the film The behaviour of this system for the oxygen reduction reaction will be different to the behaviour observed in a fuel cell where the catalyst particles are embeded into the polymeric matrix and carbon substrate. The adsorption sites on the Pt particles outside the film may possess different activity compared to the Pt particles embeded in the polymeric matrix.

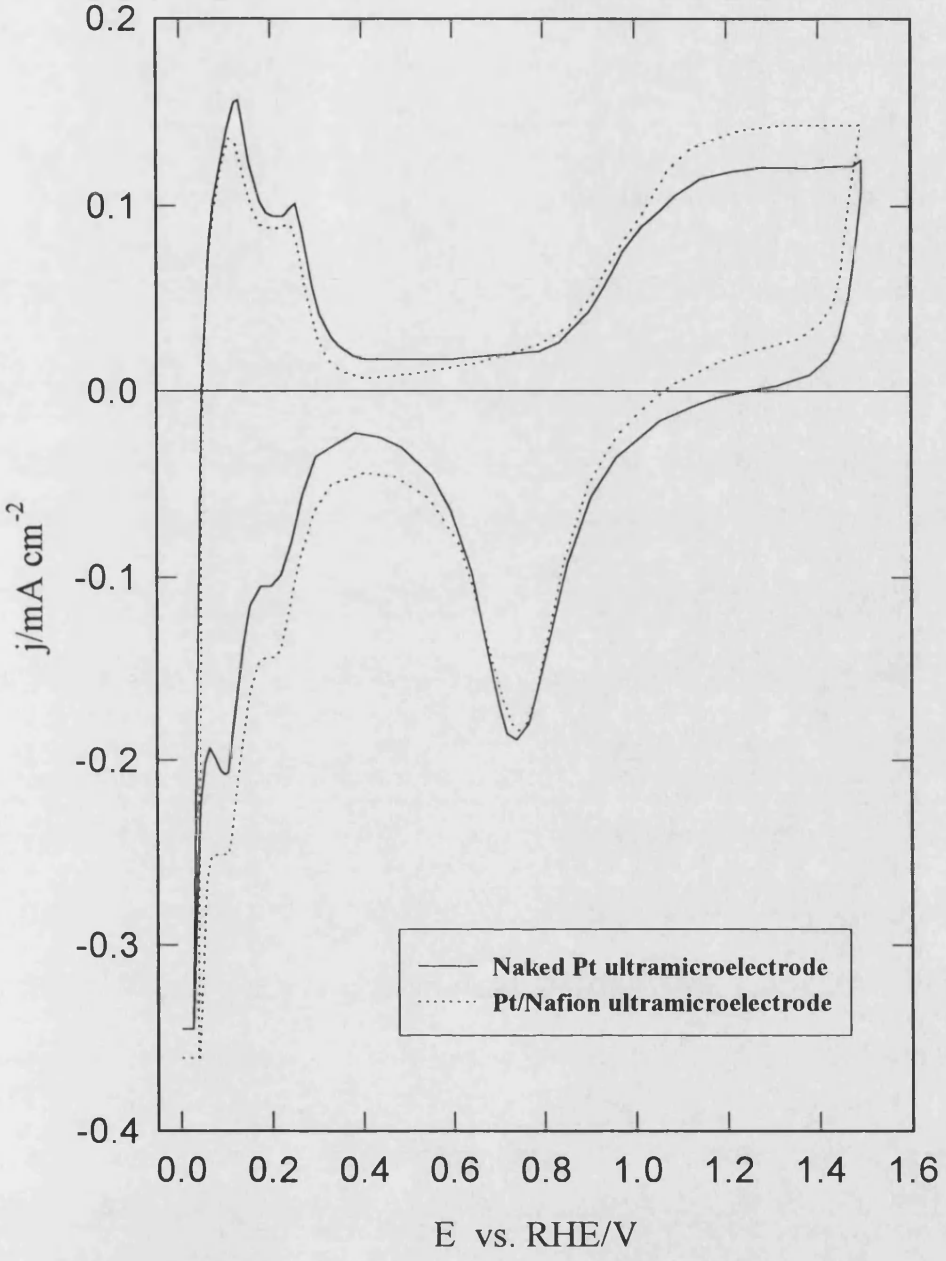

Figure 5.4. Cyclic voltammograms obtained with: A) naked Pt microelectrode (5μm radius), R= 1.88; B) Pt microelectrode modified with Nafion in 1 mol dm^{-3} H_2SO_4 at 25^0C in the absence oxygen; sweep rate: 100 mV s^{-1}.

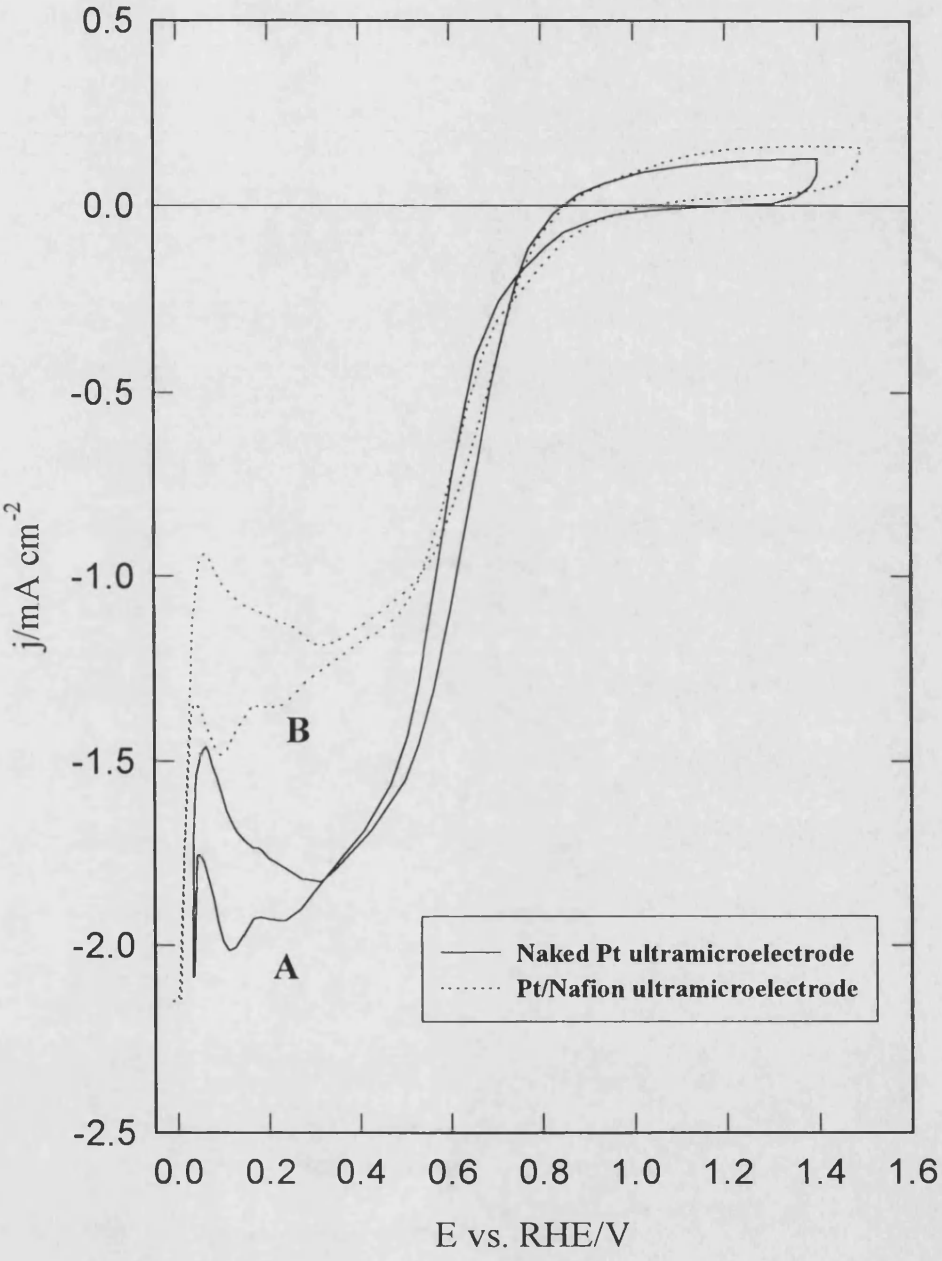

Figure 5.5. Cyclic voltammograms obtained with: A) naked Pt microelectrode (R= 1.57); B) Pt microelectrode modified with Nafion; Solution 1 mol dm^{-3} H_2SO_4 saturated with air, at 25°C (R=1.85); sweep rate= 100 mV s^{-1}.

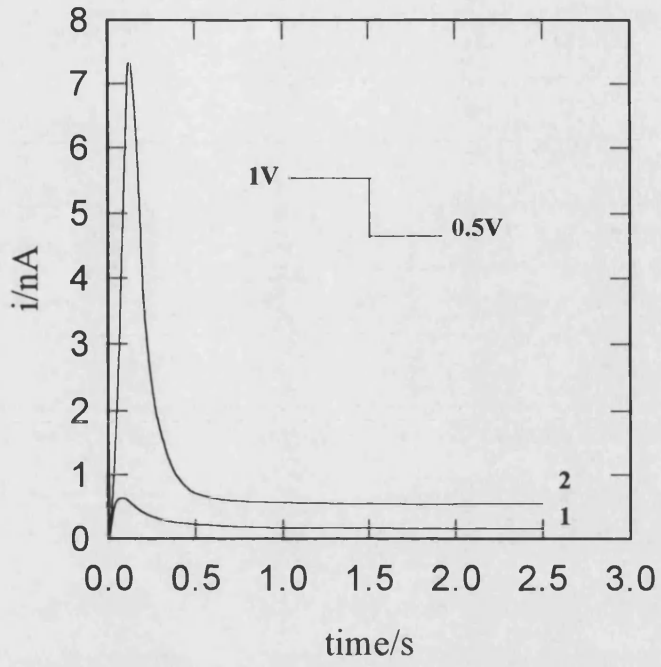

Figure 5.6a. Potential step experiment: 1) blank solution 0.01 mol dm^{-3} H_2SO_4 without oxygen; 2) 0.01 mol dm^{-3} H_2SO_4 + 5x10^{-5} mol dm^{-3} K_2PtClO_4 without oxygen.

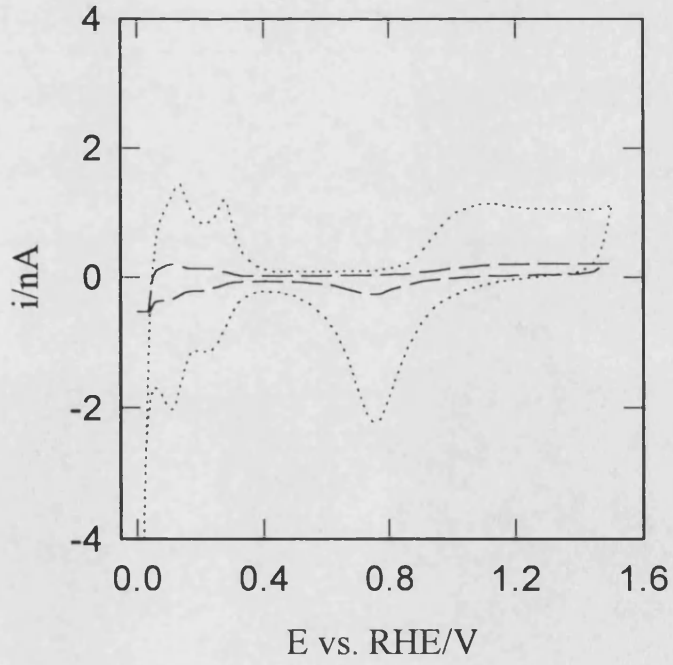

Figure 5.6b. Cyclic voltammograms obtained with: ---- Pt/Nafion ultramicroelectrode;..... Pt/Nafion ultramicroelectrode modified with Pt using potential step shown in figure 5.6a; 1 mol dm^{-3} H_2SO_4 in the absence of oxygen;ν =100 mV s^{-1}.

Figure 5.7a. Steady state voltammograms and Tafel plots.

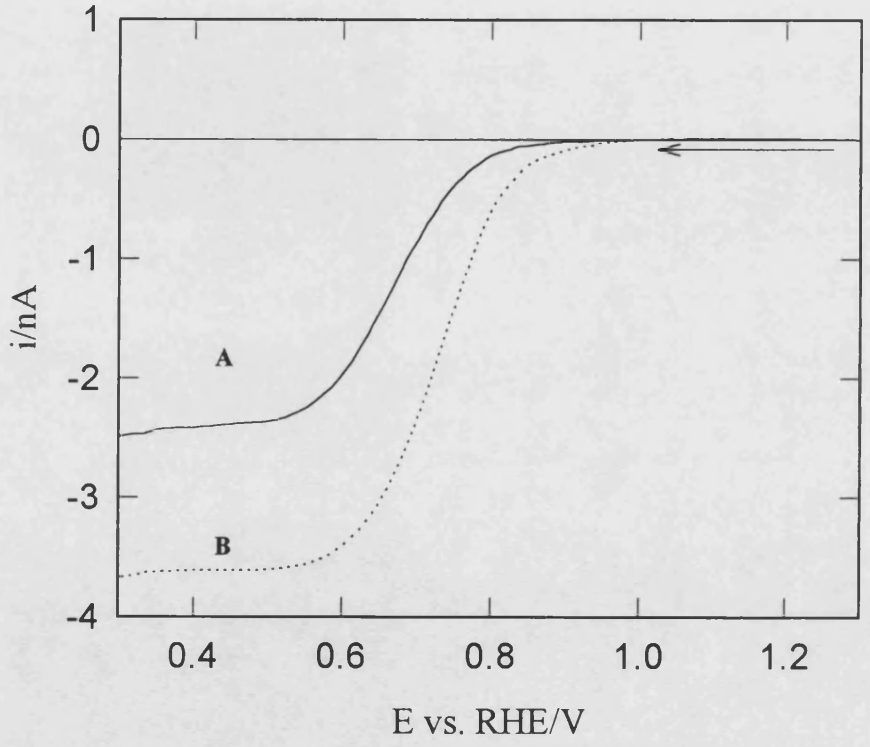

Cyclic voltammograms obtained with: A) a naked platinum microelectrode (R= 1.57); B) a Pt/Nafion/Pt microelectrode (R=15.83) in an air saturated 1 mol dm^{-3} H_2SO_4 solution, sweep rate = 10 mV s^{-1}. Data obtained from forward scan

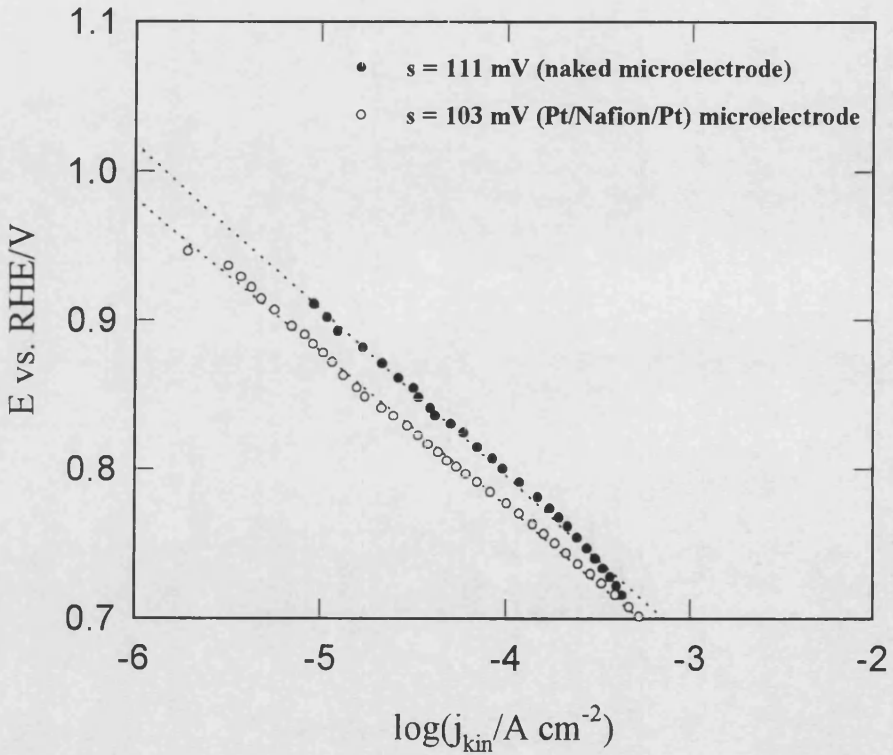

Tafel plot obtained from experimental data in figure 5.7a

Figure 5.7b. Steady state voltammograms and Tafel plots.

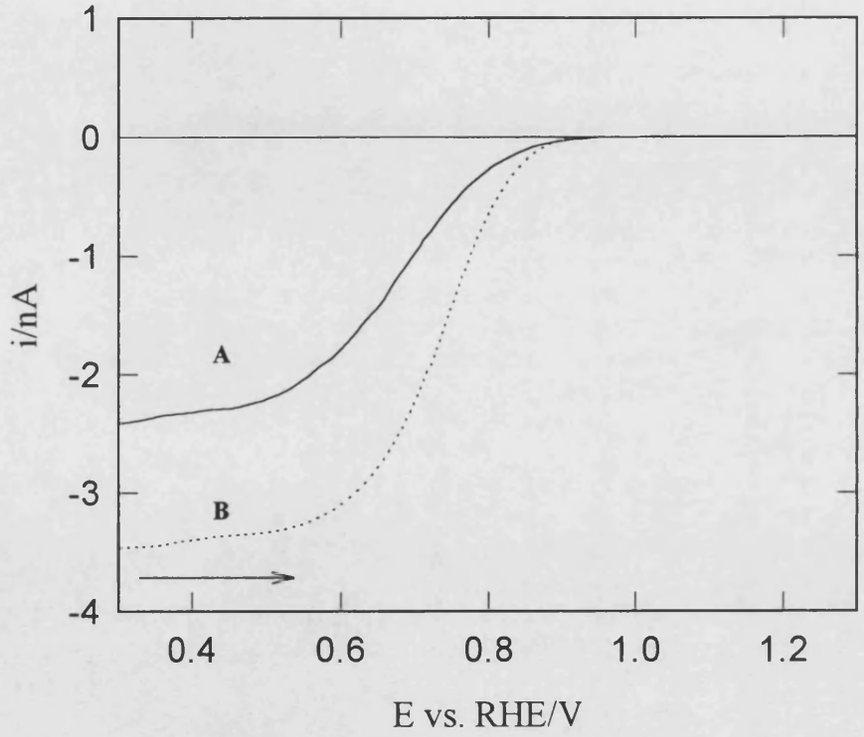

Cyclic voltammograms obtained with: A) a naked platinum microelectrode (R= 1.57); B) a Pt/Nafion/Pt microelectrode (R=15.83) in an air saturated 1 mol dm^{-3} H_2SO_4 solution, sweep rate = 10 mV s^{-1}. Data obtained during back scan

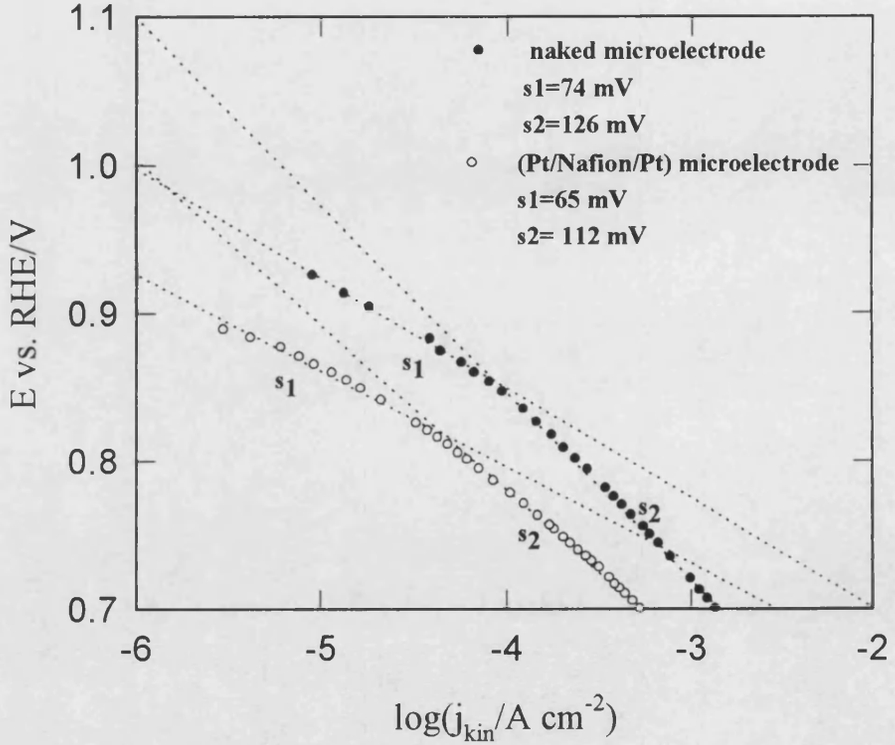

Tafel plot obtained from experimental data in figure 5.7b

5.5.3. *Experiments on platinum modified carbon substrates*

Dilute Pt(II) solutions were used to obtain mass transfer controlled deposition and hence well defined low coverages. **Figure 5.9** shows consecutive cyclic voltammograms recorded on a carbon ultramicroelectrode in 0.01 mol dm^{-3} H_2SO_4 + $5x10^{-5}$ mol dm^{-3} K_2PtCl_4 solution from 0.8V to 0V vs. RHE. It is observed that the reduction of $PtCl_4^{2-}$ occurs at 0.52 V in the first negative scan. After the first cycle cathodic, current is observed at 0.8V and increases at each cycle. The overpotential observed in the first scan for the reduction of $PtCl_4^{2-}$ may be attributed to the formation of Pt nuclei on the carbon surface. After the formation of these nuclei, the electrodeposition of Pt occurs on the Pt nuclei. Two well defined shoulders between 0.05V and 0.2V in both cathodic and anodic scans were observed after three cycles. These shoulders may be attributed to hydrogen adsorption and desorption respectively on the electrodeposited Pt.

After ultramicroelectrode modification, cyclic voltammograms were recorded in 1 mol dm^{-3} H_2SO_4 between 0.8 and 0V. A decrease of the cathodic and anodic currents was observed during the first three scans. When the ultramicro-electrode was cycled from 1.4V to 0V the voltammogram was improved, and after several cycles a reproducible voltammogram was obtained. This behaviour may be attributed to formation of a stable configuration of the deposited particles on the electrode surface. **Figure 5.10** shows the behaviour observed after obtaining the stable voltammogram, using an ultramicroelectrode which had been pretrated by cycling between 0 ans 1.4V vs. RHE. The ultramicro-electrode was left for 1 min at 1.4V prior to the experiment. For the first cycle from 1.4V to 0V, the reduction of oxide formed during the anodic polarisation at 1.4V, as well as the reduction of oxygen are clearly observed. On the second cycle the reduction of oxygen was improved in the kinetically controlled region. Under these conditions a small amount of oxide had been formed. A steady state plateau was observed on this second voltammogram in the potential range 0.6V to 0.4V vs. RHE.

The surface area of deposited platinum was determined from the anodic charge for the desorption of hydrogen. The current from the steady state plateau in the voltammogram was used to determine the apparent number of electrons

transferred during oxygen reduction reaction using equation (5.4). A value of n = 3.6 electrons was found.

Carbon ultramicroelectrodes were also modified with Pt by using a potential step deposition in a dilute solution of K_2PtCl_4. The experiments were carried out applying an initial potential of 0.85V (E_1) and a final potential of 0.5V (E_2) vs. RHE. **Figure 5.11** shows the cyclic voltammograms obtained after modification of carbon ultramicroelectrodes by deposition of different amounts of Pt.

The amount of metal deposited, the real surface area of platinum deposited, and the resulting surface roughness surface factor were determined as explained in section 5.5.2. The geometric surface area of the carbon ultramicroelectrode was $5.03x10^{-7}$ cm^2. **Table IV** is a summary of the results obtained according to the method described above.

Table IV

ultramicro-electrode	deposition method	charge (Q1) (μC)	charge (Q2) (μC)	Pt loading W ($\mu g\ cm^{-2}$)	surface area of electrodeposited Pt (cm^2)	R
1	*cv*	0.179	$4.32x10^{-3}$	359	$2.1x10^{-5}$	41
2	*ps*	$6x10^{-3}$	$2.93x10^{-3}$	12.1	$1.39x10^{-5}$	27.7
3	*ps*	$1.25x10^{-2}$	$4x10^{-3}$	25.1	$1.91x10^{-5}$	37.9

Q1 = deposition charge determined by cyclic voltammetry or potential step

Q2 = charge measured for formation of adsorbed hydrogen in cyclic voltammetry

$W = Q1xAr/2FxA_{geometric}$; where Ar is the relative atomic mass of platinum; F is Faraday's constant.

surface area of electrodeposited Pt = Q2/210 μC cm^{-2}

R = Roughness factor= $A_{real}/A_{geometric}$

cv = cyclic voltammetric; *ps*= potential step

Figures **5.12 and 5.13** show the steady state voltammograms and Tafel plots obtained with carbon/Pt ultramicroelectrodes for platinum loadings of 12.1 and 25.1μg cm^{-2}. From the steady state currents observed on the voltammograms it was found that the apparent number of electrons transferred during oxygen reduction reaction using equation (5.4) is n = 3.6 and 4 respectively. These values are in agreement with the value found on carbon/Pt ultramicroelectrodes modified by cyclic voltammetry in dilute Pt(II) solutions where also a high roughness factor was found. However, these values are in disagreement with the apparent number of electrons about ~2 found on Pt polycrystalline ultramicroelectrodes, with a roughness factor 1.57.

The catalytic effect of small particles was investigated. For evaluating this effect the current density was determined taking a reference point of potential 0.85V where it is considered that oxide is not present. **Table V** shows the parameters determined and a comparison is made with a polycrystalline Pt ultramicroelectrode:

Table V

Comparison of current densities for oxygen reduction measured at 0.85V vs. RHE for polycrystalline Pt and electrodeposited Pt on C ultramicroelectrodes

	Pt (R= 1.57)	Tafel slope (mV)	C/Pt (R=27.7)	Tafel slope (mV)	C/Pt (R=37.9)	Tafel slope (mV)
forward current density (A cm^2)	$3.9x10^{-5}$	111	$4.6x10^{-5}$	121	$3.9x10^{-5}$	111
back current density (A cm^2)	$1.0x10^{-4}$	s_1=74 s_2=118	$1.5x10^{-4}$	s_1=75 s_2=125	$1.19x10^{-4}$	s_1=54 s_2=112

The results obtained from Tafel plots at potentials less than 0.85V show that the slope is about 120 mV. This behaviour indicates that the rate determining step for the oxygen reduction is the addition of the first electron:

$$O_2 + e^- \longrightarrow O_2^- \qquad (5.7)$$

Two well-defined linear regions are observed on the Tafel plots derived from the reverse scan between 0.3V to 1.3V vs. RHE. It was observed that when the potential is > 0.85V vs. RHE, the slope changes from ~120 mV to ~60 mV. This behaviour has also been reported for oxygen reduction in other acid solutions [47]. It has been attributed to different adsorption isotherms due to changes in the coverage of oxide on the electrode surface. It seems that at potentials higher than 0.85V the oxide coverage increases. From **table V** it is observed that the current density determined at 0.85V when the ultramicroelectrode is scanned from 0.3V to 1.3V is three times larger than the value obtained when the ultramicroelectrode was scanned from 1.3V to 0.3V. In the second case there is a high oxide coverage of the electrode surface. This behaviour shows that the oxide on the electrode surface hinders the oxygen reduction reaction. It can be explained if it is considered that the first electron transfer reaction, equation (5.7), is the rate determining step both at high and at low oxide coverage, and the current density at a determined overpotential is governed by the following relationship:

$$j = j_o(1-\theta(E))\exp\left(-\frac{\alpha nF}{RT}\left(E - E^o\right)\right) \qquad (5.8)$$

where (1-θ(E)) is an additional isotherm term, which depends on the coverage grade with the potential.

The effect of particle size on the electrocatalysis of oxygen reduction is generally investigated determining the specific activity (SA) and/or mass activity (MA) which are given by the following equations:

$$SA = \frac{i}{A_{real}} = j \qquad (\mu A\ cm^{-2}) \qquad (5.9)$$

where i is the current measured at a determined potential and A_{real} is the surface area of platinum electrodeposited

$$MA = \frac{j}{W} \qquad (A\ g^{-1}) \qquad (5.10)$$

where j is the current density and W is the platinum loading

Equation (5.9) provides a measure of the electrocatalytic activity of Pt atoms in the particle surface. Equation (5.10) is frequently used in fuel cells because the cost of the electrodes depends on the amount of electrocatalysts. SA and MA were calculated measuring the activity at 0.85V (cf. **Table V**).

Table VI shows the values of MA and SA calculated:

Table VI

ultramicro -electrode	current (A)	surface area of platinum electrodeposited (cm^2)	Pt loading ($\mu g\ cm^{-2}$)	MA ($A\ gr^{-1}$)	SA ($\mu A\ cm^{-2}$)
1	a 6.45×10^{-10} b 1.95×10^{-9}	1.39×10^{-5}	12.1	a 3.83 b 11.6	a 46.4 b 140
2	a 8.14×10^{-10} b 2.46×10^{-9}	1.91×10^{-5}	25.1	a 1.7 b 5.13	a 42.6 b 128

1 and 2: carbon ultramicroelectrode (4 μm radius) modified with different amount of Pt.

a forward reaction

b back reaction

From **table VI**, it is seen that both platinum modified carbon ultramicro-electrodes exhibit similar values of SA. However the MA decrease considerably when the Pt loading is increased.

According to the experimental data obtained with polycrystalline Pt, Pt/Nafion/Pt and carbon/Pt ultramicroelectrodes using steady state voltammetry it is seen that when the roughness of the electrode surface is high (R>15), the apparent number of electrons transferred is close to 4 but when the roughness is <2, the apparent number of electrons transferred is 2. This behaviour may be explained if the following mechanisms are considered:

mechanism I:

Roughness factor <2

1) $O_2 + H^+ + e^- \longrightarrow HO_{2(ads)}$ (rate determining step) (5.11)

2) $HO_{2(ads)} + e^- + H^+ \longrightarrow H_2O_{2(ads)}$ (5.12)

3) $H_2O_{2(ads)} \xrightarrow{\text{diffusion}} H_2O_{2(solution)}$ (5.13)

mechanism II:

Roughness factor >15

1) $O_2 + H^+ + e^- \longrightarrow HO_{2(ads)}$ (rate determining step) (5.14)

2) $HO_{2(ads)} + e^- + H^+ \longrightarrow H_2O_{2(ads)}$ (5.15)

3) $H_2O_{2(ads)} \xrightarrow{\text{diffusion}} H_2O_{2(solution)}$ (5.16)

4) $H_2O_2 + 2H^+ + 2e^- \longrightarrow 2H_2O$ (5.17)

5) $2H_2O_2 \xrightarrow{\text{chemical..step}} O_2 + 2H_2O$ (5.18)

These mechanisms can be explained using the following simplified description of the high surface area Pt deposit:

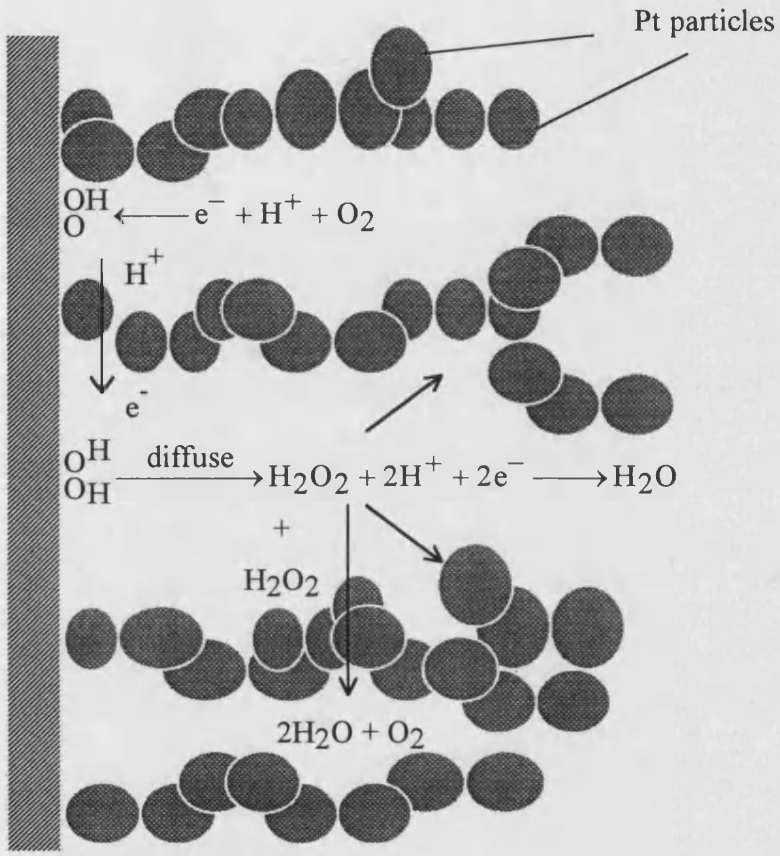

Figure 5.14. Schematic representation of the oxygen reduction on a carbon ultramicroelectrode modified with Pt particles where the roughness factor is high and further reduction or decomposition of H_2O_2 can compete favourably with diffusion

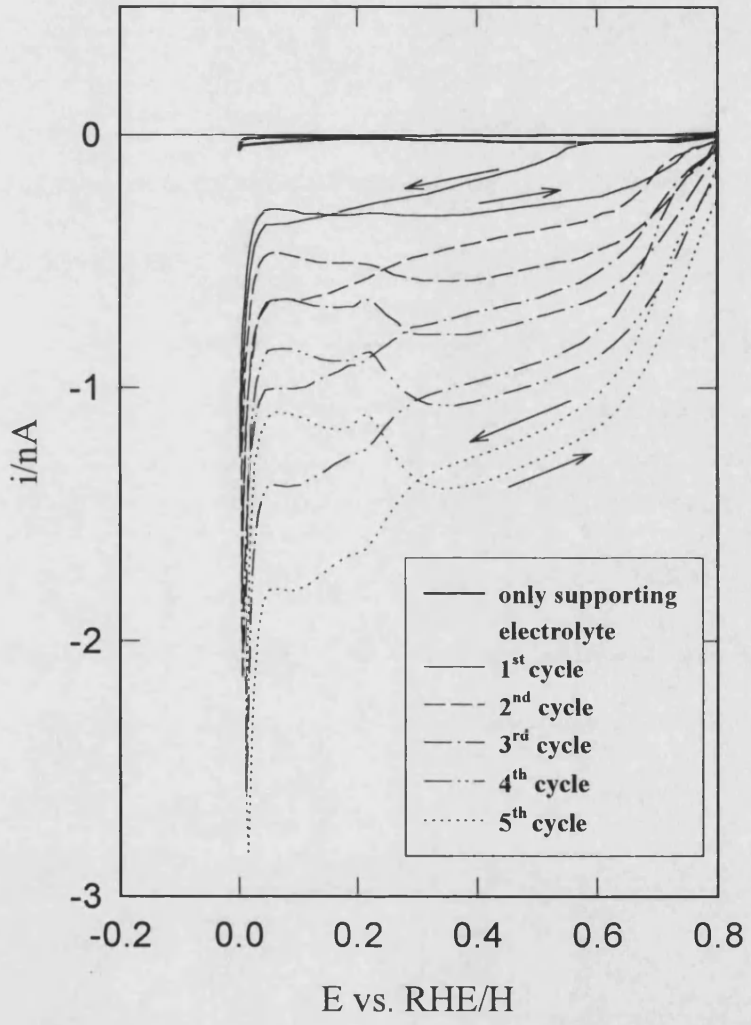

Figure 5.9. Cyclic voltammograms obtained at a carbon microlelectrode (8μm diameter) during the process of electrodeposition of platinum from 0.01 mol dm^{-3} H_2SO_4 + 5x10^{-5} mol dm^{-3} K_2PtCl_4; ν=10 mV s^{-1}.

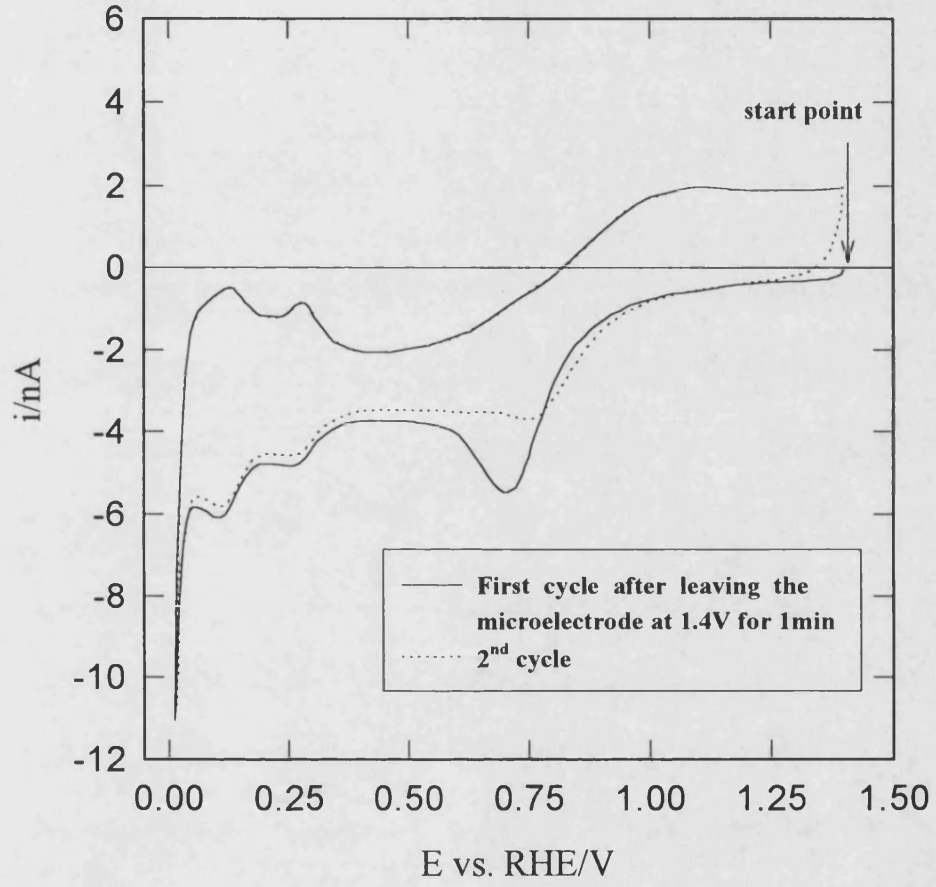

Figure 5.10. Cyclic voltammogram obtained at a carbon microelectrode modified with Pt after several cycles between 0.8V to 0.05V at 10 mV s^{-1}; Solution 1 mol dm^{-3} H_2SO_4 saturated with air at 25 ^{o}C; ν=100 mV s^{-1}

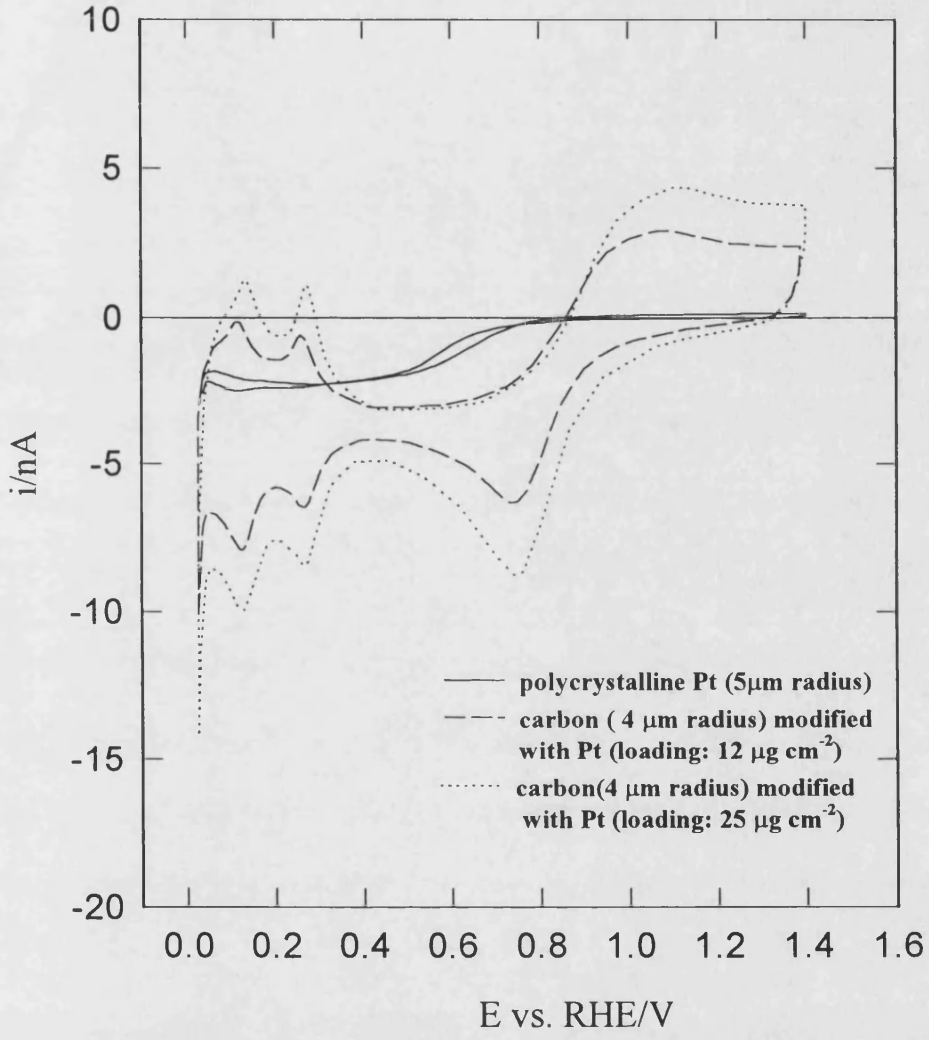

Figure 5.11. Cyclic voltammograms of a platinum microelectrode (5 μm in radius) and two carbon microelectrodes (4 μm in radius) modified with platinum. Solution 1 mol dm^{-3} H_2SO_4 saturated with air at 25°C; ν=100 mV s^{-1}

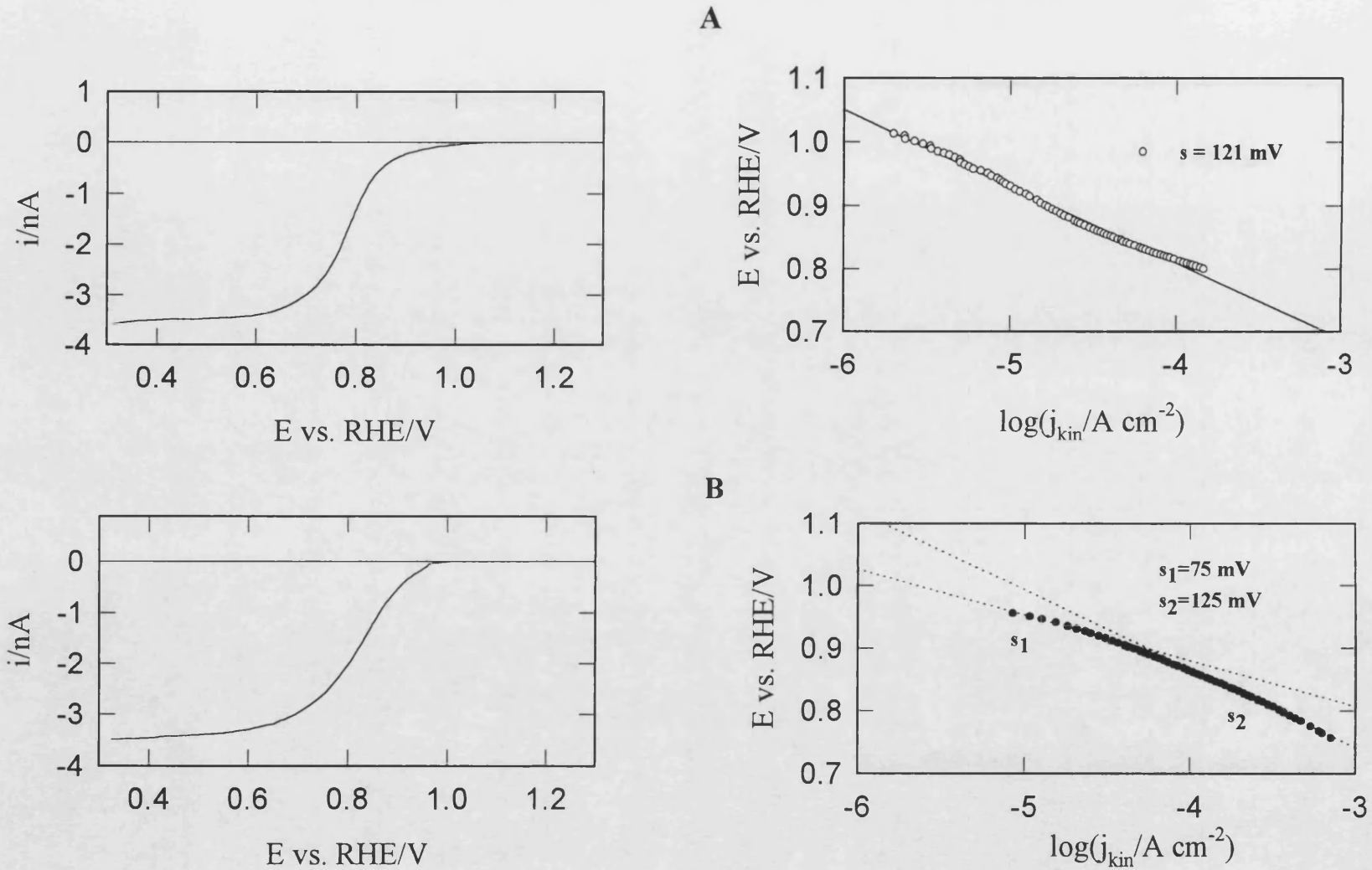

Figure 5.12. Steady state voltammogram and Tafel plots : A) forward scan; B) back scan; C/Pt microelectrode (4 μm radius); Pt loading : 12.1 μg cm^{-2}; R=27.3 in an air saturated solution 1 mol dm^{-3} H_2SO_4;ν=10 mV s^{-1}

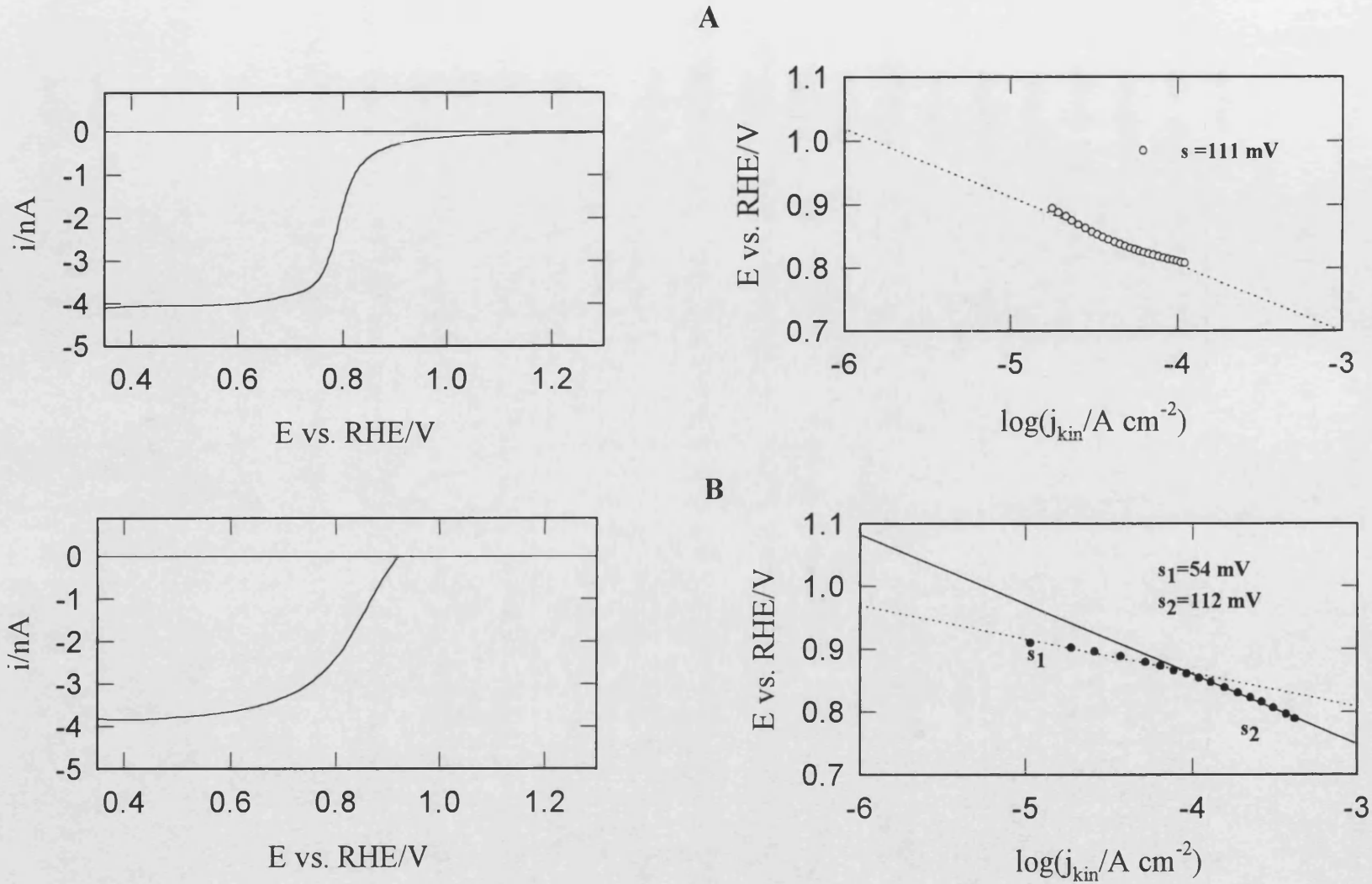

Figure 5.13. Steady state voltammogram and Tafel plots : A) forward scan; B) back scan; C/Pt microelectrode (4 μm radius); loading=25 μg cm^{-2} R=37.9 in an air saturated solution 1 mol dm^{-3} H_2SO_4;ν=10 mV s^{-1}

Although it is known that the diffusion process on the ultramicroelectrode is fast and the diffusion rate is inversely proportional to its size, the mechanism of the electrode reaction at the Pt surface seems to be dependent on the surface roughness. In this work, very dilute solutions of K_2PtCl_4 and an overpotential of about 0.25V were used during the process of electrodeposition. The high surface roughness values indicate that the deposit is highly porous. Dendritic or porous deposits are commonly found in electroplating in dilute solutions under mass transfer control [44]. Numerical simulation using diffusion-limited aggregation (DLA) models has been used for describing the different growth patterns observed during electrodeposition [45]. When metal deposits are grown far from equilibrium, the DLA model indicates that radial branching patterns or well-ordered anisotropic dendritic structures are formed. Moreover changes in the structure of the deposit have also been found when the electrolyte concentration and applied potential are varied [46,47].

From **table IV** it is seen that the Pt loading values (W) found for the modified carbon ultramicroelectrodes with roughness factors (R) of about 27.7 and 37.9, are 12.1 and 25.1 $\mu g\ cm^{-2}$ respectively. Knowing that the Pt density (ρ) is 21.45 $g\ cm^{-3}$, and assuming that the Pt deposit is a random ensemble of identical spheres, the ratio between the total volume occupied by the spheres (V_T) and the real surface area of Pt can be related with those parameters (R, W, and ρ). The total volume (V_T) occupied by the spheres is given by:

$$V_T = N\frac{4}{3}\pi r^3 \qquad (5.19)$$

where N is the total number of spheres and r is the radius of each one. The total surface area of the spheres (A_T) is given by:

$$A_T = N4\pi r^2 \qquad (5.20)$$

Combination of (5.19) and (5.20) gives:

$$\frac{V_T}{A_T} = \frac{r}{3} \qquad (5.21)$$

From this relationship the radius can be determined if it is considered that:

$$\frac{V_T}{A_T} = \frac{W}{R\rho} \qquad (5.22)$$

The radius obtained from this relationship is about 0.6 nm when the Pt loading is 12.1 μg cm^{-2} and 0.9 nm when the Pt loading is 25 μg cm^{-2}. These values indicate that Pt particle sizes in the matrix are about 1.2 and 1.8 nm respectively. Theoretical analyses of the ideal geometric structures of small Pt particles have been carried out [48]. These analyses have shown that the crystallographic sites on the particle vary with the size of the particle. **Figure (5.15)** shows a model of the cubo-octahedral structure for a platinum particle consisting of (111) and (100) crystal faces. The model represents a Pt particle of about 1.5 nm diameter. For these small particles the changes in surface concentration of the various crystallographic sites must vary dramatically with the particle size. From **table VI** it can be seen that the specific activities on both carbon ultramicroelectrodes modified are similar, which indicates that SA is independent of particle size. The MA is seen to increase as particle size decreases.

If a comparison of the specific activity is to be made between the Pt polycrystalline ultramicroelectrode and carbon ultramicroelectrodes modified with Pt, a correction of the current values must be made. At Pt ultramicroelectrodes it was demonstrated that the number of electrons transferred is 2, whereas on carbon ultramicro-electrodes modified with Pt the number of electrons transferred is 4. For a reliable comparison of the specific activities, the values of current on the Pt ultramicroelectrode must be multiplied by 2 or the values of current on the carbon ultramicroelectrode modified with Pt divided by 2. When this is done, it is observed that the specific acitivity of the electrodeposited Pt is lower by around a factor of 2 than the SA for the Pt ultramicroelectrode.

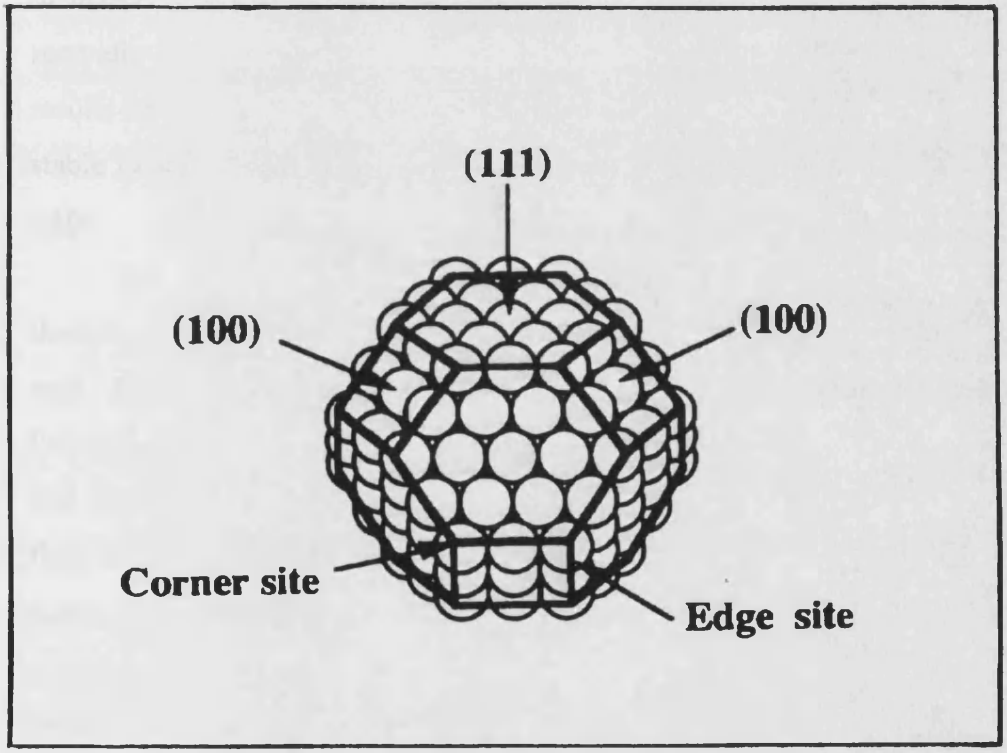

Figure 5.15. Model of a cubo-octahedral structure for platinum particles of about 1.5 nm diameter consisting of (111) and (100) crystal faces, after [8].

5.5.4 Experiments on platinum ultramicroelectrodes modified with polyaniline

A polyaniline film was formed on Pt ultramicroelectrodes (5 μm radius) provided that the electropolymerisation process was carried out using a solution which already contained oligomers of aniline. This solution was prepared by immersing a large Pt electrode in freshly prepared monomer solution together with a Pt wire electrode (counter electrode), and then cycling between -0.2V and 0.8V vs. SCE for 1 hour. When the electropolymerisation is carried out on Pt ultramicro-electrodes with this solution, the first stage of the process could be the aggregation of dissolved oligomers and precipitation on the ultramicroelectrode surface, and secondly the polymerisation of these oligomers. **Figure 5.16** shows the initial results of electropolymerisation under the conditions described. The film formed is stable under conditions where the potential applied is does not exceed 0.8V vs RHE.

Pt ultramicroelectrodes modified with polyaniline films (120-130 nm thickness) were used for studying the oxygen reduction reaction. **Figures 5.17a and 5.17b** show the cyclic voltammograms obtained when a modified Pt/Polyaniline and a Pt/polyaniline/Pt ultramicroelectrode were used in the presence and absence of oxygen. It is known that polyaniline is in the conducting emeraldine form over the potential range from 0.2V to 0.9V vs. NHE. **Figures 5.17a and 5.17b** show that there is a residual cathodic current after -0.2V vs. RHE. This suggests that the film is porous or some defects are present in the polymer film. When Pt was deposited on the film, the cathodic current increased in presence of oxygen and the cathodic current is constant at potentials where the polymer film is not conducting. This behaviour may be explained if nucleation of Pt occurs on the electrode surface through defects in the film and then growth continues through to the surface of the polymer film. This behaviour is represented in **figure 5.18**. A comparison with the voltammogram obtained on the naked Pt ultramicroelectrode can be made. Similar current densities are observed which indicates that the film surface becomes coated with platinum under the experimental conditions used.

To determine the current density, it is necessary to know the real surface area of the Pt deposited. However, no adsorption or desorption hydrogen peaks were observed since they were masked by the currents associated with redox processes in the PANi film. For this reason it was not possible to evaluate the specific activity of the Pt particles dispersed into/and on the polyaniline film. In **figures 5.17a and 5.17b**, the current density was calculated using the geometric area of the Pt ultramicroelectrode.

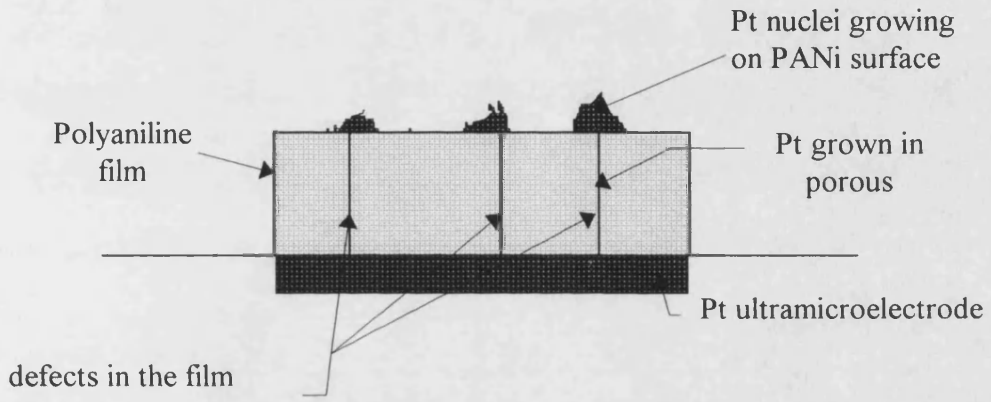

Figure 5.18. Schematic representation of electrodeposition of Pt into and on a polyaniline film

The properties of the electrode are therefore similar to those of an electrodeposited film on a conducting substrate since each platinum centre is connected by a platinum 'wire' to the ultramicroelectrode.

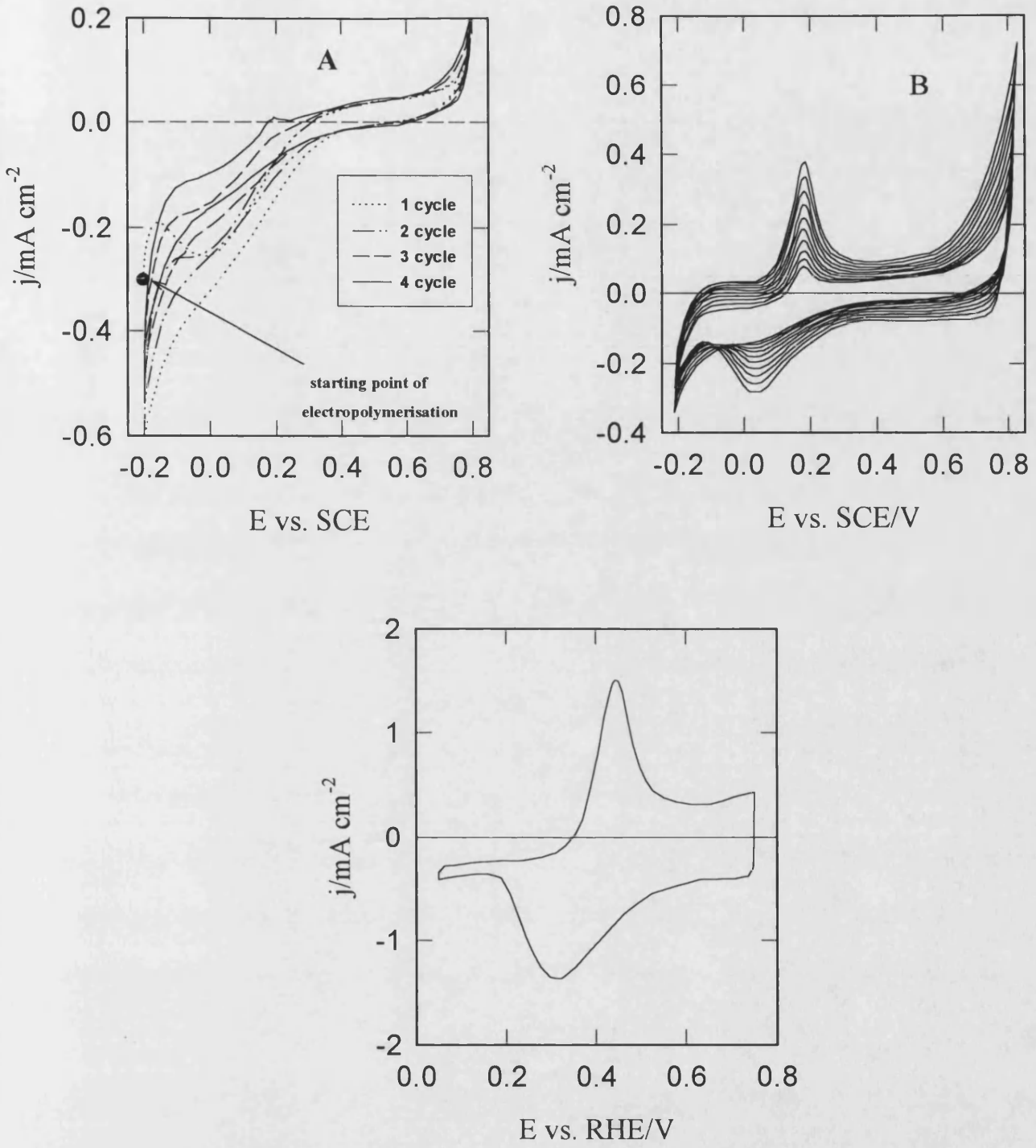

Figure 5.16. (A,B): Cyclic voltammograms of the initial stages of polymerisation of aniline 0.1 mol dm^{-3} in 1 mol dm^{-3} H_2SO_4 using a Pt ultramicroelectrode (5 μm radius), R= 1.98, ν = 50 mV s^{-1}; C) Cyclic voltammogram of the polyaniline film (130 nm thickness) in air saturated solution 1 mol dm^{-3} H_2SO_4; ν=20 mV s^{-1}.

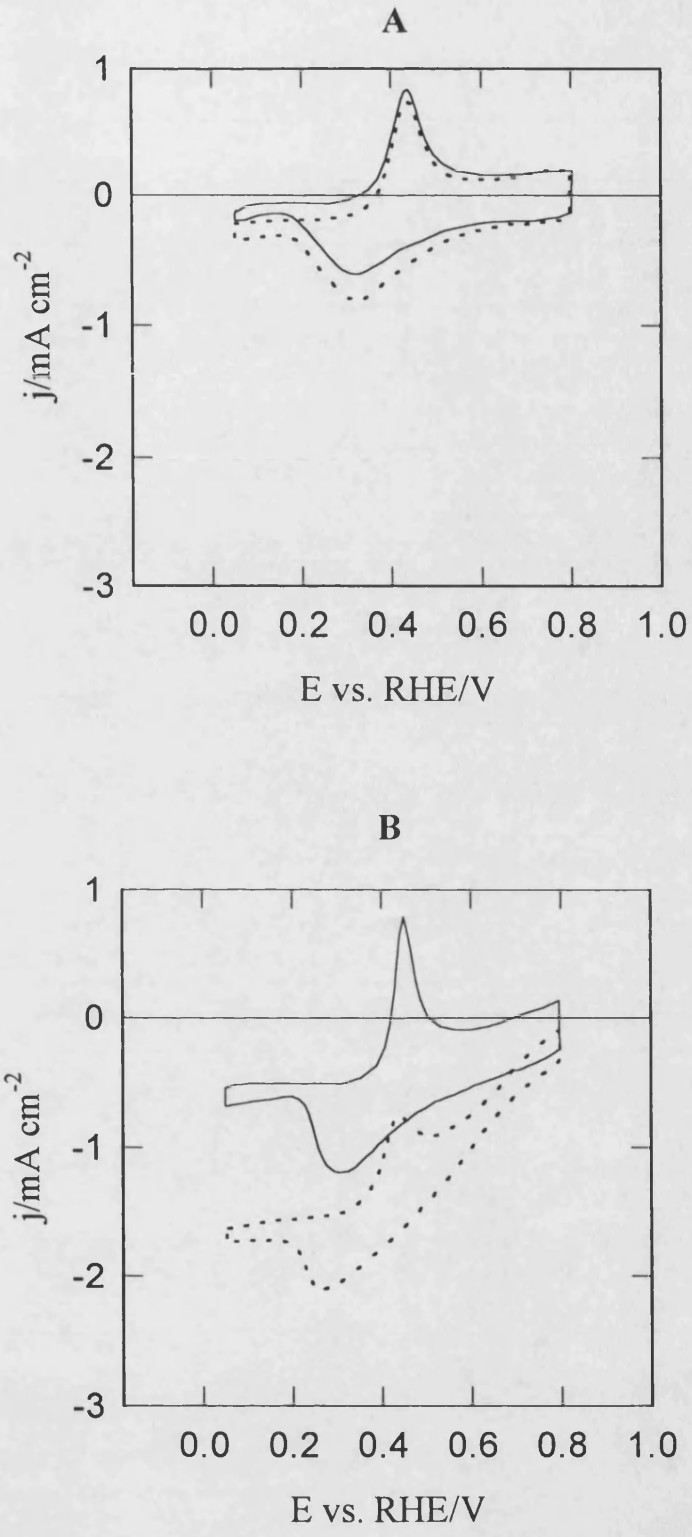

Figure 5.17. Cyclic voltammograms recorded at a: A) Pt/polyaniline ultramicroelectrode; B) Pt/polyaniline/Pt ultramicroelectrode; In absence of oxygen (—); in presence of oxygen (·····); 1 mol dm^{-3} H_2SO_4; ν=10 mV s^{-1}

5.6. Conclusions

On Pt ultramicroelectrodes (5 μm radius), the apparent number of electrons transferred during the oxygen reduction reaction in acid solution is 2. This suggests that hydrogen peroxide formed as an intermediate diffuses rapidly from the surface before decomposition or electrochemical reaction to H_2O can occur. On conventional electrodes, where mass transfer is slower than on ultramicroelectrodes, the hydrogen peroxide can be more easily reduced to water, either via the decomposition or electron transfer routes.

Although simplifying assumptions about the shape of the Pt particles deposited on carbon ultramicroelectrodes were made and 100% current efficiency assumed during the process of electrodeposition, the experimental evidence suggests strongly that very small Pt particles about 1.2 to 1.8 nm in diameter are formed when very dilute solutions of K_2PtCl_4 are used. This process of electrodeposition is completely controlled by mass transfer. The structure of the Pt deposit is highly porous, which means that it has a high roughness factor and the conversion of hydrogen peroxide to water is enhanced.

If specific sites on the surface of Pt particles size are considered to be active sites, it is expected that in Pt particles smaller than about 10 nm, changes in the surface concentration of crystallographic sites such as edges sites could affect considerably the electrocatalytic activity of these particles. However in the present work, this behaviour was not observed. The values of specific activity found for particles with 1.2 and 1.8 nm in diameter did not differ substantially from the value for bulk platinum. In conclusion, it can be said that there is no catalytic effect of the particle size on the oxygen reduction even when the Pt particles are very small. In fact the comparison shows that the smaller particles exhibit a slightly lower activity than the bulk. This decrease in activity has also been noted in other work using dispersed platinum catalysts[8].

The results indicate that H_2O_2 is produced as a solution intermediate. Whereas it can escape efficiently by diffusion from a smooth ultramicroelectrode, it reacts to form water at the highly porous platinum deposits formed on carbon ultramicroelectrodes. A similar process may occurr in fuel cells where the hydrogen

peroxide reacts at the adjacent Pt particles present in the polymer-carbon matrix to produce water.

The kinetics of oxygen reduction on Pt/Nafion/Pt ultramicroelectrodes cannot be compared with the behaviour observed in a fuel cell. In a fuell cell the Pt particles are embedded in the polymer and carbon substrate, while on ultramicro-electrodes modified in the present work, Pt is deposited inside and outside the film. The activity of the Pt particles outside the film may be different to the activity of these particles embeded in the polymer-carbon substrate.

Electropolymerisation of aniline film on ultramicroelectrodes is hindered by the high mass transfer that occurs on the ultramicroelectrode. In the present work, a stable film was obtained after oligomers were adsorbed on the electrode surface before carrying out the electropolymerisation. However, small defects in the film or the formation of a porous film are enough to produce a platinum coating on the film during the electrodeposition process even when low concentrations of K_2PtCl_4 are used. In conclusion, this behaviour does not permit small catalyst particles to be deposited inside a polyaniline film which has been grown on an ultramicro-electrode, so the catalytic effect of these small particles in the polymer film on the oxygen reduction reaction, cannot be evaluated reliably.

References (Chapter 5)

1. R.A. Van Nordstrand, A.J. Lincoln, A. Carnevale, Anal. Chem., **36**, (1964), 819
2. S. Srinivasan, J. Electrochem.Soc., **136**, (1989), 411
3. J.H. Ye, P.S. Fedkiw, Electrochimica Acta, **41**, (1996), 221
4. M. Watanabe, K. Makita, H. Usami, S. Motoo, ibid., **197**, (1986), 195
5. M. Watanabe, M. Uchida, S. Motoo, ibid., **229**, (1987), 395
6. E.J. Cairns, E.J. McInerney, J. Electrochem. Soc., **114**, (1967), 980
7. J.H. Hirschenhofer, IEEE AES Systems Magazine, november, (1993), 21
8. K.Kinoshita, *Electrochemical oxygen techology*, Wiley-Intercience, John Wiley & Sons, Inc., 1992, pp 44.
9. K. Kinoshita, P. Stonehart, in "Modern Aspects of Electrochemistry" (Edited by B.E. Conway, J.O'M. Bockris), 12, 183, Plenum Press, New York (1977)
10. K. Kinoshita, J. Electrochem. Soc., 137, (1990), 845
11. A. Damjanovic, V. Brusic, Electrochim. Acta, **12**, (1967), 615
12. J.V. Petrocelli, J. Electrochem. Soc., **114**, (1967), 1036
13. P. Delay, J. Electrochem. Soc., **97**, (1950), 198
14. A.J. Appleby, in "Modern Aspects of Electrochemistry, No9, edited by J. O'M., Bockris and B.E. Conway, Plenum Press, New York (1974)
15. J. Huang, R. Sen and E. Yeager, J. Electrochem. Soc., **126**, (1979) 785.
16. P. Fisher, J. Heitbaum, J. Electroanal. Chem., **112**, (1980), 231.
17. I. Morcos, E. Yeager, Electrochim. Acta, **15**, (1970) 953.
18. A. Damjanovic, M.A. Genshaw, J.O.M. Bockris, J. Electrochem. Soc., **114**, (1967), 1108
19. D. Pletcher, S. Sotiropoulos, J. Electroanal. Chem., **356**, (1993), 109.
20. S. Gottesfeld, I. Raistrick, S. Srinivasan, J. Electrochem.Soc., **134**, (1987), 1455
21. F.A. Uribe, T.E. Springer, S. Gottesfeld, J. Electrochem. Soc., **139**, (1992), 765

22. E.A. Ticianelli, C.R. Derovin, S. Srinivasan, J. Electroanal. Chem., **251**, (1988), 275
23. M.S. Wilson, S. Gottesfeld, J. Electrochem.Soc., **139**, (1992), L28.
24. S. Srinivasan, E.A. Ticianelli, C.R. Derouin, A.Redondo, J. Power Source, **22**, (1988), 359
25. S. Dong, Q. Qiu, J. Electroanal. Chem., **223**, (1991), 314
26. P.S. Fedkiw, W.H. Her, J. Electrochem.Soc., **136**, (1989), 899
27. H. Laborde, J.M. Leger, C. Lamy, J. Appl. Electrochem., **24**, (1994), 219
28. J. Yano, M. Kokura, K. Ogura, J. Appl. Electrochem., **24**, (1994), 1164
29. J.W. Thackeray, M.S. Wrighton, J. Phys. Chem., **90**, (1986), 6674.
30. M.S. Gholamian, J. and Contractor, A.Q. 1987.
31. H. Laborde, J.M. Leger, C. Lamy, J. Appl. Electrochem., **1019**, (1994), 1019
32. R. Schrebler, MA Delvalle, H. Gomez, C. Veas, R. Cordova, J. Electoanal. Chem., **380**, (1995), 219
33. G. Bidan, E.M. Genies, M. Lapkowki, J. Chem. Soc. Chem. Commun., 1988, 533.
34. C.S.C. Bose, K. Rajeshwar, J. Electroanal. Chem., **333**, (1992), 235
35. A. Leone, W. Marino, B.R. Scharifker, J. Electrochem. Soc., **139**, (1992), 438.
36. R.C.M., Jacobs, L.J.J. Janssen, E. Barendrecht, Electrochim. Acta, **30**, (1985), 1433
37. S. Holdcroft, L. Funt, J. Electroanal. Chem., **240**, (1988), 89
38. F.T.A. Vork, E. Barendrecht, Electrochim. Acta, **35**, (1990), 35
39. C.J. Stalder, S. Chao, M.S. Wrighton, J. Am. Chem.. Soc., **106**, (1984), 3673
40. R. Greef, M. Kalaji, L.M. Peter, Faraday Discuss. Chem. Soc., **88**, (1989), 277
41. H. Ikeuchi, M. Hayafuji, Y. Aketagawa, J. Taki, G.P. Sato, J. Electroanal. Chem., **396**, (1995), 553
42. S.E. Morris, Trends Anal. Chem., 7, (1988), 227

43. A. Damjanovic, V. Brusic., Electrochim. Acta, **12**, (1967), 615

44. D. Pletcher, F.C. Walsh, *Industrial Electrochemistry*, Blackie A. & P., London, 1990, pp 385.

45. R.M. Brady, R.C. Ball, Nature, **225**, (1984), 309

46. G.L.M.K.S. Kahanda, M. Tomkiewicz, J. Electroachem. Soc., **136**, (1989), 1497

47. C.P. Cheun, J. Jorne, J. Electrochem. Soc., **137**, (1990), 2047

48. W.Romanowski, Surf. Sci., **18**, (1969), 373